frontiers | Research Topics

Insights in renal physiology and pathophysiology 2023

Edited by
Carolyn Mary Ecelbarger, Youfei Guan and Xiaoyan Zhang

Published in
Frontiers in Physiology

ISSN 1664-8714
ISBN 978-2-8325-5818-8
DOI 10.3389/978-2-8325-5818-8

About Frontiers

Frontiers is more than just an open access publisher of scholarly articles: it is a pioneering approach to the world of academia, radically improving the way scholarly research is managed. The grand vision of Frontiers is a world where all people have an equal opportunity to seek, share and generate knowledge. Frontiers provides immediate and permanent online open access to all its publications, but this alone is not enough to realize our grand goals.

Frontiers journal series

The Frontiers journal series is a multi-tier and interdisciplinary set of open-access, online journals, promising a paradigm shift from the current review, selection and dissemination processes in academic publishing. All Frontiers journals are driven by researchers for researchers; therefore, they constitute a service to the scholarly community. At the same time, the *Frontiers journal series* operates on a revolutionary invention, the tiered publishing system, initially addressing specific communities of scholars, and gradually climbing up to broader public understanding, thus serving the interests of the lay society, too.

Dedication to quality

Each Frontiers article is a landmark of the highest quality, thanks to genuinely collaborative interactions between authors and review editors, who include some of the world's best academicians. Research must be certified by peers before entering a stream of knowledge that may eventually reach the public - and shape society; therefore, Frontiers only applies the most rigorous and unbiased reviews. Frontiers revolutionizes research publishing by freely delivering the most outstanding research, evaluated with no bias from both the academic and social point of view. By applying the most advanced information technologies, Frontiers is catapulting scholarly publishing into a new generation.

What are Frontiers Research Topics?

Frontiers Research Topics are very popular trademarks of the *Frontiers journals series*: they are collections of at least ten articles, all centered on a particular subject. With their unique mix of varied contributions from Original Research to Review Articles, Frontiers Research Topics unify the most influential researchers, the latest key findings and historical advances in a hot research area.

Find out more on how to host your own Frontiers Research Topic or contribute to one as an author by contacting the Frontiers editorial office: frontiersin.org/about/contact

Insights in renal physiology and pathophysiology: 2023

Topic editors

Carolyn Mary Ecelbarger — Georgetown University, United States
Youfei Guan — Dalian Medical University, China
Xiaoyan Zhang — East China Normal University, China

Citation

Ecelbarger, C. M., Guan, Y., Zhang, X., eds. (2024). *Insights in renal physiology and pathophysiology: 2023*. Lausanne: Frontiers Media SA.
doi: 10.3389/978-2-8325-5818-8

Table of contents

frontiers | Frontiers in Physiology

TYPE Editorial
PUBLISHED 10 December 2024
DOI 10.3389/fphys.2024.1523820

OPEN ACCESS

EDITED AND REVIEWED BY
David Mount,
Brigham and Women's Hospital and Harvard Medical School, United States

*CORRESPONDENCE
Carolyn M. Ecelbarger,
ecelbarc@georgetown.edu

RECEIVED 06 November 2024
ACCEPTED 21 November 2024
PUBLISHED 10 December 2024

CITATION
Ecelbarger CM, Zhang X and Guan Y (2024) Editorial: Insights in renal and epithelial physiology: 2023.
Front. Physiol. 15:1523820.
doi: 10.3389/fphys.2024.1523820

Editorial: Insights in renal and epithelial physiology: 2023

Carolyn M. Ecelbarger[1]*, Xiaoyan Zhang[2] and Youfei Guan[3]

[1]Department of Medicine, Division of Endocrinology and Metabolism, Washington, DC, United States, [2]Health Science Center, East China Normal University, Shanghai, China, [3]Advanced Institute for Medical Sciences, Dalian Medical University, Dalian, Liaoning, China

KEYWORDS

lithium, allograft acceptance, biomarkers, nutriceutical agents, calcium signal, acute kidney damage

Editorial on the Research Topic
Insights in renal and epithelial physiology: 2023

We were overall delighted with the high-interest generated in this second iteration of Insights in Renal Epithelial Physiology encompassing 2023–2024. We were pleased to accept 9 reviews, primary reports, and a meta-analysis on wide-ranging Research Topic from renal cell signaling mechanisms and approaches to study them, novel therapeutics and nutrition-based strategies to combat renal injury, and updates on sensitive and specific early biomarkers for renal disease. We highlight these reports below.

Lithium, used primarily in psychiatric therapy, has been associated with renal injury (Kishore and Ecelbarger, 2013). Baranovskaya et al. assessed the extent to which inflammation contributed to overall damage using a mouse model of lithium carbonate treatment. They conducted measures of renal injury including, terminal deoxynucleotidyl transferase dUTP nick end labeling (TUNEL) assay, kidney injury marker (KIM1) and neutrophil gelatinase lipocalin (NGAL). In addition, they assessed activation of the pro-inflammatory nucleotide-binding domain, leucine-rich–containing family, pyrin domain–containing-3 (NLRP3) inflammasome cascade. They determined that lithium induced activation of apoptosis, but not general inflammation, in fact inflammation was somewhat reduced (lower M1/M2 polarization ratio, caspase-1, NLRP3, and interleukin 1β levels) in the lithium-treated mice. Overall, they concluded that while lithium did insult the kidney primarily via apoptosis; the anti-inflammatory effect may be beneficial.

Guo et al. provide a mini-review on the role of bile acid receptors in water homeostasis highlighting what is known regarding the farnesoid X receptor (FXR) and the Takeda G protein-coupled receptor 5 (TGR5). While these receptors have important role in renal metabolism, less is known regarding their impact on urine concentration. FXR is a nuclear receptor primarily involved in regulating transcription, whereas, TGR5 couples to Gs-alpha (Gαs) which activates the cAMP-protein kinase A signaling (PKA) pathway. Zhang et al. (Zhang et al., 2014) showed that urine became more concentrated in mice treated with bile acids, and FXR knockout mice had impaired urine concentrating ability. In addition, activation of FXR seems to reduce renal cell apoptosis under hypertonic stress (Xu et al., 2018), and enhance activity of the sodium coupled Na-K-2Cl cotransporter (NKCC2) in the thick ascending limb. With regard to TGR5, Han et al. (Han et al., 2021) showed increased expression of aquaporin 2 in an ischemia/reperfusion model of impaired urine concentration most likely via activation of the hypoxia-inducible factor (HIF) pathway.

These findings suggest some potential therapeutic benefits of bile acids in urine concentration.

Sickle cell disease (SCD) is associated with sickle cell nephropathy (SCN) likely due to poor perfusion of capillaries with the malformation of red blood cells (Ataga et al., 2022). Early detection of nascent SCN is critical in staving off pathology. Packialakshmi et al. conducted proteomics followed by Western blotting on urine exosomes to look for early biomarkers of SCN in humanized sickle-cell disease (SCD) mice pre- and post-development of albuminuria. Potential early biomarkers they detected that correlated with albuminuria in the mice were heparanase, cathepsin C, α2-macroglobulin, and sarcoplasmic endoplasmic Ca^{2+}ATPase-3 (SERCA3). Female mice demonstrated a stronger correlation of these proteins with albuminuria. These studies provide candidates to assess in human subjects.

It is important to predict, as early as possible, whether a renal allograft will be successful. Kidney biopsies have complications and are often not reliable. Yang et al. conduct a meta-analysis to assess the diagnostic performance of graft-derived cell-free DNA (GcfDNA) in determining kidney allograft rejection rates. Eleven studies from four continents comprising 1,148 patients were statistically evaluated. GcfDNA was found to be useful particularly as a biomarker for discriminating between rejection and antibody-mediated rejection (ABMR) in transplant recipients.

Tuberous sclerosis complex (TSC) genes 1 and 2 (coding for harmatin and tuberin, respectively) are important cell growth regulators. Mutations in their function (also known as TSC), leads to cystic growth in kidney and other tissues. Soleimani reviews manifestation of this disorder in kidney and delineates how it differs from other major cystic disorders, e.g., polycystic kidney disease. Normally functioning TSC brakes over-activity of the mechanistic target of rapamycin (mTOR), upstream of growth and cell proliferation. In kidney, there appears to be involvement particularly in alpha intercalated cells via FOXI1 and upregulation of H + -ATPase signaling. Thus, there is potential for refined therapeutic targeting in TSC-associated renal cysts.

Zou provides a review on advances in the use of microRNAs to predict cardiovascular complications in chronic kidney disease (CKD). Reviewing animal and human studies, they highlighted a number of miRs that have been reported to be associated changes in vascular calcification or ventricular hypertrophy, e.g., miR-29b, miR-378-3p, and miR-30. Tables were provided showing candidate miRs and main findings. Development of a circulating prognostic panel of miRs in this patient population would move the field forward and help improve patient outcomes.

Hyperuricemia is an increasing disorder associated with metabolic syndrome, likely due to high purine and fructose metabolism (Yanai et al., 2021). Umer et al. used a potassium oxonate/bromate model of hyperuricemia in rats to study the potential therapeutic role of onion bioactive compounds, e.g., quercetin. Oral onion powder significantly reduced blood uric acid levels, in dose-wise fashion, and improved liver and kidney function and lipid profile. There were no effects on weight gain. The absolute component of the onion powder that improved metabolic profile in the rats was not determined, but these findings provide rationale for further study of underlying mechanisms.

Simpler, and more easily manipulated, model systems improve our ability to understand complex signaling in the kidney. Calcium mobilization in inner medullary collecting duct cells has been shown to be downstream of G-protein coupled signaling via exchange proteins directly activated by cyclic AMP (Epac). Using fluorescence and site-specific Ca^{2+} sensitive biosensors, Yip et al. evaluate whether murine principal kidney collecting duct cells (mpkCCD) are a reliable model for intact collecting duct with regard to Ca^{2+} mobilization characteristics. It proved reliable and they elucidated the nature of ryanodine-dependent Ca^{2+} signaling and endoplasmic reticulum (ER) mitochondrial Ca^{2+} coupling in this system.

Acute hemorrhagic events followed by necessary staunch of blood loss with a tourniquet can lead to acute kidney injury. To better treat and avoid this event, appropriate animal models are needed. Packialakshmi et al. studied the impact of hemorrhage coupled to tourniquet (lower-limb) application using a mouse model. They found hemorrhage alone did not lead to AKI (15% blood loss), but the coupling with ischemia (tourniquet) significantly exacerbated renal, as well as, lung injury associated with the ischemia. The new model system can be employed to evaluate mechanisms and therapeutic strategies.

Author contributions

CE: Writing–original draft, Writing–review and editing. XZ: Writing–review and editing. YG: Writing–review and editing.

Funding

The author(s) declare that no financial support was received for the research, authorship, and/or publication of this article.

Conflict of interest

The authors declare that the research was conducted in the absence of any commercial or financial relationships that could be construed as a potential conflict of interest.

The author(s) declared that they were an editorial board member of Frontiers, at the time of submission. This had no impact on the peer review process and the final decision.

Publisher's note

References

Ataga, K. I., Saraf, S. L., and Derebail, V. K. (2022). The nephropathy of sickle cell trait and sickle cell disease. *Nat. Rev. Nephrol.* 18, 361–377. doi:10.1038/s41581-022-00540-9

Han, M., Li, S., Xie, H., Liu, Q., Wang, A., Hu, S., et al. (2021). Activation of TGR5 restores AQP2 expression via the HIF pathway in renal ischemia-reperfusion injury. *Am. J. Physiol. Ren. Physiol.* 320, F308–F321. doi:10.1152/ajprenal.00577.2020

Kishore, B. K., and Ecelbarger, C. M. (2013). Lithium: a versatile tool for understanding renal physiology. *Am. J. Physiol. Ren. Physiol.* 304, F1139–F1149. doi:10.1152/ajprenal.00718.2012

Xu, S., Huang, S., Luan, Z., Chen, T., Wei, Y., Xing, M., et al. (2018). Farnesoid X receptor is essential for the survival of renal medullary collecting duct cells under hypertonic stress. *Proc. Natl. Acad. Sci. U. S. A.* 115, 5600–5605. doi:10.1073/pnas.1803945115

Yanai, H., Adachi, H., Hakoshima, M., and Katsuyama, H. (2021). Molecular Biological and Clinical Understanding of the Pathophysiology and Treatments of Hyperuricemia and Its Association with Metabolic Syndrome, Cardiovascular Diseases and Chronic Kidney Disease. *Int. J. Mol. Sci.* 22. 9221. doi:10.3390/ijms22179221

Zhang, X., Huang, S., Gao, M., Liu, J., Jia, X., Han, Q., et al. (2014). Farnesoid X receptor (FXR) gene deficiency impairs urine concentration in mice. *Proc. Natl. Acad. Sci. U. S. A.* 111, 2277–2282. doi:10.1073/pnas.1323977111

frontiers | Frontiers in Physiology

TYPE Original Research
PUBLISHED 29 August 2023
DOI 10.3389/fphys.2023.1250273

OPEN ACCESS

EDITED BY
Carolyn Mary Ecelbarger,
Georgetown University, United States

REVIEWED BY
Victor Babich,
Mercy College of Health Sciences, United States
David Giovannucci,
University of Toledo, United States

*CORRESPONDENCE
Kay-Pong Yip,
dyip@usf.edu

RECEIVED 29 June 2023
ACCEPTED 11 August 2023
PUBLISHED 29 August 2023

CITATION
Yip K-P, Ribeiro-Silva L, Cha B, Rieg T and Sham JSK (2023), Epac induces ryanodine receptor-dependent intracellular and inter-organellar calcium mobilization in mpkCCD cells.
Front. Physiol. 14:1250273.
doi: 10.3389/fphys.2023.1250273

Epac induces ryanodine receptor-dependent intracellular and inter-organellar calcium mobilization in mpkCCD cells

Kay-Pong Yip[1,2]*, Luisa Ribeiro-Silva[1], Byeong Cha[1], Timo Rieg[1,2,3] and James S. K. Sham[4]

[1]Department of Molecular Pharmacology and Physiology, Morsani College of Medicine, University of South Florida, Tampa, FL, United States, [2]Hypertension and Kidney Research Center, Morsani College of Medicine, University of South Florida, Tampa, FL, United States, [3]James A. Haley Veterans' Hospital, Tampa, FL, United States, [4]Division of Pulmonary and Critical Care Medicine, Johns Hopkins University School of Medicine, Baltimore, MD, United States

Arginine vasopressin (AVP) induces an increase in intracellular Ca^{2+} concentration ($[Ca^{2+}]_i$) with an oscillatory pattern in isolated perfused kidney inner medullary collecting duct (IMCD). The AVP-induced Ca^{2+} mobilization in inner medullary collecting ducts is essential for apical exocytosis and is mediated by the exchange protein directly activated by cyclic adenosine monophosphate (Epac). Murine principal kidney cortical collecting duct cells (mpkCCD) is the cell model used for transcriptomic and phosphoproteomic studies of AVP signaling in kidney collecting duct. The present study examined the characteristics of Ca^{2+} mobilization in mpkCCD cells, and utilized mpkCCD as a model to investigate the Epac-induced intracellular and intra-organellar Ca^{2+} mobilization. Ca^{2+} mobilization in cytosol, endoplasmic reticulum lumen, and mitochondrial matrix were monitored with a Ca^{2+} sensitive fluorescent probe and site-specific Ca^{2+} sensitive biosensors. Fluorescence images of mpkCCD cells and isolated perfused inner medullary duct were collected with confocal microscopy. Cell permeant ligands of ryanodine receptors (RyRs) and inositol 1,4,5 trisphosphate receptors (IP_3Rs) both triggered increase of $[Ca^{2+}]_i$ and Ca^{2+} oscillations in mpkCCD cells as reported previously in IMCD. The cell permeant Epac-specific cAMP analog Me-cAMP/AM also caused a robust Ca^{2+} mobilization and oscillations in mpkCCD cells. Using biosensors to monitor endoplasmic reticulum (ER) luminal Ca^{2+} and mitochondrial matrix Ca^{2+}, Me-cAMP/AM not only triggered Ca^{2+} release from ER into cytoplasm, but also shuttled Ca^{2+} from ER into mitochondria. The Epac-agonist induced synchronized Ca^{2+} spikes in cytosol and mitochondrial matrix, with concomitant declines in ER luminal Ca^{2+}. Me-cAMP/AM also effectively triggered store-operated Ca^{2+} entry (SOCE), suggesting that Epac-agonist is capable of depleting ER Ca^{2+} stores. These Epac-induced intracellular and inter-organelle Ca^{2+} signals were mimicked by the RyR agonist 4-CMC, but they were distinctly different from IP_3R activation. The present study hence demonstrated that mpkCCD cells retain all reported features of Ca^{2+} mobilization observed in isolated perfused IMCD. It further revealed information on the dynamics of Epac-induced RyR-dependent Ca^{2+} signaling and ER-mitochondrial Ca^{2+} transfer. ER-mitochondrial Ca^{2+} coupling may play a key role in the regulation of ATP and reactive oxygen species (ROS) production in the mitochondria along the nephron. Our data suggest that mpkCCD cells can serve as a renal cell model to address novel questions of how

mitochondrial Ca^{2+} regulates cytosolic Ca^{2+} signals, inter-organellar Ca^{2+} signaling, and renal tubular functions.

KEYWORDS

intracellular calcium stores, Epac, mitochondria-associated membrane, aquaporin-2, ryanodine receptor

Introduction

Physiological concentration of arginine vasopressin (AVP) induces intracellular Ca^{2+} mobilization in form of oscillation in isolated perfused rat inner medullary collecting duct (IMCD) (Yip, 2002). Confocal fluorescence microscopy revealed that each IMCD cells have their own unique oscillatory frequency and amplitude. Such Ca^{2+} mobilization is essential for the associated apical exocytosis, as intracellular Ca^{+2} chelators inhibit both AVP-induced Ca^{2+} mobilization and apical exocytosis in perfused IMCD. AVP exerts its actions via binding of the V_2-receptors to stimulate adenylate cyclase and cAMP production in IMCD cells (Knepper and Inoue, 1997), the latter is mediated by adenylyl cyclase 6 (Rieg et al., 2010). It has traditionally been thought that cAMP activates the protein kinase A (PKA)-dependent signaling pathway to mediate AVP-regulated osmotic water permeability of IMCD. However, our previous study found that PKA inhibitors did not prevent AVP-induced Ca^{2+} mobilization and oscillation. Instead, the cAMP analog 8-pCPT-2′-O-Me-cAMP, which specifically activates exchange protein directly activated by cAMP (Epac) but not PKA, triggered intracellular Ca^{2+} mobilization and apical exocytosis of aquaporin-2 (AQP2) in perfused IMCD (Yip, 2006). Moreover, flash photolysis of caged cADP-ribose (an endogenous ligand of ryanodine receptors) activated Ca^{2+} oscillations resembling AVP-induced Ca^{2+} response (Yip and Sham, 2011). Previous studies showed that Ca^{2+} release from ryanodine receptors (RyRs) is essential in AVP-mediated AQP2 trafficking (Chou et al., 2000; Yip, 2002), and the process is independent of the phosphoinositol signaling pathway (Chou et al., 1998). AVP could also trigger Ca^{2+} influx via the store-operated Ca^{2+} entry (SOCE) mechanism. It was concluded that AVP-induced Ca^{2+} oscillation in IMCD is mediated by an Epac-dependent mechanism through the interplay of Ca^{2+} release from ryanodine receptors and a Ca^{2+} influx mechanism involving SOCE (Yip and Sham, 2011). Epac-induced Ca^{2+} release from RYRs-gated Ca^{2+} stores have been reported in other cell types. In cardiac myocytes, Epac-activation enhances RYR activity through protein kinase $C_{epsilon}$ and Ca^{2+}/calmodulain kinase II (CaMKII)-dependent phosphorylation of RYRs (Pereira et al., 2007; Oestreich et al., 2009), leading to SR Ca^{2+} leak and arrhythmia (Pereira et al., 2013; Li et al., 2017; Pereira et al., 2017). Epac-induced activation of RYRs also causes membrane hyperpolarization and relaxation of mesenteric arteries through Ca^{2+}-sensitive K^+ channel activation (Roberts et al., 2013).

Murine principal kidney cortical collecting duct (mpkCCD) cells are commonly used cell model used for transcriptomic and phosphoproteomic studies of AVP-signaling in kidney collecting ducts (Rinschen et al., 2010; Huling et al., 2012; Sandoval et al., 2013; Yang et al., 2022; Park et al., 2023). It is assumed that mpkCCD cell retains the feature of intact collecting duct cell in AVP-induced signaling events of AQP2 trafficking. We have demonstrated cAMP-dependent vectorial trafficking and exocytosis of AQP2 tagged with photoactivable fluorescent protein in mpkCCD cells at real time (Yip et al., 2015). It has also been shown in mpkCCD cells that Wnt5A, an endogenous ligand of the non-canonical branch of the Wnt pathway, is capable of inducing AQP2 apical expression and trafficking via basolateral Fzd receptors-mediated Ca^{2+} mobilization without activation of cAMP/PKA signal pathway (Ando et al., 2016). These observations highlight the potential of targeting Ca^{2+} pathways to ameliorate polyuria associated with nephrogenic diabetes insipidus (Mortensen et al., 2020). However, there is no information on the mechanisms underlying the dynamics of intracellular Ca^{2+} mobilization in mpkCCD cells. It is also unclear whether mpkCCD cells retain the specific properties of Ca^{2+} mobilization observed in perfused IMCD. In the present study, we sought to verify mpkCCD cells as a reliable model representing collecting duct cells for the study of the intracellular Ca^{2+} stores, the mechanisms of Ca^{2+} release, and extracellular Ca^{2+} influx. Moreover, special emphasis has been placed on the Epac-induced temporal relationship of Ca^{2+} dynamics in the cytosol, endoplasmic reticulum (ER) and mitochondria. Our results demonstrate that mpkCCD cells display similar characteristics of intracellular Ca^{2+} mobilization observed in intact cells of collecting duct, and that the Epac agonist triggered intracellular Ca^{2+} mobilization and oscillation are mediated by RyR-gated Ca^{2+} release and SOCE associated with reciprocal decrease of Ca^{2+} content in the ER. Moreover, the Epac agonist can effectively shuttle ER luminal Ca^{2+} to both the cytosol and mitochondrial matrix.

Materials and methods

Cell culture

Experiments were performed on a male mouse CCD principal cell line ($mpkCCD_{C14}$, kindly provided by Dr. Douglas Eaton, Emory University) grown in AVP-free culture medium. Cells were maintained in a 1:1 mixture of DMEM/Ham's F12 medium with phenol red (Gibco), supplemented with dexamethasone (50 nM), triiodothyronine (1 nM), selenium (60 nM), insulin (5 μg/mL), mouse EGF (10 ng/mL), transferrin (5 μg/mL), and 2% fetal calf serum in a humidified atmosphere with 5% CO_2 at 37°C. mpkCCD cells between 20 and 30 passages were grown on collagen coated glass bottom dish prior to the experiments.

Monitoring of cytosolic Ca^{2+}

mpkCCD cells grown on collagen coated glass bottom dish (MatTek) were loaded with cell permeant Ca^{2+} sensitive

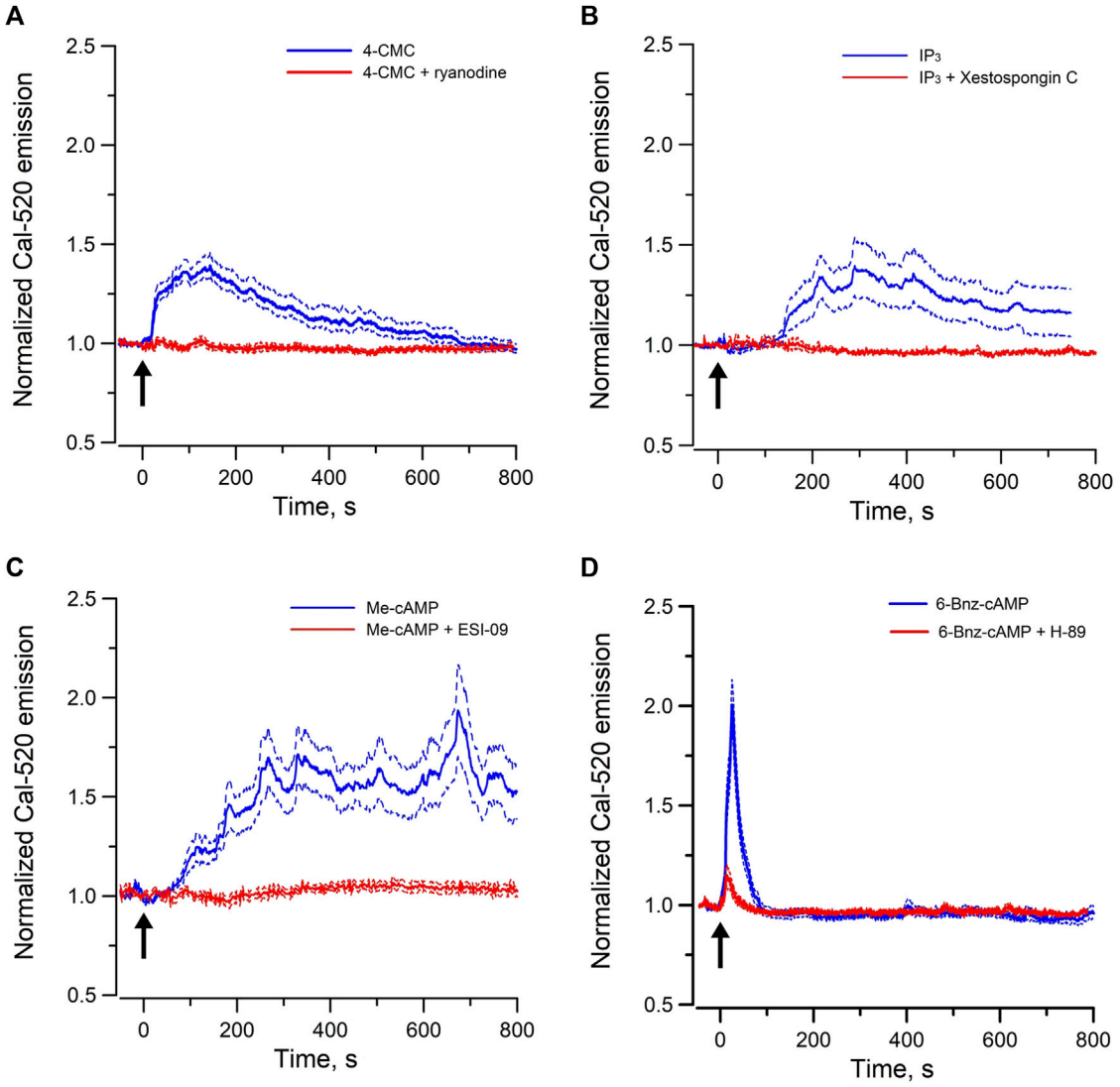

FIGURE 1
Mean normal time courses of Ca^{2+} mobilization in mpkCCD cells induced by **(A)** cell permeant ryanodine receptor agonist (50 μM 4-CMC, 54 cells/4 dishes), and **(B)** cell permeant IP_3 receptor agonist (200 μM Bt_3-Ins(1,3,5)P_3/AM, 49 cells/4 dishes), **(C)** cell permeant Epac-agonist (40 μM Me-cAMP/AM, 92 cells/6 dishes), and **(D)** cell permeant PKA-agonist (40 μM 6-Bnz-cAMP/AM, 95 cells/6 dishes). Ryanodine (50 μM, 26 cells/3 dishes), Xestospongin C (10 μM, 35 cells/3 dishes), ESI-09 (25 μM, 36 cells/3 dishes), and H-89 (10 μM, 31 cells/3 dishes) were used as the corresponding receptor blockers or antagonists. Arrow (↑) indicates application of agonist in each time course. Dash lines are standard error.

fluorescence probe (Cal-520/AM, 5 μM, AAT Bioquest) in phenol red free medium (1:1 mixture of DMEM/Ham's F12 medium, Gibco) for 30 min at 37°C, followed by 20 min for de-esterification. Fluorescent images were collected with a Leica TCS SP5 confocal imaging system using water immersion objective lens (×63, N.A. 1.2) equipped with environmental chamber. Cal-520 was excited at 488 nm, and the emission was collected with a spectral window of 495–530 nm at 1 Hz. The spatial and temporal variations of $[Ca^{2+}]_i$ in individual cells were measured from the stored images with Leica Application Suite Advanced Fluorescence software as reported previously (Yip and Sham, 2011). Store-operated calcium entry (SOCE) was induced by thapsigargin (10 μM) in calcium-free Hanks' Balanced Salt Solution (Gibco) following by re-addition of 2 mM Ca^{2+} in the extracellular buffering solution.

Monitoring of calcium in ER and mitochondria with biosensors

To monitor ER $[Ca^{2+}]$ ($[Ca^{2+}]_{ER}$) or mitochondrial $[Ca^{2+}]$ ($[Ca^{2+}]_{MITO}$) simultaneously with cytosolic $[Ca^{2+}]_i$, mpkCCD cells were transfected with either ER Ca^{2+} biosensor R-CEPIA1er (Addgene Plasmid #58216, λ_{ex}: 543 nm, λ_{em}: 560–600 nm) or mitochondrial Ca^{2+} biosensor mito-RCaMP1h (Addgene Plasmid #105013, λ_{ex}: 543 nm, λ_{em}: 560–600 nm) (Suzuki et al., 2014). Cells were seeded at 6×10^4 cells/cm^2 on collagen coated glass bottom dishes for 24 h before transfection. Cells were transfected with Lipofectamine (0.5 μg DNA/1 × 10^5 cells) for 24 h according to manufacturer's instruction. Studies were performed in transfected cells from 48 to 72 h after transfection. Cytosolic $[Ca^{2+}]_i$ was monitored simultaneously with cell permeant Ca^{2+} sensitive

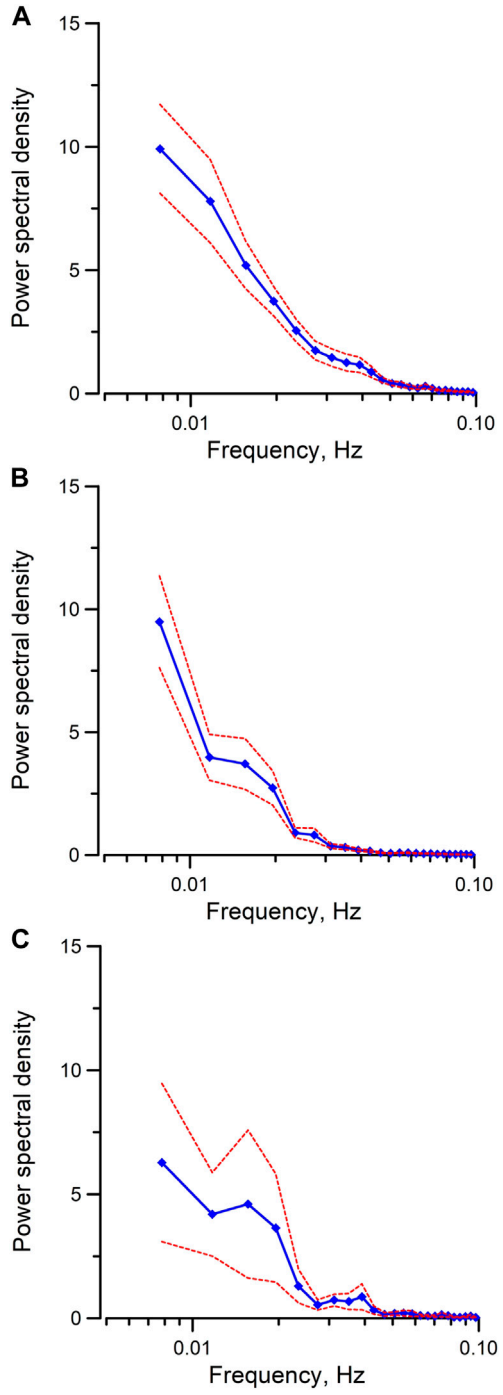

FIGURE 2
Mean power spectral spectra of cytosolic Ca^{2+} oscillations induced by **(A)** Me-cAMP/AM, **(B)** 4-CMC, **(C)** Bt_3-Ins(1,3,5)P_3/AM in mpkCCD cells. The same time series presented in Figure 1 were used for spectral analysis. By integrating the spectral power density from 0.03 Hz to 0.1 Hz in each individual power spectrum, the mean integrated spectral power density is significantly higher ($p < 0.05$) when cytosolic calcium oscillations were induced by Me-cAMP/AM than those induced by 4-CMC, or by Bt_3-Ins(1,3,5)P_3/AM. Dash lines are standard error.

fluorescence probe (Cal-520/AM) in the transfected cells incubating with phenol red free medium (1:1 mixture of DMEM/Ham's F12 medium, Gibco). To monitor ER-mitochondrial Ca^{2+} transfer in mpkCCD cells, cells were co-transfected with the ER Ca^{2+} biosensor (G-CEPIA1er, Addgene Plasmid #58215, λ_{ex}: 488 nm, λ_{em}: 510–540 nm) and mitochondrial biosensor mito-RCaMP1h. Fluorescent images were collected with the respective laser lines for excitation and spectral windows for emission using the Lecia TCS SP5 imaging system.

Perfusion of rat inner medullary collection duct (IMCD)

All animal experimentation was conducted in accordance with the National Institutes of Health Guide for Care and Use of Laboratory Animals (National Institute of Health, Bethesda, MD) and was approved by the University of South Florida Institutional Animal Care and Use Committee (PROTOCOL #R3982). IMCDs were isolated from male Sprague-Dawley rats and perfused as described previously (Yip, 2002). Cytosolic $[Ca^{2+}]i$ in perfused IMCD was monitored with fluo-4/AM (5 μM, Invitrogen) in individual IMCD cells. Confocal fluorescent images of IMCD were collected and analyzed as reported previously (Yip, 2002).

Chemicals

6-Bnz-cAMP-AM, Me-cAMP-AM (8-pCPT-2′-O-Me-cAMP-AM), and ESI-09 were purchased from Biolog (Germany). Ryanodine, SKF-96365, and Xestospongin C were purchased from MilliporeSigma (Burlington, MA). Bt_3-Ins(1,3,5)P_3/AM was purchased from SiChem. ATP, 4-CMC (4-Chloro-m-cresol), H-89, and thapsigargin were from Sigma-Aldrich (St. Louis, MO).

Data analysis

Time series of fluorescence emission variations in individual mpkCCD cells were extracted and normalized with respective to the base line from stored XYT images. Time series of Cal-520 emission from individual cells were sampled at 1 Hz for spectral analysis. Each time series was subjected to linear trend removal. 512 or 1,024 data points were used to calculate the power spectrum with an algorithm based on Fast Fourier Transform (Yip et al., 1991). Results were reported as mean ± standard error. Statistical significance was calculated by using student's t tests for paired or unpaired data and considered significant when $p < 0.05$.

Results

Intracellular Ca^{2+} mobilization in mpkCCD cells

RyRs are mainly expressed in the sarcoplasmic reticulum of skeletal, cardiac and smooth muscle cells, whereas inositol 1,4,5 trisphosphate receptors (IP_3Rs) are the predominant Ca^{2+} release channels of the ER in non-excitable cells. We have previously shown that endogenous

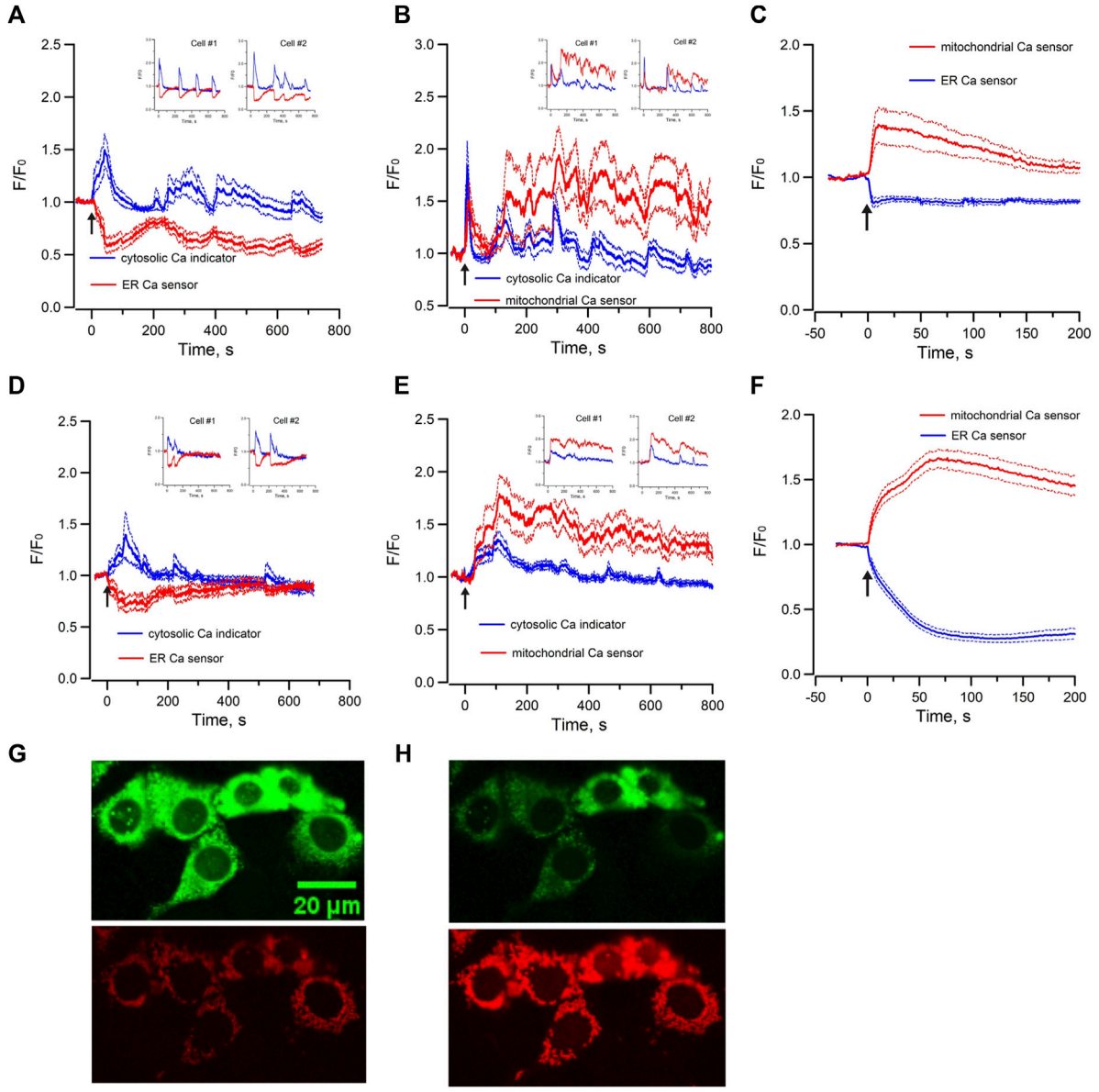

FIGURE 3
Mean normalized time courses of simultaneous changes in **(A)** cytosolic Ca^{2+} and ER luminal Ca^{2+} (15 cells/3 dishes), **(B)** cytosolic Ca^{2+} and mitochondrial matrix Ca^{2+} (20 cells/3 dishes) and **(C)** ER luminal Ca^{2+} and mitochondrial matrix Ca^{2+} (36 cells/7 dishes) induced by 40 μM Me-cAMP/AM in mpkCCD cells. Corresponding changes induced by 50 μM 4-CMC are shown in **(D)** cytosolic Ca^{2+} and ER luminal Ca^{2+} (13 cells/3 dishes), **(E)** cytosolic Ca^{2+} and mitochondrial matrix Ca^{2+} (21 cells/3 dishes), and **(F)** ER luminal Ca^{2+} and mitochondrial matrix Ca^{2+} 55 cells/9 dishes). mpkCCD cells expressing both ER biosensor (green) and mitochondrial biosensor (red) before **(G)** and after **(H)** exposure to RyR agonist 4-CMC. The Arrow (↑) indicates application of agonist in each time course. Inserts are tracings from individual cells with multiple Ca^{2+} spikes. F/F_0 is the fractional change in fluorescence emission of the fluorescent probe or biosensor. Dash lines are standard error.

agonist of RyRs and IP_3Rs triggered Ca^{2+} oscillations in individual cells of perfused IMCD, indicating both functional RyR-gated and IP_3R-gated intracellular Ca^{2+} stores are present in IMCD cells (Yip and Sham, 2011). To test whether these Ca^{2+} stores are intact in mpkCCD cells, changes in $[Ca^{2+}]_i$ were monitored with Ca^{2+} sensitive fluorescence probe when cells were stimulated with 4-CMC (a cell permeant RyR agonist) or Bt_3-Ins(1,3,5)P_3/AM (a cell permeant agonist of IP_3R). Ryanodine was used as blocker of RyRs, and Xestospongin C was used for IP_3Rs. Both agonists triggered robust intracellular Ca^{2+} mobilization and oscillations in mpkCCD cells (Figures 1A, B). The 4-CMC-induced Ca^{2+} response was almost instantaneous, compared to the delayed Bt_3-Ins(1,3,5)P_3/AM triggered Ca^{2+} response (~100–150 s). The 4-CMC-induced Ca^{2+} transient was completed at 800 s, whereas the IP_3-triggered response was more sustained. The delayed IP_3–induced Ca^{2+} response in the Ca^{2+} responses were possibly related to the rate of membrane permeation and de-esterification of Bt_3-Ins(1,3,5)P_3/AM.

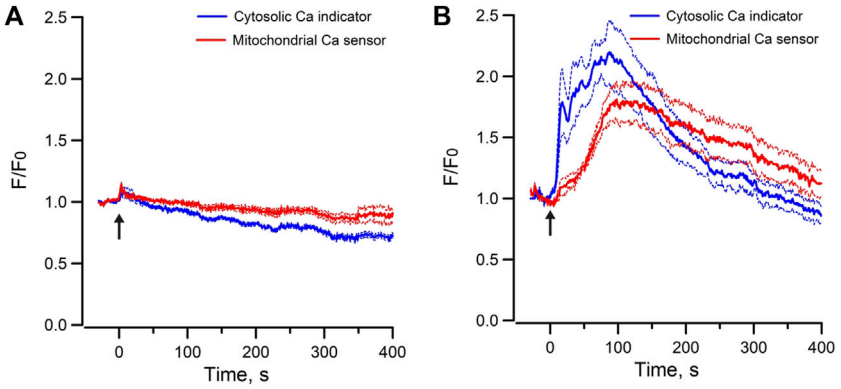

FIGURE 4
Mean normalized time courses of simultaneous changes in cytosolic Ca^{2+} and mitochondrial matrix Ca^{2+} induced by 40 μM Me-cAMP/AM in mpkCCD cells preincubated with **(A)** Ryanodine (50 μM, 19 cells/3 dishes), and **(B)** Xestospongin C (10 μM, 14 cells/3 dishes). Ryanodine but not Xestospongin C inhibits Epac-agonist induced cytosolic calcium mobilization and calcium uptake in mitochondria. Arrow (↑) indicates application of agonist in each time course. F/F_0 is the fractional change in fluorescence emission of the fluorescent probe or biosensor. Dash lines are standard error.

The differences in the kinetic profiles triggered by the two stores could be due to differences in the potency of the agonists, inactivation kinetics of the receptors, and the depletion or replenishment of the SR Ca^{2+} stores. Both 4-CMC and Bt_3-Ins(1,3,5)P_3/AM-induced Ca^{2+} responses were completely abolished in the presence of their respective receptor blockers. These observations confirmed that mpkCCD cells possess both functional RyR- and IP_3R-gated Ca^{2+} stores as in IMCD.

To examine the Epac-dependent Ca^{2+} mobilization and oscillation (Yip, 2006), mpkCCD cells were stimulated with Me-cAMP/AM. Me-cAMP/AM is a cell permeant cAMP analog which activates specifically Epac but not PKA. Me-cAMP/AM triggered larger and sustained intracellular Ca^{2+} mobilization and oscillations in mpkCCD cells compared to those induced by 4-CMC and IP_3 (Figure 1C). The Ca^{2+} response was blocked by ESI-09, an inhibitor of Epac1 and Epac2. These two Epac isoforms are expressed in IMCD and mpkCCD cells (Li et al., 2008; Kortenoeven et al., 2012). In contrast, 6-Bnz-cAMP/AM, a cell permeant cAMP analog which activates PKA but not Epac, triggered only a brief transient Ca^{2+} mobilization without Ca^{2+} oscillation (Figure 1D). The brief Ca^{2+} transient was effectively attenuated by the PKA inhibitor H-89. These observations suggested that activation of the Epac-dependent signal pathway elicits sustained Ca^{2+} mobilization and oscillation in mpkCCD cells. Spectral analysis was further applied to individual time series of Ca^{2+} signals of individual mpkCCD cells to characterize the oscillatory frequencies and the power of the Ca^{2+} oscillations. The mean power spectral density induced by Me-cAMP/AM, 4-CMC, and Bt_3-Ins(1,3,5)P_3/AM, were shown in Figure 2. All three mean power spectra had broad distribution over a range of frequencies. Most of the oscillations were confined in frequency range of 0.007–0.1 Hz, which are consistent with observations from intact IMCD cells of perfused IMCD (Yip, 2002; Yip and Sham, 2011). The power of Me-cAMP/AM, 4-CMC, and Ins(1,3,5)P_3/AM-induced Ca^{2+} oscillations were similar, except Me-cAMP/AM induced Ca^{2+} oscillation had more power at the higher frequencies (0.03–0.1 Hz frequency range).

Epac and RyR-agonist mobilize ER Ca^{2+} for cytosolic Ca^{2+} oscillation and ER-mitochondrial Ca^{2+} transfer in mpkCCD cells

To further characterize Epac-dependent activation of ER Ca^{2+} stores in mpkCCD cells, the temporal variations of cytosolic Ca^{2+} and ER luminal Ca^{2+} were monitored simultaneously with the Ca^{2+} sensitive-fluorescence probe Cal-520/AM and the ER luminal Ca^{2+} biosensor R-CEPIA1er, respectively. Me-cAMP/AM triggered an increase of cytosolic Ca^{2+} which was associated with a synchronized decrease in ER luminal Ca^{2+} content (Figure 3A). The oscillations in cytosolic Ca^{2+} were mirror images of those in ER luminal Ca^{2+}. These observations suggested that the Epac-induced increase of cytosolic Ca^{2+} was due to release of Ca^{2+} from ER intracellular Ca^{2+} stores, and the cyclic variations in luminal ER Ca^{2+} content were likely due to ER Ca^{2+} depletion and refilling by Ca^{2+} uptake via the sacroplasmic/endoplasmic reticular Ca^{2+}-ATPase (SERCA). RyR-agonist 4-CMC triggered similar response in mpkCCD cells (Figure 3D), indicating that Ca^{2+} release from RyR-gated stores generates cytosolic and ER Ca^{2+} signals comparable to those of Epac activation, congruent with reports that Epac triggered Ca^{2+} release via RyRs in IMCD and cardiomyocytes (Yip, 2006; Valli et al., 2018).

Mitochondrial Ca^{2+} concentration is important for the regulation of mitochondrial functions, and it is regulated by local Ca^{2+} concentration in the proximity of Ca^{2+} release channels of ER (Rizzuto et al., 2012; Csordas et al., 2018). To test whether there is mitochondrial matrix Ca^{2+} uptake during Epac-mediated Ca^{2+} mobilization in mpkCCD cells, the variations of cytosolic Ca^{2+} and mitochondrial matrix Ca^{2+} were monitored simultaneously with Ca^{2+} sensitive fluorescence probe and the mitochondrial matrix Ca^{2+} biosensor mito-RCaMP1h. Application of Me-cAMP/AM to mpkCCD cells activated multiple synchronized Ca^{2+} spikes in the cytosol and mitochondrial matrix (Figure 3B). These observations suggested that the Epac-agonist not only triggers

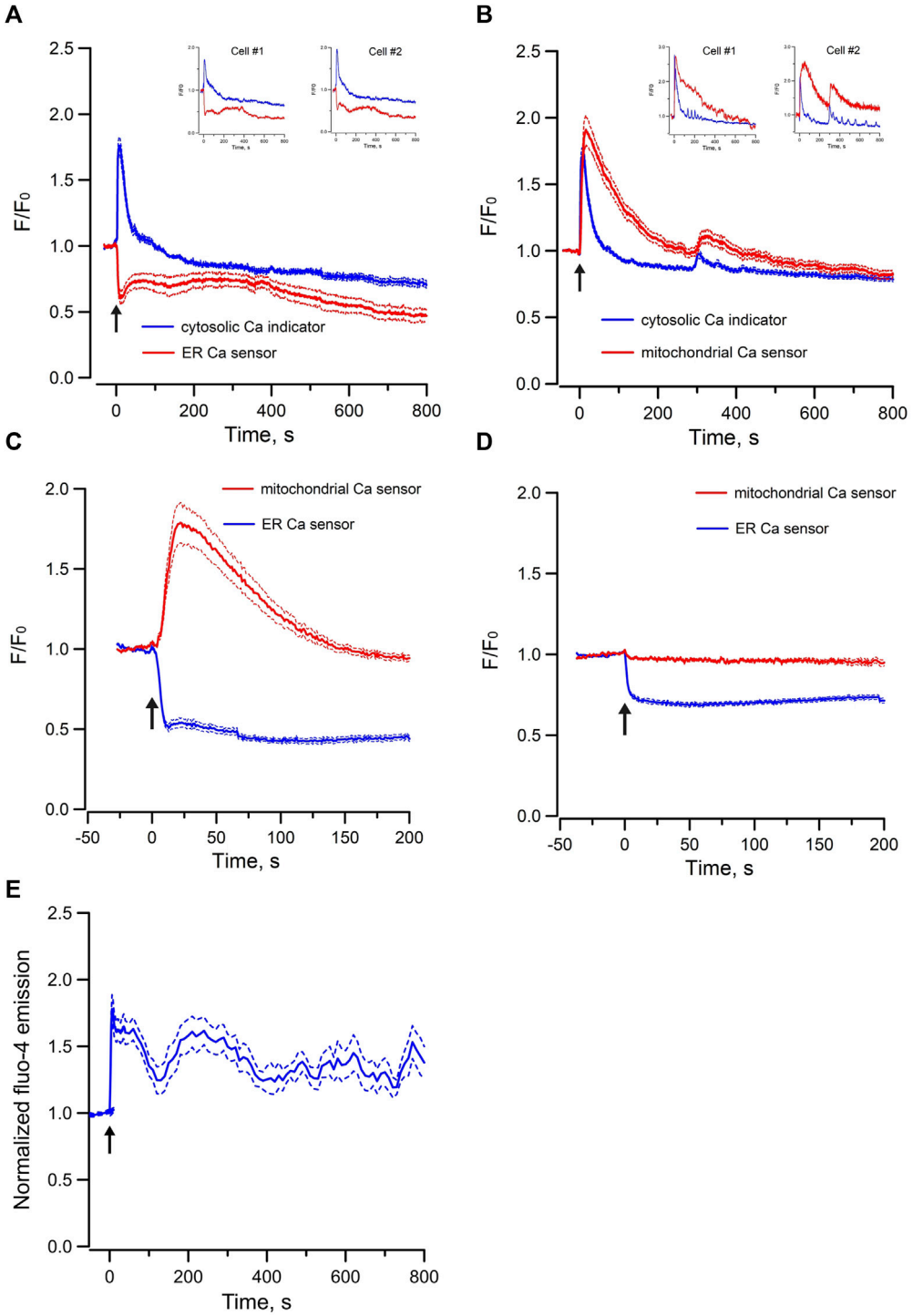

FIGURE 5
Mean normalized time courses of simultaneous changes in **(A)** cytosolic Ca^{2+} and ER luminal Ca^{2+} (15 cells/3 dishes), **(B)** cytosolic Ca^{2+} and mitochondrial matrix Ca^{2+} (9 cells/2 dishes), **(C)** ER luminal Ca^{2+} and mitochondrial matrix Ca^{2+} (32 cells/4 dishes) induced by 5 μM ATP, and **(D)** ER luminal Ca^{2+} and mitochondrial matrix Ca^{2+} induced by 200 μM Bt_3-Ins(1,3,5)P_3/AM in mpkCCD cells (45 cells/7 dishes). **(E)** mean normalized time course of cytosolic Ca^{2+} induced by 5 μM ATP in freshly isolated perfused rat IMCD (23 cells/3 tubules). The Arrow (↑) indicates application of agonist in each time course. Inserts are tracings from individual cells with multiple Ca^{2+} spikes. F/F_0 is the fractional change in fluorescence emission of the fluorescent probe or biosensor. Dash lines are standard error.

release of ER Ca^{2+} to the cytosol, but also shuttles ER Ca^{2+} into the mitochondria. RyR-agonist 4-CMC triggered a similar response with synchronized Ca^{2+} spikes in the cytosol and mitochondrial matrix (Figure 3E). To determine the temporal relationship between ER luminal Ca^{2+} and mitochondrial matrix Ca^{2+}, the ER luminal Ca^{2+} biosensor G-CEPIA1er and the mitochondrial matrix Ca^{2+}

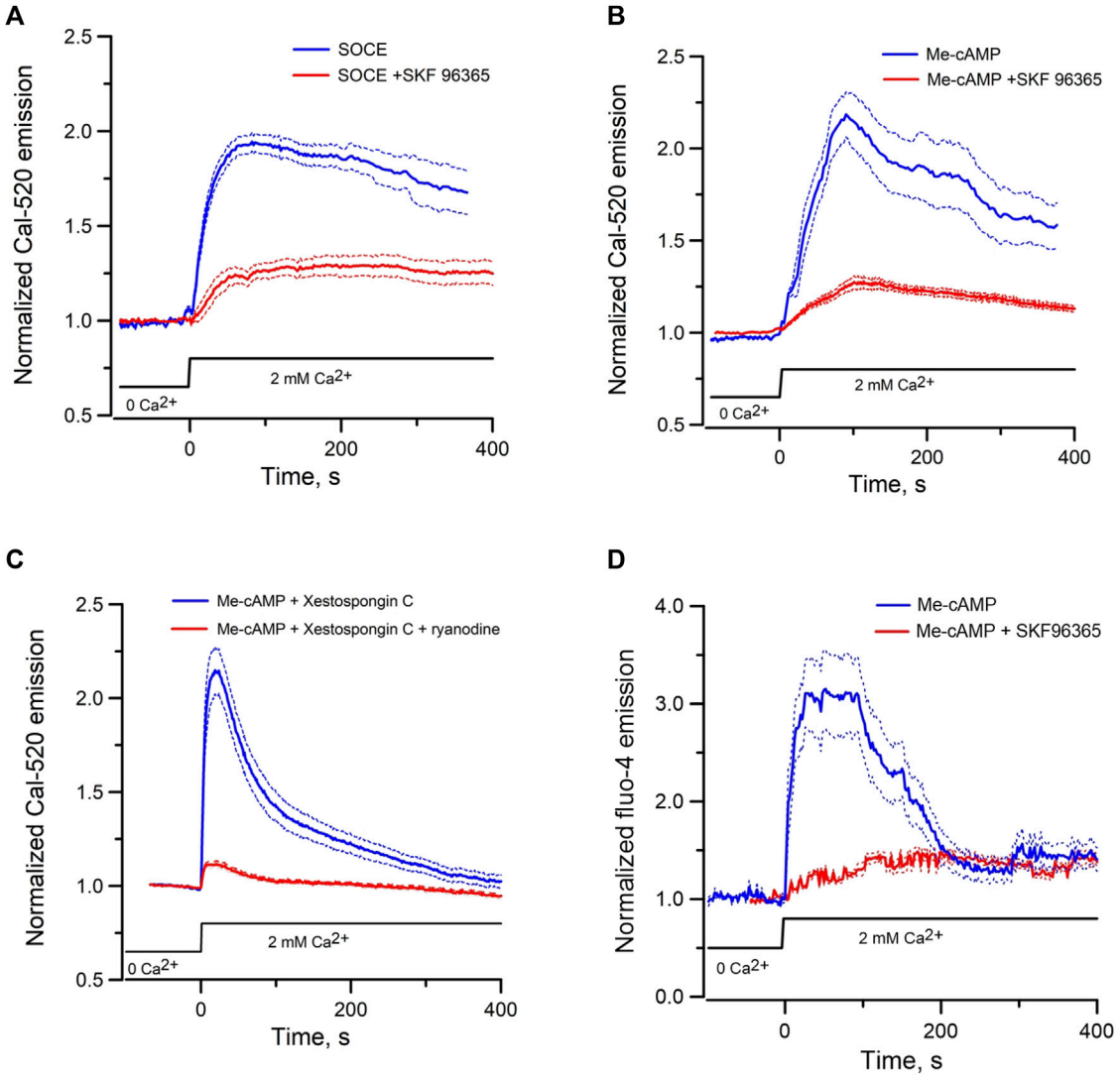

FIGURE 6
Mean normalized time courses of Ca^{2+} entry in mpkCCD cells and perfused IMCD triggered by re-addition of 2 mM of Ca^{2+}. **(A)** Store-operated Ca^{2+} entry in the absence (69 cells/4 dishes) or presence (72 cells/3 dishes) of 50 μM SKF 96365 in mpkCCD cells, **(B)** Ca^{2+} entry induced by pre-incubation of mpkCCD cells with Epac-agonist (40 μM Me-cAMP/AM) in the absence (52 cells/3 dishes) or presence (59 cells/3 dishes) of SKF 96365, **(C)** Ca^{2+} entry induced by pre-incubation of mpkCCD cells with 40 μM Me-cAMP/AM in presence of 10 μM Xestospongin C (63 cells/3 dishes), or 10 μM Xestospongin +50 μM ryanodine (79 cell/3 dishes). **(D)** Ca^{2+} entry induced by pre-incubation of perfused IMCD with 40 μM Me-cAMP/AM in the absence (39 cells/4 tubules) or presence (27 cells/3 tubules) of SKF96369. Dash lines are standard error.

biosensor mito-RCaMP1h were co-expressed in mpkCCD cells. Me-cAMP/AM triggered a decrease in ER luminal Ca^{2+}, which was associated with a concomitant increase in mitochondrial matrix Ca^{2+} (Figure 3C). RyR-agonist 4-CMC triggered a similar response (Figure 3F), indicative of effective RyR-coupled ER-mitochondrial Ca^{2+} transfer in mpkCCD cells. Figures 3G, H are fluorescence images of ER (green) and mitochondria (red) demonstrating Ca^{2+} transfer from ER to mitochondria induced by RyR agonist 4-CMC.

Moreover, the Me-cAMP/AM induced cytosolic and mitochondrial Ca^{2+} responses were completely blocked by ryanodine but were unaffected by xestospongin C (Figures 4A, B), indicating that the Epac-agonist mediated Ca^{2+} release was mainly derived from RyR-gated Ca^{2+} store to trigger mitochondrial Ca^{2+} transfer.

ATP-mediated Ca^{2+} mobilization and Ca^{2+} transfer between ER and mitochondria

In contrast, exogenous application of Bt_3-Ins(1,3,5)P_3/AM only triggered decrease in ER luminal Ca^{2+} without concomitant increase of mitochondria Ca^{2+} in mpkCCD cells (Figure 5D). To test whether increasing the abundance of endogenous IP_3 can induce Ca^{2+} transfer between ER and mitochondria, ATP was used to stimulate endogenous IP_3 production via purinergic receptors expressed in mpkCCD cells (Wildman et al., 2009). Application of ATP elicited a transient increase in cytosolic [Ca^{2+}] of less than 50 s in mpkCCD cells (Figure 5A). Of note, this was associated with a sustained decrease ER luminal Ca^{2+} (Figure 5A), and a more prolonged increase in mitochondrial

[Ca^{2+}] (Figure 5B). When ER luminal Ca^{2+} and mitochondrial matrix Ca^{2+} were monitored simultaneously, ATP triggered decrease in ER luminal Ca^{2+} and concomitant increase in mitochondrial matrix Ca^{2+} (Figure 5C). These observations suggest that endogenous activation of IP_3Rs is capable of triggering ER-mitochondrial Ca^{2+} transfer in mpkCCD cells, even though Epac-induced Ca^{2+} response is independent of the IP_3R-dependent mechanism. ATP-induced intracellular Ca^{2+} mobilization was also detected in perfused IMCD (Figure 5E), which is consistent with the observations on ATP mobilized intracellular Ca^{2+} in mpkCCD cells.

Epac-mediated store-operated Ca^{2+} entry in mpkCCD cells

Since Epac-activation mobilizes ER Ca^{2+} to elicit cytosolic Ca^{2+} signals and ER-mitochondrial Ca^{2+} transfer, the reduction in ER luminal Ca^{2+} may activate SOCE to replenish ER Ca^{2+} stores. SOCE was first examined in mpkCCD by depleting ER Ca^{2+} stores using the SERCA inhibitor thapsigargin (10 μM) in the absence of extracellular Ca^{2+}. Reintroduction of 2 mM Ca^{2+} in the external solution elicited robust Ca^{2+} entry, which was inhibited by the SOCE inhibitor SKF96365 (50 μM) (Figure 6A). Incubation of mpkCCD cells with the Epac-agonist Me-cAMP/AM in the absence of extracellular Ca^{2+} also activated SOCE similar to that induced by thapsigargin (Figure 6B). Robust Me-cAMP/AM induced Ca^{2+} entry was also observed in mpkCCD cells pretreated with xestospongin C; but the response was abolished in cells treated with both ryanodine and xestospongin C (Figure 6C). Moreover, Me-cAMP/AM-induced Ca^{2+} entry was observed in isolated perfused IMCD, and the effect was abolished by inhibition of SOCE using SKF96365 (Figure 6D). These results suggest that Epac activation is capable of inducing ER luminal Ca^{2+} depletion and SOCE in both mpkCCD and perfused IMCD.

Discussion

Epac-dependent Ca^{2+} mobilization was associated with AVP-induced apical exocytosis in perfused IMCD. mpkCCD cells have been used as the cell model for transcriptomic and phosphoproteomic studies of AVP-signaling in the collecting duct (Rinschen et al., 2010; Huling et al., 2012; Sandoval et al., 2013; Yang et al., 2022; Park et al., 2023). We have demonstrated that mpkCCD cells retain the characteristics of Epac-dependent Ca^{2+} mobilization as in intact IMCD cells. Taking advantage of expressing ER and mitochondrial specific biosensor proteins in mpkCCD cells, the dynamic properties and relationship between cytosolic Ca^{2+}, ER luminal Ca^{2+}, and mitochondrial matrix Ca^{2+} were characterized. Epac-agonist mobilized Ca^{2+} from ER Ca^{2+} stores, depleted ER luminal Ca^{2+}, and activated SOCE in mpkCCD cells. The oscillation of cytosolic Ca^{2+} triggered by Epac-agonist was entrained to Ca^{2+} oscillation in mitochondrial matrix, while 180° out-of-phase to the oscillation in ER luminal Ca^{2+}. These observations indicated that Epac-mediated oscillatory Ca^{2+} signaling event is an integrated process which involves interplay of luminal ER Ca^{2+} release and refill, Ca^{2+} entry and efflux in mitochondrial matrix, and extracellular Ca^{2+} entry secondary to ER Ca^{2+} depletion in mpkCCD cells.

Time series of Ca^{2+} oscillation extracted from mpkCCD cells were analyzed in frequency domain using algorithm based on Fast Fourier Transform. Frequencies of Epac-dependent oscillations were detected in the range between 0.007 and 0.1 Hz, which is similar to the frequency ranges induced by cADP-ribose, an endogenous agonist of RyRs, observed in intact IMCD cells (Yip, 2002; Yip and Sham, 2011). Moreover, the sustained Me-cAMP-mediated Ca^{2+} oscillation in mpkCCD cells is similar to those observed in perfused IMCD triggered by caged cyclic-ADP-ribose (Yip and Sham, 2011). However, the 4-CMC-induced Ca^{2+} transient is more transient in the IMCD cells. The disparity in the kinetic profile of 4-CMC-triggered Ca^{2+} oscillations could be related to the differences in the agonist sensitivity, the activation/inactivation kinetics, sensitization of Ca^{2+}-induced-Ca^{2+} release of the RyRs. Nevertheless, the complete inhibition of Epac-agonist-induced Ca^{2+} oscillation with ryanodine, but not by the IP_3R-antagonist xestrospongin C, suggests that RyR is the primary Ca^{2+} source contributing to the Epac-induced Ca^{2+} oscillation in the mpkCCD cells.

It has been established that AVP regulates AQP2 shuttling through a cAMP-dependent pathway, and PKA has been considered as the only effector protein of cAMP for mediating AVP-regulated water permeability in kidney collecting ducts (Knepper and Inoue, 1997). It is now known that Epac is an important effector protein of cAMP. Epac1 and Epac2 isoforms are expressed in collecting duct and mpkCCD cells (Li et al., 2008; Kortenoeven et al., 2012). Our previous study found that Epac activation, but not PKA activation, mimics AVP in triggering Ca^{2+} mobilization and oscillations and induces apical shuttling of AQP2 in perfused IMCD (Yip, 2006). In the present study, PKA specific cAMP analog (6-Bnz-cAMP/AM) did not trigger Ca^{2+} oscillations in mpkCCD cells, while Epac-specific cAMP (Me-cAMP/AM) triggered long lasting Ca^{2+} oscillations. Moreover, long-term regulation of AQP2 by AVP in mpkCCD cells is mediated by Epac but not by PKA (Kortenoeven et al., 2012). Such evidence is consistent with an Epac-dependent signal pathway for regulation of collecting duct water permeability. It is also consistent that mice lacking Epac1 or Epac2 showed impaired urinary concentration ability and augmented urinary excretion of Na^+ and urea (Cherezova et al., 2019). However, no defects in AVP-induced Ca^{2+} signaling in split-opened collecting ducts or changes in AQP2 protein abundance were observed. The urinary concentrating defect might be caused by reduced expression of the Na^+/H^+ exchanger isoform 3 (NHE3) (Cherezova et al., 2019). An inhibitory effect of Epac1 on NHE3 activity was previously shown in opossum kidney cells and mouse kidney slices (Honegger et al., 2006). A recent study reported compromised tight junctions in the collecting duct of Epac1 knockout mice in conjunction with a reduced papillary osmolarity (Sivertsen Asrud et al., 2020), suggesting Epac1 is involved in regulating paracellular permeability in the collecting duct. The reason for the discrepancies in the two knock-out mice studies is unclear but could be related to mouse dietary conditions or the existence of a different microbiome between different institutions.

Our data also show that Epac-agonist triggered Ca^{2+} oscillations resemble those activated by a RyR agonist in mpkCCD cells, suggesting that Epac-agonist mobilizes ER Ca^{2+} in mpkCCD cells via RyRs. Organelle-specific Ca^{2+}-sensitive biosensors expressed in mpkCCD

cells showed that the Epac agonist triggered synchronized Ca^{2+} spikes in cytosol and mitochondrial matrix, which are temporally correlated with reciprocal changes in ER luminal Ca^{2+}. These observations indicated that agonist-induced Epac activation not only triggered release of Ca^{2+} into cytosol, but also transferred Ca^{2+} from ER to mitochondria.

The resting $[Ca^{2+}]$ of mitochondrial matrix is comparable to the resting cytosolic $[Ca^{2+}]$. Mitochondrial Ca^{2+} uptake takes place at specialized microdomains where cytosolic $[Ca^{2+}]$ are high. Such microdomains are localized in the mitochondria-associated membranes (MAMs), where the endoplasmic reticulum membrane is within 10–30 nm from the outer mitochondrial membrane (Hajnoczky et al., 2002). Ca^{2+} released from ER enters the intermembrane space through voltage-dependent anion channels (VDACs) localized in the outer membrane, and then enters mitochondrial matrix through the mitochondrial Ca^{2+} uniporter (MCU) of the inner membrane (Patergnani et al., 2011; Giorgi et al., 2015). RyR agonist (4-CMC) triggered similar Ca^{2+} transfer from ER to mitochondria as Epac-agonist suggested that the Epac-induced ER-mitochondrial Ca^{2+} transfer is mediated by RyRs in MAMs of mpkCCD cells. IP_3Rs and RyRs have been localized in MAMs (Hajnoczky et al., 2002; Chen et al., 2012; Bartok et al., 2019), but their distribution in mpkCCD cells or native renal collecting duct cells is unclear. The current study explored on this knowledge gap. Exogenous Bt_3-Ins(1,3,5)P_3/AM, which effectively activated cytosolic Ca^{2+} oscillation, only triggered a decrease in ER luminal Ca^{2+} but not concomitantly increased mitochondria Ca^{2+} in mpkCCD cells. It is possible that IP_3Rs are less efficacious in facilitating ER-mitochondrial Ca^{2+} transfer in mpkCCD cells; or the cell permeant Bt_3-Ins(1,3,5)P_3/AM, had a poor access to the IP_3Rs in MAMs. To test the latter hypothesis, the native agonist ATP was applied to increase endogenous IP_3 abundance in mpkCCD cells. ATP triggered synchronized increase in cytosolic $[Ca^{2+}]$ with concomitant elevation in mitochondrial matrix $[Ca^{2+}]$ and depletion ER luminal Ca^{2+}. ATP-induced Ca^{2+} transfer between ER and mitochondria was also visualized in cells co-expressed with ER and mitochondrial Ca^{2+} biosensors. These observations indicated that IP_3Rs is capable of mediating Ca^{2+} transfer between ER and mitochondria in mpkCCD cells. However, the kinetics of ATP-induced cytosolic, endoplasmic, and mitochondrial Ca^{2+} responses are distinctly different from those induced by Epac or RyR agonists, distinguishing the Ca^{2+} signals activated by the two different agonists induced signaling pathways. Our studies also support that this mechanism is at play *in vivo* and it is noteworthy that 5 μM ATP also triggered Ca^{2+} mobilization and oscillations in isolated perfused IMCD (Figure 5E), confirming that purinergic receptor mediated Ca^{2+} mobilization is present in both intact IMCD cells and mpkCCD cells. Consistent with this, studies in acutely isolated connecting tubule/collecting duct of mice support that an acute increase in cytosolic $[Ca^{2+}]$ inhibits ENaC activity (Mamenko et al., 2011) mediated by $P2Y_2$ receptor activation (Pochynyuk et al., 2008).

Mitochondrial Ca^{2+}dynamics plays important roles in intracellular Ca^{2+}signaling, cell metabolism, cell survival, and other cell-type specific functions (Rizzuto et al., 2012). As described above MCU supports cytoplasmic Ca^{2+} oscillations, SOCE and Ca^{2+}-dependent gene expression in response to receptor-mediated stimulation (Samanta et al., 2014). It has been proposed that mitochondrial Ca^{2+} shuttling via MCU sustains the cytosolic Ca^{2+} signal by preventing Ca^{2+}-dependent inactivation of IP_3Rs and store-operated CRAC channels (Yoast et al., 2021). ER-mitochondrial Ca^{2+} transfer also stimulates Ca^{2+}-sensitive dehydrogenases and respiratory chain components to promote oxidative phosphorylation, ATP, and ROS production (Territo et al., 2000; Territo et al., 2001; Hou et al., 2013). The physiological implications for the ER-mitochondrial Ca^{2+} transfer in the regulation of cellular functions in renal tubular cells remain to be determined.

In conclusion, mpkCCD cells retained all reported features of Epac-induced Ca^{2+} mobilization observed in isolated perfused IMCD. The temporal relationship between cytosolic Ca^{2+}, ER luminal Ca^{2+}, and mitochondrial matrix Ca^{2+} activated by Epac and RyR-agonists are highly compatible, but is distinctly different from those induced by IP_3R stimulation. Furthermore, we have provided the first characterization of ER-mitochondrial Ca^{2+} transfer in mpkCCD cell, which can be used as a renal cell model to address novel questions of how mitochondrial Ca^{2+} regulates cytosolic Ca^{2+} signals, inter-organellar Ca^{2+} signaling, and other renal tubular functions.

Data availability statement

The raw data supporting the conclusions of this article will be made available by the authors, without undue reservation.

Ethics statement

The animal study was approved by IACUC University of South Florida. The study was conducted in accordance with the local legislation and institutional requirements.

Author contributions

K-PY, TR, and JS contributed to design and conception of the study. K-PY, LR-S, BC performed experiments. K-PY and JS interpreted results of experiments. K-PY wrote the first draft of the manuscript. K-PY, TR, BC, and JS wrote sections of the manuscript. All authors contributed to the article and approved the submitted version.

Funding

This work was supported by an American Heart Association Grant-In-Aid (K-PY). TR was supported the National Institute of Diabetes and Digestive and Kidney Diseases (NIDDK) Grant 1R01DK110621, Veterans Affairs Merit Review Award IBX004968A, and American Heart Association Transformational Research Award, 19TPA34850116. Financial support for this work was also provided by NIDDK Diabetic Complications Consortium

(RRID SCR_001415, www.diacomp.org) Grants DK076169 and DK115255.

Conflict of interest

The authors declare that the research was conducted in the absence of any commercial or financial relationships that could be construed as a potential conflict of interest.

Publisher's note

References

Ando, F., Sohara, E., Morimoto, T., Yui, N., Nomura, N., Kikuchi, E., et al. (2016). Wnt5a induces renal AQP2 expression by activating calcineurin signalling pathway. *Nat. Commun.* 7, 13636. doi:10.1038/ncomms13636

Bartok, A., Weaver, D., Golenar, T., Nichtova, Z., Katona, M., Bansaghi, S., et al. (2019). IP3 receptor isoforms differently regulate ER-mitochondrial contacts and local calcium transfer. *Nat. Commun.* 10, 3726. doi:10.1038/s41467-019-11646-3

Chen, Y., Csordas, G., Jowdy, C., Schneider, T. G., Csordas, N., Wang, W., et al. (2012). Mitofusin 2-containing mitochondrial-reticular microdomains direct rapid cardiomyocyte bioenergetic responses via interorganelle Ca(2+) crosstalk. *Circ. Res.* 111, 863–875. doi:10.1161/CIRCRESAHA.112.266585

Cherezova, A., Tomilin, V., Buncha, V., Zaika, O., Ortiz, P. A., Mei, F., et al. (2019). Urinary concentrating defect in mice lacking Epac1 or Epac2. *FASEB J.* 33, 2156–2170. doi:10.1096/fj.201800435R

Chou, C. L., Rapko, S. I., and Knepper, M. A. (1998). Phosphoinositide signaling in rat inner medullary collecting duct. *Am. J. Physiol.* 274, F564–F572. doi:10.1152/ajprenal.1998.274.3.F564

Chou, C. L., Yip, K. P., Michea, L., Kador, K., Ferraris, J. D., Wade, J. B., et al. (2000). Regulation of aquaporin-2 trafficking by vasopressin in the renal collecting duct. Roles of ryanodine-sensitive Ca2+ stores and calmodulin. *J. Biol. Chem.* 275, 36839–36846. doi:10.1074/jbc.M005552200

Csordas, G., Weaver, D., and Hajnoczky, G. (2018). Endoplasmic reticulum-mitochondrial contactology: structure and signaling functions. *Trends Cell Biol.* 28, 523–540. doi:10.1016/j.tcb.2018.02.009

Giorgi, C., Missiroli, S., Patergnani, S., Duszynski, J., Wieckowski, M. R., and Pinton, P. (2015). Mitochondria-associated membranes: composition, molecular mechanisms, and physiopathological implications. *Antioxid. Redox Signal* 22, 995–1019. doi:10.1089/ars.2014.6223

Hajnoczky, G., Csordas, G., and Yi, M. (2002). Old players in a new role: mitochondria-associated membranes, VDAC, and ryanodine receptors as contributors to calcium signal propagation from endoplasmic reticulum to the mitochondria. *Cell Calcium* 32, 363–377. doi:10.1016/s0143416002001872

Honegger, K. J., Capuano, P., Winter, C., Bacic, D., Stange, G., Wagner, C. A., et al. (2006). Regulation of sodium-proton exchanger isoform 3 (NHE3) by PKA and exchange protein directly activated by cAMP (EPAC). *Proc. Natl. Acad. Sci. U. S. A.* 103, 803–808. doi:10.1073/pnas.0503562103

Hou, T., Zhang, X., Xu, J., Jian, C., Huang, Z., Ye, T., et al. (2013). Synergistic triggering of superoxide flashes by mitochondrial Ca2+ uniport and basal reactive oxygen species elevation. *J. Biol. Chem.* 288, 4602–4612. doi:10.1074/jbc.M112.398297

Huling, J. C., Pisitkun, T., Song, J. H., Yu, M. J., Hoffert, J. D., and Knepper, M. A. (2012). Gene expression databases for kidney epithelial cells. *Am. J. Physiol. Ren. Physiol.* 302, F401–F407. doi:10.1152/ajprenal.00457.2011

Knepper, M. A., and Inoue, T. (1997). Regulation of aquaporin-2 water channel trafficking by vasopressin. *Curr. Opin. Cell Biol.* 9, 560–564. doi:10.1016/s0955-0674(97)80034-8

Kortenoeven, M. L., Trimpert, C., Van Den Brand, M., Li, Y., Wetzels, J. F., and Deen, P. M. (2012). In mpkCCD cells, long-term regulation of aquaporin-2 by vasopressin occurs independent of protein kinase A and CREB but may involve Epac. *Am. J. Physiol. Ren. Physiol.* 302, F1395–F1401. doi:10.1152/ajprenal.00376.2011

Li, M., Hothi, S. S., Salvage, S. C., Jeevaratnam, K., Grace, A. A., and Huang, C. L. (2017). Arrhythmic effects of Epac-mediated ryanodine receptor activation in Langendorff-perfused murine hearts are associated with reduced conduction velocity. *Clin. Exp. Pharmacol. Physiol.* 44, 686–692. doi:10.1111/1440-1681.12751

Li, Y., Konings, I. B., Zhao, J., Price, L. S., De Heer, E., and Deen, P. M. (2008). Renal expression of exchange protein directly activated by cAMP (Epac) 1 and 2. *Am. J. Physiol. Ren. Physiol.* 295, F525–F533. doi:10.1152/ajprenal.00448.2007

Mamenko, M., Zaika, O., Jin, M., O'Neil, R. G., and Pochynyuk, O. (2011). Purinergic activation of Ca2+-permeable TRPV4 channels is essential for mechano-sensitivity in the aldosterone-sensitive distal nephron. *PLoS One* 6, e22824. doi:10.1371/journal.pone.0022824

Mortensen, L. A., Bistrup, C., Jensen, B. L., and Hinrichs, G. R. (2020). A mini-review of pharmacological strategies used to ameliorate polyuria associated with X-linked nephrogenic diabetes insipidus. *Am. J. Physiol. Ren. Physiol.* 319, F746–F753. doi:10.1152/ajprenal.00339.2020

Oestreich, E. A., Malik, S., Goonasekera, S. A., Blaxall, B. C., Kelley, G. G., Dirksen, R. T., et al. (2009). Epac and phospholipase Cepsilon regulate Ca2+ release in the heart by activation of protein kinase Cepsilon and calcium-calmodulin kinase II. *J. Biol. Chem.* 284, 1514–1522. doi:10.1074/jbc.M806994200

Park, E., Yang, C. R., Raghuram, V., Deshpande, V., Datta, A., Poll, B. G., et al. (2023). Data resource: vasopressin-regulated protein phosphorylation sites in the collecting duct. *Am. J. Physiol. Ren. Physiol.* 324, F43–F55. doi:10.1152/ajprenal.00229.2022

Patergnani, S., Suski, J. M., Agnoletto, C., Bononi, A., Bonora, M., De Marchi, E., et al. (2011). Calcium signaling around mitochondria associated membranes (MAMs). *Cell Commun. Signal* 9, 19. doi:10.1186/1478-811X-9-19

Pereira, L., Bare, D. J., Galice, S., Shannon, T. R., and Bers, D. M. (2017). β-Adrenergic induced SR Ca2+ leak is mediated by an Epac-NOS pathway. *J. Mol. Cell Cardiol.* 108, 8–16. doi:10.1016/j.yjmcc.2017.04.005

Pereira, L., Cheng, H., Lao, D. H., Na, L., Van Oort, R. J., Brown, J. H., et al. (2013). Epac2 mediates cardiac β1-adrenergic-dependent sarcoplasmic reticulum Ca2+ leak and arrhythmia. *Circulation* 127, 913–922. doi:10.1161/CIRCULATIONAHA.12.148619

Pereira, L., Metrich, M., Fernandez-Velasco, M., Lucas, A., Leroy, J., Perrier, R., et al. (2007). The cAMP binding protein Epac modulates Ca2+ sparks by a Ca2+/calmodulin kinase signalling pathway in rat cardiac myocytes. *J. Physiol.* 583, 685–694. doi:10.1113/jphysiol.2007.133066

Pochynyuk, O., Bugaj, V., Rieg, T., Insel, P. A., Mironova, E., Vallon, V., et al. (2008). Paracrine regulation of the epithelial Na+ channel in the mammalian collecting duct by purinergic P2Y2 receptor tone. *J. Biol. Chem.* 283, 36599–36607. doi:10.1074/jbc.M807129200

Rieg, T., Tang, T., Murray, F., Schroth, J., Insel, P. A., Fenton, R. A., et al. (2010). Adenylate cyclase 6 determines cAMP formation and aquaporin-2 phosphorylation and trafficking in inner medulla. *J. Am. Soc. Nephrol.* 21, 2059–2068. doi:10.1681/ASN.2010040409

Rinschen, M. M., Yu, M. J., Wang, G., Boja, E. S., Hoffert, J. D., Pisitkun, T., et al. (2010). Quantitative phosphoproteomic analysis reveals vasopressin V2-receptor-dependent signaling pathways in renal collecting duct cells. *Proc. Natl. Acad. Sci. U. S. A.* 107, 3882–3887. doi:10.1073/pnas.0910646107

Rizzuto, R., De Stefani, D., Raffaello, A., and Mammucari, C. (2012). Mitochondria as sensors and regulators of calcium signalling. *Nat. Rev. Mol. Cell Biol.* 13, 566–578. doi:10.1038/nrm3412

Roberts, O. L., Kamishima, T., Barrett-Jolley, R., Quayle, J. M., and Dart, C. (2013). Exchange protein activated by cAMP (Epac) induces vascular relaxation by activating Ca2+-sensitive K+ channels in rat mesenteric artery. *J. Physiol.* 591, 5107–5123. doi:10.1113/jphysiol.2013.262006

Samanta, K., Douglas, S., and Parekh, A. B. (2014). Mitochondrial calcium uniporter MCU supports cytoplasmic Ca2+ oscillations, store-operated Ca2+ entry and Ca2+-dependent gene expression in response to receptor stimulation. *PLoS One* 9, e101188. doi:10.1371/journal.pone.0101188

Sandoval, P. C., Slentz, D. H., Pisitkun, T., Saeed, F., Hoffert, J. D., and Knepper, M. A. (2013). Proteome-wide measurement of protein half-lives and translation rates in vasopressin-sensitive collecting duct cells. *J. Am. Soc. Nephrol.* 24, 1793–1805. doi:10.1681/ASN.2013030279

Sivertsen Asrud, K., Bjornstad, R., Kopperud, R., Pedersen, L., Van Der Hoeven, B., Karlsen, T. V., et al. (2020). Epac1 null mice have nephrogenic diabetes insipidus with deficient corticopapillary osmotic gradient and weaker collecting duct tight junctions. *Acta Physiol. (Oxf)* 229, e13442. doi:10.1111/apha.13442

Suzuki, J., Kanemaru, K., Ishii, K., Ohkura, M., Okubo, Y., and Iino, M. (2014). Imaging intraorganellar Ca2+ at subcellular resolution using CEPIA. *Nat. Commun.* 5, 4153. doi:10.1038/ncomms5153

Territo, P. R., French, S. A., Dunleavy, M. C., Evans, F. J., and Balaban, R. S. (2001). Calcium activation of heart mitochondrial oxidative phosphorylation: rapid kinetics of mVO2, nadh, and light scattering. *J. Biol. Chem.* 276, 2586–2599. doi:10.1074/jbc.M002923200

Territo, P. R., Mootha, V. K., French, S. A., and Balaban, R. S. (2000). Ca(2+) activation of heart mitochondrial oxidative phosphorylation: role of the F(0)/F(1)-ATPase. *Am. J. Physiol. Cell Physiol.* 278, C423–C435. doi:10.1152/ajpcell.2000.278.2.C423

Valli, H., Ahmad, S., Sriharan, S., Dean, L. D., Grace, A. A., Jeevaratnam, K., et al. (2018). Epac-induced ryanodine receptor type 2 activation inhibits sodium currents in atrial and ventricular murine cardiomyocytes. *Clin. Exp. Pharmacol. Physiol.* 45, 278–292. doi:10.1111/1440-1681.12870

Wildman, S. S., Boone, M., Peppiatt-Wildman, C. M., Contreras-Sanz, A., King, B. F., Shirley, D. G., et al. (2009). Nucleotides downregulate aquaporin 2 via activation of apical P2 receptors. *J. Am. Soc. Nephrol.* 20, 1480–1490. doi:10.1681/ASN.2008070686

Yang, H. H., Su, S. H., Ho, C. H., Yeh, A. H., Lin, Y. J., and Yu, M. J. (2022). Glucocorticoid receptor maintains vasopressin responses in kidney collecting duct cells. *Front. Physiol.* 13, 816959. doi:10.3389/fphys.2022.816959

Yip, K. P., Cha, B. J., Tse, C. M., Amin, M. E., and Amin, J. (2015). Functional expression of aquaporin-2 tagged with photoconvertible fluorescent protein in mpkCCD cells. *Cell Physiol. Biochem.* 36, 670–682. doi:10.1159/000430129

Yip, K. P. (2002). Coupling of vasopressin-induced intracellular Ca(2+) mobilization and apical exocytosis in perfused rat kidney collecting duct. *J. Physiol.* 538, 891–899. doi:10.1113/jphysiol.2001.012606

Yip, K. P. (2006). Epac-mediated Ca(2+) mobilization and exocytosis in inner medullary collecting duct. *Am. J. Physiol. Ren. Physiol.* 291, F882–F890. doi:10.1152/ajprenal.00411.2005

Yip, K. P., Holstein-Rathlou, N. H., and Marsh, D. J. (1991). Chaos in blood flow control in genetic and renovascular hypertensive rats. *Am. J. Physiol.* 261, F400–F408. doi:10.1152/ajprenal.1991.261.3.F400

Yip, K. P., and Sham, J. S. (2011). Mechanisms of vasopressin-induced intracellular Ca2+ oscillations in rat inner medullary collecting duct. *Am. J. Physiol. Ren. Physiol.* 300, F540–F548. doi:10.1152/ajprenal.00544.2009

Yoast, R. E., Emrich, S. M., Zhang, X., Xin, P., Arige, V., Pathak, T., et al. (2021). The Mitochondrial Ca(2+) uniporter is a central regulator of interorganellar Ca(2+) transfer and NFAT activation. *J. Biol. Chem.* 297, 101174. doi:10.1016/j.jbc.2021.101174

frontiers | Frontiers in Physiology

TYPE Review
PUBLISHED 08 November 2023
DOI 10.3389/fphys.2023.1289388

OPEN ACCESS

EDITED BY
Carolyn Mary Ecelbarger,
Georgetown University, United States

REVIEWED BY
Liming Chen,
Huazhong University of Science and Technology, China
Masashi Suzuki,
Tokyo Gakugei University, Japan

*CORRESPONDENCE
Manoocher Soleimani,
msoleimani@salud.unm.edu,
manoocher.soleimani@va.gov

RECEIVED 05 September 2023
ACCEPTED 18 October 2023
PUBLISHED 08 November 2023

CITATION
Soleimani M (2023), Not all kidney cysts are created equal: a distinct renal cystogenic mechanism in tuberous sclerosis complex (TSC).
Front. Physiol. 14:1289388.
doi: 10.3389/fphys.2023.1289388

Not all kidney cysts are created equal: a distinct renal cystogenic mechanism in tuberous sclerosis complex (TSC)

Manoocher Soleimani[1,2]*

[1]Department of Medicine, New Mexico Veterans Health Care Center, Albuquerque, NM, United States, [2]Department of Medicine, University of New Mexico School of Medicine, Albuquerque, NM, United States

Tuberous Sclerosis Complex (TSC) is an autosomal dominant genetic disease caused by mutations in either *TSC1* or *TSC2* genes. Approximately, two million individuals suffer from this disorder worldwide. TSC1 and TSC2 code for the proteins harmartin and tuberin, respectively, which form a complex that regulates the mechanistic target of rapamycin complex 1 (mTORC1) and prevents uncontrollable cell growth. In the kidney, TSC presents with the enlargement of benign tumors (angiomyolipomas) and cysts whose presence eventually causes kidney failure. The factors promoting cyst formation and tumor growth in TSC are poorly understood. Recent studies on kidney cysts in various mouse models of TSC, including mice with principal cell- or pericyte-specific inactivation of TSC1 or TSC2, have identified a unique cystogenic mechanism. These studies demonstrate the development of numerous cortical cysts that are predominantly comprised of hyperproliferating A-intercalated (A-IC) cells that express both TSC1 and TSC2. An analogous cellular phenotype in cystic epithelium is observed in both humans with TSC and in $TSC2^{+/-}$ mice, confirming a similar kidney cystogenesis mechanism in TSC. This cellular phenotype profoundly contrasts with kidney cysts found in Autosomal Dominant Polycystic Kidney Disease (ADPKD), which do not show any notable evidence of A-IC cells participating in the cyst lining or expansion. RNA sequencing (RNA-Seq) and confirmatory expression studies demonstrate robust expression of Forkhead Box I1 (FOXI1) transcription factor and its downstream targets, including apical H^+-ATPase and cytoplasmic carbonic anhydrase 2 (CAII), in the cyst epithelia of *Tsc1* (or *Tsc2*) knockout (KO) mice, but not in Polycystic Kidney Disease (*Pkd1*) mutant mice. Deletion of FOXI1, which is vital to H^+-ATPase expression and intercalated (IC) cell viability, completely inhibited mTORC1 activation and abrogated the cyst burden in the kidneys of *Tsc1* KO mice. These results unequivocally demonstrate the critical role that FOXI1 and A-IC cells, along with H^+-ATPase, play in TSC kidney cystogenesis. This review article will discuss the latest research into the causes of kidney cystogenesis in TSC with a focus on possible therapeutic options for this devastating disease.

KEYWORDS

intercalated cells, kidney cysts, FOXI1, mTORC1, c-KIT, AVPR1A

Introduction and discussion

TSC is caused by mutations in either TSC1 or TSC2 genes and affects multiple organs; including the kidney, heart, lung, and brain (Sampson and Harris, 1994; Crino et al., 2006; Henske et al., 2016; Rosset et al., 2017). TSC renal disease is characterized by the development and enlargement of cysts and benign tumors (angiomyolipomas) whose presence results in the decline of kidney function and eventually leads to end stage renal disease (Bissler et al., 2008; Henske et al., 2014; Bissler and Kingswood, 2018; Gallo-Bernal et al., 2022). The incidence of renal cell carcinoma (RCC) is increased in TSC, specifically affecting younger individuals afflicted with disease (Henske et al., 2016). Although the initiating event in TSC1 or TSC2 is well described, the factors that promote the kidney disease phenotype and progression are poorly understood.

The role of mTORC1 in cyst and tumor growth in TSC kidneys

Loss of function of TSC1 or TSC2 activates mTORC1, a ubiquitous protein kinase complex that integrates systemic signals, such as growth factors and cytokines, with local signals that sense the availability of nutrients (e.g., amino acids, glucose and oxygen), in order to regulate cell growth (Urbanska et al., 2013; Kim and Guan, 2019). The mTORC1 activation is the principal mechanism driving growth in benign tumors (angiomyolipomas) and cystogenesis in TSC kidneys (Bissler et al., 2008; Henske et al., 2014; Bissler and Kingswood, 2018; Gallo-Bernal et al., 2022) by initiating transcriptional, translational, and post-translational processes that promote a multitude of anabolic activities; including inhibiting cellular catabolic processes resulting in cell growth and proliferation (Sarbassov et al., 2005; Düvel et al., 2010; Howell et al., 2013).

The mTORC1 is under the control of the TSC1-TSC2 complex and the Ras-Homolog Enriched in Brain (RHEB). RHEB plays a vital role in regulation of growth and cell proliferation through the insulin/mTOR/S6 Kinase (S6K) signaling pathway (Sarbassov et al., 2005; Düvel et al., 2010; Howell et al., 2013; Urbanska et al., 2013; Kim and Guan, 2019). The TSC1-TSC2 complex inhibits mTORC1 by negatively regulating RHEB-GTPase (Fingar and Blenis, 2004; Kwiatkowski and Manning, 2005; Sarbassov et al., 2005; Düvel et al., 2010; Howell et al., 2013; Henske et al., 2014; Bissler and Kingswood, 2018). In the presence of inactivating mutations in TSC1 or TSC2, RHEB-GTPase is no longer under the inhibitory control of TSC1/TSC2, and in its GTP-bound form can activate mTORC1, which then phosphorylates the downstream elements, S6K and the eIF4E-binding proteins (4-EBP), leading to cell proliferation and growth (Fingar and Blenis, 2004; Kwiatkowski and Manning, 2005; Sancak et al., 2010; Ögmundsdóttir et al., 2012; Showkat et al., 2014).

Angiomyolipomas are benign kidney tumors consisting of fat, muscle, and blood vessels. They are usually accompanied by cysts and are subject to progressive growth and hemorrhage (Bissler et al., 2008; Henske et al., 2014; Bissler and Kingswood, 2018; Gallo-Bernal et al., 2022). Because of robust mTORC1 activation and its role in cell proliferation, mTORC1 inhibitors (e.g., sirolimus or everolimus) have been used in the treatment of kidney disease in TSC patients (Bissler et al., 2008; Henske et al., 2014). Unfortunately, a significant portion of individuals with TSC do not respond to this therapy. Further, kidney lesions can return to their baseline size when drugs are discontinued (Bissler et al., 2019a).

Loss of heterozygosity in TSC gene in angiomyolipomas vs. cysts in TSC kidney

Kidney cysts are usually composed of cells that express intact TSC1 and TSC2 proteins in both mouse models, as well as in humans with TSC renal cystic disease (Onda et al., 1999; Bonsib et al., 2016). This occurrence is distinct from the angiomyolipomas which show a loss of TSC gene and function (Bonsib et al., 2016; Giannikou et al., 2016). These results may suggest that the factors and pathways that promote cyst growth and expansion are unique and different from those promoting the formation of angiomyolipomas in the kidneys of individuals with TSC.

While expressing phenotypically distinct cell types lining the cysts, both ADPKD and TSC kidney cysts display mTORC1 activation (Shillingford et al., 2006; Henske et al., 2014; Bissler and Kingswood, 2018). Yet, the role of mTORC1 activation in ADPKD cystogenesis remains conflicting. In humans with TSC, inhibition of mTORC1 or S6K profoundly blunts the overgrowth of cells, tumors, and cysts in the kidney, as long as patients remain on these inhibitors (Bissler et al., 2008; Henske et al., 2014; Bissler and Kingswood, 2018). In contrast, the inhibition of mTORC1 in humans with ADPKD did not exhibit a significant beneficial impact on kidney function and cyst volume (Serra et al., 2010). These results display contrasting effects of mTORC1 in cystogenesis in TSC vs. ADPKD. With the exception of mTORC1 inhibitors, there are no therapeutic (druggable) molecular targets to alleviate kidney cysts or tumors in TSC.

Distinct cell phenotype in cyst epithelia in TSC

The first studies examining the identity of cells lining the cysts in TSC came from heterozygote *Tsc2* (*Tsc2*$^{+/-}$) mice, which showed a predominance of IC cells within the cyst epithelia (Onda et al., 1999). A more recent report on *Tsc1* inactivation in mouse principal cells showed that kidney cysts exhibited a gradual loss of Aquaporin 2 (AQP-2)-positive cells in their epithelium (Chen et al., 2014). The disappearance of AQP-2-positive cells was attributed to the dedifferentiation of principal cells (Chen et al., 2014). However, there were no detailed characterizations of the non–AQP-2–expressing cells lining the cysts (Chen et al., 2014). Recently, we showed that in mice with either *Tsc1* or *Tsc2* deletion in kidney principal cells, the epithelia lining the cysts are predominantly comprised of cells exhibiting apical H^+-ATPase and basolateral Cl^-/HCO_3^- exchanger AE1 (SLC4A1) (Bissler et al., 2019b; Barone et al., 2021; Zahedi et al., 2022; Barone et al., 2023). These results convincingly identified the cells lining the kidney cysts in TSC as A-IC cells (Bissler et al., 2019b; Barone et al., 2021; Zahedi et al., 2022; Barone et al., 2023) and demonstrate that the loss of AQP-2 positive cells was due to the disappearance of

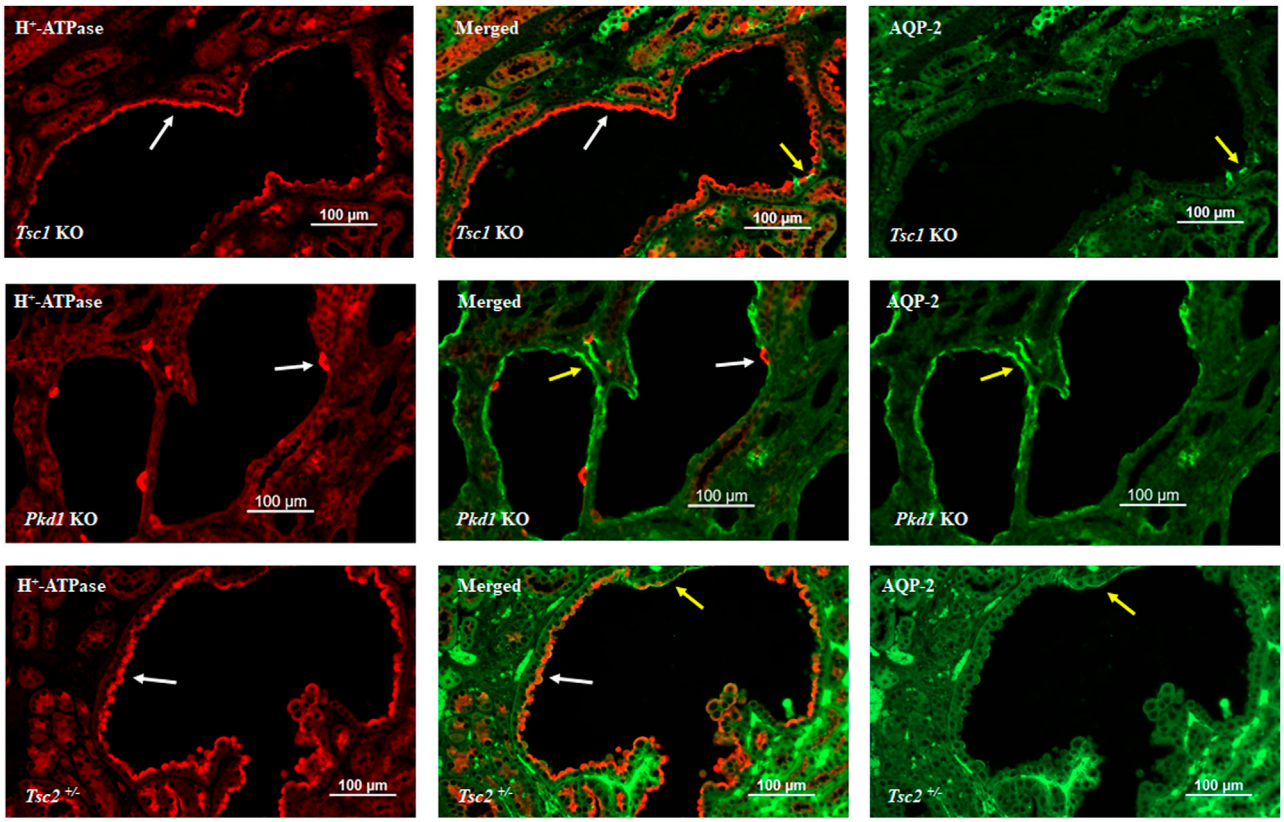

FIGURE 1
Double immunofluorescence labeling with H^+-ATPase and AQP-2 in the kidney cysts of mice with principal cell-specific inactivation of *Tsc1* (top panel), principal cell-specific inactivation of *Pkd1* (middle panel), and *Tsc2* haploinsufficiency ($Tsc2^{+/-}$). As indicated, H^+-ATPase shows abundant and widespread expression on the apical membrane of cells lining the cysts, with very few AQP-2 labeling in *Tsc1* KO mice (top panel). The H^+-ATPase expression in *Pkd1* mice is shown for comparison (middle panel) and indicates a completely different labeling pattern. There are few H^+-ATPase positive cells lining the cysts; whereas, AQP-2 labeling is very robust in *Pkd1* cyst epithelia (middle panel). The expression of H^+-ATPase was almost uniform in $Tsc2^{+/-}$ mice (bottom panel). Created with BioRender.com by Sharon Barone.

principal cells and their replacement with A-intercalated cells in the cyst lining.

In addition to the apical H^+-ATPase and basolateral AE1 expression, cells lining the cysts expressed the proliferation marker Proliferating Cell Nuclear Antigen (PCNA), along with the intact TSC locus (Bissler et al., 2019b; Barone et al., 2021). These results strongly support the view that the cyst epithelial cells are hyperproliferating A-IC cells that are genotypically normal and express both TSC1 and TSC2 (Bissler et al., 2019b; Barone et al., 2021). A similar cell phenotype was observed in kidney cysts in mice with pericyte-specific inactivation of TSC1 (Bissler et al., 2019b; Barone et al., 2021). Furthermore, an identical cell phenotype was observed in the cystic epithelium of humans with TSC, confirming a similar TSC kidney cystogenesis mechanism (Bissler et al., 2019b; Barone et al., 2021). The epithelial cells lining the cysts in individuals with ADPKD and in mutant *Pkd*1 mouse models do not show any notable evidence of IC cell presence or their participation in cyst expansion (Holthöfer et al., 1990; Shibazaki et al., 2008).

Figure 1 depicts double immunofluorescence labeling with H^+-ATPase and AQP-2 in kidney cysts of mice with principal cell inactivation of *Tsc1* (top panel), kidney-specific inactivation of *Pkd1* (middle panel), and *Tsc2* haploinsufficiency ($Tsc2^{+/-}$). H^+-ATPase shows abundant and widespread expression on the apical membrane of cells lining the cysts, with very few AQP-2 positive cells in *Tsc1* KO mice (top panel). The H^+-ATPase expression in *Pkd1* mice is shown for comparison (middle panel) and indicates a completely different pattern, with few cells lining the cysts expressing H^+-ATPase, whereas labeling with AQP-2 is very robust in cyst epithelia in *Pkd1* mutant mice (middle panel). The expression of H^+-ATPase was almost uniform in $Tsc2^{+/-}$ mice (bottom panel). Please see legend to Figure 1.

H^+-ATPase and mTORC1 interaction: the essential role of the lysosome

The presence of apical H^+-ATPase in cells lining the cysts has brought new attention to the role of this molecule in TSC renal cystic disease (Bissler et al., 2019b; Barone et al., 2021; Zahedi et al., 2022; Barone et al., 2023). Vacuolar H^+-ATPase (V H^+-ATPase) is a large, multi-subunit H^+ pump composed of V0 (membrane-spanning) and V1 (catalytic) complexes, and couples the energy of ATP hydrolysis to H^+ translocation across plasma and intracellular membranes (Forgac, 2007; Hinton et al., 2009). Examination of the role of V H^+-ATPase has revealed a crucial role for this pump in luminal acidification in several intracellular organelles, including late

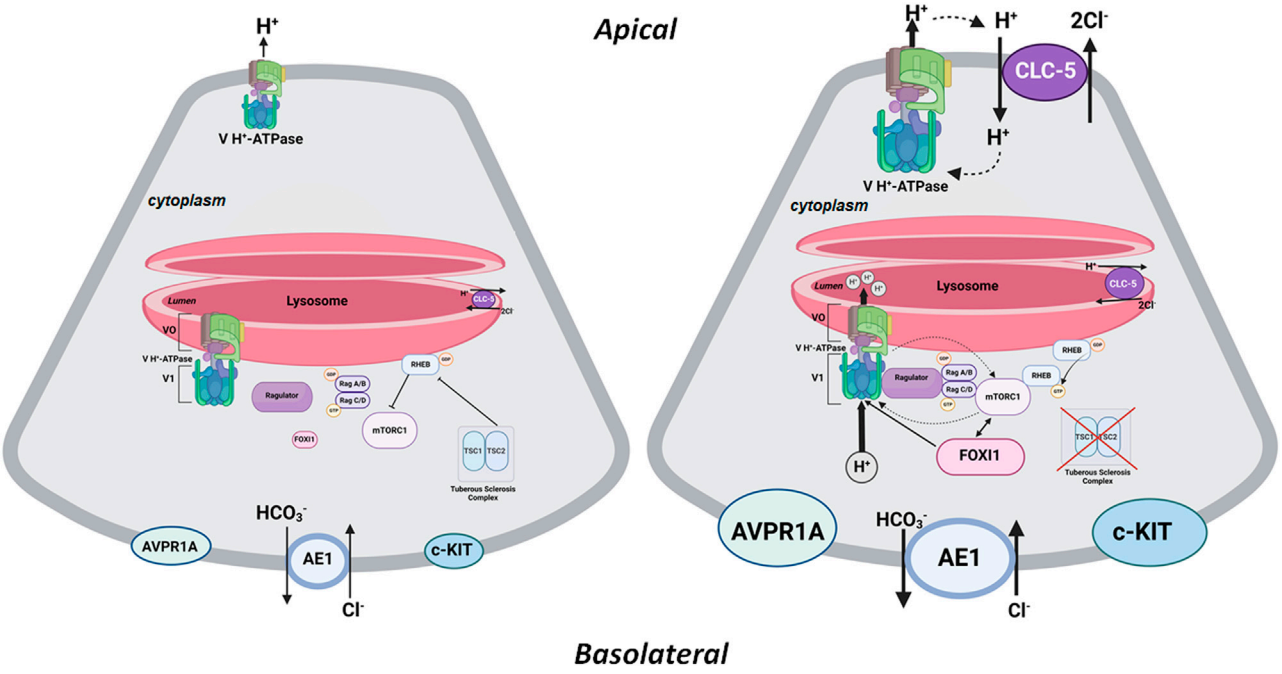

FIGURE 2
A schematic diagram depicting the interaction of mTORC1 and H^+-ATPase on the lysosomal membrane. The left panel depicts a baseline state where the TSC1/TSC2 complex is intact and prevents RHEB from activating mTORC1. See additional description in the text under the heading, "The Central Role of FOXI1 in Kidney Cystogenesis in TSC." The right panel depicts mTORC1 activation consequent to inactivating mutations or phosphorylation of TSC1 or TSC2. In its activated state, RHEB is released from the TSC1/TSC2 complex, resulting in the activation of mTORC1, which enhances the expression and assembly of V0 and V1 H^+-ATPase subcomplexes (as depicted by bold arrows); therefore, resulting in increased H^+-ATPase-mediate H^+ transport. The feedback loop between mTORC1 and H^+-ATPase also indicates the stimulatory effect of H^+-ATPase on mTORC1 by enabling its recruitment and activation on the lysosomal membrane. In all mouse models of TSC examined thus far (Bissler et al., 2019b; Barone et al., 2021; Zahedi et al., 2022; Barone et al., 2023), mTORC1 is associated with enhanced expression of FOXI1 which activates H^+-ATPase by enhancing the expression and activity of its subunits. Inhibition or inactivation of FOXI1 completely abrogates kidney cystogenesis and inhibits mTORC1 in TSC kidneys. The HCO_3^- exit via the basolateral Cl^-/HCO_3^- exchange system (AE1; SLC4A1) is enhanced under an activated mTORC1 state. Created with BioRender.com by Sharon Barone.

endosomes and lysosomes (Forgac, 2007; Hinton et al., 2009). Essential to mTORC1 activation is its recruitment to the lysosomal surface, which has brought additional attention to this organelle as a signaling hub since it incorporates many contributing signals required for cell proliferation and growth (Sancak et al., 2010; Ögmundsdóttir et al., 2012; Showkat et al., 2014).

Vacuolar H^+-ATPase and mTORC1 have a reciprocal activating effect on each other in the lysosomal membrane. Recent studies have identified a network of signals/molecules that link mTORC1 to V H^+-ATPase, a critical component of lysosomes. mTORC1 was able to enhance the expression of V H^+-ATPases both in cells and mice (Peña-Llopis et al., 2011). The crosstalk between V H^+-ATPase and mTORC1 on lysosome membranes is dependent on lysosomal biogenesis, which is regulated by Transcription factor EB (TFEB) (Peña-Llopis et al., 2011). Concurrently, increased H^+-ATPase assembly and activity in the lysosomal membrane is necessary for amino acid-dependent mTORC1 recruitment (and activation) through interactions with the Rag GTPases, which are tethered to the lysosomal membrane by the Ragulator complex (Zoncu et al., 2011; Bar-Peled et al., 2013; Bar-Peled and Sabatini, 2014; Alesi et al., 2021). The inhibition or inactivation of H^+-ATPase occurs through the decoupling of H^+-ATPase from the Rag GTPases, leading to the inhibition of mTORC1 signaling (Forgac, 2007; Hinton et al., 2009; Nada et al., 2014). This inactivation leads to the neutralization of the luminal pH in lysosomes. It should be noted that the luminal lysosomal acidification consequent to the inward H^+-ATPase-mediated H^+ transport can simultaneously lead to the cytosolic alkalinization, which has further been implicated in the regulation of lysosomal perinuclear clustering (lysosomal topology) and mTORC1 (Chung et al., 2019). Taken together, these studies demonstrate the reciprocal stimulating effect of mTORC1 and H^+-ATPase; mTORC1 enhances H^+-ATPase expression and activity (Peña-Llopis et al., 2011; Alesi et al., 2021), while H^+-ATPase plays a critical role in recruiting mTORC1 and sustaining its activation (Zoncu et al., 2011; Bar-Peled et al., 2013; Bar-Peled and Sabatini, 2014; Nada et al., 2014; Chung et al., 2019). Please see Figure 2 for more details.

mTORC1 activation in cyst epithelium is mainly detected in H^+-ATPase–overexpressing intercalated cells

The renal cyst epithelia in all mouse models of TSC display a robust mTORC1 activation as demonstrated by the presence of significantly elevated phospho-S6K levels (Bissler et al., 2019b; Barone et al., 2021). Active proliferation of A-IC cells in cyst

epithelia was verified by a remarkable co-localization of PCNA and H^+-ATPase in the same cells (Bissler et al., 2019b; Barone et al., 2021). These results indicate the activation of mTORC1 in A-IC cells lining the cysts and demonstrate that A-IC cells are the primary cells that are robustly proliferating in the epithelium of renal cysts.

Vacuolar H^+-ATPase in kidney A-IC cells: from intracellular organelles to the plasma membrane

V H^+-ATPase is essential for the luminal acidification of intracellular organelles in all cells (Forgac, 2007; Hinton et al., 2009). This process includes acidifying the lumen of endosomes, lysosomes, and phagosomes; as well as several other intracellular organelles (Forgac, 2007; Hinton et al., 2009). In a few specialized cells, including kidney IC cells, pancreatic beta cells, and osteoclasts, V H^+-ATPase plays two distinct roles. It pumps acid (H^+) into the lumen of organelles, as well as across the plasma membrane into the extracellular compartment (Forgac, 2007; Hinton et al., 2009; Korolchuk et al., 2011; Soleimani and Rastegar, 2016; Do et al., 2022).

There is evidence supporting the recycling of V H^+-ATPase between the plasma membrane and specialized intracellular vesicles (compartments) in kidney IC cells in response to either pH alteration or various stimuli, including several hormones, glucose, or signaling pathways (Carraro-Lacroix and Malnic, 2006; Brown et al., 2009; Alzamora et al., 2010; Gong et al., 2010; Ueno et al., 2014; Merkulova et al., 2015; Smith et al., 2016; Stransky et al., 2016; Eaton et al., 2021). One major pathway enhancing the trafficking of H^+-ATPase from the specialized intracellular compartments to the plasma membrane is the activation of PKA by intracellular cAMP, which causes phosphorylation of several H^+-ATPase subunits (Alzamora et al., 2010; Gong et al., 2010; Eaton et al., 2021). In A-IC cells, H^+-ATPase plays an essential role in pumping H^+ into the lumen of the collecting duct, thus regulating the systemic acid base balance (Soleimani and Rastegar, 2016; Bissler et al., 2019b; Barone et al., 2021; Do et al., 2022; Barone et al., 2023).

In addition to H^+-ATPase, the electrogenic $2Cl^-/H^+$ exchanger (CLC5) is also expressed on lysosomal membranes and works in tandem with H^+-ATPase to maintain the luminal acidity of this crucial organelle in several nephron segments (Günther et al., 1998; Satoh et al., 2017). Both CLC5 and H^+-ATPase are known to be expressed in A-IC cells (Chen et al., 2017; Park et al., 2018), and show co-localization on both the intracellular organelle membranes and the apical membrane of A-IC cells (Günther et al., 1998; Satoh et al., 2017). In kidneys of various mouse models of TSC (*Tsc1* or *Tsc2* KO in principal cells, *Tsc1* KO in pericytes, as well in $Tsc2^{+/-}$), V H^+-ATPase and CLC5 show robust expression and remarkable co-localization on the apical membrane of A-IC cells lining the cysts (Barone et al., 2023).

The mode of transport of CLC5 is electrogenic and comprises the inward movement of $2Cl^-$ in exchange for an outward movement of H^+ from the lysosomal lumen (Günther et al., 1998; Satoh et al., 2017). The co-localization of V H^+-ATPase and CLC5 in both the lysosomal membrane and the plasma membrane support the view that both molecules may traffic from the intracellular compartments to the plasma membrane in A-IC cells in TSC (Barone et al., 2023). It has been speculated that CLC5 co-localization with H^+-ATPase on the apical membrane of A-IC cells could provide a mechanism for continued chloride secretion while maintaining the gradient for continuous H^+-ATPase H^+ secretion into the cyst lumen (Barone et al., 2023).

The central role of FOXI1 in kidney cystogenesis in TSC

RNA sequencing (RNA-Seq) and confirmatory expression studies in our laboratories demonstrated robust expression of FOXI1 and its downstream targets, including H^+-ATPase and cytoplasmic carbonic anhydrase 2 (CAII), in the cyst epithelia of *Tsc1* (or *Tsc2*) knockout (KO) mice, but not in *Pkd1* mutant mice (Barone et al., 2021; Barone et al., 2023). FOXI1 belongs to a large family of transcription factors that are important in cell-type specification during organogenesis (Benayoun et al., 2011). In the kidney, FOXI1 is exclusively expressed in IC cells and is necessary for expression of many H^+-ATPase subunits in this nephron segment (Al-Awqati and Schwartz, 2004; Blomqvist et al., 2004; Vidarsson et al., 2009). In addition, FOXI1 is likely a major determinant for proper assembly of H^+-ATPase subcomplexes and its activation at both the plasma membrane and the membranes of intracellular organelles.

Deletion of FOXI1, which is vital to H^+-ATPase expression and IC cell development (Blomqvist et al., 2004), completely inhibited mTOR activation and abrogated the cyst burden in *Tsc1* KO mice (Barone et al., 2021). These results unequivocally demonstrate the critical role that IC cells, along with their H^+-ATPase and acid secreting machinery, play in TSC kidney cystogenesis. The collecting ducts of the FOXI1 null mice and the Tsc1/Foxi1 double KO (dKO) mice contained primitive cells that expressed both intercalated cell and principal cell transporters (Blomqvist et al., 2004; Barone et al., 2021). Deletion of FOXI1 resulted in profound suppression of several activated H^+-ATPase subunits in the IC cells of Tsc1 KO mice (Barone et al., 2021).

Figure 2 is a schematic diagram that depicts the interaction of mTORC1 and H^+-ATPase on the lysosomal membrane. The left panel depicts the state of mTORC1 in an inactivated state. As noted, the TSC1-TSC2 complex inhibits mTORC1 by negatively regulating RHEB-GTPase. Inactivating mutations in TSC1 or TSC2 remove the inhibitory effect of TSC complex on RHEB-GTPase leading to the activation of mTORC1, which then phosphorylates the downstream elements, S6K, and the eIF4E-binding proteins (4-EBP), enhancing cell proliferation and growth. The feedback loop between mTORC1 and H^+-ATPase facilitates enhanced expression and assembly of H^+-ATPase subcomplexes, and its activation by mTORC1. At the same time, the stimulatory effect of H^+-ATPase on mTORC1 enables its recruitment and activation on lysosomal membrane. Unique to the kidney in TSC is the activation of FOXI1 transcription factor consequent to the activation of mTORC1 (Barone et al., 2021; Barone et al., 2023). FOXI1 is a master regulator of H^+-ATPase subunits and its inactivation completely abrogated cystogenesis and mTORC1 activation in kidneys of TSC1 KO mice (Barone et al., 2021). As indicated the electrogenic Cl-transporter, CLC-5, is enhanced and translocated to the apical membrane of A-IC cells in addition to its original location

on the lysosomal membrane. The CLC-5 maybe involved in movement of Cl- into the cyst lumen and expansion.

FOXI1-dependent signaling pathways and kidney cystogenesis in TSC

To discern the molecular basis of kidney cystogenesis in *Tsc1* KO mice, we analyzed and contrasted the RNA transcriptomes in: 1) *Tsc1* single KO mice which have numerous cysts and cyst adenomas; and compared it to 2) *Tsc1/Foxi1* dKO mice that do not exhibit any kidney cysts. Our results identified the proto-oncogene c-KIT and the vasopressin receptor 1A (AVPR1A) as robustly enhanced transcripts in kidneys of *Tsc1* KO mice (Zahedi et al., 2022; Zahedi et al., 2023). Both molecules exhibit enhanced expression at the mRNA and protein levels in kidney cysts in TSC1 KO mice. Both transcripts were completely suppressed in *Tsc1/Foxi1* dKO mice (Zahedi et al., 2022; Zahedi et al., 2023). Both molecules are known to be expressed in A-IC cells under baseline conditions (Chen et al., 2017; Park et al., 2018).

Transfection of cultured m-IMCD cells with the full length FOX1 cDNA strongly induced the expression of c-KIT and AVPR1A (Zahedi et al., 2022; Zahedi et al., 2023). These results demonstrate that FOXI1 which is critical to the kidney cystogenesis in TSC (Barone et al., 2021), directly induces the expression of c-KIT and AVPR1A in cystic kidneys. Both genes, c-KIT (Hirota et al., 1998; Wiedmann and Caca, 2005; Larkin and Eisen, 2006; Bosbach et al., 2017; Lasota et al., 2019) and AVPR1A (Miller et al., 2013; Fenner, 2019; Zhao et al., 2019; Heidman et al., 2022), are known to play essential roles in enhancing cell proliferation in several uroepithelial cancers and other malignancies in part via mTORC1 activation. Both c-KIT and AVPR1A exhibit predominant expression in IC cells (Chen et al., 2017), with AVPR1A playing a crucial role in H^+-ATPase stimulation in IC cells and acid secretion into the lumen of the collecting ducts (Yasuoka et al., 2013; Giesecke et al., 2019). This is in stark contrast with the cyst epithelia in ADPKD, which contain abundant principal cells with very few IC cells (Barone et al., 2021) and do not show any upregulation of c-KIT or AVPR1A (Zahedi et al., 2022; Zahedi et al., 2023).

c-KIT is a receptor tyrosine kinase that is expressed in several cell types and plays a critical role in enhancing cell proliferation and growth (Miettinen et al., 2005; de Toledo et al., 2023; Krimmer et al., 2023; Sternberg et al., 2023). Published reports indicate that increased activity of the kinase domain of c-KIT significantly contributes to the increased incidence of cancer consequent to uncontrolled cell proliferation. Such aberrant activity of c-KIT has been implicated in the pathogenesis of gastrointestinal stromal tumors (GISTs), mastocytosis, and hematological malignancies (Wiedmann and Caca, 2005; Bosbach et al., 2017; Lasota et al., 2019).

In the kidney, AVPR1A plays a key role secreting acid into the lumen of the collecting duct via stimulation of H^+- secretion in A-IC cells (Yasuoka et al., 2013; Giesecke et al., 2019). Basolateral treatment of isolated perfused medullary collecting ducts with the AVPR1A agonist or vasopressin increased intracellular calcium levels in IC cells, enhanced apical abundance of H^+-ATPase, and stimulated H^+ secretion (Yasuoka et al., 2013; Giesecke et al., 2019). AVPR1A is essential in increasing cell proliferation in several tissues including prostate epithelial cells (Miller et al., 2013; Fenner, 2019; Zhao et al., 2019). The treatment of Castration-resistant prostate cancer (CRPC) cells with the AVPR1A ligand, arginine vasopressin (AVP), activated cAMP response element-binding protein (CREB) via the RAS-MAPK transduction cascade (Zhao et al., 2019). Inhibition by the selective AVPR1A antagonist, relcovaptan, decreased CRPC proliferation in mouse models (Miller et al., 2013). In addition, depletion of AVPR1A in CRPC significantly inhibited cell proliferation (Miller et al., 2013; Fenner, 2019).

Conclusion

The studies that are discussed in this review article demonstrate that in TSC renal cysts, A-IC cells that express both TSC1 and TSC2 constitute the cyst epithelium, and that FOXI1 plays a critical role in the process of cystogenesis. Currently, the only therapeutic option for TSC renal cystic disease is treatment with mTORC1 inhibitors, such as everolimus, which is fraught with many limitations, including resistance to treatment or the return of cysts and tumors to their original size upon discontinuation of therapy. Development of a thorough understanding of the process of renal cystogenesis in TSC should provide us with novel druggable targets for the treatment of this disorder. Delineating specific molecules and pathways that maybe critical to cyst expansion are part of the systemic approach aimed at understanding the mechanistic basis of TSC renal cystogenesis and developing novel and effective therapies for its treatment. The identification of c-KIT and AVPR1A as two differentially expressed genes with known effects on promotion of cell growth and mTORC1 activation in uroepithelial carcinomas and other malignancies is likely a first step toward the exciting discovery of new therapies for this devastating disease.

Author contributions

MS: Conceptualization, Visualization, Writing–original draft, Writing–review and editing.

Funding

The author(s) declare financial support was received for the research, authorship, and/or publication of this article. The author is supported by the United States Veterans Administration Department Merit Review Award (Grant Number: 2I01BX001000-10), Dialysis Clinic Inc. (Grant Number: DCI C-4149), and the National Institutes of Health (Grant Number: NIH/NHLBIT32HL007736; PI T. Resta). This research made use of the Fluorescence Microscopy and Cell Imaging Shared Resource, which is supported partially by the University of New Mexico (UNM) Comprehensive Cancer Center Support Grant NCIP30CA118100. The author is a Senior Clinician Scientist Investigator with the Department of Veterans Health Administration.

Acknowledgments

The critical review of this manuscript by Sharon Barone and Kamyar Zahedi is greatly appreciated. The *Tsc2*$^{+/-}$ mice were generous gifts from Dr. Jane Yu at the University of Cincinnati. Kidney sections from *Pkd1* mutant mice were generous gifts from Dr. Stephen Somlo at Yale University.

Conflict of interest

The author declares that the research was conducted in the absence of any commercial or financial relationships that could be construed as a potential conflict of interest.

The author declared that they were an editorial board member of Frontiers, at the time of submission. This had no impact on the peer review process and the final decision.

Publisher's note

References

Al-Awqati, Q., and Schwartz, G. J. (2004). A fork in the road of cell differentiation in the kidney tubule. *J. Clin. Invest.* 113 (11), 1528–1530. doi:10.1172/JCI22029

Alesi, N., Akl, E. W., Khabibullin, D., Liu, H. J., Nidhiry, A. S., Garner, E. R., et al. (2021). TSC2 regulates lysosome biogenesis via a non-canonical RAGC and TFEB-dependent mechanism. *Nat. Commun.* 12 (1), 4245. doi:10.1038/s41467-021-24499-6

Alzamora, R., Thali, R. F., Gong, F., Smolak, C., Li, H., Baty, C. J., et al. (2010). PKA regulates vacuolar H^+-ATPase localization and activity via direct phosphorylation of the a subunit in kidney cells. *J. Biol. Chem.* 285 (32), 24676–24685. doi:10.1074/jbc.M110.106278

Barone, S., Brooks, M., Zahedi, K., Holliday, L. S., Bissler, J., Yu, J. J., et al. (2023). Identification of an electrogenic $2Cl^-/H^+$ exchanger, ClC5, as a chloride-secreting transporter candidate in kidney cyst epithelium in tuberous sclerosis. *Am. J. Pathol.* 193 (2), 191–200. doi:10.1016/j.ajpath.2022.10.007

Barone, S., Zahedi, K., Brooks, M., Henske, E. P., Yang, Y., Zhang, E., et al. (2021). Kidney intercalated cells and the transcription factor FOXi1 drive cystogenesis in tuberous sclerosis complex. *Proc. Natl. Acad. Sci. U. S. A.* 118 (6), e2020190118. doi:10.1073/pnas.2020190118

Bar-Peled, L., Chantranupong, L., Cherniack, A. D., Chen, W. W., Ottina, K. A., Grabiner, B. C., et al. (2013). A tumor suppressor complex with GAP activity for the Rag GTPases that signal amino acid sufficiency to mTORC1. *Science* 340 (6136), 1100–1106. doi:10.1126/science.1232044

Bar-Peled, L., and Sabatini, D. M. (2014). Regulation of mTORC1 by amino acids. *Trends Cell Biol.* 24 (7), 400–406. doi:10.1016/j.tcb.2014.03.003

Benayoun, B. A., Caburet, S., and Veitia, R. A. (2011). Forkhead transcription factors: key players in health and disease. *Trends Genet.* 27 (6), 224–232. doi:10.1016/j.tig.2011.03.003

Bissler, J. J., Budde, K., Sauter, M., Franz, D. N., Zonnenberg, B. A., Frost, M. D., et al. (2019a). Effect of everolimus on renal function in patients with tuberous sclerosis complex: evidence from EXIST-1 and EXIST-2. *Nephrol. Dial. Transpl.* 34 (6), 1000–1008. doi:10.1093/ndt/gfy132

Bissler, J. J., and Kingswood, J. C. (2018). Renal manifestation of tuberous sclerosis complex. *Am. J. Med. Genet. C Semin. Med. Genet.* 178 (3), 338–347. doi:10.1002/ajmg.c.31654

Bissler, J. J., McCormack, F. X., Young, L. R., Elwing, J. M., Chuck, G., Leonard, J. M., et al. (2008). Sirolimus for angiomyolipoma in tuberous sclerosis complex or lymphangioleiomyomatosis. *N. Engl. J. Med.* 358, 140–151. doi:10.1056/NEJMoa063564

Bissler, J. J., Zadjali, F., Bridges, D., Astrinidis, A., Barone, S., Yao, Y., et al. (2019b). Tuberous sclerosis complex exhibits a new renal cystogenic mechanism. *Physiol. Rep.* 7 (2), e13983. doi:10.14814/phy2.13983

Blomqvist, S. R., Vidarsson, H., Fitzgerald, S., Johansson, B. R., Ollerstam, A., Brown, R., et al. (2004). Distal renal tubular acidosis in mice that lack the forkhead transcription factor Foxi1. *J. Clin. Invest.* 113 (11), 1560–1570. doi:10.1172/JCI20665

Bonsib, S. M., Boils, C., Gokden, N., Grignon, D., Gu, X., Higgins, J. P., et al. (2016). Tuberous sclerosis complex: hamartin and tuberin expression in renal cysts and its discordant expression in renal neoplasms. *Pathol. Res. Pract.* 212 (11), 972–979. doi:10.1016/j.prp.2016.04.005

Bosbach, B., Rossi, F., Yozgat, Y., Loo, J., Zhang, J. Q., Berrozpe, G., et al. (2017). Direct engagement of the PI3K pathway by mutant KIT dominates oncogenic signaling in gastrointestinal stromal tumor. *Proc. Natl. Acad. Sci. U. S. A.* 114 (40), E8448–E8457. doi:10.1073/pnas.1711449114

Brown, D., Paunescu, T. G., Breton, S., and Marshansky, V. (2009). Regulation of the V-ATPase in kidney epithelial cells: dual role in acid-base homeostasis and vesicle trafficking. *J. Exp. Biol.* 212 (11), 1762–1772. doi:10.1242/jeb.028803

Carraro-Lacroix, L. R., and Malnic, G. (2006). Signaling pathways involved with the stimulatory effect of angiotensin II on vacuolar H^+-ATPase in proximal tubule cells. *Pflugers Arch.* 452 (6), 728–736. doi:10.1007/s00424-006-0085-2

Chen, L., Lee, J. W., Chou, C. L., Nair, A. V., Battistone, M. A., Păunescu, T. G., et al. (2017). Transcriptomes of major renal collecting duct cell types in mouse identified by single-cell RNA-seq. *Proc. Natl. Acad. Sci. U. S. A.* 114 (46), E9989–E9998. doi:10.1073/pnas.1710964114

Chen, Z., Dong, H., Jia, C., Song, Q., Chen, J., Zhang, Y., et al. (2014). Activation of mTORC1 in collecting ducts causes hyperkalemia. *J. Am. Soc. Nephrol.* 25, 534–545. doi:10.1681/ASN.2013030225

Chung, C. Y., Shin, H. R., Berdan, C. A., Ford, B., Ward, C. C., Olzmann, J. A., et al. (2019). Covalent targeting of the vacuolar H+-ATPase activates autophagy via mTORC1 inhibition. *Nat. Chem. Biol.* 15 (8), 776–785. doi:10.1038/s41589-019-0308-4

Crino, P. B., Nathanson, K. L., and Henske, E. P. (2006). The tuberous sclerosis complex. *N. Engl. J. Med.* 355, 1345–1356. doi:10.1056/NEJMra055323

de Toledo, M. A. S., Fu, X., Maié, T., Buhl, E. M., Götz, K., Schmitz, S., et al. (2023). KIT D816V mast cells derived from induced pluripotent stem cells recapitulate systemic mastocytosis transcriptional profile. *Int. J. Mol. Sci.* 24 (6), 5275. doi:10.3390/ijms24065275

Do, C., Vasquez, P. C., and Soleimani, M. (2022). Metabolic alkalosis pathogenesis, diagnosis, and treatment: core curriculum 2022. *Am. J. Kidney Dis.* 80 (4), 536–551. doi:10.1053/j.ajkd.2021.12.016

Düvel, K., Yecies, J. L., Menon, S., Raman, P., Lipovsky, A. I., Souza, A. L., et al. (2010). Activation of a metabolic gene regulatory network downstream of mTOR complex 1. *Mol. Cell* 39 (2), 171–183. doi:10.1016/j.molcel.2010.06.022

Eaton, A. F., Merkulova, M., and Brown, D. (2021). The H^+-ATPase (V-ATPase): from proton pump to signaling complex in health and disease. *Am. J. Physiol. Cell Physiol.* 320 (3), C392–C414. doi:10.1152/ajpcell.00442.2020

Fenner, A. (2019). AVPR1A: a target in CRPC? *Nat. Rev. Urol.* 16 (9), 508. doi:10.1038/s41585-019-0218-y

Fingar, D. C., and Blenis, J. (2004). Target of rapamycin (TOR): an integrator of nutrient and growth factor signals and coordinator of cell growth and cell cycle progression. *Oncogene* 23, 3151–3171. doi:10.1038/sj.onc.1207542

Forgac, M. (2007). Vacuolar ATPases: rotary proton pumps in physiology and pathophysiology. *Nat. Rev. Mol. Cell Biol.* 8 (11), 917–929. doi:10.1038/nrm2272

Gallo-Bernal, S., Kilcoyne, A., Gee, M. S., and Paul, E. (2022). Cystic kidney disease in tuberous sclerosis complex: current knowledge and unresolved questions. *Pediatr. Nephrol.* 38, 3253–3264. doi:10.1007/s00467-022-05820-x

Giannikou, K., Malinowska, I. A., Pugh, T. J., Yan, R., Tseng, Y. Y., Oh, C., et al. (2016). Whole exome sequencing identifies TSC1/TSC2 biallelic loss as the primary and sufficient driver event for renal angiomyolipoma development. *PLoS Genet.* 12 (8), e1006242. doi:10.1371/journal.pgen.1006242

Giesecke, T., Himmerkus, N., Leipziger, J., Bleich, M., Koshimizu, T. A., Fähling, M., et al. (2019). Vasopressin increases urinary acidification via V1a receptors in collecting duct intercalated cells. *J. Am. Soc. Nephrol.* 30 (6), 946–961. doi:10.1681/ASN.2018080816

Gong, F., Alzamora, R., Smolak, C., Li, H., Naveed, S., Neumann, D., et al. (2010). Vacuolar H^+-ATPase apical accumulation in kidney intercalated cells is regulated by PKA and AMP-activated protein kinase. *Am. J. Physiol. Ren. Physiol.* 298 (5), F1162–F1169. doi:10.1152/ajprenal.00645.2009

Günther, W., Lüchow, A., Cluzeaud, F., Vandewalle, A., and Jentsch, T. J. (1998). ClC-5, the chloride channel mutated in Dent's disease, colocalizes with the proton pump in endocytotically active kidney cells. *Proc. Natl. Acad. Sci. U.S.A.* 95 (14), 8075–8080. doi:10.1073/pnas.95.14.8075

Heidman, L. M., Peinetti, N., Copello, V. A., and Burnstein, K. L. (2022). Exploiting dependence of castration-resistant prostate cancer on the arginine vasopressin signaling Axis by repurposing vaptans. *Mol. Cancer Res.* 20 (8), 1295–1304. doi:10.1158/1541-7786.MCR-21-0927

Henske, E. P., Jóźwiak, S., Kingswood, J. C., Sampson, J. R., and Thiele, E. A. (2016). Tuberous sclerosis complex. *Nat. Rev. Dis. Prim.* 2, 16035. doi:10.1038/nrdp.2016.35

Henske, E. P., Rasooly, R., Siroky, B., and Bissler, J. (2014). Tuberous sclerosis complex, mTOR, and the kidney: report of an NIDDK-sponsored workshop. *Am. J. Physiol. Ren. Physiol.* 306, F279–F283. doi:10.1152/ajprenal.00525.2013

Hinton, A., Bond, S., and Forgac, M. (2009). V-ATPase functions in normal and disease processes. *Pflugers Arch.* 457 (3), 589–598. doi:10.1007/s00424-007-0382-4

Hirota, S., Isozaki, K., Moriyama, Y., Hashimoto, K., Nishida, T., Ishiguro, S., et al. (1998). Gain-of-function mutations of c-kit in human gastrointestinal stromal tumors. *Science* 279 (5350), 577–580. doi:10.1126/science.279.5350.577

Holthöfer, H., Kumpulainen, T., and Rapola, J. (1990). Polycystic disease of the kidney. Evaluation and classification based on nephron segment and cell-type specific markers. *Lab. Invest.* 62 (3), 363–369.

Howell, J. J., Ricoult, S. J., Ben-Sahra, I., and Manning, B. D. (2013). A growing role for mTOR in promoting anabolic metabolism. *Biochem. Soc. Trans.* 41, 906–912. doi:10.1042/BST20130041

Kim, J., and Guan, K. L. (2019). mTOR as a central hub of nutrient signalling and cell growth. *Nat. Cell Biol.* 21 (1), 63–71. doi:10.1038/s41556-018-0205-1

Korolchuk, V. I., Saiki, S., Lichtenberg, M., Siddiqi, F. H., Roberts, E. A., Imarisio, S., et al. (2011). Lysosomal positioning coordinates cellular nutrient responses. *Nat. Cell Biol.* 13 (4), 453–460. doi:10.1038/ncb2204

Krimmer, S. G., Bertoletti, N., Suzuki, Y., Katic, L., Mohanty, J., Shu, S., et al. (2023). Cryo-EM analyses of KIT and oncogenic mutants reveal structural oncogenic plasticity and a target for therapeutic intervention. *Proc. Natl. Acad. Sci. U. S. A.* 120 (13), e2300054120. doi:10.1073/pnas.2300054120

Kwiatkowski, D. J., and Manning, B. D. (2005). Tuberous sclerosis: a GAP at the crossroads of multiple signaling pathways. *Hum. Mol. Genet.* 14, R251–R258. doi:10.1093/hmg/ddi260

Larkin, J. M., and Eisen, T. (2006). Kinase inhibitors in the treatment of renal cell carcinoma. *Crit. Rev. Oncol. Hematol.* 60 (3), 216–226. doi:10.1016/j.critrevonc.2006.06.008

Lasota, J., Kowalik, A., Felisiak-Golabek, A., Zięba, S., Wang, Z. F., and Miettinen, M. (2019). New mechanisms of mTOR pathway activation in KIT-mutant malignant GISTs. *Appl. Immunohistochem. Mol. Morphol.* 27 (1), 54–58. doi:10.1097/PAI.0000000000000541

Merkulova, M., Păunescu, T. G., Azroyan, A., Marshansky, V., Breton, S., and Brown, D. (2015). Mapping the H(+) (V)-ATPase interactome: identification of proteins involved in trafficking, folding, assembly and phosphorylation. *Sci. Rep.* 5, 14827. doi:10.1038/srep14827

Miettinen, M., and Lasota, J. (2005). KIT (CD117): a review on expression in normal and neoplastic tissues, and mutations and their clinicopathologic correlation. *Appl. Immunohistochem. Mol. Morphol.* 13 (3), 205–220. doi:10.1097/01.pai.0000173054.83414.22

Miller, R. L., Sandoval, P. C., Pisitkun, T., Knepper, M. A., and Hoffert, J. D. (2013). Vasopressin inhibits apoptosis in renal collecting duct cells. *Am. J. Physiol. Ren. Physiol.* 304 (2), F177–F188. doi:10.1152/ajprenal.00431.2012

Nada, S., Mori, S., Takahashi, Y., and Okada, M. (2014). p18/LAMTOR1: a late endosome/lysosome-specific anchor protein for the mTORC1/MAPK signaling pathway. *Methods Enzymol.* 535, 249–263. doi:10.1016/B978-0-12-397925-4.00015-8

Ögmundsdóttir, M. H., Heublein, S., Kazi, S., Reynolds, B., Visvalingam, S. M., Shaw, M. K., et al. (2012). Proton-assisted amino acid transporter PAT1 complexes with Rag GTPases and activates TORC1 on late endosomal and lysosomal membranes. *PloS One* 7 (5), e36616. doi:10.1371/journal.pone.0036616

Onda, H., Lueck, A., Marks, P. W., Warren, H. B., and Kwiatkowski, D. J. (1999). Tsc2(+/-) mice develop tumors in multiple sites that express gelsolin and are influenced by genetic background. *J. Clin. Invest.* 104, 687–695. doi:10.1172/JCI7319

Park, J., Shrestha, R., Qiu, C., Kondo, A., Huang, S., Werth, M., et al. (2018). Single-cell transcriptomics of the mouse kidney reveals potential cellular targets of kidney disease. *Science* 360 (6390), 758–763. doi:10.1126/science.aar2131

Peña-Llopis, S., Vega-Rubin-de-Celis, S., Schwartz, J. C., Wolff, N. C., Tran, T. A., Zou, L., et al. (2011). Regulation of TFEB and V-ATPases by mTORC1. *EMBO J.* 30 (16), 3242–3258. doi:10.1038/emboj.2011.257

Rosset, C., Netto, C. B. O., and Ashton-Prolla, P. (2017). TSC1 and TSC2 gene mutations and their implications for treatment in Tuberous Sclerosis Complex: a review. *Genet. Mol. Biol.* 40, 69–79. doi:10.1590/1678-4685-GMB-2015-0321

Sampson, J. R., and Harris, P. C. (1994). The molecular genetics of tuberous sclerosis. *Hum. Mol. Genet.* 3, 1477–1480. doi:10.1093/hmg/3.suppl_1.1477

Sancak, Y., Bar-Peled, L., Zoncu, R., Markhard, A. L., Nada, S., and Sabatini, D. M. (2010). Ragulator-Rag complex targets mTORC1 to the lysosomal surface and is necessary for its activation by amino acids. *Cell* 141 (2), 290–303. doi:10.1016/j.cell.2010.02.024

Sarbassov, D. D., Ali, S. M., and Sabatini, D. M. (2005). Growing roles for the mTOR pathway. *Curr Opin Cell Biol* 17, 596–603. doi:10.1016/j.ceb.2005.09.009

Satoh, N., Suzuki, M., Nakamura, M., Suzuki, A., Horita, S., Seki, G., et al. (2017). Functional coupling of V-ATPase and CLC-5. *World J. Nephrol.* 6 (1), 14–20. doi:10.5527/wjn.v6.i1.14

Serra, A. L., Poster, D., Kistler, A. D., Krauer, F., Raina, S., Young, J., et al. (2010). Sirolimus and kidney growth in autosomal dominant polycystic kidney disease. *N. Engl. J. Med.* 363 (9), 820–829. doi:10.1056/NEJMoa0907419

Shibazaki, S., Yu, Z., Nishio, S., Tian, X., Thomson, R. B., Mitobe, M., et al. (2008). Cyst formation and activation of the extracellular regulated kinase pathway after kidney specific inactivation of Pkd1. *Hum. Mol. Genet.* 17 (11), 1505–1516. doi:10.1093/hmg/ddn039

Shillingford, J. M., Murcia, N. S., Larson, C. H., Low, S. H., Hedgepeth, R., Brown, N., et al. (2006). The mTOR pathway is regulated by polycystin-1, and its inhibition reverses renal cystogenesis in polycystic kidney disease. *Proc. Natl. Acad. Sci. U. S. A.* 103 (14), 5466–5471. doi:10.1073/pnas.0509694103

Showkat, M., Beigh, M. A., and Andrabi, K. I. (2014). mTOR signaling in protein translation regulation: implications in cancer genesis and therapeutic interventions. *Mol. Biol. Int.* 2014, 686984. doi:10.1155/2014/686984

Smith, G. A., Howell, G. J., Phillips, C., Muench, S. P., Ponnambalam, S., and Harrison, M. A. (2016). Extracellular and luminal pH regulation by vacuolar H+-ATPase isoform expression and targeting to the plasma membrane and endosomes. *J. Biol. Chem.* 291 (16), 8500–8515. doi:10.1074/jbc.M116.723395

Soleimani, M., and Rastegar, A. (2016). Pathophysiology of renal tubular acidosis: core curriculum 2016. *Am. J. Kidney Dis.* 68 (3), 488–498. doi:10.1053/j.ajkd.2016.03.422

Sternberg, C. N., Davis, I. D., Mardiak, J., Szczylik, C., Lee, E., Wagstaff, J., et al. (2023). Pazopanib in locally advanced or metastatic renal cell carcinoma: results of a randomized phase III trial. *J. Clin. Oncol.* 41 (11), 1957–1964. doi:10.1200/JCO.22.02622

Stransky, L., Cotter, K., and Forgac, M. (2016). The function of V-ATPases in cancer. *Physiol. Rev.* 96 (3), 1071–1091. doi:10.1152/physrev.00035.2015

Ueno, K., Saito, M., Nagashima, M., Kojima, A., Nishinoaki, S., Toshima, J. Y., et al. (2014). V-ATPase-dependent luminal acidification is required for endocytic recycling of a yeast cell wall stress sensor, Wsc1p. *Biochem. Biophys. Res. Commun.* 443 (2), 549–555. doi:10.1016/j.bbrc.2013.12.008

Urbanska, M., Macias, M., Skalecka, A., and Jaworski, J. (2013). Beyond control of protein translation: what we have learned about the non-canonical regulation and function of mammalian target of rapamycin (mTOR). *Malik Ar. Biochim. Biophys. Acta* 1834 (7), 1434–1448. doi:10.1016/j.bbapap.2012.12.010

Vidarsson, H., Westergren, R., Heglind, M., Blomqvist, S. R., Breton, S., and Enerbäck, S. (2009). The forkhead transcription factor Foxi1 is a master regulator of vacuolar H-ATPase proton pump subunits in the inner ear, kidney and epididymis. *PLoS One* 4 (2), e4471. doi:10.1371/journal.pone.0004471

Wiedmann, M. W., and Caca, K. (2005). Molecularly targeted therapy for gastrointestinal cancer. *Curr. Cancer Drug Targets* 5 (3), 171–193. doi:10.2174/1568009053765771

Yasuoka, Y., Kobayashi, M., Sato, Y., Zhou, M., Abe, H., Okamoto, H., et al. (2013). The intercalated cells of the mouse kidney OMCD(is) are the target of the vasopressin V1a receptor axis for urinary acidification. *Clin. Exp. Nephrol.* 17 (6), 783–792. doi:10.1007/s10157-013-0783-y

Zahedi, K., Barone, S., Brooks, M., Murray Stewart, T., Casero, R. A., Jr, and Soleimani, M. (2022). Renal transcriptome and metabolome in mice with principal cell-specific ablation of the Tsc1 gene: derangements in pathways associated with cell metabolism, growth and acid secretion. *Int. J. Mol. Sci.* 23 (18), 10601. doi:10.3390/ijms231810601

Zahedi, K., Barone, S., Zaidman, N., and Soleimani, M. (2023). "Identification of transcripts critical to tsc-mTOR Axis dysregulation in tuberous sclerosis complex renal disease," in *American society of nephrology (ASN) kidney week* (Berlin, Germany: Springer).

Zhao, N., Peacock, S. O., Lo, C. H., Heidman, L. M., Rice, M. A., Fahrenholtz, C. D., et al. (2019). Arginine vasopressin receptor 1a is a therapeutic target for castration-resistant prostate cancer. *Sci. Transl. Med.* 11 (498), eaaw4636. doi:10.1126/scitranslmed.aaw4636

Zoncu, R., Bar-Peled, L., Efeyan, A., Wang, S., Sancak, Y., and Sabatini, D. M. (2011). mTORC1 senses lysosomal amino acids through an inside out mechanism that requires the vacuolar H(+)-ATPase. *Science* 334 (6056), 678–683. doi:10.1126/science.1207056

frontiers | Frontiers in Physiology

TYPE Original Research
PUBLISHED 08 November 2023
DOI 10.3389/fphys.2023.1240352

OPEN ACCESS

EDITED BY
Carolyn Mary Ecelbarger,
Georgetown University, United States

REVIEWED BY
Adam Deak,
University of Debrecen, Hungary
Yanyang Li,
Northwestern University, United States

*CORRESPONDENCE
Xiaoming Zhou,
xiaoming.zhou@usuhs.edu

RECEIVED 14 June 2023
ACCEPTED 09 October 2023
PUBLISHED 08 November 2023

CITATION
Packialakshmi B, Burmeister DM, Anderson JA, Morgan J, Cannon G, Kiang JG, Feng Y, Lee S, Stewart IJ and Zhou X (2023), A clinically-relevant mouse model that displays hemorrhage exacerbates tourniquet-induced acute kidney injury.
Front. Physiol. 14:1240352.
doi: 10.3389/fphys.2023.1240352

A clinically-relevant mouse model that displays hemorrhage exacerbates tourniquet-induced acute kidney injury

Balamurugan Packialakshmi[1], David M. Burmeister[1], Joseph A. Anderson[2], Judah Morgan[3], Georgetta Cannon[4], Juliann G. Kiang[1,4,5], Yuanyi Feng[6], Sang Lee[2], Ian J. Stewart[1] and Xiaoming Zhou[1]*

[1]Department of Medicine, Uniformed Services University of the Health Sciences, Bethesda, MD, United States, [2]Department of Laboratory Animal Resources, Uniformed Services University of the Health Sciences, Bethesda, MD, United States, [3]Internal Medicine Residency Program at Madigan Army Medical Center, Joint Base Lewis-McChord, Tacoma, WA, United States, [4]Armed Forces Radiobiology Research Institute, Uniformed Services University of the Health Sciences, Bethesda, MD, United States, [5]Department of Pharmacology and Molecular Therapeutics, Uniformed Services University of the Health Sciences, Bethesda, MD, United States, [6]Department of Biochemistry and Molecular Biology, Uniformed Services University of the Health Sciences, Bethesda, MD, United States

Hemorrhage is a leading cause of death in trauma. Tourniquets are effective at controlling extremity hemorrhage and have saved lives. However, tourniquets can cause ischemia reperfusion injury of limbs, leading to systemic inflammation and other adverse effects, which results in secondary damage to the kidney, lung, and liver. A clinically relevant animal model is critical to understanding the pathophysiology of this process and developing therapeutic interventions. Despite the importance of animal models, tourniquet-induced lower limb ischemia/reperfusion (TILLIR) models to date lack a hemorrhage component. We sought to develop a new TILLIR model that included hemorrhage and analyze the subsequent impact on kidney, lung and liver injuries. Four groups of mice were examined: group 1) control, group 2) hemorrhage, group 3) tourniquet application, and group 4) hemorrhage and tourniquet application. The hemorrhagic injury consisted of the removal of 15% of blood volume through the submandibular vein. The tourniquet injury consisted of orthodontic rubber bands applied to the inguinal area bilaterally for 80 min. Mice were then placed in metabolic cages individually for 22 h to collect urine. Hemorrhage alone did not significantly affect transcutaneous glomerular filtration rate (tGFR), blood urea nitrogen (BUN) or urinary kidney injury molecule-1 (KIM-1) levels. Without hemorrhage, TILLIR decreased tGFR by 46%, increased BUN by 162%, and increased KIM-1 by 27% ($p < 0.05$ for all). With hemorrhage, TILLIR decreased the tGFR by 72%, increased BUN by 395%, and increased urinary KIM-1 by 37% ($p < 0.05$ for all). These differences were statistically significant ($p < 0.05$). While hemorrhage had no significant effect on TILLIR-induced renal tubular degeneration and necrosis, it significantly increased TILLIR-induced lung total

Abbreviations: AKI, acute kidney injury; KIM-1, kidney injury molecule-1; BUN, serum urea nitrogen; tGFR, transcutaneous glomerular filtration rate; TILLIR, tourniquet-induced lower limb ischemia reperfusion.

10.3389/fphys.2023.1240352

injury scores and congestion, and fatty liver. In conclusion, hemorrhage exacerbates TILLIR-induced acute kidney injury and structural damage in the lung and liver.

KEYWORDS

lower limb, ischemia/reperfusion, rhabdomyolysis, systemic inflammation, lung injury, liver injury

Introduction

Hemorrhage accounts for approximately 40% of deaths in traumatic injury worldwide (Curry et al., 2011). Tourniquets are the first-line therapy to control extremity hemorrhage both in civilian and military care settings (Kragh et al., 2008; Scerbo et al., 2017; Muñoz et al., 2020; Gallo et al., 2021; Hinojosa-Laborde et al., 2022). It is estimated that tourniquets may have saved as many as 2,000 lives in the U.S. Military operations in Iraq and Afghanistan (Andersen et al., 2012). Tourniquets are also used as an adjunct procedure in limb surgery to create a bloodless field (Gallo et al., 2021; Tirumala et al., 2021). However, prolonged application and release of tourniquets induces ischemia/reperfusion injury to limbs, releasing myoglobin, damage-associated molecular patterns, cytokines, chemokines, and other harmful molecules, leading to systemic inflammation (Yassin et al., 1998; Cai et al., 2009; Foster et al., 2017). Systemic inflammation increases vascular permeability and leakage, resulting in hypovolemia and hypoperfusion of the kidney and other organs (De Rosa et al., 2018; Simon et al., 2018). Therefore, prolonged use of tourniquets can induce secondary distal organ injuries such as acute kidney, lung and liver injures (Morsey et al., 2003; Arora et al., 2015;

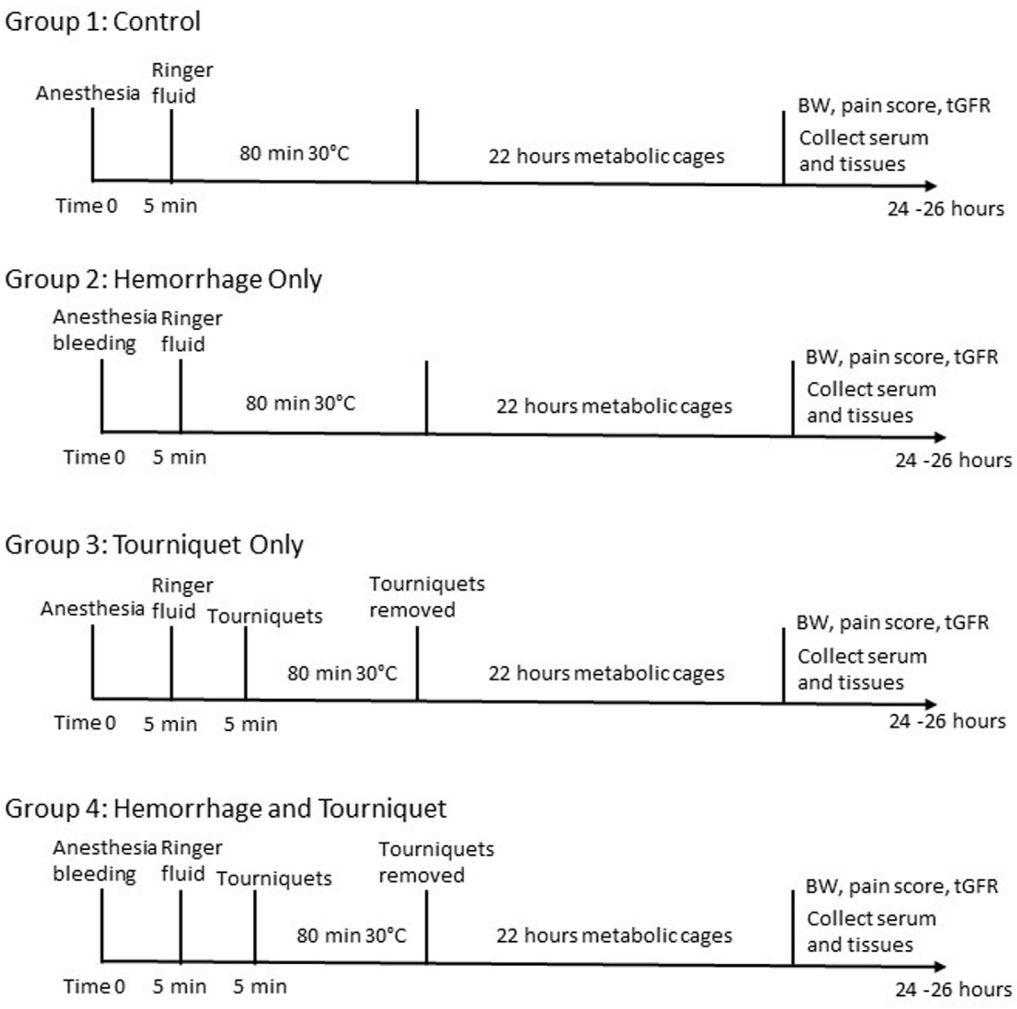

FIGURE 1
Experimental design and procedures. BW, body weight; tGFR, transcutaneous glomerular filtration rate.

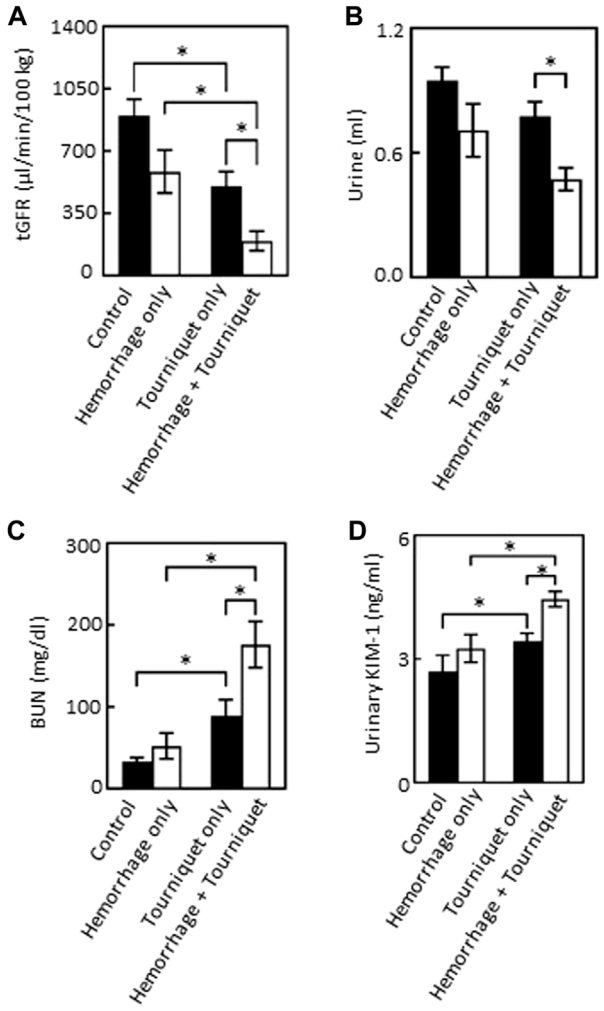

FIGURE 2
Hemorrhage exacerbates TILLIR-induced reduction in the renal function as assessed by tGFR, urinary output, BUN and urinary KIM-1 levels. **(A)** Tourniquet alone reduced tGFR as compared with the control, addition of hemorrhage further decreased tourniquet-induced reduction of tGFR compared either with hemorrhage only or tourniquet only. The tGFR was measured by disappearance of FITC-sinistrin from the blood. $n = 5$ for the control, $n = 6$ for the hemorrhage only, $n = 12$ for the tourniquet only, and $n = 11$ for the hemorrhage + tourniquet. **(B)** Tourniquet alone did not significantly reduce urinary output, but combining tourniquet with hemorrhage decreased urinary output as compared with the tourniquet only group. Urine was collected through metabolic cages for 22 h $n = 5$ for the control, $n = 6$ for the hemorrhage only, $n = 11$ for the tourniquet only or hemorrhage + tourniquet. **(C)** Tourniquet alone increased serum urea nitrogen (BUN) as compared with the control, the combination of tourniquet with hemorrhage further elevated tourniquet-induced increase in BUN compared either with hemorrhage only or tourniquet only. BUN was measured with a colorimetric method. $n = 5$ for the control or hemorrhage only, $n = 9$ for the tourniquet only, and $n = 10$ for hemorrhage + tourniquet. **(D)** Tourniquets alone increased urinary KIM-1 level as compared with the control. Adding hemorrhage further elevated tourniquet-induced increase in urinary KIM-1 concentrations compared either with hemorrhage only or tourniquet only. The KIM-1 concentrations were measured with an ELISA kit from Abcam (ab213477). $n = 5$ for the control or hemorrhage only, $n = 10$ for the tourniquet only and hemorrhage + tourniquet, respectively. *$p < 0.05$, Two-way ANOVA.

Chavez et al., 2016; De Rosa et al., 2018; Leurcharusmee et al., 2018; Kasepalu et al., 2020; BenÍtez et al., 2021). The incidences of acute kidney injury (AKI) associated with tourniquet use range from 0.8% to 17.2%, depending on whether patients are diabetic (Morsey et al., 2003; Arora et al., 2015; Chavez et al., 2016; De Rosa et al., 2018; Leurcharusmee et al., 2018; Kasepalu et al., 2020; BenÍtez et al., 2021; Pottecher et al., 2021; Paquette et al., 2022). There is no specific prevention or treatment for tourniquet-induced AKI or other organ injury (Zhou, 2023).

An animal model closely mimicking the clinical setting is important to understanding pathophysiology and testing therapeutic approaches. Although pigs are more similar to humans in physical size, physiology and immunology than rodents (Packialakshmi et al., 2020; Zhou, 2022), rodents are easy to handle, quickly reproduce and have contributed significantly to deciphering pathophysiology and developing novel therapies. As such, a majority of tourniquet-induced lower limb ischemia/reperfusion (TILLIR) injury in the literature has been produced in rodents, and a variety of therapies have been tested using rodent models (Klausner et al., 1989; Adachi et al., 2006; Hsu et al., 2012; Mansour et al., 2014; Kao et al., 2015a; Kao et al., 2015b; Karahan et al., 2016; Onody et al., 2016; Foster et al., 2017; Shih et al., 2018; İnce et al., 2019).

However, these models were produced by applying a tourniquet either unilaterally or bilaterally to the hindlimbs without inducing hemorrhage. In a clinical setting, however, it is unlikely that a tourniquet can be placed prior to significant blood loss. Hemorrhage induces hypoperfusion, metabolic derangement, coagulopathy and systemic inflammation, all of which play a critical role in the pathogenesis of multi-organ injury (Denk et al., 2018). As a result, these models have missed a crucial factor in TILLIR-induced organ injury. To address this gap, we sought to develop a novel, clinically relevant mouse model of TILLIR by inducing hemorrhage prior to tourniquet application and examined the subsequent impact of TILLIR, with and without hemorrhage, on end-organ damage with a focus on AKI. We hypothesized that hemorrhage would exacerbate TILLIR-induced organ injury.

Materials and methods

Mice

The protocol for use of mice was approved by the institutional animal care and use committee of the Uniformed Services University of the Health Sciences. Male C57BL/6 mice (8–10 weeks old, The Jackson Laboratory) were chosen because they are more prone to develop AKI compared to females (Park et al., 2004; Kher et al., 2005). Mice were kept on a 12:12 light:dark cycle with regular food and water *ad libitum*. Mice were adapted to the facility for at least 3 days before their use for experiments. The experimental design and procedures are outlined in Figure 1. Mice were divided into 4 groups. Group 1 is the control in which mice received the same procedures as other groups, but did not undergo hemorrhage or tourniquet application. Group 2 mice were bled up to 15% blood volume (Class I shock) through the submandibular vein. Group 3 mice had tourniquets (an orthodontic rubber band, 3.2 mm, heavy force 4.5 Oz, purchased from Amazon) applied bilaterally in the inguinal regions for 80 min. Group 4 mice received both tourniquets (80 min) and hemorrhage (15% of blood volume). Blood volume

TABLE 1 Effects of tourniquets and hemorrhage on body weight.

	Pain score	Body weight (g)		Difference	n
		At beginning	At end		
Control	0	23.8 ± 1.4	21.6 ± 1.5	2.2 ± 0.4	5
Hemorrhage only	0.2 ± 0.2	22.7 ± 0.9	20.6 ± 0.8	2.1 ± 0.5	6
Tourniquet only	2.6 ± 0.2	22.8 ± 0.4	21.6 ± 0.4	1.2 ± 0.2	12
Hemorrhage + Tourniquet	3.5 ± 0.3*	22.7 ± 0.6	21.4 ± 0.5	1.4 ± 0.4	11

*$p < 0.05$ vs. Tourniquet only.

was calculated using an estimation of 1.4 mL/20 g of body weight. Mice were weighed and injected intraperitoneally with ketamine (100 mg/kg) and xylazine (4 mg/kg) in sterile PBS for anesthesia. Buprenex (0.1 mg/kg) was injected subcutaneously for analgesia. All mice were resuscitated with 1 mL Ringer's solution subcutaneously with 0.5 mL on each side. Mice were shaved in the right lumbar region to prepare for measuring transcutaneous glomerular filtration rate (tGFR) the next day. All mice were placed at 30°C in an incubator while they were under anesthesia to maintain body temperature. All mice were then placed individually in metabolic cages to collect urine for 22 h. At the end of 22 h, mice were again weighed and scored on the severity of the symptoms such as hind limb mobility, appearance and provoked response (Koch et al., 2016). After tGFR measurements, the mice were euthanized using an intraperitoneal injection of ketamine (100 mg/kg) and xylazine (4 mg/kg), followed by cervical dislocation.

tGFR measurement

tGFR was measured transdermally with the clearance of FITC-sinistrin (Scarfe et al., 2018). Briefly, under isoflurane anesthesia, mice were injected with FITC-sinistrin (5 mg/100 g body weight; Mannheim Pharma and Diagnostics GmbH) via retro- orbital route and the disappearance of the FITC fluorescence was monitored by a Medibeacon NIC-Kidney units with internal memory (Mannheim Pharma and Diagnostics GmbH) mounted on the lumbar region. The animals were placed in cages individually for an hour and then the data were transferred to a computer and analyzed with the MPD 1.0 software. The half-time of reduction in the blood FITC-sinistrin concentrations is proportional to GFR, which was calculated based on the manufacturer's formula.

Blood urea nitrogen measurement

Blood urea nitrogen (BUN) levels were detected with the diacetyl monoxime method (Rahmatullah and Boyde, 1980). Briefly, a chromogen was freshly prepared by mixing Reagent A (10 mg of ferric chloride dissolved in 10 mL of 1.48 M phosphoric acid mixed with 30 mL of 5.52 M sulfuric acid and 60 mL of distilled water) and Reagent B (50 mg of diacetyl monoxime and 1 mg of thiosmicarbazide dissolved in 10 mL of water) at 2: 1. The serum samples were diluted 10 times with de-ionized water. Proteins in the diluted serum were precipitated with 0.61 M trichloroacetic acid solution, and the supernatants were incubated with the chromogen at 80°C for 5 min. The absorption was measured at 490 nm.

Urinary KIM-1 assay

Urinary kidney injury molecule (KIM-1) was measured with the Mouse KIM-1 ELISA kit from Abcam (ab213477) according to the manufacturer's protocol and normalized to urinary creatinine levels that were measured with the Jaffe's method (Toora and Rajagopal, 2002). Briefly, 50 µL mouse urine sample (diluted 5 times) was incubated with 25 µL mixture of 0.75 N NaOH and 1% picric acid (1:1) at room temperature for 15 min. The absorption was recorded at 490 nm.

Histology

The kidney, lung, and liver fixed with 10% formalin for 48 h and then transferred to 70% ethanol. The tissues were embedded in a Paraplast Plus Tissue Infiltration/Embedding Medium (McCormick Scientific), sectioned at 4 µm, and stained with hematoxylin/eosin. Two to four sections of each tissue were examined by a board-certified veterinary pathologist in a blinded fashion using an Olympus BX43 light microscope with magnification ranging from 1.25X-60X. The kidney histopathology was scored based on tubular degeneration and necrosis, cast, congestion and hemorrhage. Lung histopathology was graded based on hemorrhage, congestion, pigment, edema, atelectasis and bronchio-alveolar hyperplasia. Liver histopathology was quantified based on fatty change, infiltration of neutrophils and mononuclear cells, oval cell hyperplasia, focal necrosis, congestion, karyocytomegaly, and multinucleated hepatocytes. The total score is the summation of all averages of histological change in an organ. Tissues were scored semiquantitatively by determining the percentage of relevant cells affected as follows: 0 = Normal: tissue considered to be normal under the conditions of the study. 1 = Minimal: amount of change barely exceeds normal, up to 5%; 2 = Mild: the lesion is easily identified but of limited severity, 6%–15%; 3 = Moderate: the lesion is prominent, but there is significant potential for increased severity, 16%–50%; 4 = Marked: the lesion occupies the majority of the examined tissue section but there is still potential for increased severity, 51%–90%; 5 = Severe: the degree of change is as complete as possible and unlikely to be potential for increased severity, >90%.

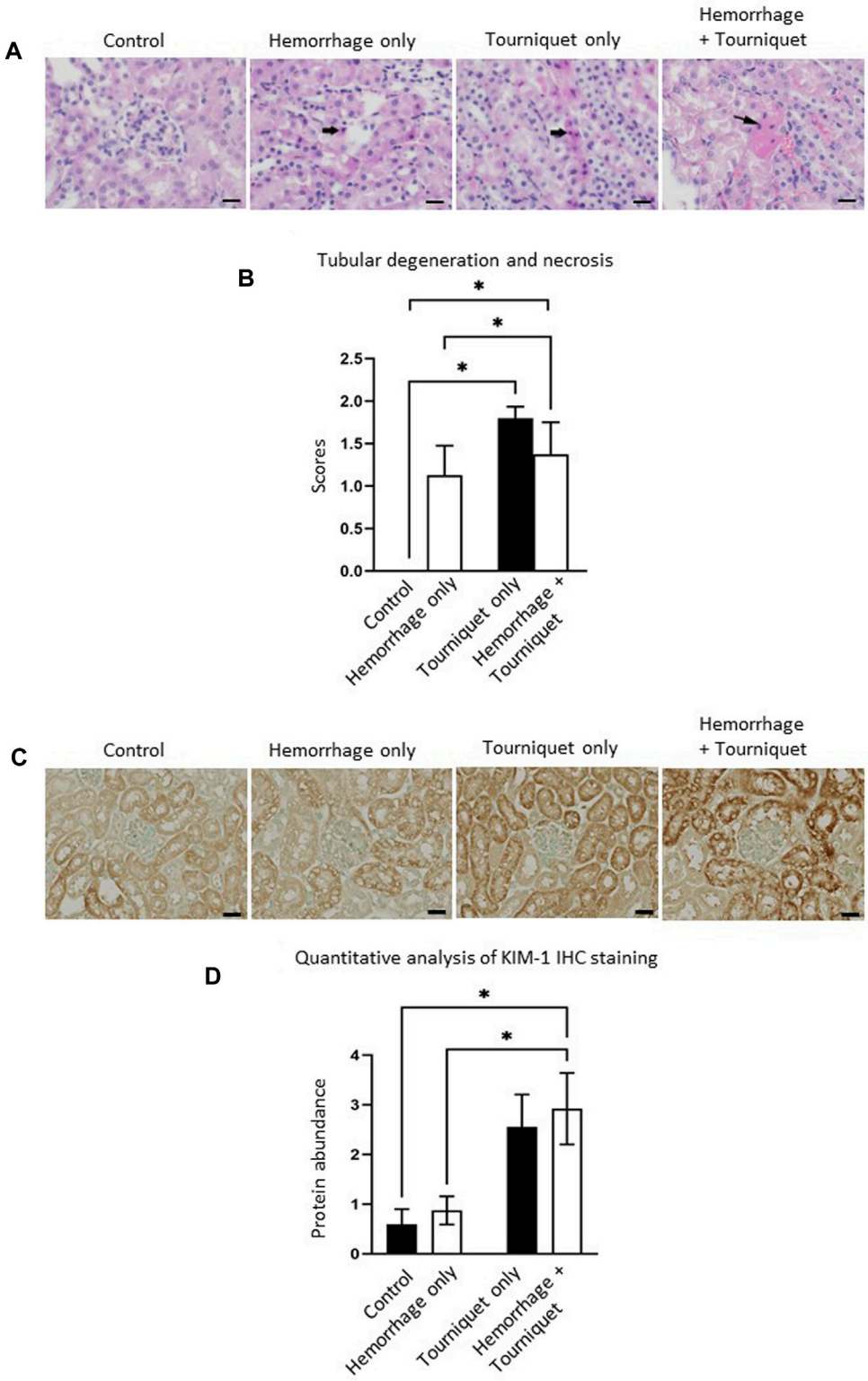

FIGURE 3
Hemorrhage potentiates TILLIR-induced injury in the renal cortex. **(A)** Representatives of TILLIR-induced renal tubular degeneration and necrosis. Increased hematoxylin/eosin staining indicates tubular degeneration and necrosis (arrow). **(B)** Compared with Control, TILLIR increased renal tubular degeneration and necrosis, but hemorrhage had no additive effect. **(C)** Representatives of TILLIR-induced increase of KIM-1 immunohistochemical staining. **(D)** TILLIR did not significantly increase KIM-1 protein abundance in the absence of hemorrhage. However, it showed a significant increase in KIM-1 protein abundance in the presence of hemorrhage when compared to the hemorrhage only group. In A and B, $n = 6$ for the control, $n = 8$ for the hemorrhage only, $n = 9$ for the tourniquet only and hemorrhage + tourniquet, respectively. In **(C,D)**, $n = 8$. *$p < 0.05$, Two-way ANOVA. Scale bars: 20 μm.

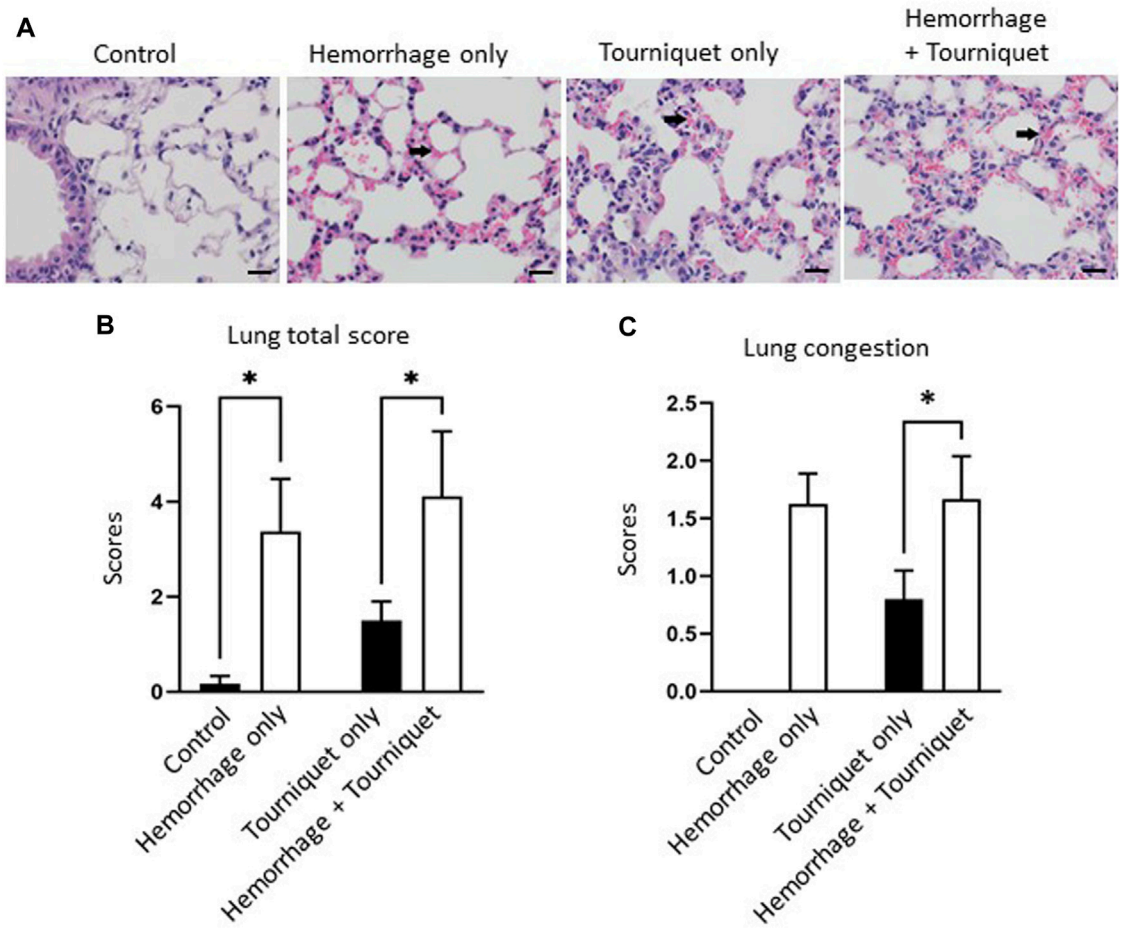

FIGURE 4
Hemorrhage potentiates TILLIR-induced structural damage in the lung. **(A)** Representatives of TILLIR-induced congestion in the lung (arrow). **(B)** Hemorrhage only increased total lung injury scores compared with the control, whereas tourniquet only did not. However, addition of hemorrhage increased total lung injury scores compared with tourniquet only. **(C)** Neither hemorrhage only nor tourniquet only induced congestion, but combination of these two did compared with tourniquet only. $n = 6$ for the control, $n = 8$ for the hemorrhage only, $n = 9$ for the tourniquet only and hemorrhage + tourniquet, respectively. *$p < 0.05$, Two-way ANOVA. Scale bars: 20 μm.

Immunohistochemistry

Immunohistochemical staining of KIM-1 was performed essentially as previously described (Packialakshmi et al., 2022). Briefly, paraffin-embedded kidney slides (4 μm) were deparaffinized and rehydrated sequentially with xylene, ethanol, and water. Endogenous peroxidase was blocked using a blocking buffer from a DAB (3,3′-Diaminobenzidine) kit (AB64264, Abcam), following the manufacturer's protocol. Antigens were exposed by incubating the slides in Antigen Retrieval Buffer (BUF025A, Bio-Rad) at 90°C for 20 min. Non-specific binding was inhibited using a blocking solution included in the DAB kit. Subsequently, slides were incubated with an anti-KIM-1 antibody (1:500 dilution, PA520244, Thermo Fisher) at room temperature for 60 min. Following washing, KIM-1 antibody binding was visualized using the DAB kit and quantified with ImageJ. The percentage of pixels in the cortex above a set threshold represented the protein abundance of KIM-1. Nuclei were stained with 1% Methyl Green (4800-30-18, R&D Systems).

Serum cytokine and chemokine assay

Blood was collected via cardiac puncture using a heparin-free needle and syringe, and then transferred into an Eppendorf tube. The sample was allowed to sit at room temperature for 30 min before being centrifuged at 1,400 rpm for 15 min at 4°C. Serum was then collected. A total of 23 cytokine and chemokine concentrations in serum were analyzed using the Bio-Plex Pro™ Mouse Cytokine Panel Plex (Bio-Rad) as previously described (Kiang et al., 2017). These cytokines and chemokines were IL-1α, IL-1β, IL-2, IL-3, IL-4, IL-5, IL-6, IL-9, IL-10, IL-12 (p40), IL-12 (p70), IL-13, IL-17, eotaxin, G-CSF, GM-CSF, IFN-γ, KC, MCP-1, MIP-1α, MIP-1β, RANTES, and TNF-α. Briefly, serum from each mouse was diluted four-fold and examined. The cytokine and chemokine levels were analyzed using Bio-Plex 200 (Bio-Rad) and quantified using MiraiBio MasterPlexH CT and QT Software (Hitachi Software Engineering America Ltd.), and concentrations were expressed in pg/mL.

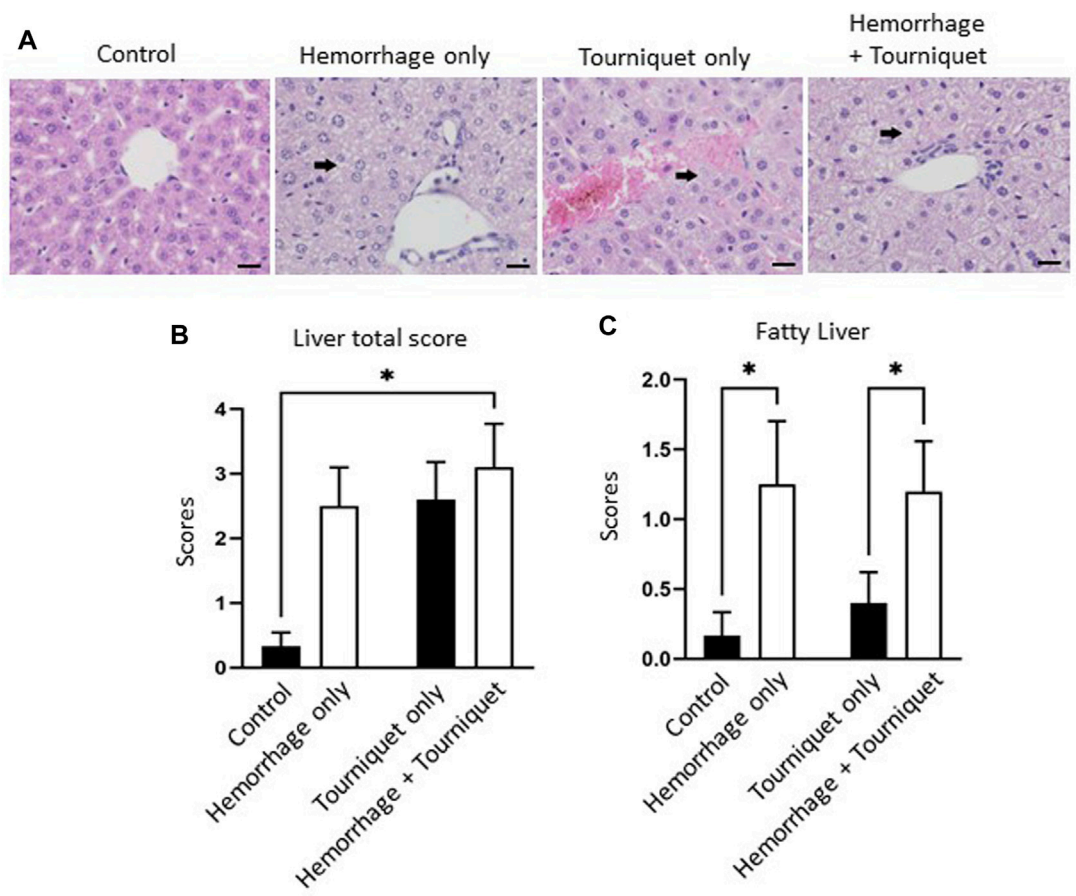

FIGURE 5
Hemorrhage potentiates TILLIR-induced structural damage in the liver. **(A)** Representatives of TILLIR-induced fat deposit in the liver (arrow). **(B)** Compared with the control, neither hemorrhage only nor tourniquet only significantly increased total liver injury scores, but combination of the two did. **(C)** In the absence of hemorrhage, tourniquet only did not increase fatty liver compared with the control, although hemorrhage only did. However, hemorrhage potentiated tourniquet-induced fatty liver. n = 6 for the control, n = 8 for the hemorrhage only, n = 9 for the tourniquet only and hemorrhage + tourniquet, respectively. *p < 0.05, Two-way ANOVA. Scale bars: 20 μm.

Statistical analysis

Data are expressed as means ± standard error of the mean. Data were analyzed with two-way ANOVA (GraphPad Prism 9.0.2). After identifying the overall significant effects of tourniquet and hemorrhage, multiple comparisons were made with Tukey's analysis. The significant effects between tourniquet and control and tourniquet and tourniquet plus hemorrhage are reported. p < 0.05 was considered significant.

Results

Hemorrhage worsens TILLIR-induced reduction in the renal function

We found that hemorrhage alone had no significant effect on tGFR, urine output, BUN or urinary KIM-1 levels as compared with the control group. Tourniquet alone significantly reduced tGFR from 928 ± 215 μL/min/100 g to 502 ± 87 μL/min/100 g, and increased BUN from 30.5 ± 7.8 mg/dL to 80.0 ± 22.2 mg/dL, urinary KIM-1 from 2.7 ± 0.4 ng/mL to 3.4 ± 0.2 ng/mL and pain score from zero to 2.5 without significantly affecting urinary output (0.9 ± 0.2 mL vs. 0.8 ± 0.1 mL) compared with the control group. However, the combination of hemorrhage with tourniquets significantly reduced tGFR and urinary output by 61% and 38%, and increased BUN, KIM-1 and pain score by 127%, 24%, and 35%, respectively, compared with tourniquet alone (Figure 2; Table 1). Neither hemorrhage alone nor the combination of hemorrhage with tourniquets had a significant effect on body weight (Table 1).

Hemorrhage potentiates TILLIR-induced structural damages in the kidney, lung and liver

Hemorrhage only, tourniquet only or hemorrhage combined with tourniquet had no significant effect on total injury scores in the kidney compared with the control or among themselves (data not shown).

TABLE 2 Averages of histopathological scores in their respective categories.

Kidney	Control	Hemorrhage only	Tourniquet only	Hemorrhage + Tourniquet
Tubular degeneration and necrosis	0.00 ± 0.00	1.13 ± 0.35	1.80 ± 0.13*	1.38 ± 0.38#
Cast	0.00 ± 0.00	0.13 ± 0.13	0.00 ± 0.00	0.25 ± 0.16
Congestion	0.00 ± 0.00	0.88 ± 0.30	1.05 ± 0.33	1.00 ± 0.38
Hemorrhage	0.00 ± 0.00	0.25 ± 0.16	0.00 ± 0.00	0.13 ± 0.13
Total scores	0.00 ± 0.00	2.38 ± 0.78	2.80 ± 0.39	2.75 ± 0.88
Lung				
Congestion	0.00 ± 0.00	1.63 ± 0.26	0.80 ± 0.25	1.67 ± 0.37&
Hemorrhage	0.17 ± 0.17	0.88 ± 0.44	0.50 ± 0.22	0.89 ± 0.45
Pigment	0.00 ± 0.00	0.38 ± 0.26	0.10 ± 0.10	0.44 ± 0.29
Edema	0.00 ± 0.00	0.25 ± 0.25	0.00 ± 0.00	0.22 ± 0.22
Atalectasis	0.00 ± 0.00	0.25 ± 0.25	0.00 ± 0.00	0.67 ± 0.33
Bronchio-Alveolar hyperplasia	0.00 ± 0.00	0.00 ± 0.00	0.10 ± 0.10	0.00 ± 0.00
Total scores	0.17 ± 0.17	3.38 ± 1.10*	1.50 ± 0.40	4.11 ± 1.37&
Liver				
Fatty change	0.17 ± 0.17	1.25 ± 0.45*	0.40 ± 0.22	1.20 ± 0.36&
Neutrophil infiltration	0.17 ± 0.17	0.00 ± 0.00	0.10 ± 0.10	0.20 ± 0.20
Mononuclear cell infiltration	0.00 ± 0.00	0.13 ± 0.13	0.10 ± 0.10	0.00 ± 0.00
Oval cell hyperplasia	0.00 ± 0.00	0.00 ± 0.00	0.30 ± 0.15	0.40 ± 0.16
Focal necrosis	0.00 ± 0.00	0.00 ± 0.00	0.10 ± 0.10	0.20 ± 0.20
Congestion	0.00 ± 0.00	0.63 ± 0.32	0.90 ± 0.31	1.10 ± 0.31
Karyocytomegaly	0.50 ± 0.34	1.00 ± 0.38	0.80 ± 0.25	1.40 ± 0.34
Multinucleated hepatocytes	0.83 ± 0.31	1.00 ± 0.38	0.70 ± 0.26	1.30 ± 0.30
Total scores	1.67 ± 0.61	4.00 ± 0.98	3.40 ± 0.50	5.80 ± 1.28*

*$p < 0.05$ vs. Control. #$p < 0.05$ vs. Hemorrhage only. &$p < 0.05$ vs. Tourniquet only.

TILLIR caused renal tubular degeneration and necrosis irrespective of hemorrhage, and combination of hemorrhage and tourniquet had no additive effect (Figure 3). In eight experiments, TILLIR exhibited a tendency to elevate the abundance of KIM-1 protein in the renal cortex when compared to the control group in the absence of hemorrhage. However, TILLIR showed a significant increase in KIM-1 protein abundance in the presence of hemorrhage when compared to the hemorrhage only (Figure 3). Compared with the control, hemorrhage only significantly increased total lung injury scores, whereas tourniquet only did not. However, combination of hemorrhage with tourniquet increased total lung injury scores as well as congestion compared with tourniquet only (Figure 4). Compared with the control, neither hemorrhage only nor tourniquet only significantly increased total liver injury scores, but combination of the two did (Figure 5). In the absence of hemorrhage, tourniquet only did not significantly increase fatty liver compared with the control, although hemorrhage only did. However, hemorrhage potentiated tourniquet-induced fatty liver (Figure 5). Averages of histopathological scores in their respective categories were provided in Table 2.

Hemorrhage only has a minor effect on TILLIR-induced cytokine and chemokine profiles in the serum

Tourniquets alone increased the concentrations of various cytokines and chemokines in the serum as compared with the control group (Table 2). Addition of hemorrhage had no significant effect on a majority of tourniquet alone-induced increases of cytokines or chemokines except for decreasing IFN-γ and RANTES levels in the serum (Table 3).

Discussion

Limb hemorrhage often occurs in both civilian and military trauma patients (Morsey et al., 2003; Arora et al., 2015; Chavez et al., 2016; De Rosa et al., 2018; Leurcharusmee et al., 2018; Kasepalu et al., 2020; BenÍtez et al., 2021; Pottecher et al., 2021; Hinojosa-Laborde et al., 2022; Paquette et al., 2022). Tourniquets are an

TABLE 3 Effects of hemorrhage on serum cytokine and chemokine concentrations (pg/mL).

	Control	Hemorrhage only	Tourniquet only	Hemorrhage + Tourniquet
IL-1α	4.2 ± 3.7	1.9 ± 1.7	27.3 ± 8.0	15.6 ± 5.8
IL-1β	7.0 ± 4.2	10.1 ± 3.3	25.1 ± 5.2	14.8 ± 3.1
IL-5	11.7 ± 10.5	69.6 ± 42.4	208.4 ± 61.9	402.2 ± 103.7*
IL-6	261.4 ± 168.8	335.5 ± 216.4	1637.4 ± 370.3*	803.9 ± 195.1
IL-10	310.9 ± 278.0	461.4 ± 412.7	3558.7 ± 965.2	2652.6 ± 926.0
IL-12 (p40)	2588.2 ± 982.6	2678.8 ± 637.2	3514.1 ± 1081.3	1245.3 ± 199.8
IL-17	ND	247.7 ± 172.3	604.0 ± 221.4	147.5 ± 71.0
KC	2149.5 ± 596.9	1776.3 ± 344.5	4594.8 ± 1290.5	2840.0 ± 354.2
G-CSF	5026.1 ± 2434.5	9214.1 ± 2502.9	28939.3 ± 6221.4*	17989.6 ± 3376.9
GM-CSF	59.8 ± 53.5	225.9 ± 116.1	821.7 ± 152.2	532.9 ± 123.7
Eotaxin	15271.5 ± 1372.3	23218.4 ± 4129.9	37404.5 ± 6012.5	29093.1 ± 6585.9
IFN-γ	ND	68.2 ± 26.6	368.4 ± 108.4*	27.9 ± 26.1$^{\&}$
TNF-α	1.0 ± 0.9	203.0 ± 83.9	532.3 ± 157.6	143.9 ± 56.1
RANTES	2972.5 ± 949.8	3041 ± 309.8	4332.2 ± 525.8	1855.9 ± 137.6$^{\&}$
MIP-1α	30.3 ± 16.7	83.9 ± 16.1	217.7 ± 59.6	90.4 ± 25.3
MIP-1β	565.7 ± 335.2	983.1 ± 379.5	2932.9 ± 936.0	723.5 ± 230.5
MCP-1	14671.5 ± 4885.0	10083.3 ± 1543.5	24807.3 ± 7309.5	13074.2 ± 1054.6

Serum cytokine and chemokine concentrations were analyzed with the Bio-Plex Pro™ Mouse Cytokine Panel Plex (Bio-Rad). *$p < 0.05$ vs. the control, $^{\&}p < 0.05$ vs. the tourniquet only (Two-way ANOVA). $n = 5$ for the control and hemorrhage only groups, $n = 10$ for the tourniquet only group and $n = 8$ for the hemorrhage + tourniquet group. ND, not detectable.

effective first-line therapy to stop extremity bleeding. In practical terms, there would be no reason to deploy tourniquets in the absence of active hemorrhage. However, conventional murine models in the literature were produced with application of tourniquets without hemorrhage (Klausner et al., 1989; Adachi et al., 2006; Hsu et al., 2012; Yang et al., 2012; Mansour et al., 2014; Kao et al., 2015a; Kao et al., 2015b; Karahan et al., 2016; Onody et al., 2016; Foster et al., 2017; Shih et al., 2018; İnce et al., 2019; Packialakshmi et al., 2022). We describe a new TILLIR injury model, which was produced by first inducing hemorrhage then applying tourniquets.

We found that this new model resulted in a greater decline in renal function and damage (as defined by tGFR, BUN, KIM-1 and urine output) compared to either hemorrhage or tourniquet placement alone. There was also the indication that combined hemorrhage and tourniquet application increased histologic damage to the liver and lung. These data indicate that hemorrhage exacerbates tourniquet-induced organ damage. These findings are consistent with the observations from clinical studies showing that hemorrhage markedly increases AKI incidence in trauma patients. For example, a 3-year multicenter observational study found that the rate of AKI in trauma patients was higher in those that presented with hemorrhagic shock (42%) compared to patients presenting without hemorrhagic shock (13%) (Harrois et al., 2018).

Multiple types of tourniquets including McGivney hemorrhoidal ligator band, controlled tension tourniquet and orthodontic rubber band have been used in murine models (Crawford et al., 2007). The orthodontic rubber band stops blood flow to the hindlimb similarly as other two types of tourniquets in mice, but causes significantly less neuromuscular dysfunction (Crawford et al., 2007). Therefore, orthodontic rubber bands have become the method of choice for tourniquets in murine models. Orthodontic rubber bands have been applied to a hindlimb either unilaterally for 3–4 h (Kato et al., 2009; Corrick et al., 2018) or bilaterally for 2–3 h (Kato et al., 2009; Yang et al., 2012). Unilateral application of tourniquets is advantageous to study neuromuscular injury in the hindlimb, because the contralateral hindlimb can serve as a control. Bilateral application of tourniquets induces severe systemic inflammation and is a good model to study tourniquet-induced secondary organ injures. As such, bilateral application of tourniquets has been used to induce acute kidney, lung and liver injures in a majority of studies (Wunder et al., 2005; Yang et al., 2012; Shih et al., 2018; Wang et al., 2022). We bled mice and then applied orthodontic rubber bands bilaterally only for 80 min. It appears that shorter times are required for tourniquets to induce organ damage in the presence of hemorrhage. However, the diameters and force of orthodontic bands used in the previous studies are not available (Wunder et al., 2005; Yang et al., 2012; Shih et al., 2018; Wang et al., 2022), therefore the variations in the severity of ischemia between our and previous studies cannot be ruled out as a potential cause. In the present study we measured GFR with a transdermal method as opposed to the serum creatinine levels, which is less sensitive than the transdermal method (Yang et al., 2012; Scarfe et al., 2018).

It is noteworthy that tourniquet alone for 80 min in the present study only induced mild AKI, whereas tourniquet alone for 76 min induced severe AKI in our previous study (Packialakshmi et al., 2022). The reason is that mice received 1 mL Ringer's solution in the present study, whereas mice in the previous study did not. It is well

known that fluid resuscitation is beneficial to most types of AKI and therefore it is commonly done in the clinical setting (Prowle and Bellomo, 2015; Michelsen et al., 2019). This is another factor that makes our new model of TILLIR more clinically relevant.

Tourniquets alone increased serum levels of various cytokines and chemokines as compared with the control. Yet, addition of hemorrhage had no significant effects on tourniquet-induced cytokines and chemokines except for reducing tourniquet-induced increase in IFN-γ (Table 2). However, whether tourniquets induce increases in cytokine and chemokine levels in the kidney and whether adding hemorrhage enhances the effects of the cytokines and chemokines remain unknown. Furthermore, we measured the serum cytokine and chemokine levels at the end of the experiments. Whether hemorrhage alters tourniquet-induced cytokines and chemokines more acutely remains to be determined.

This model still has several limitations. The amount of hemorrhage was relatively modest (up to 15% of blood volume). The impact of more severe hemorrhage on TILLIR injury remains to be elucidated. Mice were resuscitated with Ringer's solution instead of blood products, which are the first line resuscitation for hemorrhage clinically. This model lacks a skeletal muscle injury component, which is known to exacerbate AKI in rats (Xiang et al., 2021). Further, only male mice were used in the present study.

In summary, we have developed a clinically relevant mouse model of TILLIR injury by incorporating hemorrhage before applying tourniquets. With this model we have found that hemorrhage exacerbates TILLIR-induced AKI and also potentiated TILLIR-induced structural damages in the lung and liver. Further work with this model can better define the pathophysiology of TILLIR-induced multi-organ injury and identify potential therapeutic targets.

Data availability statement

The original contributions presented in the study are included in the article/supplementary material, further inquiries can be directed to the corresponding author.

Ethics statement

The animal study was approved by The institutional animal care and use committee of the Uniformed Services University of the Health Sciences. The study was conducted in accordance with the local legislation and institutional requirements.

Author contributions

DB, JK, YF, IS, and XZ designed the experiments. BP, JA, GC, SL, and XZ performed the experiments. DB, JA, JK, IS, and XZ analyzed the data. BP, JA, IS, and XZ prepared the figures. JM and XZ wrote the manuscript. DB, JA, JK, IS, and XZ revised and edited the manuscript. IS conceived the original idea and supervised the project. All authors contributed to the article and approved the submitted version.

Funding

This work was supported in part by the Departments of Medicine and Surgery at the Uniformed Services University, the Uniformed Services University Sanford Endowment Fund, the United States of America Department of Defense grants W81XWH-22-2-0068 and MED-83-12715.

Acknowledgments

Authors greatly appreciate Dr. Kevin K. Chung for his support during the course of the study, and Dr. Hong Wang for performing immunohistochemical analysis of KIM-1. Authors thank Ms. Lisa Myers and Dr. Dennis McDaniel at the Biomedical Instrument Center of the Uniformed Services University for their help in histology assay and imaging, respectively.

Conflict of interest

The authors declare that the research was conducted in the absence of any commercial or financial relationships that could be construed as a potential conflict of interest.

Publisher's note

All claims expressed in this article are solely those of the authors and do not necessarily represent those of their affiliated organizations, or those of the publisher, the editors and the reviewers. Any product that may be evaluated in this article, or claim that may be made by its manufacturer, is not guaranteed or endorsed by the publisher.

Author disclaimer

The content and views expressed in this article are the sole responsibility of the authors and do not necessarily reflect the views or policies of the Uniformed Services University or Department of Defense. Mention of trade names, commercial products, or organizations does not imply endorsement by the Uniformed Services University or Department of Defense.

References

Adachi, J., Kurisaki, E., Kudo, R., Nakagawa, K., Hatake, K., Hiraiwa, K., et al. (2006). Enhanced lipid peroxidation in tourniquet-release mice. *Clin. Chim. Acta* 371, 79–84. doi:10.1016/j.cca.2006.02.024

Andersen, R. C., Shawen, S. B., Kragh, J. F., Jr., Lebrun, C. T., Ficke, J. R., Bosse, M. J., et al. (2012). Special topics. *J. Am. Acad. Orthop. Surg.* 20 (1), S94–S98. doi:10.5435/jaaos-20-08-s94

Arora, P., Davari-Farid, S., Pourafkari, L., Gupta, A., Dosluoglu, H. H., and Nader, N. D. (2015). The effect of acute kidney injury after revascularization on the development of chronic kidney disease and mortality in patients with chronic limb ischemia. *J. Vasc. Surg.* 61, 720–727. doi:10.1016/j.jvs.2014.10.020

BenÍtez, C. Y., Ottolino, P., Pereira, B. M., Lima, D. S., Guemes, A., Khan, M., et al. (2021). Tourniquet use for civilian extremity hemorrhage: systematic review of the literature. *Rev. Col. Bras. Cir.* 48, e20202783. doi:10.1590/0100-6991e-20202783

Cai, B., Deitch, E. A., Grande, D., and Ulloa, L. (2009). Anti-inflammatory resuscitation improves survival in hemorrhage with trauma. *J. Trauma* 66, 1632–1639. doi:10.1097/TA.0b013e3181a5b179

Chavez, L. O., Leon, M., Einav, S., and Varon, J. (2016). Beyond muscle destruction: a systematic review of rhabdomyolysis for clinical practice. *Crit. Care* 20, 135. doi:10.1186/s13054-016-1314-5

Corrick, R. M., Tu, H., Zhang, D., Barksdale, A. N., Muelleman, R. L., Wadman, M. C., et al. (2018). Dexamethasone protects against tourniquet-induced acute ischemia-reperfusion injury in mouse hindlimb. *Front. Physiol.* 9, 244. doi:10.3389/fphys.2018.00244

Crawford, R. S., Hashmi, F. F., Jones, J. E., Albadawi, H., McCormack, M., Eberlin, K., et al. (2007). A novel model of acute murine hindlimb ischemia. *Am. J. Physiol. Heart Circ. Physiol.* 292, H830–H837. doi:10.1152/ajpheart.00581.2006

Curry, N., Hopewell, S., Dorée, C., Hyde, C., Brohi, K., and Stanworth, S. (2011). The acute management of trauma hemorrhage: a systematic review of randomized controlled trials. *Crit. Care* 15, R92. doi:10.1186/cc10096

De Rosa, S., Villa, G., Inaba, K., Samoni, S., and Ronco, C. (2018). Acute renal replacement therapy in patients with major extremity injuries. *Minerva Anestesiol.* 84, 747–755. doi:10.23736/S0375-9393.18.12474-6

Denk, S., Weckbach, S., Eisele, P., Braun, C. K., Wiegner, R., Ohmann, J. J., et al. (2018). Role of hemorrhagic shock in experimental polytrauma. *Shock* 49, 154–163. doi:10.1097/SHK.0000000000000925

Foster, A. D., Vicente, D., Sexton, J. J., Johnston, L., Clark, N., Leonhardt, C., et al. (2017). Administration of FTY720 during tourniquet-induced limb ischemia reperfusion injury attenuates systemic inflammation. *Mediat. Inflamm.* 2017, 4594035. doi:10.1155/2017/4594035

Gallo, L. K., Ramos, C. R., Rajani, R. R., and Benarroch-Gampel, J. (2021). Management and outcomes after upper versus lower extremity vascular trauma. *Ann. Vasc. Surg.* 76, 152–158. doi:10.1016/j.avsg.2021.05.007

Harrois, A., Soyer, B., Gauss, T., Hamada, S., Raux, M., Duranteau, J., et al. (2018). Prevalence and risk factors for acute kidney injury among trauma patients: a multicenter cohort study. *Crit. Care* 22, 344. doi:10.1186/s13054-018-2265-9

Hinojosa-Laborde, C., Hudson, I. L., Ross, E., Xiang, L., and Ryan, K. L. (2022). Pathophysiology of hemorrhage as it relates to the warfighter. *Physiol. (Bethesda)* 37, 141–153. doi:10.1152/physiol.00028.2021

Hsu, K. Y., Chen, C. H., Shih, P. C., and Huang, C. J. (2012). Adverse effects of bilateral lower limb ischemia-reperfusion on inducing kidney injuries in rats could be ameliorated by platonin. *Acta Anaesthesiol. Taiwan* 50, 63–68. doi:10.1016/j.aat.2012.05.010

İnce, İ., Akar, İ., and Arıcı, A. (2019). Renoprotective effect of edaravone in acute limb ischemia/reperfusion injury. *Turk Gogus Kalp Damar Cerrahisi Derg.* 28, 274–281. doi:10.5606/tgkdc.dergisi.2020.18905

Kao, M. C., Chung, C. Y., Chang, Y. Y., Lin, C. K., Sheu, J. R., and Huang, C. J. (2015a). Salutary effects of cepharanthine against skeletal muscle and kidney injuries following limb ischemia/reperfusion. *Evid. Based Complement. Altern. Med.* 2015, 504061. doi:10.1155/2015/504061

Kao, M. C., Yang, C. H., Chou, W. C., Sheu, J. R., and Huang, C. J. (2015b). Cepharanthine mitigates lung injury in lower limb ischemia-reperfusion. *J. Surg. Res.* 199, 647–656. doi:10.1016/j.jss.2015.06.041

Karahan, M. A., Yalcin, S., Aydogan, H., Buyukfirat, E., Kucuk, A., Kocarslan, S., et al. (2016). Curcumin and dexmedetomidine prevents oxidative stress and renal injury in hind limb ischemia/reperfusion injury in a rat model. *Ren. Fail* 38, 693–698. doi:10.3109/0886022X.2016.1157746

Kasepalu, T., Kuusik, K., Lepner, U., Starkopf, J., Zilmer, M., Eha, J., et al. (2020). Remote ischaemic preconditioning reduces kidney injury biomarkers in patients undergoing open surgical lower limb revascularisation: a randomised trial. *Oxid. Med. Cell Longev.* 2020, 7098505. doi:10.1155/2020/7098505

Kato, N., Abe, S., Suto, M., and Hiraiwa, K. (2009). Comparison of renal dysfunction in wild-type, IL-6 KO and iNOS KO mice hind limb tourniquet-reperfusion model. *Leg. Med. (Tokyo)* 11 (1), S248–S251. doi:10.1016/j.legalmed.2009.03.006

Kher, A., Meldrum, K. K., Wang, M., Tsai, B. M., Pitcher, J. M., and Meldrum, D. R. (2005). Cellular and molecular mechanisms of sex differences in renal ischemia-reperfusion injury. *Cardiovasc Res.* 67, 594–603. doi:10.1016/j.cardiores.2005.05.005

Kiang, J. G., Smith, J. T., Anderson, M. N., Elliott, T. B., Gupta, P., Balakathiresan, N. S., et al. (2017). Hemorrhage enhances cytokine, complement component 3, and caspase-3, and regulates microRNAs associated with intestinal damage after whole-body gamma-irradiation in combined injury. *PLoS One* 12, e0184393. doi:10.1371/journal.pone.0184393

Klausner, J. M., Paterson, I. S., Kobzik, L., Valeri, C. R., Shepro, D., and Hechtman, H. B. (1989). Leukotrienes but not complement mediate limb ischemia-induced lung injury. *Ann. Surg.* 209, 462–470. doi:10.1097/00000658-198904000-00012

Koch, A., Gulani, J., King, G., Hieber, K., Chappell, M., and Ossetrova, N. (2016). Establishment of early endpoints in mouse total-body irradiation model. *PLoS One* 11, e0161079. doi:10.1371/journal.pone.0161079

Kragh, J. F., Jr., Walters, T. J., Baer, D. G., Fox, C. J., Wade, C. E., Salinas, J., et al. (2008). Practical use of emergency tourniquets to stop bleeding in major limb trauma. *J. Trauma* 64, S38–S49. doi:10.1097/TA.0b013e31816086b1

Leurcharusmee, P., Sawaddiruk, P., Punjasawadwong, Y., Chattipakorn, N., and Chattipakorn, S. C. (2018). The possible pathophysiological outcomes and mechanisms of tourniquet-induced ischemia-reperfusion injury during total knee arthroplasty. *Oxid. Med. Cell Longev.* 2018, 8087598. doi:10.1155/2018/8087598

Mansour, Z., Charles, A. L., Kindo, M., Pottecher, J., Chamaraux-Tran, T. N., Lejay, A., et al. (2014). Remote effects of lower limb ischemia-reperfusion: impaired lung, unchanged liver, and stimulated kidney oxidative capacities. *Biomed. Res. Int.* 2014, 392390. doi:10.1155/2014/392390

Michelsen, J., Cordtz, J., Liboriussen, L., Behzadi, M. T., Ibsen, M., Damholt, M. B., et al. (2019). Prevention of rhabdomyolysis-induced acute kidney injury - a DASAIM/DSIT clinical practice guideline. *Acta Anaesthesiol. Scand.* 63, 576–586. doi:10.1111/aas.13308

Morsey, H., Aslam, M., and Standfield, N. (2003). Patients with critical ischemia of the lower limb are at risk of developing kidney dysfunction. *Am. J. Surg.* 185, 360–363. doi:10.1016/s0002-9610(02)01406-x

Muñoz, B., Schobel, S. A., Lisboa, F. A., Khatri, V., Grey, S. F., Dente, C. J., et al. (2020). Clinical risk factors and inflammatory biomarkers of post-traumatic acute kidney injury in combat patients. *Surgery* 168, 662–670. doi:10.1016/j.surg.2020.04.064

Onody, P., Aranyi, P., Turoczi, Z., Stangl, R., Fulop, A., Dudas, E., et al. (2016). Levosimendan administration in limb ischemia: multicomponent signaling serving kidney protection. *PLoS One* 11, e0163675. doi:10.1371/journal.pone.0163675

Packialakshmi, B., Stewart, I. J., Burmeister, D. M., Chung, K. K., and Zhou, X. (2020). Large animal models for translational research in acute kidney injury. *Ren. Fail* 42, 1042–1058. doi:10.1080/0886022X.2020.1830108

Packialakshmi, B., Stewart, I. J., Burmeister, D. M., Feng, Y., McDaniel, D. P., Chung, K. K., et al. (2022). Tourniquet-induced lower limb ischemia/reperfusion reduces mitochondrial function by decreasing mitochondrial biogenesis in acute kidney injury in mice. *Physiol. Rep.* 10, e15181. doi:10.14814/phy2.15181

Paquette, R., Wampler, D., Schaefer, R., Blume, A., Casillas, H., Echols, B., et al. (2022). Prehospital tourniquet usage and diabetes mellitus associated with increased incidence, odds, and risk of acute kidney injury: a pilot study. *Prehosp Disaster Med.* 37, 360–364. doi:10.1017/S1049023X2200067X

Park, K. M., Kim, J. I., Ahn, Y., Bonventre, A. J., and Bonventre, J. V. (2004). Testosterone is responsible for enhanced susceptibility of males to ischemic renal injury. *J. Biol. Chem.* 279, 52282–52292. doi:10.1074/jbc.M407629200

Pottecher, J., Lefort, H., Adam, P., Barbier, O., Bouzat, P., Charbit, J., et al. (2021). Guidelines for the acute care of severe limb trauma patients. *Anaesth. Crit. Care Pain Med.* 40, 100862. doi:10.1016/j.accpm.2021.100862

Prowle, J. R., and Bellomo, R. (2015). Sepsis-associated acute kidney injury: macrohemodynamic and microhemodynamic alterations in the renal circulation. *Semin. Nephrol.* 35, 64–74. doi:10.1016/j.semnephrol.2015.01.007

Rahmatullah, M., and Boyde, T. R. (1980). Improvements in the determination of urea using diacetyl monoxime; methods with and without deproteinisation. *Clin. Chim. Acta* 107, 3–9. doi:10.1016/0009-8981(80)90407-6

Scarfe, L., Schock-Kusch, D., Ressel, L., Friedemann, J., Shulhevich, Y., Murray, P., et al. (2018). Transdermal measurement of glomerular filtration rate in mice. *J. Vis. Exp.*, 58520. doi:10.3791/58520

Scerbo, M. H., Holcomb, J. B., Taub, E., Gates, K., Love, J. D., Wade, C. E., et al. (2017). The trauma center is too late: major limb trauma without a pre-hospital tourniquet has increased death from hemorrhagic shock. *J. Trauma Acute Care Surg.* 83, 1165–1172. doi:10.1097/TA.0000000000001666

Shih, J. M., Shih, Y. M., Hou, Y. C., Pai, M. H., Yeh, C. L., and Yeh, S. L. (2018). Effects of fish oil-based lipid emulsion on inflammation and kidney injury in mice subjected to unilateral hind limb ischemia/reperfusion. *Cytokine* 111, 49–57. doi:10.1016/j.cyto.2018.07.035

Simon, F., Oberhuber, A., Floros, N., Busch, A., Wagenhäuser, M. U., Schelzig, H., et al. (2018). Acute limb ischemia-much more than just a lack of oxygen. *Int. J. Mol. Sci.* 19, 374. doi:10.3390/ijms19020374

Tirumala, V., Klemt, C., Oganseyan, R., Walker, P., Padmanabha, A., and Kwon, Y. M. (2021). Outcomes of tourniquet-less revision total knee arthroplasty: a matched cohort analysis. *J. Am. Acad. Orthop. Surg.* 29, e1343–e1352. doi:10.5435/JAAOS-D-20-00796

Toora, B. D., and Rajagopal, G. (2002). Measurement of creatinine by Jaffe's reaction-determination of concentration of sodium hydroxide required for maximum color development in standard, urine and protein free filtrate of serum. *Indian J. Exp. Biol.* 40, 352–354.

Wang, L., Ding, Y., Bai, Y., Shi, J., Li, J., and Wang, X. (2022). The activation of SIRT3 by dexmedetomidine mitigates limb ischemia-reperfusion-induced lung injury. *Ann. Transl. Med.* 10, 319. doi:10.21037/atm-22-711

Wunder, C., Brock, R. W., Frantz, S., Göttsch, W., Morawietz, H., Roewer, N., et al. (2005). Carbon monoxide, but not endothelin-1, plays a major role for the hepatic microcirculation in a murine model of early systemic inflammation. *Crit. Care Med.* 33, 2323–2331. doi:10.1097/01.ccm.0000182794.42733.71

Xiang, L., Calderon, A. S., Klemcke, H. G., Hudson, I. L., Hinojosa-Laborde, C., Chung, K. K., et al. (2021). Extremity trauma exacerbates acute kidney injury following prolonged hemorrhagic hypotension. *J. Trauma Acute Care Surg.* 91, S113–s123. doi:10.1097/TA.0000000000003311

Yang, X. H., Wang, Y. H., Wang, J. J., Liu, Y. C., Deng, W., Qin, C., et al. (2012). Role of angiotensin-converting enzyme (ACE and ACE2) imbalance on tourniquet-induced remote kidney injury in a mouse hindlimb ischemia-reperfusion model. *Peptides* 36, 60–70. doi:10.1016/j.peptides.2012.04.024

Yassin, M. M., Barros D'Sa, A. A., Parks, T. G., Soong, C. V., Halliday, M. I., McCaigue, M. D., et al. (1998). Lower limb ischaemia-reperfusion injury causes endotoxaemia and endogenous antiendotoxin antibody consumption but not bacterial translocation. *Br. J. Surg.* 85, 785–789. doi:10.1046/j.1365-2168.1998.00717.x

Zhou, X. (2022). A step forward toward establishing a novel preclinical porcine model to study ischemia/reperfusion-induced acute and chronic kidney injures. *Transl. Androl. Urol.* 11, 575–577. doi:10.21037/tau-22-176

Zhou, X. (2023). Reducing oxygen demand to alleviate acute kidney injury. *Front. Biosci. (Landmark Ed.* 28, 62. doi:10.31083/j.fbl2803062

frontiers | Frontiers in Physiology

TYPE Mini Review
PUBLISHED 15 November 2023
DOI 10.3389/fphys.2023.1322288

OPEN ACCESS

EDITED BY
Belisario Enrique Fernandez,
University Institute of Health Sciences, Argentina

REVIEWED BY
Silvana Lorena Della Penna,
University of Twente, Netherlands

*CORRESPONDENCE
Xiaoyan Zhang,
xyzhang@hsc.ecnu.edu.cn

RECEIVED 16 October 2023
ACCEPTED 07 November 2023
PUBLISHED 15 November 2023

CITATION
Guo Y, Luo T, Xie G and Zhang X (2023), Bile acid receptors and renal regulation of water homeostasis.
Front. Physiol. 14:1322288.
doi: 10.3389/fphys.2023.1322288

Bile acid receptors and renal regulation of water homeostasis

Yanlin Guo[1,2], Taotao Luo[1], Guixiang Xie[1] and Xiaoyan Zhang[1,2]*

[1]Division of Nephrology, Wuhu Hospital, East China Normal University, Wuhu, China, [2]Health Science Center, East China Normal University, Shanghai, China

The kidney is the key organ responsible for maintaining the body's water and electrolyte homeostasis. About 99% of the primary urine filtered from the Bowman's capsule is reabsorbed along various renal tubules every day, with only 1–2 L of urine excreted. Aquaporins (AQPs) play a vital role in water reabsorption in the kidney. Currently, a variety of molecules are found to be involved in the process of urine concentration by regulating the expression or activity of AQPs, such as antidiuretic hormone, renin-angiotensin-aldosterone system (RAAS), prostaglandin, and several nuclear receptors. As the main bile acid receptors, farnesoid X receptor (FXR) and membrane G protein-coupled bile acid receptor 1 (TGR5) play important roles in bile acid, glucose, lipid, and energy metabolism. In the kidney, FXR and TGR5 exhibit broad expression across all segments of renal tubules, and their activation holds significant therapeutic potential for numerous acute and chronic kidney diseases through alleviating renal lipid accumulation, inflammation, oxidative stress, and fibrosis. Emerging evidence has demonstrated that the genetic deletion of FXR or TGR5 exhibits increased basal urine output, suggesting that bile acid receptors play a critical role in urine concentration. Here, we briefly summarize the function of bile acid receptors in renal water reabsorption and urine concentration.

KEYWORDS

FXR, tgr5, aquaporin, kidney, water homeostasis

Introduction

The kidney is a vital organ that receives 20%–25% of an adult human's cardiac output and controls the metabolism of salt and water. About 180 L of filtrate are produced daily by an adult human kidney, but only 1–2 L of urine are expelled, with 99% of the primary urine being reabsorbed along various renal tubules.

Many factors are involved in the progress of urine concentration. Firstly, the hypertonic environment of the inner medullary is a necessary condition for urine concentration, which promotes the reabsorption of water. The hypertonic environment is mainly due to the accumulation of urea and sodium chloride in the inner medullary, where $Na^+/K^+/2Cl^-$cotransporter (NKCC2) and urea transporters play an important role in this process. Secondly, aquaporins also play important roles in this process. Eight aquaporins, including AQP1-7 and AQP11, have been identified in the kidney (Noda et al., 2010). Among them, AQP1 is expressed on both the apical and basolateral membrane of the proximal tubule, as well as the thin descending limb of the loop of Henle and the vasa recta (Chou et al., 1999), responsible for the reabsorption of about 80% of the water in primary urine. AQP2 is highly expressed in the apical membrane and subapical vesicles of principal cells in the renal collecting duct, responsible for about 20% of water reabsorption (Kwon et al., 2013). Mice that do not have AQP1, AQP2, AQP3, or AQP4 genes exhibit a significant increase in urine production (Yang et al., 2001). Finally, The Epithelial sodium

channel (ENaC) is important for sodium and water reabsorption, which is located in the apical membrane of the collecting ducts. ENaC facilitates Na^+ reabsorption and then the movement of Na^+ creates an osmotic gradient, allowing water to follow in the same direction.

Currently, it has been reported that a variety of molecules are involved in regulating the reabsorption of water in the kidney. Antidiuretic hormone (ADH) or arginine vasopressin (AVP) is a critical hormone synthesized in the hypothalamus that plays a key role in water homeostasis. In the renal collecting duct, AVP binds to the V2 receptor (V2R) and increases the phosphorylation of AQP2 by the cAMP-PKA pathway. Recently, increasing evidence has demonstrated that AVP played a critical role in facilitating urinary concentration via activating ENaC (Mironova et al., 2012; Mironova et al., 2015; Stockand et al., 2022; Wang et al., 2022). Moreover, AVP also rapidly increased water and urea transport in the terminal inner medullary collecting duct (IMCD) by increasing the expression and apical membrane trafficking of the urea transporter A1 (UT-A1) (Sands et al., 2011). The renin-angiotensin-aldosterone system (RAAS) additionally contributes to the regulation of water and sodium reabsorption in the kidney. Angiotensin II has different effects on different parts of the kidneys. In the proximal tubules, it heightens the activity of sodium/hydrogen exchanger and sodium-bicarbonate cotransporter through binding to the Angiotensin II receptor type 1 (AT1) receptor. In the distal tubule and collecting ducts, Angiotensin II further amplifies the activity of sodium-chloride cotransporter (NCC) and ENaC, which increases the reabsorption of water and sodium. Additionally, Angiotensin II increases aldosterone levels, which promotes sodium reabsorption by binding to the mineralocorticoid receptor (Harrison-Bernard, 2009; Zaika et al., 2013). Prostaglandin E2 (PGE2) is the main cyclooxygenase metabolite of arachidonic acid (AA). It is primarily synthesized in the medullary collecting tubule of the kidney (Bonvalet et al., 1987). EP1-4 are the 4 G protein-coupled receptors (GPCRs) of PGE2. Among these, EP1 and EP3 have high expression in the basolateral membrane of the collecting duct, respectively. When these receptors are activated, less sodium chloride and water are absorbed, which increases the excretion of sodium ions and urine (Ando and Asano, 1995; Guan et al., 1998; Breyer and Breyer, 2001; Nasrallah et al., 2018). In the kidney, EP2 expression is low, however, the activation of EP2 increased AQP2 membrane targeting (Olesen et al., 2016). The primary function of EP4, which is mostly expressed in glomeruli, is to control the release of renin (Breyer and Breyer, 2001). In the collecting ducts, disruption of EP4 impaired urinary concentration via decreasing AQP2 through the cAMP/PKA pathway (Gao et al., 2015). Several nuclear receptors have been implicated in regulating water homeostasis. Activation of peroxisome proliferator-activated receptor γ (PPARγ) increased the water and sodium reabsorption through the ENaC and AQP2 (Guan et al., 2005; Zhou et al., 2015). The activation of the glucocorticoid receptor (GR) enhanced the AQP2 gene expression induced by AVP in the collecting duct cell (Su et al., 2020). Liver X receptor β (LXRβ) knockout mice also exhibited polyuria due to decreased AVP and AQP1 (Gabbi et al., 2012), and increased ubiquitination of AQP2 protein (Su et al., 2017). The administration of estradiol decreased the expression of AQP2 by binding to estrogen receptor α, consequently leading to an increase in urine output in ovariectomized rats (Cheema et al., 2015).

Increasing evidence suggests that bile acid receptors play a crucial role in regulating renal water and sodium reabsorption. In this article, we will review the general functions of two bile acid receptors, nuclear receptor FXR, and membrane receptor TGR5, and finally focus on their roles in renal water and sodium homeostasis, offering novel strategies for addressing disorders related to water and salt metabolism, such as diabetes insipidus.

Classification and general function of bile acid receptors

The liver is responsible for the synthesis of primary bile acids, specifically cholic acid (CA) and chenodeoxycholic acid (CDCA). These primary bile acids are subsequently conjugated and excreted into the intestine. Within the gut, they were metabolized by the gut microbiota, leading to the formation of secondary bile acids, namely, lithocholic acid (LCA) and deoxycholic acid (DCA) (Wang et al., 1999). In the intestine, roughly 95% of bile acids are reabsorbed into hepatocytes, with only a small fraction entering the bloodstream. Initially, these circulating bile acids go through glomerular filtration but are nearly completely reabsorbed in the proximal renal tubules, facilitated by the apical sodium-dependent bile acid transporter (ASBT) and the basolateral Organic Solute Transporter α/β (OSTα/β). Consequently, only about 5% of the filtered bile acids end up in the urine each day (Stiehl, 1974; Herman-Edelstein et al., 2018). Bile acids play crucial roles in various physiological and pathophysiological processes by binding and activating the nuclear receptor FXR and the membrane G protein-coupled receptor TGR5.

FXR is a member of the nuclear receptor (NR) superfamily that controls the transcription of specific target genes. It exhibits prominent expression in organs such as the liver, kidney, and small intestine. As the endogenous ligand of FXR, bile acids activate FXR in the following order: CDCA > DCA > LCA > CA (Wang et al., 1999). Upon activation, FXR assumes critical roles in the regulation of various metabolic pathways, including bile acid, glucose, and lipid metabolism (Guo et al., 2023). Notably, it acts to inhibit the production and accumulation of bile acids in the liver and intestines (Liu et al., 2003; Boyer et al., 2006; Landrier et al., 2006). Additionally, the activation of FXR increases glycogen synthesis and reduces glycolysis (Zhang et al., 2006; Caron et al., 2013; Dong et al., 2019). Furthermore, it reduced the accumulation of lipids in the kidney in insulin-resistance animal models (Nakahara et al., 2002; Zhang et al., 2006; Lai et al., 2022). Recently, several studies reported that overexpression of FXR in the kidney substantially alleviated hypertension and elevated renal nitric oxide (NO) levels, which was achieved by stimulating the expression of endothelial nitric oxide synthase (eNOS) in a mouse model of hypertension induced by an 8-week regimen of 20% fructose in drinking water combined with a 4% sodium chloride diet (referred to as HFS) (Ghebremariam et al., 2013; Li et al., 2015). In the kidney, activation of FXR attenuated acute kidney injury caused by cisplatin and renal ischemia–reperfusion (I/R) through regulating apoptosis, ferroptosis, and autophagy (Bae et al., 2014; Gai et al., 2017; Luan et al., 2021; Zhang et al., 2022). Additionally, FXR agonists also improved renal inflammation, fibrosis, lipid accumulation, and glucose metabolism disorders, which prevented the progression of chronic kidney disease (Evans et al., 2009; Wang et al., 2010; Zhou et al., 2016; Marquardt et al., 2017).

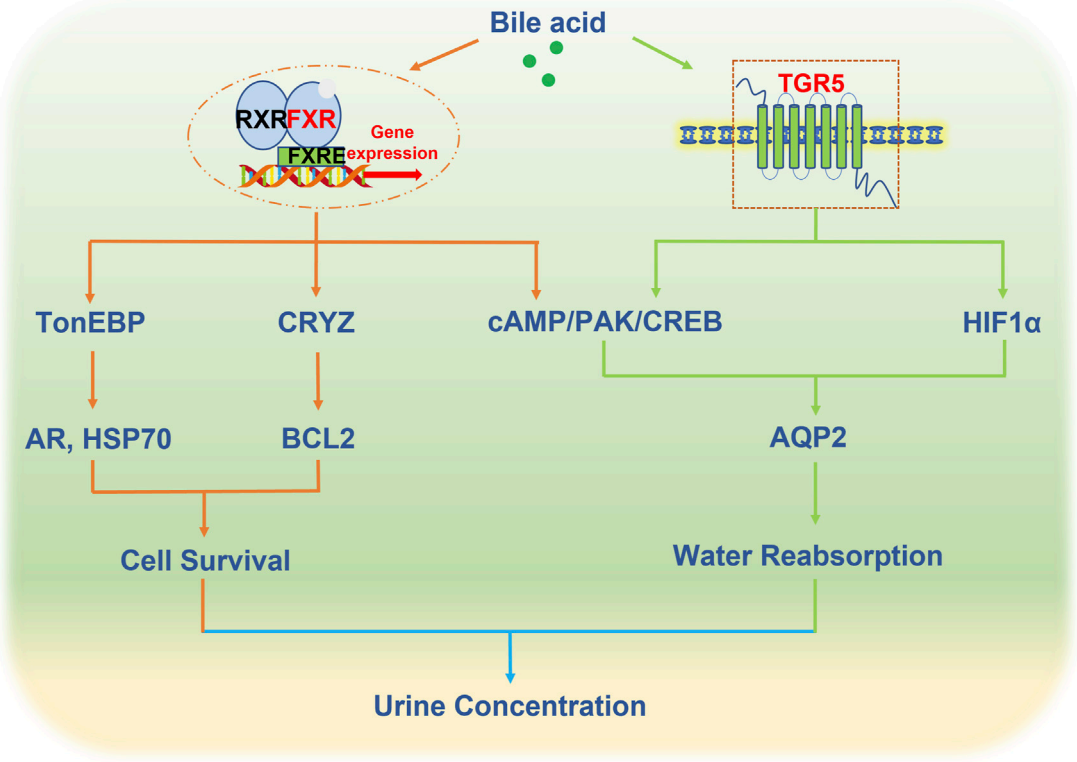

FIGURE 1
Bile acid receptors in the regulation of urine concentration.

TGR5 is a membrane receptor of bile acids, which can be bound and activated by various endogenous bile acids, especially LCA. TGR5 is expressed in various tissues, such as the kidney, liver, digestive tract, and central nervous system (Poole et al., 2010). Many studies have demonstrated that it plays a significant role in multiple physiological processes, as well as the pathogenesis of various metabolic diseases (Reich et al., 2021; Tian et al., 2022; Chen et al., 2023). Activation of TGR5 results in coupling with a stimulatory G-alpha-protein (Gαs) which, in turn, activates the cAMP-PKA signaling pathway. This cascade of events results in the phosphorylation of the cAMP response element binding protein (CREB) and its subsequent nuclear import, ultimately leading to the activation of the target genes. When activated, TGR5 promotes GLP-1 secretion from enteroendocrine L cells (Li et al., 2017), mitochondrial thermogenesis in adipocytes (Velazquez-Villegas et al., 2018), and protected against lipopolysaccharide (LPS)-induced liver inflammation by decreasing inflammatory cytokine secretion (Wang et al., 2011). In the kidney, TGR5 activation has been found to alleviate renal I/R injury by reducing inflammation and macrophage migration (Zhang et al., 2019). Furthermore, it has also been observed that the activation of TGR5 can prevent renal inflammation and fibrosis by inhibiting the NF-κB pathway in diabetic mice induced by streptozotocin (STZ) (Xiao et al., 2020). Moreover, a selective TGR5 agonist INT-777 has been shown to ameliorate proteinuria and podocyte injury in diabetic db/db mice (Wang et al., 2016). In addition, TGR5 activation also decreased the high glucose-induced fibrosis in glomerular mesangial cells (GMCs) (Yang et al., 2016). Recently studies have also revealed that the deubiquitination of TGR5 at K306 residue also restored TGR5 expression and protected db/db mice from diabetic nephropathy (Lin et al., 2023).

Currently, there are some studies on dual FXR and TGR5 agonists in the kidney. Diabetic mice treated with the dual FXR/TGR5 agonist INT-767 showed an improvement in proteinuria and prevention of podocyte injury, mesangial expansion, and tubulointerstitial fibrosis (Wang et al., 2016). The same dual agonist reduced the proteinuria and fibronectin accumulation in aging mice (Wang et al., 2017). These findings indicate a potential role of dual FXR/TGR5 agonists in the regulation of many kidney diseases.

Bile acid receptors and kidney water homeostasis

As mentioned above, about 95% of the bile acids synthesized from the liver are recycled through the enterohepatic circulation. In the kidney, approximately 100 μmol bile acids are filtered in the glomeruli per day, and almost all of them are reabsorbed in the proximal tubule. Only 1–2 μmol/day is excreted in the urine (Dawson et al., 2009). The renal tubules, especially the collecting duct, express high levels of bile acid receptors FXR and TGR5, where water is reabsorption through aquaporins to complete the final step of urine concentration, suggesting that FXR and TGR5 may play an important role in the regulation of water homeostasis. Whether the activation of the bile acid receptor in collecting ducts plays a significant role in water homeostasis is worth studying.

Farnesoid X receptor and renal water reabsorption

In the kidney, FXR exhibits high expression levels in various renal tubules, especially the collecting duct. However, the current study of FXR in water reabsorption only reveals its role in collecting ducts. FXR plays a pivotal role in the regulation of urine volume. FXR knockout mice displayed diminished urine concentrating ability in comparison to WT mice, and its activation by binding with CDCA or a synthetic agonist GW4064 increased urinary concentrating capacity, mainly by increasing renal AQP2 expression (Zhang et al., 2014). Moreover, MCDs are exposed to a massive hypertonic environment, which is critical in regulating urine concentration. FXR can prevent hypertonic-induced apoptosis of MCDs by activating tonicity response enhancer-binding protein (TonEBP), a critical transcription factor responsible for facilitating the cellular accumulation of organic osmolytes to resist the hyperosmotic stress through increasing the expression of the target genes, including aldose reductase (AR) and heat shock protein 70 (HSP70) (Xu et al., 2018). Recently, studies revealed that crystallin zeta (CRYZ), a direct target gene of FXR, increased the NKCC2 expression to help maintain medullary hyperosmotic gradient. Additionally, overexpressing CRYZ reduced the cell death caused by hypertonicity by elevating the expression of B-cell lymphoma 2 (BCL2). These data demonstrated that FXR plays a critical role in the regulation of urine volume by increasing the expression of AQP2 and promoting the survival of MCDs in a dehydrated state. The above results proved the physiological function of FXR in water reabsorption, but its role in the pathophysiological state such as diabetes insipidus is still unclear. Moreover, recent evidence also showed that enhanced urinary excretion of bile acids in some conditions such as cholestasis may cause the injury of tubular epithelial cells, and FXR agonist obeticholic acid (OCA) ameliorated the renal tubular damage in bile duct ligation (BDL) induced hepatorenal syndrome (HRS) (Tsai et al., 2020). Low urine volume also existed in HRS mainly caused by a reduction in renal blood flow, it is not known the effect of increased bile acids in renal tubules on the expression of AQPs and water reabsorption.

TGR5 and renal water reabsorption

In normal kidney tissue, TGR5 exhibited high expression in collecting ducts, distal convoluted tubules, and the thin loop of Henle, with minimal or sporadic weak staining in the proximal tubules (Zhao et al., 2018). Different from the study of FXR in water reabsorption focusing on physiological levels, the study of TGR5 in AQP2 regulation is mainly carried out in kidney diseases. Lithium is a frequently prescribed medication for managing bipolar disorder, which may cause multiple endocrinopathies including nephrogenic diabetes insipidus (NDI). In a mouse model of lithium-induced nephrogenic diabetes insipidus, the activation of TGR5 by INT-777 or INT-767 elevated the expression of AQP2 through the cAMP/PKA signaling pathway (Li et al., 2018). Acute kidney injury is a common clinical disease, accompanied by changes in urine output. With the progression of the disease, oliguria, anuria, and polyuria can occur. In the I/R-induced AKI rat model, urinary output was significantly decreased, accompanied by the loss of renal AQP1, AQP2, and AQP3 in the cortex and outer medulla (Hussein et al., 2012; Asvapromtada et al., 2018; Liu et al., 2021). While the activation of TGR5 by LCA or INT-777 effectively prevented the downregulation of renal AQP2 in I/R-induced kidney injury through activating HIF-1α signaling (Han et al., 2021). These findings support the potential role of TGR5 in the regulation of renal water reabsorption.

Perspectives

FXR and TGR5, as bile acid receptors, play an important role in renal water homeostasis through regulating the expression and trafficking of AQP2, which provides a novel therapeutic for the treatment of water and salt metabolism disorders such as diabetes insipidus (Figure 1). However, the mechanism of bile acids in the regulation of water homeostasis is largely unknown. Firstly, there are 8 types of aquaporins in the kidney, in addition to affecting AQP2, whether the activation of bile acid receptors affects other aquaporins is worth exploring. Secondly, AVP synthesized in the hypothalamus regulates AQP2 expression. Recently studies revealed that FXR and TGR5 were expressed in the hypothalamus (Castellanos-Jankiewicz et al., 2021; Deckmyn et al., 2021), and circulating bile acids can also reach the hypothalamus (Xu, 2018). Whether bile acid receptors affect AVP secretion remains to be investigated. Thirdly, in addition to aquaporins, other ion channels such as ENac can also indirectly affect water reabsorption. At present, research has not delved into the direct regulation of ENaC by either FXR or TGR5 in the kidney, but several studies have reported that ENaC is regulated by bile acids in overexpressed human ENaC *Xenopus laevis* oocytes (Ilyaskin et al., 2016; Wang et al., 2019).

Author contributions

YG: Writing–original draft. TL: Writing–original draft. GX: Writing–original draft. XZ: Funding acquisition, Writing–review and editing.

Funding

The author(s) declare financial support was received for the research, authorship, and/or publication of this article. The following funding sources provided support for this project: Grants 82270703, 81970606, and 81970595 from the National Natural Science Foundation of China, as well as the East China Normal University Medicine and Health Joint Fund (2022JKXYD03001).

Conflict of interest

The authors declare that the research was conducted in the absence of any commercial or financial relationships that could be construed as a potential conflict of interest.

Publisher's note

References

Ando, Y., and Asano, Y. (1995). Luminal prostaglandin E2 modulates sodium and water transport in rabbit cortical collecting ducts. *Am. J. Physiology-Renal Physiology* 268, F1093–F1101. doi:10.1152/ajprenal.1995.268.6.F1093

Asvapromtada, S., Sonoda, H., Kinouchi, M., Oshikawa, S., Takahashi, S., Hoshino, Y., et al. (2018). Characterization of urinary exosomal release of aquaporin-1 and -2 after renal ischemia-reperfusion in rats. *Am. J. Physiol. Ren. Physiol.* 314, F584-F601–f601. doi:10.1152/ajprenal.00184.2017

Bae, E. H., Choi, H. S., Joo, S. Y., Kim, I. J., Kim, C. S., Choi, J. S., et al. (2014). Farnesoid X receptor ligand prevents cisplatin-induced kidney injury by enhancing small heterodimer partner. *PLoS One* 9, e86553. doi:10.1371/journal.pone.0086553

Bonvalet, J. P., Pradelles, P., and Farman, N. (1987). Segmental synthesis and actions of prostaglandins along the nephron. *Am. J. Physiol.* 253, F377–F387. doi:10.1152/ajprenal.1987.253.3.F377

Boyer, J. L., Trauner, M., Mennone, A., Soroka, C. J., Cai, S.-Y., Moustafa, T., et al. (2006). Upregulation of a basolateral FXR-dependent bile acid efflux transporter OSTalpha-OSTbeta in cholestasis in humans and rodents. *Am. J. Physiology-Gastrointestinal Liver Physiology* 290, G1124–G1130. doi:10.1152/ajpgi.00539.2005

Breyer, M. D., and Breyer, R. M. (2001). G protein-coupled prostanoid receptors and the kidney. *Annu. Rev. Physiol.* 63, 579–605. doi:10.1146/annurev.physiol.63.1.579

Caron, S., Huaman Samanez, C., Dehondt, H., Ploton, M., Briand, O., Lien, F., et al. (2013). Farnesoid X receptor inhibits the transcriptional activity of carbohydrate response element binding protein in human hepatocytes. *Mol. Cell Biol.* 33, 2202–2211. doi:10.1128/MCB.01004-12

Castellanos-Jankiewicz, A., Guzmán-Quevedo, O., Fénelon, V. S., Zizzari, P., Quarta, C., Bellocchio, L., et al. (2021). Hypothalamic bile acid-TGR5 signaling protects from obesity. *Cell Metab.* 33, 1483–1492.e10. doi:10.1016/j.cmet.2021.04.009

Cheema, M. U., Irsik, D. L., Wang, Y., Miller-Little, W., Hyndman, K. A., Marks, E. S., et al. (2015). Estradiol regulates AQP2 expression in the collecting duct: a novel inhibitory role for estrogen receptor α. *Am. J. Physiol. Ren. Physiol.* 309, F305–F317. doi:10.1152/ajprenal.00685.2014

Chen, B., Bai, Y., Tong, F., Yan, J., Zhang, R., Zhong, Y., et al. (2023). Glycoursodeoxycholic acid regulates bile acids level and alters gut microbiota and glycolipid metabolism to attenuate diabetes. *Gut Microbes* 15, 2192155. doi:10.1080/19490976.2023.2192155

Chou, C. L., Knepper, M. A., Hoek, A. N., Brown, D., Yang, B., Ma, T., et al. (1999). Reduced water permeability and altered ultrastructure in thin descending limb of Henle in aquaporin-1 null mice. *J. Clin. Invest.* 103, 491–496. doi:10.1172/JCI5704

Dawson, P. A., Lan, T., and Rao, A. (2009). Bile acid transporters. *J. Lipid Res.* 50, 2340–2357. doi:10.1194/jlr.R900012-JLR200

Deckmyn, B., Domenger, D., Blondel, C., Ducastel, S., Nicolas, E., Dorchies, E., et al. (2021). Farnesoid X receptor activation in brain alters Brown adipose tissue function via the sympathetic system. *Front. Mol. Neurosci.* 14, 808603. doi:10.3389/fnmol.2021.808603

Dong, R., Yang, X., Wang, C., Liu, K., Liu, Z., Ma, X., et al. (2019). Yangonin protects against non-alcoholic fatty liver disease through farnesoid X receptor. *Phytomedicine* 53, 134–142. doi:10.1016/j.phymed.2018.09.006

Evans, M. J., Mahaney, P. E., Borges-Marcucci, L., Lai, K., Wang, S., Krueger, J. A., et al. (2009). A synthetic farnesoid X receptor (FXR) agonist promotes cholesterol lowering in models of dyslipidemia. *Am. J. Physiol. Gastrointest. Liver Physiol.* 296, G543–G552. doi:10.1152/ajpgi.90585.2008

Gabbi, C., Kong, X., Suzuki, H., Kim, H. J., Gao, M., Jia, X., et al. (2012). Central diabetes insipidus associated with impaired renal aquaporin-1 expression in mice lacking liver X receptor β. *Proc. Natl. Acad. Sci. U. S. A.* 109, 3030–3034. doi:10.1073/pnas.1200588109

Gai, Z., Chu, L., Xu, Z., Song, X., Sun, D., and Kullak-Ublick, G. A. (2017). Farnesoid X receptor activation protects the kidney from ischemia-reperfusion damage. *Sci. Rep.* 7, 9815. doi:10.1038/s41598-017-10168-6

Gao, M., Cao, R., Du, S., Jia, X., Zheng, S., Huang, S., et al. (2015). Disruption of prostaglandin E2 receptor EP4 impairs urinary concentration via decreasing aquaporin 2 in renal collecting ducts. *Proc. Natl. Acad. Sci. U. S. A.* 112, 8397–8402. doi:10.1073/pnas.1509565112

Ghebremariam, Y. T., Yamada, K., Lee, J. C., Johnson, C. L., Atzler, D., Anderssohn, M., et al. (2013). FXR agonist INT-747 upregulates DDAH expression and enhances insulin sensitivity in high-salt fed Dahl rats. *PLoS One* 8, e60653. doi:10.1371/journal.pone.0060653

Guan, Y., Hao, C., Cha, D. R., Rao, R., Lu, W., Kohan, D. E., et al. (2005). Thiazolidinediones expand body fluid volume through PPARgamma stimulation of ENaC-mediated renal salt absorption. *Nat. Med.* 11, 861–866. doi:10.1038/nm1278

Guan, Y., Zhang, Y., Breyer, R. M., Fowler, B., Davis, L., Hébert, R. L., et al. (1998). Prostaglandin E2 inhibits renal collecting duct Na+ absorption by activating the EP1 receptor. *J. Clin. Invest.* 102, 194–201. doi:10.1172/JCI2872

Guo, Y., Xie, G., and Zhang, X. (2023). Role of FXR in renal Physiology and kidney diseases. *Int. J. Mol. Sci.* 24, 2408. doi:10.3390/ijms24032408

Han, M., Li, S., Xie, H., Liu, Q., Wang, A., Hu, S., et al. (2021). Activation of TGR5 restores AQP2 expression via the HIF pathway in renal ischemia-reperfusion injury. *Am. J. Physiology-Renal Physiology* 320, F308–F321. doi:10.1152/ajprenal.00577.2020

Harrison-Bernard, L. M. (2009). The renal renin-angiotensin system. *Adv. Physiology Educ.* 33, 270–274. doi:10.1152/advan.00049.2009

Herman-Edelstein, M., Weinstein, T., and Levi, M. (2018). Bile acid receptors and the kidney. *Curr. Opin. Nephrol. Hypertens.* 27, 56–62. doi:10.1097/MNH.0000000000000374

Hussein, A. A., El-Dken, Z. H., Barakat, N., and Abol-Enein, H. (2012). Renal ischaemia/reperfusion injury: possible role of aquaporins. *Acta Physiol. (Oxf)* 204, 308–316. doi:10.1111/j.1748-1716.2011.02372.x

Ilyaskin, A. V., Diakov, A., Korbmacher, C., and Haerteis, S. (2016). Activation of the human epithelial sodium channel (ENaC) by bile acids involves the degenerin site. *J. Biol. Chem.* 291, 19835–19847. doi:10.1074/jbc.M116.726471

Kwon, T. H., Frøkiær, J., and Nielsen, S. (2013). Regulation of aquaporin-2 in the kidney: a molecular mechanism of body-water homeostasis. *Kidney Res. Clin. Pract.* 32, 96–102. doi:10.1016/j.krcp.2013.07.005

Lai, C. R., Tsai, Y. L., Tsai, W. C., Chen, T. M., Chang, H. H., Changchien, C. Y., et al. (2022). Farnesoid X receptor overexpression decreases the migration, invasion and angiogenesis of human bladder cancers via AMPK activation and cholesterol biosynthesis inhibition. *Cancers (Basel)* 14, 4398. doi:10.3390/cancers14184398

Landrier, J.-F., Eloranta, J. J., Vavricka, S. R., and Kullak-Ublick, G. A. (2006). The nuclear receptor for bile acids, FXR, transactivates human organic solute transporter-alpha and -beta genes. *Am. J. Physiology-Gastrointestinal Liver Physiology* 290, G476–G485. doi:10.1152/ajpgi.00430.2005

Li, C., Li, J., Weng, X., Lan, X., and Chi, X. (2015). Farnesoid X receptor agonist CDCA reduces blood pressure and regulates vascular tone in spontaneously hypertensive rats. *J. Am. Soc. Hypertens.* 9, 507–516. doi:10.1016/j.jash.2015.04.006

Li, S., Qiu, M., Kong, Y., Zhao, X., Choi, H. J., Reich, M., et al. (2018). Bile acid G protein-coupled membrane receptor TGR5 modulates aquaporin 2-mediated water homeostasis. *J. Am. Soc. Nephrol.* 29, 2658–2670. doi:10.1681/ASN.2018030271

Li, Y., Cheng, K. C., Niu, C. S., Lo, S. H., Cheng, J. T., and Niu, H. S. (2017). Investigation of triamterene as an inhibitor of the TGR5 receptor: identification in cells and animals. *Drug Des. Devel Ther.* 11, 1127–1134. doi:10.2147/DDDT.S131892

Lin, Z., Li, S., Xiao, H., Xu, Z., Li, C., Zeng, J., et al. (2023). The degradation of TGR5 mediated by Smurf1 contributes to diabetic nephropathy. *Cell Rep.* 42, 112851. doi:10.1016/j.celrep.2023.112851

Liu, Q., Kong, Y., Guo, X., Liang, B., Xie, H., Hu, S., et al. (2021). GSK-3β inhibitor TDZD-8 prevents reduction of aquaporin-1 expression via activating autophagy under renal ischemia reperfusion injury. *Faseb J.* 35, e21809. doi:10.1096/fj.202100549R

Liu, Y., Binz, J., Numerick, M. J., Dennis, S., Luo, G., Desai, B., et al. (2003). Hepatoprotection by the farnesoid X receptor agonist GW4064 in rat models of intra-and extrahepatic cholestasis. *J. Clin. investigation* 112, 1678–1687. doi:10.1172/JCI18945

Luan, Z. L., Ming, W. H., Sun, X. W., Zhang, C., Zhou, Y., Zheng, F., et al. (2021). A naturally occurring FXR agonist, alisol B 23-acetate, protects against renal ischemia-reperfusion injury. *Am. J. Physiol. Ren. Physiol.* 321, F617–f628. doi:10.1152/ajprenal.00193.2021

Marquardt, A., Al-Dabet, M. M., Ghosh, S., Kohli, S., Manoharan, J., Elwakiel, A., et al. (2017). Farnesoid X receptor agonism protects against diabetic tubulopathy: potential add-on therapy for diabetic nephropathy. *J. Am. Soc. Nephrol.* 28, 3182–3189. doi:10.1681/ASN.2016101123

Mironova, E., Bugaj, V., Roos, K. P., Kohan, D. E., and Stockand, J. D. (2012). Aldosterone-independent regulation of the epithelial Na+ channel (ENaC) by vasopressin in adrenalectomized mice. *Proc. Natl. Acad. Sci. U. S. A.* 109, 10095–10100. doi:10.1073/pnas.1201978109

Mironova, E., Chen, Y., Pao, A. C., Roos, K. P., Kohan, D. E., Bugaj, V., et al. (2015). Activation of ENaC by AVP contributes to the urinary concentrating mechanism and dilution of plasma. *Am. J. Physiol. Ren. Physiol.* 308, F237–F243. doi:10.1152/ajprenal.00246.2014

Nakahara, M., Fujii, H., Maloney, P. R., Shimizu, M., and Sato, R. (2002). Bile acids enhance low density lipoprotein receptor gene expression via a MAPK cascade-mediated stabilization of mRNA. *J. Biol. Chem.* 277, 37229–37234. doi:10.1074/jbc.M206749200

Nasrallah, R., Zimpelmann, J., Eckert, D., Ghossein, J., Geddes, S., Beique, J. C., et al. (2018). PGE(2) EP(1) receptor inhibits vasopressin-dependent water reabsorption and sodium transport in mouse collecting duct. *Lab. Invest.* 98, 360–370. doi:10.1038/labinvest.2017.133

Noda, Y., Sohara, E., Ohta, E., and Sasaki, S. (2010). Aquaporins in kidney pathophysiology. *Nat. Rev. Nephrol.* 6, 168–178. doi:10.1038/nrneph.2009.231

Olesen, E. T., Moeller, H. B., Assentoft, M., Macaulay, N., and Fenton, R. A. (2016). The vasopressin type 2 receptor and prostaglandin receptors EP2 and EP4 can increase aquaporin-2 plasma membrane targeting through a cAMP-independent pathway. *Am. J. Physiol. Ren. Physiol.* 311, F935-F944–f944. doi:10.1152/ajprenal.00559.2015

Poole, D. P., Godfrey, C., Cattaruzza, F., Cottrell, G. S., Kirkland, J. G., Pelayo, J. C., et al. (2010). Expression and function of the bile acid receptor GpBAR1 (TGR5) in the murine enteric nervous system. *Neurogastroenterol. Motil.* 22 (814-25), 814–825. doi:10.1111/j.1365-2982.2010.01487.x

Reich, M., Spomer, L., Klindt, C., Fuchs, K., Stindt, J., Deutschmann, K., et al. (2021). Downregulation of TGR5 (GPBAR1) in biliary epithelial cells contributes to the pathogenesis of sclerosing cholangitis. *J. Hepatol.* 75, 634–646. doi:10.1016/j.jhep.2021.03.029

Sands, J. M., Blount, M. A., and Klein, J. D. (2011). Regulation of renal urea transport by vasopressin. *Trans. Am. Clin. Climatol. Assoc.* 122, 82–92.

Stiehl, A. (1974). Bile salt sulphates in cholestasis. *Eur. J. Clin. Invest.* 4, 59–63. doi:10.1111/j.1365-2362.1974.tb00373.x

Stockand, J. D., Mironova, E. V., Xiang, H., Soares, A. G., Contreras, J., Mccormick, J. A., et al. (2022). Chronic activation of vasopressin-2 receptors induces hypertension in Liddle mice by promoting Na(+) and water retention. *Am. J. Physiol. Ren. Physiol.* 323, F468–f478. doi:10.1152/ajprenal.00384.2021

Su, S.-H., Ho, C.-H., and Yu, M.-J. (2020). Glucocorticoid receptor maintains vasopressin-regulated water reabsorption pathway in the kidney collecting duct cells. *FASEB J.* 34, 1. doi:10.1096/fasebj.2020.34.s1.05129

Su, W., Huang, S. Z., Gao, M., Kong, X. M., Gustafsson, J., Xu, S. J., et al. (2017). Liver X receptor β increases aquaporin 2 protein level via a posttranscriptional mechanism in renal collecting ducts. *Am. J. Physiol. Ren. Physiol.* 312, F619-F628–f628. doi:10.1152/ajprenal.00564.2016

Tian, F., Xu, W., Chen, L., Chen, T., Feng, X., Chen, J., et al. (2022). Ginsenoside compound K increases glucagon-like peptide-1 release and L-cell abundance in db/db mice through TGR5/YAP signaling. *Int. Immunopharmacol.* 113, 109405. doi:10.1016/j.intimp.2022.109405

Tsai, Y. L., Liu, C. W., Hsu, C. F., Huang, C. C., Lin, M. W., Huang, S. F., et al. (2020). Obeticholic acid ameliorates hepatorenal syndrome in ascitic cirrhotic rats by down-regulating the renal 8-iso-PGF2α-activated COX-TXA2 pathway. *Clin. Sci. (Lond)* 134, 2055–2073. doi:10.1042/CS20200452

Velazquez-Villegas, L. A., Perino, A., Lemos, V., Zietak, M., Nomura, M., Pols, T. W. H., et al. (2018). TGR5 signalling promotes mitochondrial fission and beige remodelling of white adipose tissue. *Nat. Commun.* 9, 245. doi:10.1038/s41467-017-02068-0

Wang, H., Chen, J., Hollister, K., Sowers, L. C., and Forman, B. M. (1999). Endogenous bile acids are ligands for the nuclear receptor FXR/BAR. *Mol. Cell* 3, 543–553. doi:10.1016/s1097-2765(00)80348-2

Wang, X. P., Im, S. J., Balchak, D. M., Montalbetti, N., Carattino, M. D., Ray, E. C., et al. (2019). Murine epithelial sodium (Na(+)) channel regulation by biliary factors. *J. Biol. Chem.* 294, 10182–10193. doi:10.1074/jbc.RA119.007394

Wang, X. P., Tomilin, V., Nickerson, A. J., Tian, R., Ertem, M., Mckernan, A., et al. (2022). Bile acids regulate the epithelial Na(+) channel in native tissues through direct binding at multiple sites. *J. Physiol.* 600, 4695–4711. doi:10.1113/JP283318

Wang, X. X., Edelstein, M. H., Gafter, U., Qiu, L., Luo, Y., Dobrinskikh, E., et al. (2016). G protein-coupled bile acid receptor TGR5 activation inhibits kidney disease in obesity and diabetes. *J. Am. Soc. Nephrol.* 27, 1362–1378. doi:10.1681/ASN.2014121271

Wang, X. X., Jiang, T., Shen, Y., Caldas, Y., Miyazaki-Anzai, S., Santamaria, H., et al. (2010). Diabetic nephropathy is accelerated by farnesoid X receptor deficiency and inhibited by farnesoid X receptor activation in a type 1 diabetes model. *Diabetes* 59, 2916–2927. doi:10.2337/db10-0019

Wang, X. X., Luo, Y., Wang, D., Adorini, L., Pruzanski, M., Dobrinskikh, E., et al. (2017). A dual agonist of farnesoid X receptor (FXR) and the G protein-coupled receptor TGR5, INT-767, reverses age-related kidney disease in mice. *J. Biol. Chem.* 292, 12018–12024. doi:10.1074/jbc.C117.794982

Wang, Y. D., Chen, W. D., Yu, D., Forman, B. M., and Huang, W. (2011). The G-protein-coupled bile acid receptor, Gpbar1 (TGR5), negatively regulates hepatic inflammatory response through antagonizing nuclear factor κ light-chain enhancer of activated B cells (NF-κB) in mice. *Hepatology* 54, 1421–1432. doi:10.1002/hep.24525

Xiao, H., Sun, X., Liu, R., Chen, Z., Lin, Z., Yang, Y., et al. (2020). Gentiopicroside activates the bile acid receptor Gpbar1 (TGR5) to repress NF-kappaB pathway and ameliorate diabetic nephropathy. *Pharmacol. Res.* 151, 104559. doi:10.1016/j.phrs.2019.104559

Xu, A. W. (2018). Hypothalamic sensing of bile acids, a gut feeling. *Trends Endocrinol. Metab.* 29, 363–366. doi:10.1016/j.tem.2018.02.001

Xu, S., Huang, S., Luan, Z., Chen, T., Wei, Y., Xing, M., et al. (2018). Farnesoid X receptor is essential for the survival of renal medullary collecting duct cells under hypertonic stress. *Proc. Natl. Acad. Sci. U. S. A.* 115, 5600–5605. doi:10.1073/pnas.1803945115

Yang, B., Ma, T., and Verkman, A. S. (2001). Erythrocyte water permeability and renal function in double knockout mice lacking aquaporin-1 and aquaporin-3. *J. Biol. Chem.* 276, 624–628. doi:10.1074/jbc.M008664200

Yang, Z., Xiong, F., Wang, Y., Gong, W., Huang, J., Chen, C., et al. (2016). TGR5 activation suppressed S1P/S1P2 signaling and resisted high glucose-induced fibrosis in glomerular mesangial cells. *Pharmacol. Res.* 111, 226–236. doi:10.1016/j.phrs.2016.05.035

Zaika, O., Mamenko, M., Staruschenko, A., and Pochynyuk, O. (2013). Direct activation of ENaC by angiotensin II: recent advances and new insights. *Curr. Hypertens. Rep.* 15, 17–24. doi:10.1007/s11906-012-0316-1

Zhang, L., Fu, X., Gui, T., Wang, T., Wang, Z., Kullak-Ublick, G. A., et al. (2019). Effects of farnesiferol B on ischemia-reperfusion-induced renal damage, inflammation, and NF-κB signaling. *Int. J. Mol. Sci.* 20, 6280. doi:10.3390/ijms20246280

Zhang, L., Li, A., Huang, Z., Wang, Y., and Yi, B. (2022). Knockout of farnesoid X receptor gene aggravates cisplatin-induced kidney injury. *Zhong Nan Da Xue Xue Bao Yi Xue Ban.* 47, 174–182. doi:10.11817/j.issn.1672-7347.2022.210423

Zhang, X., Huang, S., Gao, M., Liu, J., Jia, X., Han, Q., et al. (2014). Farnesoid X receptor (FXR) gene deficiency impairs urine concentration in mice. *Proc. Natl. Acad. Sci. U. S. A.* 111, 2277–2282. doi:10.1073/pnas.1323977111

Zhang, Y., Lee, F. Y., Barrera, G., Lee, H., Vales, C., Gonzalez, F. J., et al. (2006). Activation of the nuclear receptor FXR improves hyperglycemia and hyperlipidemia in diabetic mice. *Proc. Natl. Acad. Sci.* 103, 1006–1011. doi:10.1073/pnas.0506982103

Zhao, C. L., Amin, A., Hui, Y., Yang, D., and Cao, W. (2018). TGR5 expression in normal kidney and renal neoplasms. *Diagn. Pathol.* 13, 22. doi:10.1186/s13000-018-0700-5

Zhou, B., Feng, B., Qin, Z., Zhao, Y., Chen, Y., Shi, Z., et al. (2016). Activation of farnesoid X receptor downregulates visfatin and attenuates diabetic nephropathy. *Mol. Cell. Endocrinol.* 419, 72–82. doi:10.1016/j.mce.2015.10.001

Zhou, L., Panasiuk, A., Downton, M., Zhao, D., Yang, B., Jia, Z., et al. (2015). Systemic PPARγ deletion causes severe disturbance in fluid homeostasis in mice. *Physiol. Genomics* 47, 541–547. doi:10.1152/physiolgenomics.00066.2015

frontiers | Frontiers in Physiology

TYPE Review
PUBLISHED 23 November 2023
DOI 10.3389/fphys.2023.1283597

OPEN ACCESS

EDITED BY
Youfei Guan,
Dalian Medical University, China

REVIEWED BY
Giuseppe Coppolino,
University Magna Graecia of Catanzaro, Italy
Francisco Rodriguez-Esparragón,
Servicio Canario de la Salud, Spain

*CORRESPONDENCE
Chenchen Zou,
nlkbjyczcc@163.com

RECEIVED 26 August 2023
ACCEPTED 13 November 2023
PUBLISHED 23 November 2023

CITATION
Zou C (2023), Advances in the study of miRNAs in chronic kidney disease with cardiovascular complications.
Front. Physiol. 14:1283597.
doi: 10.3389/fphys.2023.1283597

Advances in the study of miRNAs in chronic kidney disease with cardiovascular complications

Chenchen Zou*

Department of Geriatrics, Jiangyin Hospital of Traditional Chinese Medicine, Wuxi, Jiangsu, China

Chronic kidney disease (CKD) is characterised by gradual loss of renal function and cardiovascular disease (CVD) as its principal consequence. CVD is a substantial source of morbidity and death in the CKD population and a growing global concern. Because there are no reliable early biomarkers to follow the progression of CKD and predict the risk of complications, research into such molecules continues. Many studies have demonstrated that miRNAs are potentially important variables in CKD, are very stable in blood, and may be employed as diagnostic and prognostic markers for various disorders. Vascular calcification (VC) is a cell-mediated process that necessitates genetic defects in the combined cardiovascular issues of CKD and may be modulated in part by miRNAs. Numerous miRNAs have been linked to the progression of vascular calcification. Many miRNAs have been discovered as being important in ventricular hypertrophy, including miRNA-30, miRNA-212, and miRNA-133. Endothelium miR-126, miR-92a-3p, and others are important regulators of angiogenesis, endothelium repair, and homeostasis. Several interesting non-invasive miRNA biomarkers in CKD/CVD have been found, with the potential to enhance diagnostic accuracy, predict prognosis, track disease progression, and serve as novel therapy targets. However, large-scale clinical studies are still needed to determine the therapeutic utility of miRNA.

KEYWORDS

chronic kidney disease, cardiovascular disease, miRNAs, advanced manufacturing, study

Introduction

Chronic kidney disease (CKD) is a progressive chronic condition with a high morbidity and death rate, particularly in people with diabetes and high blood pressure. It is a major public health concern that can potentially become the world's fifth leading cause of death (Kalantar-Zadeh et al., 2021). The risk of cardiovascular disease (CVD) for those with CKD is commonly acknowledged to be increasing, and adverse cardiovascular events continuously increase as the illness worsens. Cardiovascular diseases are a common cause of death in people with chronic kidney disease (CKD) and those with end-stage kidney disease (ESKD), accounting for a significant portion of the deaths in the dialysis community, accounting for more than half of all documented cases. The United States Renal Data System (USRDS) determined in 2020 that the burden imposed by cardiovascular disease (CVD) was much greater on those with chronic kidney disease (CKD) than on those without this illness (Matsushita et al., 2022). CVD was more frequent in advanced CKD patients, with a prevalence of 75.3% in CKD stage 4–5 patients, compared to 66.6% and 63.4% in CKD stage 3 patients and CKD stage 1–2 patients, respectively. The incidence of CVD was 37.5% greater in patients without CKD than in persons with CKD. A recent CCDFRS study (Wang et al., 2023) found that the

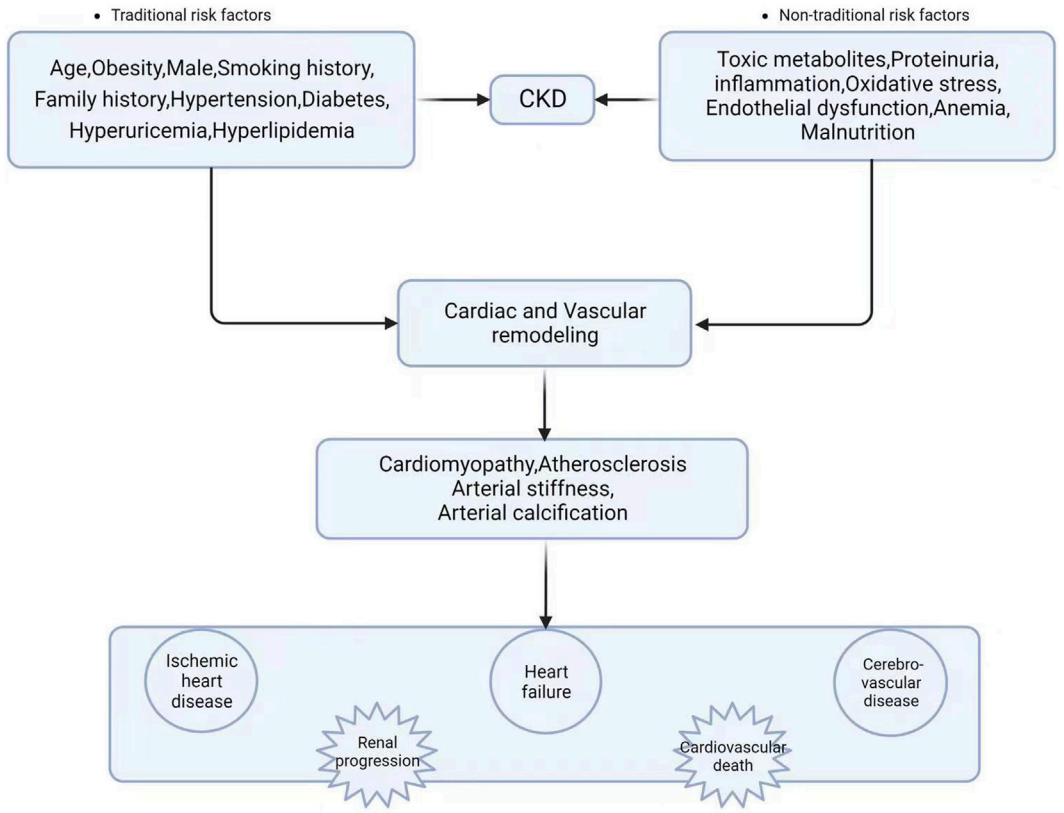

FIGURE 1
Risk factors associated with CKD combined with CVD and complications (Created with BioRender).

prevalence of CKD in Chinese adults was 8.2%, with CVD occurring at a rate of 20.6%. CVD mortality has increased in ESKD patients, accounting for 51% of known fatalities among ESKD patients from 2011 to 2013 and 53% and 55% of known deaths among peritoneal dialysis and hemodialysis patients, respectively, in 2018 (Doshi and Wish, 2022). While it is widely assumed that traditional risk factors for cardiovascular disease, such as hypertension, advanced age, dyslipidemia, and diabetes mellitus, are frequently observed in people with chronic kidney disease (CKD), it is important to note that there are additional, unconventional risk factors that are unique to CKD patients. Figure 1 (Sarnak et al., 2003) shows that these "nontraditional" factors include malnutrition, volume overload, anaemia, inflammation, and oxidative stress. Cardiovascular issues such as cardiomyopathy, left ventricular hypertrophy, vascular calcification, and atherosclerosis are more common in CKD patients due to impaired renal function (Sarnak et al., 2003). As a result, CVD increases the risk of morbidity and mortality in CKD patients and is the major cause of death (Lim et al., 2021). Furthermore, the chance of chronic kidney disease (CKD) advancing to end-stage kidney disease (ESKD) increases in tandem with the severity of hypertension. Specifically, CKD patients with mean arterial pressures of 180/100 mmHg had a 15-fold higher risk of developing ESKD than CKD patients with normal blood pressure values (Lim et al., 2021). Troponin and brain natriuretic peptide (BNP), two of the most often utilised indicators in this field, remain increased in CKD patients, perhaps due to decreased renal clearance (Mirna et al., 2020). As a result, their clinical utility in CKD patients is limited. As a result, novel biomarkers are particularly needed to improve the diagnosis and risk stratification of various disease entities for proactive prevention, early detection, prompt intervention, and to reduce the financial burden on patients.

Serum microRNAs are highly stable in the circulatory system and are excellent diagnostic indicators in various diseases (Carracedo et al., 2020). A relationship between miRNA levels and CKD has been discovered in cellular and animal models. Numerous studies have shown that miRNAs have the potential to be indispensable in the area of CKD, and changed miRNA expression has been linked to the initiation and progression of numerous pathological processes, including diabetic nephropathy, renal cancer, and kidney damage. Moreover, because of their intrinsic stability and varied amounts inside both strong and damaged physiological tissues, circulating miRNAs in the circulation play an important role in maintaining the balance of cardiovascular dynamics. Numerous studies have demonstrated that miRNAs can operate as important regulators in CKD-associated CVD signalling pathways, and they are also thought to be biomarkers for the diagnosis and prognosis of a range of illnesses, notably CKD-associated CVDs (Carracedo et al., 2020).

miRNAs——the core of gene regulation

The participation of a recently discovered category of particles known as short non-coding RNAs (200 nucleotides, which includes

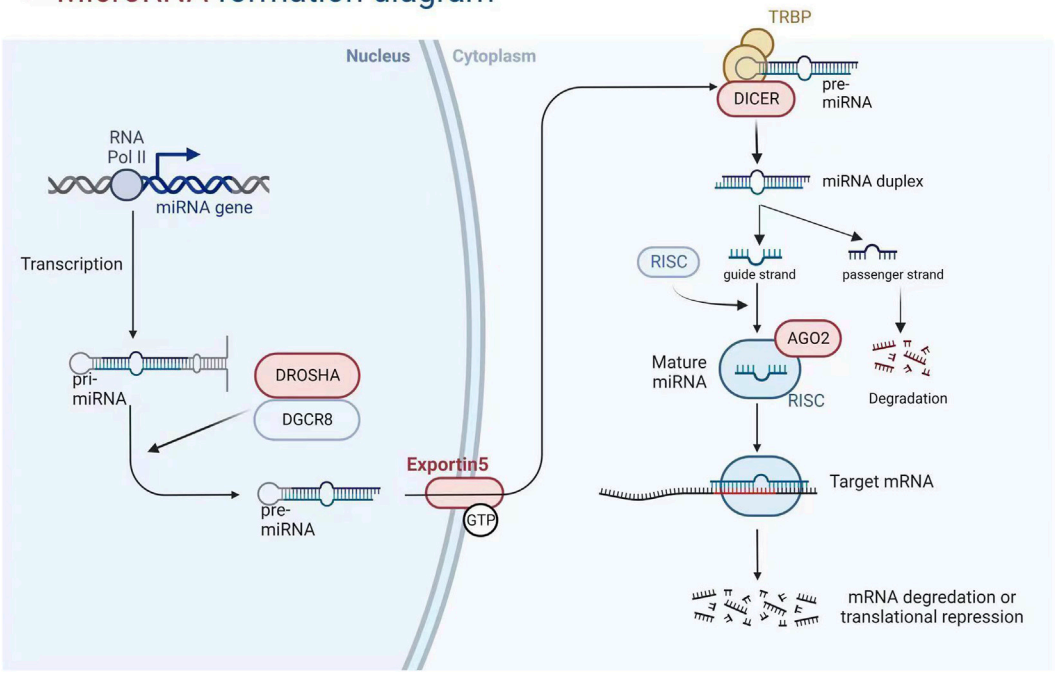

FIGURE 2
MicroRNA formation diagram (Created with BioRender).

miRNA, snoRNA, and piRNA) or long non-coding RNAs (lncRNA and circular RNA, >200 nucleotides) is required for gene regulation (Papaioannou et al., 2014; Metzinger-Le Meuth and Metzinger, 2019). We will look at miRNAs in this investigation. These particles are endogenous non-coding RNAs acting as negative gene expression regulators by degrading or trans-suppressing their target mRNAs (Metzinger-Le Meuth et al., 2019). RNA polymerase II converts the miRNA into a longer RNA product (called Pri-miRNA), which is subsequently cleaved in the nucleus by RNase III (Drosha) and DiGeorge syndrome critical region 8 (DGCR8), resulting in miRNA maturation. The length of the produced pre-miRNA hairpin is around 60–70 nt. The export protein transfers it to the cytoplasm, cleaving it into a double-stranded miRNA/miRNA duplex (about 22 bp) by Dicer RNase III. Finally, one of the threads becomes tightly intertwined inside the RISC assembly, known as the RNA-induced silencing complex, allowing it to be transported to the appropriate messenger RNA to inhibit genetic expression. Concurrently, the second thread disintegrates quickly or produces a unique miRNA with clear, albeit variable, biological repercussions (see Figure 2) (Metzinger-Le Meuth and Metzinger, 2019). Although the seed region of mature miRNAs has consistent sequences, some mismatches are common outside this region, allowing a single miRNA to regulate the expression of multiple target genes by repressing target mRNA translation or promoting their degradation, thereby affecting many horizontal developmental pathways (Metzinger-Le Meuth and Metzinger, 2019). MiRNAs can interfere with the start and elongation of particular proteins during translation, reducing their synthesis. They can also isolate and destroy particular mRNAs in cytoplasmic processing bodies. Additionally, targeting promoter regions has been linked to transcriptional gene silencing (Franczyk et al., 2022). The presence of perfect or incomplete complementarity between miRNAs and their target mRNAs allows for regulating several genes. MiRNA-associated gene expression has permanently activated signalling pathways, facilitated cellular phenotypic change in pathological conditions, and accelerated disease progression (Mirna et al., 2020). Long non-coding RNAs (lncRNAs) can improve the functional activity of certain miRNAs by working through "sponge-like" effects or chromatin remodelling. Several studies have discovered that the interaction between these two non-coding RNAs has a role in the genesis and progression of various illnesses (Rong et al., 2017; Metzinger-Le Meuth et al., 2019). MiRNAs are now being studied as predictive biomarkers for illness diagnosis, severity determination, and progression tracking. Several miRNAs are abundantly expressed in the kidney and may play important roles in regulating CKD-related cardiovascular problems. In CKD, paradoxical miRNA expression has an impact on various biological processes and downstream genes that are important for disease initiation or progression.

miRNAs and CKD-related cardiovascular complications

miRNAs and vascular calcification

Vascular calcification (VC) is highly prevalent in individuals with chronic kidney disease (CKD) and is strongly linked to major cardiovascular events with devastating consequences. The key underlying process of vascular calcification involves the transformation of vascular smooth muscle cells (VSMCs) into

osteoblast-like cells, particularly in the presence of elevated levels of both phosphorus (hyperphosphatemia) and calcium (hypercalcemia). Additionally, the production of matrix vesicles plays a crucial role in facilitating the deposition of calcium and phosphate within the walls of blood vessels (Jansen et al., 2009; Shanahan et al., 2011). Vascular calcification can occur in the vessel's middle and inner layers, and both calcifications can occur in CKD patients. However, calcification in the intermediate layer is more characteristic of CKD. Initially, vascular calcification was reported in individuals with stage 2 CKD. Vascular calcification affects around 25% of CKD stage 3–4 patients and up to 50%–80% of patients on maintenance hemodialysis. VC accelerates the degradation of renal function. Mineral metabolism disorders, hyperphosphatemia, and excessive use of calcium-binding drugs in the setting of uremia, in addition to established risk factors such as hypertension, dyslipidemia, and inflammation, have emerged as substantial risk factors for VC in CKD. VSMCs are also required for vascular calcification in CKD. Previously, it was believed that vascular calcification (VC) associated with chronic kidney disease (CKD) was a passive phenomenon, characterized by the accumulation of hydroxyapatite within the inner layer of arterial walls due to alterations in calcium and phosphorus metabolism. This process consequently leads to heightened arterial stiffness. Contrary to previous beliefs, recent studies have unveiled vascular calcification (VC) as an active and regulated biological process, resembling the intricate mechanisms involved in bone formation. This process entails the transformation of vascular smooth muscle cells (VSMCs) into osteoblast-like cells, accompanied by the implementation of a cellular program that promotes the deposition of bone matrix within the blood vessels (Leopold, 2015). Under normal circumstances, contractile vascular smooth muscle cells (VSMCs) exhibit a slow rate of proliferation. However, in the presence of mineral dysregulation within a uremic environment, these cells can undergo a phenotypic transformation into an active synthetic phenotype. This transformation leads to an accelerated proliferation rate and enhanced secretory capabilities of the VSMCs (Durham et al., 2018). The initiation of medial calcification has been attributed to the phenotypic transition of VSMCs, which is subsequently accompanied by the degradation of elastin (Disthabanchong and Srisuwarn, 2019). This process involves the downregulation of mineralization inhibitors and the upregulation of molecules that promote calcification. Additionally, the absence of smooth muscle cell indicators (such as SM22a and SMa-actin) and the presence of acquired osteogenic markers [including alkaline phosphatase (ALP), Runx2, and bone morphogenetic protein-2 (BMP-2)] contribute to this phenomenon (Liu and Zhang, 2021). Recent investigations have shed light on the complex and multifaceted progression of vascular calcification. These studies have revealed the presence of inhibitory mechanisms such as fetuin-A, klotho, and the vitamin K-dependent matrix Gla protein (MGP) and Gla-rich protein (GRP). These findings have enhanced our understanding of the intricate processes involved in preventing vascular calcification (Schurgers et al., 2013; Viegas et al., 2019). The detrimental consequences of the pathological condition of CKD, which is distinguished by the occurrence of hypercalcemia, hyperphosphatemia, hyperthyroidism, oxidative stress, inflammation, α Klotho deficiency, and the buildup of uremic toxins such as indole sulfate (is) and advanced glycosylation end products (AGEs) (Zhang et al., 2021). In recent years, miRNA has garnered significant attention as a crucial intercellular signalling molecule and an emerging participant in the field of vascular calcification. It is recognized for its capacity to regulate various processes involved in the development of vascular calcification, thereby serving as an information transporter that promotes this pathological condition.

Runx2, a transcription factor essential for osteoblast and chondrocyte maturation, is involved in VSMC calcification. Runx2 expression is low under normal settings but drastically increased in calcified atherosclerotic plaques, showing that Runx2 may play a role in vascular calcification. Several studies have revealed that miRNAs promote osteogenesis by affecting Runx2 expression directly or indirectly. Overexpression of miR-133a suppresses cytosolic calcification, resulting in the downregulation of RUNX2 and OCN, according to Li et al. (2022) MiR-133a, via targeting the RUNX2 gene, can directly control cytosolic calcification and play a role in the aetiology of end-stage renal disease. MiR-29a and miR-125b target Runx2 indirectly via co-repressors or co-activators, which may result in increased or reduced control of osteoblast differentiation (Narayanan et al., 2019). MiR-125b, according to Chao et al. (2017), might be used as a predictive biomarker for VC. MiR-125b levels in the blood were shown to be inversely related to the severity of VC, meaning that miR-125b may be used as a risk factor for VC in uremia. Endogenous miR-125b inhibition improved osteogenic transdifferentiation, alkaline phosphatase activity, and matrix mineralisation. According to expression data, miR-125 b targets the osteoblast transcription factor SP7 (osterix). ApoE knockout mice corroborated this (Goettsch et al., 2011). In an *in vitro* biomineralisation model, a discernible difference in osteocalcin expression was observed between VSMC that underwent transfection with miR-125b and the control VSMC (Chao et al., 2017). The corroboration of these findings can be ascertained by the observation that a decrease in the circulation of miR-125b among patients suffering from chronic kidney disease is intricately linked to a significant deterioration in renal function (Chen et al., 2013). Significant correlations have been found between the levels of miR-125b and the severity of vascular calcification (VC), as well as the levels of fetuin-A and the mediators of mineral bone disease, osteoprotegerin, and FGF-23 (Chao et al., 2017; Chao et al., 2019). High blood osteoprotegerin levels and low serum miR-125b levels enhanced VC risk assessment in one investigation (Chao et al., 2019). Hyperparathyroidism manifests itself in early CKD and can be noticed in dialysis patients, where elevated parathyroid hormone levels are a symptom of bone and mineral abnormalities (Lee et al., 2019). Recently, the role of microRNAs in parathyroid function has been studied. Shilo et al. (2017) discovered that miR148 and let-7 control parathyroid hormone production in secondary hyperparathyroidism, with let-7 members inhibiting PTH secretion and miR-148 members promoting it. Increased parathyroid let-7 expression and miR-148 members in CKD may lead to SHP formation. Future research may reveal miRNAs as new therapeutic targets for SHP management. It is uncertain what causes the present study's direct link between miRNAs and parathyroid hormone levels. As a result, additional investigation into this relationship is required. In a rat model of CKD, miR-302b levels dropped in chronic renal failure (CRF) animals. Upregulation of

miR-302b, on the other hand, may increase calcium and phosphorus metabolic activity and prevent the development of ectopic VC, thereby alleviating the condition of CRF that may be related to the BMP-2/Runx2/Osterix signalling pathway, thereby providing a novel concept for identifying effective CKD treatments (Sun et al., 2018). Exosomes generated from mesenchymal stem cells in the bone marrow, also known as BMSC-Exo, have significantly reduced calcification caused by hyperphosphatemia inside vascular smooth muscle cells (VMSCs). This finding implies that BMSC-Exo has enormous potential in treating chronic kidney disease-associated vascular calcification (CKD-VC). However, the particular mechanical foundations of this event remain unknown and deserve additional exploration. A scientific study used hyperphosphate-stimulated human aortic smooth muscle cells (HA-VSMCs) in conjunction with a 5/6 complete nephrectomy (SNx) rat model to investigate the complicated workings of BMSC-Exo. This study sought to determine the underlying mechanism of action of BMSC-Exo using both human and animal experimental models. The current study discovered that BMSC-Exo effectively inhibits the progression of apoptosis and calcification *in vivo* and *in vitro* via the mediating influence of microRNA-381-3p (miR-381-3p). In addition, it has been unequivocally demonstrated that miR-381-3p effectively inhibits the production of nuclear factor 5 (NFAT5) in vibrant T cells via its astute binding to the 3′ untranslated region. Furthermore, the presence of significant arterial calcification among dialysis patients has been found to have a negative correlation with the level of miR-381-3p while having a positive correlation with the expression of NFAT5. This study concluded that BMSC-Exo had anti-calcification and anti-apoptotic effects in CKD by providing closed miR-381-3p and directly targeting NFAT5 mRNA (Liu et al., 2022). In a built-rat CRF model, overexpression of miR-93 in the aorta of CRF rats significantly reduced the production of OPN, OCN, RUNX2, and BMP-2. MiR-93 inhibited aortic calcification by delaying VSMC osteogenic differentiation. MiR-93 may reduce Wnt/- signalling pathway activity and VC-related gene expression to enhance renal function in CRF rats and relieve vascular calcification in CRF, establishing the framework for VC-targeted treatment in CRF (Peng et al., 2022).

SULF1, which encodes heparan sulphate lyase 1, is widely distributed in tissues and has the ability to influence Wnt, FGF, and BMP pathways by modifying extracellular proteoglycans. The role of SULF1 in vascular smooth muscle cell (VSMC) physiology cannot be overstated. Evidence suggests that increased SULF1 expression in VSMC causes a decrease in adhesive properties while simultaneously increasing the propensity for apoptosis, migration, and chemotaxis (Sala-Newby et al., 2005). Moreover, SULF1 stimulation of vascular tissue Wnt signalling has been established (Sahota and Dhoot, 2009), while induction of the Wnt/-catenin pathway promotes the formation of vascular calcification (Nie et al., 2019). The incorporation of SULF1 is postulated as a potential modulator in the regulation of angiotensin II receptor expression and consequently, it exhibits the ability to augment osteogenic differentiation, as alluded to by previous studies (Cha et al., 2018; Matsushita et al., 2015). MiR-378a-3p, wi-th its interaction with BMP2 and ERK2, purportedly assumes a pivotal function in terms of skeletogenesis and calcification. Notably, higher BMP2 levels have been regularly found in the setting of calcified aneurysms, making it a widely recognised marker. Surprisingly, lowering BMP2 levels has been shown to reduce the severity of vascular calcification (VC). Activation of ERK1/2, an intracellular signalling pathway, has been linked to the transdifferentiation of vascular smooth muscle cells (VSMCs) into osteoblasts. A notable corollary could be the increased potential for vascular calcification (VC) achieved by using compounds that inhibit ERK1/2 expression. Another potential target of miR-378a-3p, Ca2+/calmodulin-dependent protein kinase II (CAMKK2), has been shown to induce stem cell differentiation in the osteoblast lineage (Chao et al., 2021). Chao et al. (2021) discovered that serum miR-378a-3p, when combined with their matched gene SULF1, was independently linked with serum VC and VC severity in sera from patients with nondialysis CKD and dialysis-dependent ESRD, outperforming clinical characteristics alone or target proteins alone. Finally, miRNA-target gene pairings functionally govern the pathogenic process of VC and may be therapeutic targets. The findings of this study constitute a significant step forward in identifying uremic individuals at high risk using molecular regulation-based (miRNA-mRNA) paired biomarkers.

IS, the representative uremic toxin, can induce osteogenic differentiation in vascular smooth muscle cells (VSMCs) by enhancing oxidative stress levels, changes in methylation patterns, and changes in the expression of microRNAs (miRNAs) specifically involved in osteogenic differentiation. These molecular mechanisms result in a condition known as vascular calcification (VC), which has a strong association with the presence of VC in patients with chronic kidney disease (CKD) (He et al., 2020). Matrix GLa protein (MGP) is a calcification inhibitor that plays an important role in VC. MGP was reduced in calcified arteries *in vitro* by IS through activation of ROS/NF-B signalling to suppress MGP expression in HASMCs in parallel with osteogenic differentiation, and further investigation revealed that IS induced NF-B-responsive microRNA (miR)-155. The rise in miR-155-5p mimic overexpression enhanced the decrease in MGP generated by IS and osteogenic cell differentiation. However, these states were alleviated by silencing miR-155-5p. IS induces a phenotypic change in HASMCs by reducing MGP expression via ROS/NF-B/miR-155-5p signalling, shedding light on the pathophysiology of IS-induced VC (He et al., 2020). IS was found to have a dual effect on human aortic smooth muscle cells (HASMCs), causing a decrease in miR-29b expression while increasing calcification. MiR-29b mimics strongly suppressed IS-induced expression of Runt-related transcription factor 2 and Osteopontin, but miR-29b anti-miR was significantly enhanced. In comparison to control participants, patients with end-stage renal disease had higher levels of Wnt7b/-catenin expression in the radial arteries. Additionally, it was observed that the influence of IS resulted in an intensified manifestation of Wnt7b/β-catenin in human aortic smooth muscle cells (HASMCs), whereby this augmentation occurred within a mere duration of 3 days following the initiation of stimulation. Moreover, miR-29b mimics inhibited Wnt7b/β-catenin protein expression in HASMCs while miR-29b anti-mir enhances it, demonstrating that miR-29b adversely controls Wnt7b/β-catenin signalling. The protein known as Dickkopf-1 was shown to have an inhibitory effect on the calcification process in human airway smooth muscle cells

(HASMC). This calcification is induced by the presence of anti-miR-29b, a factor of significant influence in the suppression of the Wnt/β-catenin signalling pathway. As a result, the findings of this study suggest that the suppression of miR-29b and the activation of Wnt/β-catenin signalling may emerge as a pivotal mechanism in the occurrence of vascular calcification stimulated by IS in the context of chronic renal disease (Zhang et al., 2018). However, given the intricacy of the process's regulation and the diversity of miRNAs involved, additional research is needed to find the best candidate miRNAs for targeting (See Table 1).

miRNAs and left ventricular hypertrophy

The presence of left ventricular hypertrophy (LVH) is a prevalent characteristic of cardiac alterations observed in individuals with chronic renal illness, contributing to the development of heightened cardiovascular abnormalities (Shimizu and Minamino, 2016). Left ventricular hypertrophy is observed in the first phases of chronic kidney disease (CKD) and is prevalent in around 65% of patients who have not yet initiated dialysis (Parfrey et al., 1990). Hemodynamic overload has been widely recognised as a significant catalyst for the occurrence of left ventricular hypertrophy (LVH) in individuals with chronic kidney disease (CKD) (Zoccali et al., 2017). Additionally, various detrimental factors linked to CKD, including the renin-angiotensin system (RAS), uremic toxins, microinflammatory states, and disturbances in phosphorus metabolism, have shown a strong correlation with LVH (Wang and Shapiro, 2019). Identification of a shared mechanism underlying cardiac hypertrophy generated by these causal variables has the potential to establish a foundation for understanding left ventricular hypertrophy in chronic kidney disease (CKD) and subsequently enhance the efficacy of therapy for CKD patients with cardiovascular problems. MicroRNAs (miRNAs) are a category of brief, non-coding ribonucleic acids (RNAs) that govern the modulation of gene expression subsequent to transcription. MicroRNAs (miRNAs) play a significant role in the development of cardiac hypertrophy and have the potential to serve as mediators in the progression of hypertrophy. The expression of miR-30 is significantly upregulated in cardiac tissues and downregulated in hypertrophic circumstances, indicating its crucial role in cardiac function. The miR-30 family has high levels of expression in cardiac tissues during normal physiological settings (Mcgahon et al., 2013; Ludwig et al., 2016), indicating their significant involvement in heart function. Following the surgical removal of a kidney (nephrectomy), the occurrence of cardiac hypertrophy and inhibition of myofibrillar miR-30 were observed. These findings primarily indicate a potential association between miR-30 inhibition and the advancement of cardiac hypertrophy in chronic kidney disease (CKD). Bao et al. (2021) conducted a study that revealed the inhibition of endogenous miR-30 in cardiomyocytes resulted in the development of pathological cardiac hypertrophy. Additionally, this inhibition augmented the activity of calmodulin phosphatase, leading to increased phosphorylation, and facilitated the translocation of NFATc3 to the nucleus. In addition, the transfection of miR-30 sponge plasmid into cardiomyocytes resulted in the manifestation of cardiomyocyte enlargement and increased intranuclear NFATc3 concentrations. Moreover, cardiomyocyte hypertrophy was inhibited upon treatment with the particular calmodulin inhibitor FK506. Significantly, the mRNAs of Ppp3ca and Nfatc3 are directly regulated by miR-30. In addition, it was shown that miR-30 had a mitigating effect on calcineurin signalling inside the myocardium of rats with chronic kidney disease (CKD) and mice treated with fibroblast growth factor-23 (FGF-23). Thus, it can be inferred that the association between calmodulin/NFATc3 and miR-30 contributes to cardiac hypertrophy. Reducing miR-30 is of utmost importance in developing left ventricular hypertrophy produced by chronic kidney disease. A recent study conducted by Chuppa et al. (2018) demonstrated that the suppression of miR-21 has a protective effect against left ventricular hypertrophy (LVH) and leads to an improvement in left ventricular (LV) function in rats with 5/6 nephrectomy. This beneficial effect was seen to occur through the activation of the peroxisome proliferator-activated receptor alpha (PPAR-α) pathway. Furthermore, there have been reports indicating that the activation of Na+/K+-ATPase signalling results in the suppression of miR-29b expression in the heart, hence promoting elevated collagen production in individuals with chronic kidney disease (Drummond et al., 2016). Furthermore, the downregulation of miR-29b and miR-30c has been implicated in the development of cardiac fibrosis in chronic kidney disease (CKD). These microRNAs play a crucial role in regulating collagen-1a1, matrix metalloproteinase 2, and connective tissue growth factors, all of which are well-established promoters of fibrosis (Panizo et al., 2017). The suppression of miR-208 in the cardiac system has been observed to be linked to cardiac hypertrophy in individuals with chronic kidney disease (CKD) (Prado-Uribe et al., 2013).

The role of miR-212 as a crucial regulator of pathological left ventricular hypertrophy in heart failure generated by pressure overload has been demonstrated through its regulation of the FOXO3/calreticulin/nuclear factor of activated T cells (NFAT) pathway. In a recent study conducted by Sárközy et al. (2019), the researchers investigated the potential role of miR-212 and its associated targets, including FOXO3, extracellular signal-regulated kinase 2 (ERK2), and AMP-activated protein kinase (AMPK), in the pathogenesis of heart failure with preserved ejection fraction (HFpEF) within the context of chronic kidney disease (CKD) patients. Chronic kidney disease (CKD) was experimentally created in male Wistar rats using a surgical procedure known as 5/6 nephrectomy. The echocardiography and histological examinations revealed the presence of left ventricular hypertrophy, fibrosis, maintained systolic function, and diastolic dysfunction in the group with chronic kidney disease (CKD) at the end of 8 and/or 9 weeks, in comparison to the animals who underwent sham surgery. The expression of miR-212 in the left ventricle was considerably upregulated in the group with chronic kidney disease (CKD). Nevertheless, the mRNA and protein levels of FOXO3, AMPK, and ERK2 remained relatively unchanged. The protein kinase B (AKT)/FOXO3 and AKT/mammalian target of rapamycin (mTOR) pathways have been implicated as potential mechanisms involved in the regulation of left ventricular hypertrophy (LVH) induced by pressure overload. It is worth noting that the ratio of phosphorylated-AKT to total AKT was found to be elevated in individuals with chronic kidney disease

TABLE 1 Comparison of miRNAs in vascular calcification.

miRNAs	Population/Methods	Function	Key-findings
miR-133a Li et al. (2022)	Rat smooth muscle A7r5 cells	MiR-133a is mainly expressed in myocardial and skeletal muscle cells, which regulates their proliferation and differentiation	● miR-133a can indirectly regulate cellular calcification through RUNX2 gene expression. The results of this study provide insight into miR-133a as a molecular target for the diagnosis of vascular calcification in end-stage renal disease
miR-125b Goettsch et al. (2011); Chao et al. (2017)	rat and human aortic vascular smooth muscle cells	miR-125b plays a role in atherosclerotic plaque formation, including inflammation, apoptosis, and angiogenesis	● serum miR-125b levels are associated with VC severity and serve as a novel predictive marker for the risk of uremia-associated calcification progression ● It demonstrate that miR-125b is involved in the osteogenic transdifferentiation of VSMCs, at least in part by targeting SP7, and implicate miRs as a novel link for the common mechanisms of vascular calcification and bone remodeling
miR-148 Shilo et al. (2017)	male Sprague Dawley rats and C57BL/6 mice	miR-148 family has been linked with various neoplastic diseases, and inhibition of miR-148 was reported to downregulate insulin mRNA in pancreatic islet cells	● let-7 members restrict PTH secretion, whereas miR-148 members promote secretion. In CKD, the expression of parathyroid let-7 and the increase in miR-148 members may contribute to the development of SHP. Future studies may identify miRNAs as new therapeutic targets for the management of SHP, a common complication of CKD and a source of morbidity and mortality in these patients
miR-302b (Sun et al., 2018)	male clean-grade Sprague-Dawley rats	miR-302 could promote the activation of BMP signaling pathway in undifferentiated human embryonic stem cells	● miR-302b was shown to be decreased in rats with CRF, and upregulation of miR-302b may improve calciumphosphorous metabolism and prevent the progression of ectopic VC, thus relieving the conditions of CRF possibly associated with BMP-2/Runx2/Osterix signaling pathway, which provided a new idea for finding effective therapeutic approach to CRF.
miR-381-3p Liu et al. (2022)	Human aortic smooth muscle cells (HAVSMCs) and 5/6 subtotal nephrectomy (SNx) rat	miR-381-3p as a dual suppressor of TNF-induced apoptosis and necroptosis in multiple cancer cells	● BMSC-derived exosomal miR-381- 3p could downregulate NFAT5, therefore alleviate the cellular apoptosis and VC. This study reveals the significant role of miR-381-3p/NFAT5 in regulating apoptosis/Vascular calcification。
miR-93 Peng et al. (2022)	Sprague Dawley (SD) male rats	miR-93 in the development, progression and drug tolerance of multiple tumors, but also pointed out its critical roles in senescence, hyperglycemia and osteoblast calcification	● MiR-93, via inhibiting the activity of Wnt/β-catenin pathway by targeting TCF4, can improve the renal function of CRF rats, thereby mitigating the vascular calcification of CRF.
miR-378a-3p Chao et al. (2021)	rat aortic vascular smooth muscle cells (VSMCs) A7r5 and human aortic smooth muscle cells (ASMCs)	miR-378a-3p exhibits multifaceted effects on angiogenesis, muscle cell proliferation and differentiation, and it promotes myogenesis, myocyte survival and inhibits apoptosis	● After analyzing and screening the probability of incorporating miR-378a-3p and SULF1 into these miRNA/protein biomarkers for the measurement of uremic VC, it is possible that significant improvements could be made in how we diagnose uremic VC.We believe that a combined biomarker set including miRNAs and their target proteins may represent a potentially useful approach for identifying patients who are prone to VC or who may experience ESRD patients with worsening VC
miR-155-5p He et al. (2020)	human aortic smooth muscle cells (HASMCs)	MiR-155-5p is a typical NF-κB-responsive miRNA, as a NF-κB-binding site is present in its promoter, which has marked effects on endothelial dysfunction, vascular inflammation, and VSMC phenotypic	● IS promotes the HASMCs phenotype switch by suppressing MGP expression via ROS/NF-κB/miR-155-5p signaling and provide a new insight for the pathogenesis of IS-induced VC.
miR-29b Zhang et al. (2018)	human aortic smooth muscle cells (HASMCs)	A feedback loop exists between the miR-29 family and wnt signaling, which contributes to osteoblastic differentiation of MSCs	● miR-29b as an important protective factor of VSMC calcification by repressing wnt/β-catenin signaling, which represents a novel mechanism regulating vascular calcification. This finding may provide a new perspective on pathogenesis and treatment of vascular calcification in chronic kidney disease

(CKD), with no significant impact on the phosphorylation of FOXO3 or mTOR. In summary, the cardiac overexpression of miR-212 in chronic kidney disease (CKD) did not have any impact on the downstream targets that have been previously linked to hypertrophy. Therefore, it can be inferred that the molecular processes responsible for the development of left ventricular hypertrophy (LVH) in chronic kidney disease (CKD) are not influenced by FOXO3, ERK1/2, AMPK, and AKT/mTOR-mediated pathways. This implies that this particular kind of LVH possesses distinct characteristics. This work is the initial investigation documenting the co-occurrence of left ventricular hypertrophy (LVH) and fibrosis with discernible overexpression of miR-212 in the left ventricle among individuals with chronic kidney disease (CKD). Further inquiry is imperative in order to ascertain whether the upregulation of miR-212 in cardiac tissue serves as a driving force or a consequence of left ventricular hypertrophy associated with chronic kidney disease.

Li et al. (2020) conducted a study on ventricular hypertrophy and demonstrated that circRNA_000203 exhibited upregulation in cardiac hypertrophy. Moreover, the researchers observed that circRNA_000203 contributed to the augmentation of heart hypertrophic growth both *in vivo* and *in vitro*. Circular RNA 000203 has the ability to sequester miR-26b-5p and miR-140-3p, resulting in an upregulation of GATA4 expression, hence facilitating the development of cardiac hypertrophy. The study also determined that the activation of the NF-κB signalling pathway had a role in the increased expression of circRNA_000203 during cardiac hypertrophy. The microRNA known as miR-133a has putative regulatory functions in the context of cardiac hypertrophy. The activation of hypertrophic signalling through the involvement of NFAT (nuclear factor of activated T cells) is a crucial regulatory response to hypertrophic stimuli. The transcription factor NFATc4, which is related to hypertrophy, is a target of negative regulation by miR-133a. Moreover, the *in vitro* upregulation of miR-133 or miR-1 showed inhibitory effects on cardiac hypertrophy. On the contrary, the induction of hypertrophy by the use of a "decoy" sequence to block miR-133 exhibited a greater degree of prominence compared to the hypertrophy caused by conventional inducers. The induction of heart hypertrophy is shown as a persistent and significant outcome when miR-133 is inhibited *in vivo* with a single transfection of antigametophytes. The particular targets of miR-133 have been identified as rhoA, a protein responsible for GDP-GTP exchange and regulation of cardiac hypertrophy; Cdc42, a signalling kinase involved in hypertrophy; and Nelf-A/WHSC2, a nuclear factor implicated in cardiogenesis (Care et al., 2007). In addition, the presence of myocardial ischemia, along with the measurement of circulating miR-133a, has the potential to serve as a biomarker for the prediction of cardiac hypertrophy in individuals undergoing chronic hemodialysis and those who have had valve replacement due to aortic stenosis (Xiao et al., 2019). In a murine model of ventricular hypertrophy produced by Ang II, the exosome miR-21 generated from cardiac fibroblasts has a hypertrophy-promoting influence by selectively targeting the Z-lineage-associated proteins SORBS2 and PDLIM5 (Fang et al., 2022). In a similar vein, a recent study has demonstrated that the expression of miR-27a is increased in hearts affected by infarction, leading to the promotion of hypertrophic gene expression. This effect is achieved through the targeting of PDLIM5, which in turn facilitates the process of cardiomyocyte hypertrophy (Tian et al., 2020). The upregulation of miR-217 expression was seen in both transverse aortic constriction (TAC) mice models and people with heart failure (HF) (Nie et al., 2018). According to a recent study, the process of converting fibroblasts into induced pluripotent stem cells (iPSCs) was shown to have a mitigating effect on cardiac hypertrophy. This effect was achieved by the reduction of exosomal miR-22, as indicated by the study (Huang et al., 2013).

Paterson et al. (2019) conducted a compelling study to examine the gender-specific impact of miR-146b-5p on cardiology within a rat model of chronic kidney disease (CKD). Following the administration of 5/6 Nx, female miR-146b−/− rats did not exhibit observable cardiac hypertrophy as compared to their wild-type counterparts. However, it is worth noting that aberrant renal function was seen in the former group. The expression of this trait was partially diminished with the use of a preventive ovariectomy procedure. On the other hand, the removal of miR-146b-5p did not result in any significant impact on the hypertrophic response in males. Instead, men displayed noticeable left ventricular hypertrophy and cardiac chamber dilatation after undergoing 5/6 Nx when compared to miR-146b−/− males but not when compared to wild-type males. The results of sophisticated computational calculations demonstrated that the primary target of miR-146b-5p activity was the downregulation of TGFB1 protein production in the TGF-B pathway, together with the suppression of waveform protein (Vim) and e-calmodulin (Cdh1). The administration of β-estrogen resulted in a decrease in the expression of Vim induced by TGF-β. Conversely, treatment with pre-miR-146b significantly reduced collagen expression in cells exposed to both TGF-β and β-estrogen but not in cells incubated solely with TGF-β. These findings suggest that the effects of miR-146b-5p are influenced by sex hormones. Therefore, it may be inferred that miR-146-5p in women with wild-type (WT) genes may enhance the beneficial impacts of oestrogen. This might potentially elucidate the reason for the disruption of gonadotropin signalling and the deterioration of chronic kidney disease (CKD) when miR-146b-5p is inhibited. Further investigation is required to explore the potential involvement of additional miRNA families in regulating hormonal responses to cardiac pathology during chronic kidney disease (CKD) (D'Agostino et al., 2023). The aforementioned studies not only provide insights into a hitherto unidentified mechanism of left ventricular hypertrophy (LVH) production in chronic kidney disease (CKD) but also propose prospective therapeutic targets for managing cardiac hypertrophy in CKD patients (refer to Table 2).

miRNAs and endothelial dysfunction

Endothelial dysfunction, a pathological condition affecting the inner lining of blood vessels, is a primary contributor to the development of chronic kidney disease and significantly increases the likelihood of cardiovascular complications (Roumeliotis et al., 2020). Several recently discovered endothelium damage indicators can be utilised to assess this process in CKD (Glorieux et al., 2021). Syndecan-1 (Sdc-1) belongs to the transmembrane heparan sulfate glycoprotein family, serving as a reservoir for growth factors and chemokines that play crucial roles in numerous cellular activities

TABLE 2 Comparison of miRNAs in Ventricular Hypertrophy.

miRNAs	Population/Methods	Function	Key-findings
miR-30 Bao et al. (2021)	male Sprague-Dawley rats	miR-30 regulates autophagy, apoptosis and oxidative stress	● MiR-30 suppression may result in cardiac hypertrophy via calcineurin/ NFATc3 activation in LVH.
miR-21-5p Chuppa et al. (2018)	Male Sprague Dawley rats	miR-21 has a role in acute and chronic pathology in several organs. Short term cardiac upregulation of miR-21 is protective in ischemia/reperfusion injury, while chronic upregulation has been associated with pathologic changes.miR-21 suppression has also been reported to be renoprotective in models of acute renal injury/fibrosis and Alport nephropathy	● Inhibition of miR-21-5p protects 5/ 6 nephrectomized rats from developing left ventricular hypertrophy and improves left ventricular function ● MiR-21-5p inhibition altered gene expression of the left ventricular peroxisome proliferator-activated receptor α (PPAR α) regulatory pathway. PPAR α, a miR-21-5p target, is the predominant PPAR isoform in the heart and plays an important role in the regulation of fatty acid metabolism.Therapeutic administration of a low-dose PPAR α agonist (clofibrate) to 5/6 nephrectomized rats improved cardiac function and prevented left ventricular dilatation
miR-29b and miR-30c Panizo et al. (2017)	male Wistar rats	miR-29 targets genes encoding collagen types I and IV and MMP-2, among others. Downregulation of miR-29 by TGF-b1/ Smad3 is part of the mechanism by which this signalling pathway induces renal fibrosis. In addition, the loss of miR-30 in the course of LV hypertrophy intensifies pro-fibrotic signalling, in part through increases in CTGF levels	● Vitamin D receptor activators (VDRAs), particularly paricalcitol, attenuated cardiac fibrosis acting on COL1A1, MMP-2 and CTGF expression, partly through regulation of miR-29b and miR-30c
miR-208 Prado-Uribe et al. (2013)	Male Sprague Dawley rats	microRNA-208 (mir-208), is selectively expressed in myocardial tissue and is involved in the control of heart remodeling because it regulates the expression of b-MHC and myocardial fibrosis in response to various stimuli	● Decreased plasma level of thyroid hormones or sensitivity at tissue level observed in chronic kidney disease induced by 5/6Nx has an important effect in heart remodeling processes, some of it related or mediated by mir-208 and TGF-b expression in the heart
miR-212 Sárközy et al. (2019)	adult male Wistar rats	miR-212 overexpression plays a role in the development of LVH and heart failure through fetal gene reprogramming in the human heart. In addition, the prohypertrophic potential of miR-212 was confirmed in primary neonatal rat cardiomyocytes	● cardiac overexpression of miR-212 in CKD failed to affect its previously implicated hypertrophy-associated downstream targets. thus, the molecular mechanism of the development of LVH in CKD seems to be independent of the FOXO3, ERK1/2, AMPK, and AKT/mTOR-mediated pathways indicating unique features in this form of LVH.
miR-133a Care et al. (2007)	10–12 week old C57BL/6 female mice (Harlan)	miR-133a inhibits angiogenesis, apoptosis, fibrosis, hypertrophy, and inflammation while promoting therapeutic cardiac remodeling	● MiR-133 has a critical role in determining cardiomyocyte hypertrophy ● Overexpression of miR-133 or miR-1 *in vitro* inhibited cardiac hypertrophy. In contrast, induction of hypertrophy by miR-133 was inhibited by a "decoy" sequence, which was more pronounced than after stimulation with conventional hypertrophy inducers ● We identified specific targets of miR-133: RhoA, a GDP-GTP exchange protein that regulates cardiac hypertrophy; Cdc42, a signaling kinase implicated in hypertrophy; and Nelf-A/WHSC2, a nuclear factor involved in cardiogenesis ● MiR-133 and possibly miR-1 are key regulators of cardiac hypertrophy, suggesting their therapeutic application in heart disease
miR-27a Tian et al. (2020)	male Sprague-Dawley rats	MicroRNA-27a (miRNA-27a) is the major microRNA contained in cardiac fibroblast-derived EVs and contributes to oxidative stress as well as expression of hypertrophic genes in cardiomyocytes	● Secretion of miRNA27a*-rich EVs by cardiac fibroblasts may serve as a paracrine signaling mediator of cardiac hypertrophy with potential as a new therapeutic target.

(Continued on following page)

TABLE 2 (*Continued*) Comparison of miRNAs in Ventricular Hypertrophy.

miRNAs	Population/Methods	Function	Key-findings
miR-217 Nie et al. (2018)	Seventeen heart samples were collected from cardiac transplant patients with CHF, and nine heart samples were from accident victims. Male C57BL/6 mice	MiR-217 plays multiple roles in physiological and pathological processes. For example, mir-217 promotes inflammation and fibrosis through the SIRT1/HIF-1a signaling pathway in high glucose-cultured rat glomerular mesangial cells. miR-217 mediates the protective effects of dopamine D2 receptors against fibrosis by targeting Wnt5a in human renal proximal tubule cells. Overexpression of transforming growth factor b1 (TGF-b1) triggers dysregulation of the miR-217-SIRT1 pathway, which then promotes the epithelial-mesenchymal transition process	● The findings reveal that miR-217 is highly expressed in the hearts of CHF patients and aggravate pressure overload-induced cardiac hypertrophy and dysfunction by suppressing PTEN expression. Cardiomyocyte-derived miR-217-containing exosomes induce fibroblast proliferation and may promote cardiac fibrosis (Figure 7). These findings suggest that miR-217 plays important roles in cardiac hypertrophy and dysfunction, providing therapeutic targets for heart failure
miR-22 Huang et al. (2013)	This study established mouse models of global and cardiac-specific miR-22 deletion	miRNA-22 (miR-22) was previously reported as a tumorsuppressive miRNA that induces cellular senescence in cancer cell lines. miR-22 was shown to repress hypertrophy in cultured cardiomyocytes.miR-22 was required for the heart to adapt to pressure overload–induced cardiac hypertrophy	● miR-22 as a critical regulator of cardiomyocyte hypertrophy and cardiac remodeling
miR-146b-5p Paterson et al. (2019)	miR-146b-5p knockout rats	miR-146b-5p, is an important mediator in renal cardiac pathophysiology. Increased abundance of miR-146b-5p has been reported in clinical studies in renal pathology and experimental disease models; including hypertension, AKI, renal fibrosis and CKD.	● MiR-146b rats exhibited functional knockout of miR-146b-5p in both kidney and heart ● Although 5/6 nephrectomy resulted in tissue hypertrophy, miR-146b−/− female rats showed exacerbated renal hypertrophy ● In addition, miR-146b female rats exhibited significantly elevated renal fibrosis and marked renal insufficiency, but lower blood pressure and less pronounced cardiac remodeling. These phenotypic differences were not demonstrated in miR-146b−/− male rats ● Ovariectomy improved renal pathology and eliminated genotypic differences

(De Luca et al., 2010). VCAM-1 (vascular cell adhesion molecule) is a glycosylated protein located on the surface of endothelial cells. Its primary function is to facilitate the recruitment of macrophages to the renal vasculature in response to vascular injury (Chow et al., 2005). During tissue remodeling, matrix metalloproteinase-7 (MMP-7) plays a crucial role in the breakdown of the extracellular matrix (Bradshaw, 2009). MMP-7 is found to be increased in individuals suffering from chronic renal illness, positioning it as a significant biomarker for assessing endothelial dysfunction (Liu et al., 2020). Angiopoietin-2 (ANGPT2) influences endothelial cell death, migration, and proliferation via altering cell-matrix interaction (David et al., 2010). The buildup of uremic toxins in the blood is another characteristic of chronic renal failure (Barreto et al., 2009). On the basis of their molecular weights and protein-binding capacity, uremic toxins are classified as (a) water-soluble small molecular compounds (e.g., inorganic phosphates), (b) medium molecular compounds, and (c) protein-bound compounds [e.g., indole sulphate (IS)]. Uremic toxins can induce endothelial dysfunction in patients with chronic kidney disease (CKD). Indeed, the endothelium monolayer structure is altered in chronic kidney disease patients, and studies have demonstrated that uremic toxins cause cell-cell junction loss and increased permeability. Uremic toxins induce oxidative stress within these cells, triggering the activation of signaling pathways including the aryl hydrocarbon receptor (AhR), nuclear factor-B (NF-B), and mitogen-activated protein kinase (MAPK). When these pathways are activated, pro-inflammatory proteins (e.g., monocyte chemotactic protein-1, E-selectin) and pro-thrombotic proteins (e.g., tissue factor) are overexpressed. Uremic toxins have been found to induce the production of endothelial cell microparticles (EMPs), leading to the activation and subsequent dysfunction of various cellular components. These toxins also disrupt the expression of microRNAs, critical regulators of cellular functions (Cunha et al., 2020). As a result, uremic toxins and the pathways they control may be viable therapeutic targets for improving CKD therapy.

According to Cunha et al., individuals with miR-126 levels below the median exhibited a poorer survival rate, along with an elevated incidence of cardiovascular and renal events (Fourdinier et al., 2021). Recent findings by Scullion et al. (2021) have revealed that the serum levels of miR-126 were significantly lower in rats with nephrotoxic nephritis and individuals with acute endothelial and renal damage compared to healthy controls. There was a link between Sdc-1 and miR-126 in multivariate analysis. The endothelial glycocalyx (eGC) is a protective layer comprised of negatively charged polymers that coats the luminal surface of endothelial cells. It acts as a shield, safeguarding the vascular wall from potential damage that could trigger endothelial dysfunction.

Sdc-1 shedding from eGC has been found to be elevated in individuals with chronic renal disease (Padberg et al., 2014). Interestingly, this was more prevalent among dialysis patients, indicating that this connection is connected to the degree of CKD (Liew et al., 2021). Sdc-1 mRNA upregulation predicts the development of acute damage in chronic renal disease (Jiang et al., 2021). Sdc-1 mRNA upregulation predicts the development of acute damage in chronic renal disease (Jiang et al., 2021). The research conducted by Cunha et al. (Fourdinier et al., 2021) solidified the notion of an association between miR-126 levels and endothelial dysfunction in a substantial cohort of patients with chronic kidney disease (CKD). In addition, it has been discovered that miR-126 promotes CXCL12-induced angiogenesis through its target gene Spred-1, indicating that the expression of miR-126 plays a role in angiogenesis and tissue regeneration (Bassand et al., 2021). MiR-126 suppression inhibited CXCL12-induced angiogenesis and migration in HUVEC endothelial cells. A notable correlation has been revealed between the cellular levels of miR-126 and the expression of Sdc-1 in prostate cancer cells. It has been observed that a reduction in Sdc-1 expression leads to a corresponding decrease in miR-126 expression (Fujii et al., 2015). MiR-126 reduces cell proliferation and promotes senescence in this model. IS and other protein-bound toxins have been shown to be harmful in the course of chronic renal disease. MiR-126 levels linked with free IS levels in multivariate studies. Higher levels of free IS have been linked to a higher relative risk of mortality when compared to total levels, suggesting that free IS levels are linked to miR-126 but not total IS (Liabeuf et al., 2011). Cunha et al. discovered that free IS enhanced IDI when the interaction was predictive, suggesting the additional predictive effect of this possible novel biomarker on critical CKD outcomes above and beyond existing prognostic indicators (e.g., baseline eGFR). Total pCG levels were also shown to be related to miR-126 but not free pCG levels. There was no link observed between free or total pCS. Cresol conjugation by bacteria yields mostly pCS and, to a lesser extent, pCG (Fourdinier et al., 2021). In a recent analysis of this cohort, free pCS was most linked with cardiovascular prognosis in non-dialyzed patients with chronic renal disease (Glorieux et al., 2021). IS is more effective in vascular remodelling, but pCS reduces endothelial cell survival. Moreover, Carmona et al. reported that IS triggers endothelial cells to create microvesicles and that the number of miRNAs in these microvesicles may be changed (Carmona et al., 2017). According to the findings of the identical research group, it has been revealed that microvesicles generated by pCS-treated endothelial cells impede the process of endothelial cell healing and expedite the aging of adult endothelial cells (Guerrero et al., 2020).

The equilibrium between vasoconstriction and vasodilation in vascular tone is regulated by factors released from the endothelium (Furchgott and Zawadzki, 1980). The levels of miR-142-3p in the blood are not only closely associated with vasodilatory markers in patients with end-stage renal disease (ESRD) and uremic mice, but also have a potential pathogenic function. By inhibiting the decrease of miR-142-3p expression, the restoration of ACh-mediated vasodilation occurs (Kétszeri et al., 2019). These findings are congruent with those of Sharma et al. (2012), who found that miR-142 plays an important role in adaptive cardiac overstretching in response to hemodynamic stress. According to Kétszeri et al. (2019), the presence of blood miR-142-3p serves as not only a biomarker for impaired renal function and endothelial dysfunction, but also as a direct facilitator of decreased ACh-mediated vasorelaxation in uremic patients. This suggests that targeting this molecule could potentially mitigate arterial stiffness and further complications in individuals with uremia. Uremia is characterized by prominent vascular lesions that affect the function of both VSMC and endothelial cells. These lesions have been closely associated with notable rates of morbidity and mortality due to cardiovascular complications. According to the data, it is evident that miRs play a crucial role in the development of uremic mesothelial sclerosis; however, further evidence is emerging regarding their potential involvement in vascular function impairment.

Endothelial dysfunction in atherosclerosis increases an inflammatory response to cholesterol and fat buildup inside the artery wall. The suppression of protective endothelium genes, specifically KLF2 and KLF4, through targeted targeting has revealed the critical role of miR-92a-3p as a regulator of angiogenesis and endothelial dysfunction (Wiese et al., 2019). Inhibiting miR-92a-3p in mice lacking the low-density lipoprotein receptor (Ldlr−/−) decreases the atherosclerotic load (Loyer et al., 2014). MiR-92a-3p levels in CKD sufferers' blood are higher, and adenine-induced rise of aortic miR-92a-3p levels in CKD rats has been described (Shang et al., 2017). Therefore, impeding the activity of endothelial miR-92a-3p shows great potential as a treatment approach for atherosclerosis in chronic kidney disease. Wiese et al. (2019) conducted a study in which they administered LNA miRNA inhibitors to aortic endothelial cells *in vivo* via HDL, resulting in the discovery of a promising approach for reducing atherosclerosis in a renal injury model (ApoE−/−;5/6Nx). Specifically, the team found that simultaneous inhibition of miR-92a-3p and miR-489-3p yielded positive results in decreasing atherosclerosis. When compared to ApoE/control animals with undamaged kidneys, atherogenic miRNA (miR-92a-3p) levels were considerably higher in the vascular endothelium of ApoE/control mice. A recent research investigation has unveiled a novel miR-92a-3p/FAM220A/STAT3 pathway within human coronary artery epithelial cells (HCAEC) that exhibits potential in mitigating atherosclerosis in a rat model of renal injury. Wiese et al. (2019) discovered new miRNA targets, Tgfb2 and Fam220a, which were validated using real-time PCR and gene reporter experiments. Furthermore, there is a possibility that the presence of miR-92a-3p may have an impact on the pro-atherosclerotic activity of STAT3 through indirect means. This can be achieved by exerting direct control over FAM220A, a negative regulator of STAT3. According to numerous studies, STAT3 serves as a pro-inflammatory transcription factor within vascular endothelial cells, leading to the manifestation of vascular endothelial dysfunction and atherosclerosis (Lim and Fu, 2012; Dutzmann et al., 2015). Thus, dual inhibition of these miRNAs may alleviate atherosclerosis by activating the anti-inflammatory pathway (TGF) while inhibiting the pro-inflammatory route (STAT3). As a result, our data suggest the feasibility of using a dual inhibition strategy of LNA-based miRNAs to treat atherosclerosis in the context of CKD. It is evident that the use of endothelial miRNAs has promising prospects as a means of treating atherosclerosis and could potentially offer a more effective therapeutic approach for individuals with chronic kidney disease (CKD), especially those with advanced CKD who have not responded well to lipid-lowering therapies (see Table 3).

TABLE 3 Comparison of miRNAs in endothelial dysfunction.

miRNAs	Population/Methods	Function	Key-findings
miR-126 Barreto et al. (2009); Padberg et al. (2014)	Patient serum/Sprague-Dawley rats	miR-126 is enriched in endothelial cells and is a regulator of vascular integrity and angiogenesis. The -3p and -5p forms of miR-126 have activity in endothelial cells – 3p is anti-inflammatory and 5p is pro-proliferative。	● miR-126 induces CXCL12-induced angiogenesis through its target gene Spred-1, suggesting that miR-126 expression may be involved in angiogenesis and tissue regeneration. In HUVEC endothelial cells, CXCL12-induced angiogenesis and migration were abolished after miR-126 was inhibited
miR-142-3p Carmona et al. (2017); Guerrero et al. (2020)	p300 transgenic (p300tg) and wild-type (wt) mice/Patient serum	miR-142-3p is not only a biomarker of impaired renal function and endothelial dysfunction, but also a direct mediator of impaired acetylcholine-mediated vasodilation in uremia	● Downregulation of miR-142 is required to enable cytokine-mediated survival signalling during cardiac growth in response to haemodynamic stress and is a critical element of adaptive hypertrophy ● Pharmacological exploitation of naturally occurring miRs and especially miR-142-3p could be a potential avenue to counteract vascular dysfunction in uremia and might thus ultimately prevent deleterious cardiovascular endpoints in patients with ESRD.
miR-92a-3p Furchgott and Zawadzki (1980)	Apolipoprotein E−/− (Apoe−/−) B6.129P2-Apoetm1Unc/J mice	miR-92a-3p has been identified as an important regulator of angiogenesis and endothelial dysfunction by targeting and repressing protective endothelial genes, including kruppel-like factors 2 (KLF2) and 4 (KLF4)	● Elevated aortic endothelial miRNA expression is associated with kidney injury and hypercholesterolemia. Inhibition of miR-92a-3p and miR-489-3p by a dual LNA treatment strategy significantly attenuated atherosclerosis and altered endothelial gene expression. The analysis identified Tgfb2 and Fam220a as novel target genes for miR-489-3p and miR-92a-3p, respectively ● In addition, FAM220A was demonstrated to be a direct target of miR-92a-3p in HCAEC, and the regulatory role of FAM220A on STAT3 phosphorylation in endothelial cells was verified. Thus, these findings support the potential of a dual LNA-based miRNA inhibition strategy for the treatment of atherosclerosis in CKD patients

Summary and outlook

The focus of our investigation is the involvement of microRNAs (miRNAs) in cardiovascular problems associated with chronic kidney disease (CKD). The goal of this study is to highlight the significant promise of multiple miRNAs as new biomarkers and therapeutic targets in the setting of cardiovascular disease (CVD) associated with CKD. Numerous studies have offered persuasive data supporting the use of microRNAs (miRNAs) as effective biological markers of early vascular calcification, allowing for timely intervention to halt the evolution of this disease (Panizo et al., 2016). Additionally, microRNAs show significant promise as feasible targets for the prevention of arterial calcification and its associated negative cardiovascular consequences. Through the use of antisense miRNA inhibitors, the future treatment option for the management and prevention of vascular calcification is the suppression of the miRNAs that activate this process. This approach has greater promise than using nanocarrier-based approaches or vascular-specific carriers to reduce vascular calcification (Metzinger-Le Meuth et al., 2017). Chronic kidney disease (CKD) risk factors, including fibroblast growth factor-23, a uremic toxin, angiotensin II, and transforming growth factor-β, have been reported to inhibit the expression of cardiac miRNA-30. Nonetheless, the addition of additional miRNA-30 has shown a significant decrease in cardiomyocyte enlargement caused by the aforementioned variables. The findings establish a fresh conceptual framework for the pathophysiology of CKD-induced LVH while also identifying a potential focal area for therapeutic intervention aimed at reducing LVH in CKD patients (Bao et al., 2021). MiRNAs have the potential to become sensitive and specific biomarkers for renal disorders due to their tissue specificity and stability in a variety of biological components. The constant development of new perspectives in the domain of microRNAs (miRNAs) is a long-term result of the continued use of animal models, *in vitro* tests, and human subject research. However, the real challenges are in translating these scientific insights into accurate clinical diagnostic tools. Numerous intriguing non-invasive miRNA biomarkers have been discovered in the realm of kidney disease, holding promise for improving prognosis prediction and diagnostic precision, while also monitoring disease progression and treatment efficacy. Individuals with differing degrees of chronic kidney disease (CKD) and those receiving hemodialysis therapy have different

levels of expression of the cellular regulatory molecules known as miRNAs. Patients with chronic kidney disease (CKD) stages III-V who are receiving hemodialysis had elevated expressions of miR-143, miR-145, and miR-223. In contrast, lower amounts of these microRNAs have been seen in kidney transplant patients. In contrast, miR-126 and miR-155 can be identified by their increased abundance in people with CKD stages III-V, followed by a decrease in manifestation among those on hemodialysis, and finally by a more pronounced decrease in renal transplant recipients. These observed differences in miRNA levels illustrate the complex interaction between physiological perturbations and the resulting alteration of gene regulatory systems. This highlights miRNAs' potential as viable diagnostic and therapeutic targets in the management of CKD and its subsequent treatment approaches (Franczyk et al., 2022). Significant clinical trials with a broad patient population, on the other hand, are necessary to test miRNAs' clinical relevance and confirm their accuracy and prevalence. In conclusion, there is a hypothesis indicating the involvement of miRNA in clinical diagnosis; nevertheless, additional research is required. As we move forward, it is extremely likely that microRNAs (miRNAs) will provide significant advantages to current advances in diagnostics and therapies, notably in chronic kidney disease (CKD) and its related cardiovascular illnesses (CVD). MiRNAs are poised to serve a critical and vital function in this respect.

Author contributions

CZ: Writing–review and editing.

Funding

The author(s) declare that no financial support was received for the research, authorship, and/or publication of this article.

Conflict of interest

The author declares that the research was conducted in the absence of any commercial or financial relationships that could be construed as a potential conflict of interest.

Publisher's note

References

Bao, J., Lu, Y., She, Q., Dou, W., Tang, R., Xu, X., et al. (2021). MicroRNA-30 regulates left ventricular hypertrophy in chronic kidney disease. *JCI Insight* 6 (10), e138027. doi:10.1172/jci.insight.138027

Barreto, F. C., Barreto, D. V., Liabeuf, S., Meert, N., Glorieux, G., Temmar, M., et al. (2009). Serum indoxyl sulfate is associated with vascular disease and mortality in chronic kidney disease patients. *Clin. J. Am. Soc. Nephrol.* 4, 1551–1558. doi:10.2215/CJN.03980609

Bassand, K., Metzinger, L., Naïm, M., Mouhoubi, N., Haddad, O., Assoun, V., et al. (2021). miR-126-3p is essential for CXCL12-induced angiogenesis. *J. Cell Mol. Med.* 25, 6032–6045. doi:10.1111/jcmm.16460

Bradshaw, A. D. (2009). The role of SPARC in extracellular matrix assembly. *J. Cell Commun. Signal.* 3, 239–246. doi:10.1007/s12079-009-0062-6

Care, A., Catalucci, D., Felicetti, F., Bonci, D., Addario, A., Gallo, P., et al. (2007). MicroRNA-133 controls cardiac hypertrophy. *Nat. Med.* 13 (5), 613–618. doi:10.1038/nm1582

Carmona, A., Guerrero, F., Buendia, P., Obrero, T., Aljama, P., and Carracedo, J. (2017). Microvesicles derived from indoxyl sulfate TreatedEndothelial cells induce endothelial progenitor cells dysfunction. *Front. Physiol.* 8, 666. doi:10.3389/fphys.2017.00666

Carracedo, J., Alique, M., Vida, C., Bodega, G., Ceprián, N., Morales, E., et al. (2020). Mechanisms of cardiovascular disorders in patients with chronic kidney disease: a process related to accelerated senescence. *Front. Cell Dev. Biol.* 8, 185. doi:10.3389/fcell.2020.00185

Cha, H. J., Kim, H. Y., and Kim, H. S. (2018). Sulfatase 1 mediates the attenuation of Ang II-induced hypertensive effects by CCL5 in vascular smooth muscle cells from spontaneously hypertensive rats. *Cytokine* 110, 1–8. doi:10.1016/j.cyto.2017.12.027

Chao, C., Yuan, T., Yeh, H., Chen, H. Y., Huang, J. W., and Chen, H. W. (2019). Risk factors associated withaltered circulating microRNA-125b and their influences on uremicvascular calcification among patients with end-stage renal disease. *J. Am. Heart Assoc.* 8, e010805. doi:10.1161/JAHA.118.010805

Chao, C. T., Liu, Y. P., Su, S. F., Yeh, H. Y., Chen, H. Y., Lee, P. J., et al. (2017). Circulating MicroRNA-125b predicts the presence and progression of uremic vascular calcification. *Arterioscler. Thromb. Vasc. Biol.* 37 (7), 1402–1414. doi:10.1161/ATVBAHA.117.309566

Chao, C. T., Yeh, H. Y., Tsai, Y. T., Chiang, C. K., and Chen, H. W. (2021). A combined microRNA and target protein-based panel for predicting the probability and severity of uraemic vascular calcification: a translational study. *Cardiovasc Res.* 117 (8), 1958–1973. doi:10.1093/cvr/cvaa255

Chen, N. X., Kiattisunthorn, K., O'Neill, K. D., Chen, X., Moorthi, R. N., Gattone, V. H., et al. (2013). DecreasedmicroRNA is involved in the vascular remodeling abnormalities inchronic kidney disease (CKD). *PLoS One* 8, e64558. doi:10.1371/journal.pone.0064558

Chow, F. Y., Nikolic-Paterson, D. J., Ozols, E., Atkins, R. C., and Tesch, G. H. (2005). Intercellular adhesion molecule-1 deficiency is protectiveagainst nephropathy in type 2 diabetic db/db mice. *J. Am. Soc. Nephrol.* 16, 1711–1722. doi:10.1681/ASN.2004070612

Chuppa, S., Liang, M., Liu, P., Liu, Y., Casati, M. C., Cowley, A. W., et al. (2018). MicroRNA-21 regulates peroxisome proliferator-activated receptor alpha, a molecular mechanism of cardiac pathology in Cardiorenal Syndrome Type 4. *Kidney Int.* 93, 375–389. doi:10.1016/j.kint.2017.05.014

Cunha, R. S. D., Santos, A. F., Barreto, F. C., and Stinghen, A. E. M. (2020). How do uremic toxins affect the endothelium? *Toxins (Basel).* 12 (6), 412. doi:10.3390/toxins12060412

D'Agostino, M., Mauro, D., Zicarelli, M., Carullo, N., Greco, M., Andreucci, M., et al. (2023). miRNAs in uremic cardiomyopathy: a comprehensive review. *Int. J. Mol. Sci.* 24 (6), 5425. Published 2023 Mar 12. doi:10.3390/ijms24065425

David, S., Kümpers, P., Lukasz, A., Fliser, D., Martens-Lobenhoffer, J., Bode-Böger, S. M., et al. (2010). Circulating angiopoietin-2 levels increase with progress of chronic kidney disease. *Nephrol. Dial. Transpl.* 25, 2571–2576. doi:10.1093/ndt/gfq060

De Luca, M., Klimentidis, Y. C., Casazza, K., Chambers, M. M., Cho, R., Harbison, S. T., et al. (2010). A conserved role for syndecan family members in the regulation of whole-body energy metabolism. *PLoSONE* 5, e11286. doi:10.1371/journal.pone.0011286

Disthabanchong, S., and Srisuwarn, P. (2019). Mechanisms of vascular calcification in kidney disease. *Adv. Chronic Kidney Dis.* 26, 417–426. doi:10.1053/j.ackd.2019.08.014

Doshi, S. M., and Wish, J. B. (2022). Past, present, and future of phosphate management. *Kidney Int. Rep.* 7, 688–698. doi:10.1016/j.ekir.2022.01.1055

Drummond, C. A., Hill, M. C., Shi, H., Fan, X., Xie, J. X., Haller, S. T., et al. (2016). Na/K-ATPase signaling regulates collagen synthesis through microRNA-29b-3p in cardiac fibroblasts. *Physiol. Genomics.* 48, 220–229. doi:10.1152/physiolgenomics.00116.2015

Durham, A. L., Speer, M. Y., Scatena, M., Giachelli, C. M., and Shanahan, C. M. (2018). Role of smooth muscle cells in vascular calcification: implications in atherosclerosis and arterial stiffness. *Cardiovasc Res.* 114, 590–600. doi:10.1093/cvr/cvy010

Dutzmann, J., Daniel, J. M., Bauersachs, J., Hilfiker-Kleiner, D., and Sedding, D. G. (2015). Emerging translational approaches to target STAT3 signalling and its impact on vascular disease. *Cardiovasc Res.* 106 (3), 365–374. doi:10.1093/cvr/cvv103

Fang, J., Zhang, Y., Chen, D., Zheng, Y., and Jiang, J. (2022). Exosomes and exosomal cargos: a promising world for ventricular remodeling following myocardial infarction. *Int. J. Nanomedicine* 17, 4699–4719. Published 2022 Oct 4. doi:10.2147/IJN.S377479

Fourdinier, O., Glorieux, G., Brigant, B., Diouf, M., Pletinck, A., Vanholder, R., et al. (2021). Syndecan-1 and free indoxyl sulfate levels are associated with miR-126 in chronic kidney disease. *Int. J. Mol. Sci.* 22 (19), 10549. doi:10.3390/ijms221910549

Franczyk, B., Gluba-Brzózka, A., Olszewski, R., Parolczyk, M., Rysz-Górzyńska, M., and Rysz, J. (2022). miRNA biomarkers in renal disease. *Int. urology Nephrol.* 54 (3), 575–588. doi:10.1007/s11255-021-02922-7

Fujii, T., Shimada, K., Tatsumi, Y., Fujimoto, K., and Konishi, N. (2015). Syndecan-1 responsive microRNA-126 and 149 regulate cellproliferation in prostate cancer. *Biochem. Biophys. Res. Commun.* 456, 183–189. doi:10.1016/j.bbrc.2014.11.056

Furchgott, R. F., and Zawadzki, J. V. (1980). The obligatory role of endothelial cells in the relaxation of arterial smooth muscle by acetylcholine. *Nature* 288, 373–376. doi:10.1038/288373a0

Glorieux, G., Vanholder, R., Van Biesen, W., Pletinck, A., Schepers, E., Neirynck, N., et al. (2021). Free P-cresyl sulfate shows the highest association with cardiovascular outcome in chronic kidney disease. *Nephrol. Dial.Transplant.* 36, 998–1005. doi:10.1093/ndt/gfab004

Goettsch, C., Rauner, M., Pacyna, N., Hempel, U., Bornstein, S. R., and Hofbauer, L. C. (2011). miR-125b regulates calcification of vascularsmooth muscle cells. *Am. J. Pathol.* 179, 1594–1600. doi:10.1016/j.ajpath.2011.06.016

Guerrero, F., Carmona, A., Obrero, T., Jiménez, M. J., Soriano, S., Moreno, J. A., et al. (2020). Role of endothelialmicrovesicles released by p-cresol on endothelial dysfunction. *Sci. Rep.* 10, 10657. doi:10.1038/s41598-020-67574-6

He, X., Wang, Z., Wei, L., Cheng, X., Chen, L., Gao, F., et al. (2020). Indoxyl sulfate promotes osteogenic differentiation of vascular smooth muscle cells by miR-155-5p-dependent downregulation of matrix Gla protein via ROS/NF-κB signaling. *Exp. Cell Res.* 397 (1), 112301. doi:10.1016/j.yexcr.2020.112301

Huang, Z.-P., Chen, J., Seok, H. Y., Zhang, Z., Kataoka, M., Hu, X., et al. (2013). MicroRNA-22 regulates cardiac hypertrophy and remodeling in response to stress. *Circ. Res.* 112 (9), 1234–1243. doi:10.1161/CIRCRESAHA.112.300682

Jansen, F. H., Krijgsveld, J., van Rijswijk, A., van den Bemd, G. J., van den Berg, M. S., van Weerden, W. M., et al. (2009). Exosomal secretion of cytoplasmic prostate cancer xenograft-derived proteins. *Mol. Cell Proteomics* 8, 1192–1205. doi:10.1074/mcp.M800443-MCP200

Jiang, W., Wang, X., Geng, X., Gu, Y., Guo, M., Ding, X., et al. (2021). Novel predictive biomarkers for acute injury superimposed onchronic kidney disease. *Nefrología* 41, 165–173. doi:10.1016/j.nefro.2020.06.007

Kalantar-Zadeh, K., Jafar, T. H., Nitsch, D., Neuen, B. L., and Perkovic, V. (2021). Chronic kidney disease. *lancet* 398 (10302), 786–802. doi:10.1016/S0140-6736(21)00519-5

Kétszeri, M., Kirsch, A., Frauscher, B., Moschovaki-Filippidou, F., Mooslechner, A. A., et al. (2019). MicroRNA-142-3p improves vascular relaxation in uremia. *Atherosclerosis* 280, 28–36. doi:10.1016/j.atherosclerosis.2018.11.024

Lee, C. T., Lee, Y. T., Tain, Y. L., Ng, H. Y., and Kuo, W. H. (2019). Circulating microRNAs and vascular calcification in hemodialysis patients. *J. Int. Med. Res.* 47 (7), 2929–2939. doi:10.1177/0300060519848949

Leopold, J. A. (2015). Vascular calcification: mechanisms of vascular smooth muscle cell calcification. *Trends Cardiovasc Med.* 25, 267–274. doi:10.1016/j.tcm.2014.10.021

Li, H., Xu, J. D., Fang, X. H., Zhu, J. N., Yang, J., Pan, R., et al. (2020). Circular RNA circRNA_000203 aggravates cardiac hypertrophy via suppressing miR-26b-5p and miR-140-3p binding to Gata4. *Cardiovasc Res.* 116 (7), 1323–1334. doi:10.1093/cvr/cvz215

Li, S., Zhi, F., Hu, M., Xue, X., and Mo, Y. (2022). MiR-133a is a potential target for arterial calcification in patients with end-stage renal disease. *Int. Urol. Nephrol.* 54 (1), 217–224. doi:10.1007/s11255-021-02906-7

Liabeuf, S., Drüeke, T. B., and Massy, Z. A. (2011). Protein-bound uremic toxins: new insight from clinical studies. *Toxins* 3, 911–919. doi:10.3390/toxins3070911

Liew, H., Roberts, M. A., Pope, A., and McMahon, L. P. (2021). Endothelial glycocalyx damage in kidney disease correlates with uraemictoxins and endothelial dysfunction. *BMC Nephrol.* 22, 21. doi:10.1186/s12882-020-02219-4

Lim, C. P., and Fu, X. Y. (2012). Multiple roles of STAT3 in cardiovascular inflammatory responses. *Prog. Mol. Biol. Transl. Sci.* 106, 63–73. doi:10.1016/B978-0-12-396456-4.00010-9

Lim, Y. J., Sidor, N. A., Tonial, N. C., Che, A., and Urquhart, B. L. (2021). Uremic toxins in the progression of chronic kidney disease and cardiovascular disease: mechanisms and therapeutic targets. *Toxins* 13 (2), 142. doi:10.3390/toxins13020142

Liu, S., and Zhang, N. (2021). Narrative review of exosomes: novel players in vascular calcification of chronic kidney disease. *Ann. Palliat. Med.* 10 (12), 13002–13008. doi:10.21037/apm-20-910

Liu, Y., Guo, Y., Bao, S., Huang, H., Liu, W., and Guo, W. (2022). Bone marrow mesenchymal stem cell-derived exosomal microRNA-381-3p alleviates vascular calcification in chronic kidney disease by targeting NFAT5. *Cell Death Dis.* 13 (3), 278. Published 2022 Mar 28. doi:10.1038/s41419-022-04703-1

Liu, Z., Tan, R. J., and Liu, Y. (2020). The many faces of matrix metalloproteinase-7 in kidney diseases. *Biomolecules* 10, 960. doi:10.3390/biom10060960

Loyer, X., Potteaux, S., Vion, A. C., Guérin, C. L., Boulkroun, S., Rautou, P. E., et al. (2014). Inhibition of microRNA-92a prevents endothelial dysfunction and atherosclerosis in mice. *Circ. Res.* 114 (3), 434–443. doi:10.1161/CIRCRESAHA.114.302213

Ludwig, N., Leidinger, P., Becker, K., Backes, C., Fehlmann, T., Pallasch, C., et al. (2016). Distribution of miRNA expression across human tissues. *Nucleic Acids Res.* 44 (8), 3865–3877. doi:10.1093/nar/gkw116

Matsushita, K., Ballew, S. H., Wang, A. Y. M., Kalyesubula, R., Schaeffner, E., and Agarwal, R. (2022). Epidemiology and risk of cardiovascular disease in populations with chronic kidney disease. *Nat. Rev. Nephrol.* 18 (11), 696–707. doi:10.1038/s41581-022-00616-6

Matsushita, K., Wu, Y., Pratt, R. E., and Dzau, V. J. (2015). Blockade of angiotensin II type 2 receptor by PD123319 inhibits osteogenic differentiation of human mesenchymal stem cells via inhibition of extracellular signal-regulated kinase signaling. *J. Am. Soc. Hypertens.* 9, 517–525. doi:10.1016/j.jash.2015.06.006

Mcgahon, M. K., Yarham, J. M., Daly, A., Guduric-Fuchs, J., Ferguson, L. J., Simpson, D. A., et al. (2013). Distinctive profile of IsomiR expression and novel microRNAs in rat heart left ventricle. *PLoS One* 8 (6), e65809. doi:10.1371/journal.pone.0065809

Metzinger-Le Meuth, V., Burtey, S., Maitrias, P., Massy, Z. A., and Metzinger, L. (2017). microRNAs in the pathophysiology of CKD-MBD: biomarkers and innovative drugs. *Biochim. Biophys. Acta* 1863, 337–345. doi:10.1016/j.bbadis.2016.10.027

Metzinger-Le Meuth, V., Fourdinier, O., Charnaux, N., Massy, Z. A., and Metzinger, L. (2019). The expanding roles of microRNAs in kid-ney pathophysiology. *Nephrol. Dial. Transpl.* 34, 7–15. doi:10.1093/ndt/gfy140

Metzinger-Le Meuth, V., and Metzinger, L. (2019). miR-223 and other miRNA's evaluation in chronic kidney disease: innovative bio-markers and therapeutic tools. *Noncoding RNA Res.* 4, 30–35. doi:10.1016/j.ncrna.2019.01.002

Mirna, M., Topf, A., Wernly, B., Rezar, R., Paar, V., Jung, C., et al. (2020). Novel biomarkers in patients with chronic kidney disease: an analysis of patients enrolled in the GCKD-study. *J. Clin. Med.* 9 (3), 886. doi:10.3390/jcm9030886

Narayanan, A., Srinaath, N., Rohini, M., and Selvamurugan, N. (2019). Regulation of Runx2 by MicroRNAs in osteoblast differentia-tion. *Life Sci.* 232, 116676. doi:10.1016/j.lfs.2019.116676

Nie, B., Zhang, S.-y., Guan, S.-m., Zhou, S.-q., and Fang, X. (2019). Role of wnt/β-catenin pathway in the arterial medial calcification and its effect on the OPG/RANKL system. *Curr. Med. Sci.* 39, 28–36. doi:10.1007/s11596-019-1996-4

Nie, X., Fan, J., Li, H., Yin, Z., Zhao, Y., Dai, B., et al. (2018). miR-217 promotes cardiac hypertrophy and dysfunction by targeting PTEN. *Mol. Ther. Nucleic Acids* 12, 254–266. doi:10.1016/j.omtn.2018.05.013

Padberg, J.-S., Wiesinger, A., Di Marco, G. S., Reuter, S., Grabner, A., Kentrup, D., et al. (2014). Damage of the endothelial glycocalyx in chronic kidney disease. *Atherosclerosis* 234, 335–343. doi:10.1016/j.atherosclerosis.2014.03.016

Panizo, S., Carrillo-López, N., Naves-Díaz, M., Solache-Berrocal, G., Martínez-Arias, L., Rodrigues-Díez, R. R., et al. (2017). Regulation of miR-29b and miR-30c by vitamin D receptor activators contributes to attenuate uraemia-induced cardiac fibrosis. *Nephrol. Dial. Transpl.* 32, 1831–1840. doi:10.1093/ndt/gfx060

Panizo, S., Naves-Díaz, M., Carrillo-López, N., Martínez-Arias, L., Fernández-Martín, J. L., Ruiz-Torres, M. P., et al. (2016). MicroRNAs 29b, 133b, and 211 regulate vascular smooth muscle calcification mediated by high phosphorus. *J. Am. Soc. Nephrol.* 27, 824–834. doi:10.1681/ASN.2014050520

Papaioannou, G., Mirzamohammadi, F., and Kobayashi, T. (2014). MicroRNAs involved in bone formation. *Cell Mol. Life Sci.* 71, 4747–4761. doi:10.1007/s00018-014-1700-6

Parfrey, P. S., Harnett, J. D., Griffiths, S. M., Taylor, R., Hand, J., King, A., et al. (1990). The clinical course of left ventricular hypertrophy in dialysis patients. *Nephron* 55 (2), 114–120. doi:10.1159/000185937

Paterson, M. R., Geurts, A. M., and Kriegel, A. J. (2019). miR-146b-5p has a sex-specific role in renal and cardiac pathology in a rat model of chronic kidney disease. *Kidney Int.* 96 (6), 1332–1345. doi:10.1016/j.kint.2019.07.017

Peng, J., Qin, C., Tian, S. Y., and Peng, J. Q. (2022). MiR-93 inhibits the vascular calcification of chronic renal failure by suppression of Wnt/β-catenin pathway. *Int. Urol. Nephrol.* 54 (1), 225–235. doi:10.1007/s11255-021-02907-6

Prado-Uribe, M. D., Soto-Abraham, M. V., Mora-Villalpando, C. J., Gallardo, J. M., Bonilla, E., Avila, M., et al. (2013). Role of thyroid hormones and mir-208 in myocardial remodeling in 5/6 nephrectomized rats. *Arch. Med. Res.* 44 (8), 616–622. doi:10.1016/j.arcmed.2013.11.005

Rong, D., Sun, H., Li, Z., Liu, S., Dong, C., Fu, K., et al. (2017). An emerging function of circRNA-miRNAs-mRNA axis in human diseases. *Oncotarget* 8, 73271–73281. doi:10.18632/oncotarget.19154

Roumeliotis, S., Mallamaci, F., and Zoccali, C. (2020). Endothelial dysfunction in chronic kidney disease, from biology to clinical outcomes:A 2020 update. *JCM* 9, 2359. doi:10.3390/jcm9082359

Sahota, A. P., and Dhoot, G. K. (2009). A novel SULF1 splice variant inhibits Wnt signalling but enhances angiogenesis by opposing SULF1 activity. *Exp. Cell Res.* 315, 2752–2764. doi:10.1016/j.yexcr.2009.06.029

Sala-Newby, G. B., George, S. J., Bond, M., Dhoot, G. K., and Newby, A. C. (2005). Regulation of vascular smooth muscle cell proliferation, migration and death by heparan sulfate 6-O-endosulfatase1. *FEBS Lett.* 579, 6493–6498. doi:10.1016/j.febslet.2005.10.026

Sárközy, M., Gáspár, R., Zvara, Á., Siska, A., Kővári, B., Szűcs, G., et al. (2019). Chronic kidney disease induces left ventricular overexpression of the pro-hypertrophic microRNA-212. *Sci. Rep.* 9 (1), 1302. doi:10.1038/s41598-018-37690-5

Sarnak, M. J., Levey, A. S., Schoolwerth, A. C., Coresh, J., Culleton, B., Hamm, L. L., et al. (2003). Kidney disease as a risk factor for development of cardiovascular disease: a statement from the American heart association councils on kidney in cardiovascular disease, high blood pressure research, clinical cardiology, and epidemiology and prevention. *Circulation* 108 (17), 2154–2169. doi:10.1161/01.CIR.0000095676.90936.80

Schurgers, L. J., Uitto, J., and Reutelingsperger, C. P. (2013). Vitamin K-dependent carboxylation of matrix Gla-protein: a crucial switchto control ectopic mineralization. *Trends Mol. Med.* 19, 217–226. doi:10.1016/j.molmed.2012.12.008

Scullion, K. M., Vliegenthart, A. D. B., Rivoli, L., Oosthuyzen, W., Farrah, T. E., Czopek, A., et al. (2021). Circulating argonaute-bound microRNA-126 reports vascular dysfunction and treatment response in acute andchronic kidney disease. *iScience* 24, 101937. doi:10.1016/j.isci.2020.101937

Shanahan, C. M., Crouthamel, M. H., Kapustin, A., and Giachelli, C. M. (2011). Arterial calcification in chronic kidney disease: key roles for calcium and phosphate. *Circ. Res.* 109, 697–711. doi:10.1161/CIRCRESAHA.110.234914

Shang, F., Wang, S. C., Hsu, C. Y., Miao, Y., Martin, M., Yin, Y., et al. (2017). MicroRNA-92a mediates endothelial dysfunction in CKD. *J. Am. Soc. Nephrol.* 28 (11), 3251–3261. doi:10.1681/ASN.2016111215

Sharma, S., Liu, J., Wei, J., Yuan, H., Zhang, T., and Bishopric, N. H. (2012). Repression of miR-142 by p300 and MAPK is required for survival signalling via gp130 during adaptive hypertrophy. *EMBO Mol. Med.* 4, 617–632. doi:10.1002/emmm.201200234

Shilo, V., Mor-Yosef Levi, I., Abel, R., Mihailović, A., Wasserman, G., Naveh-Many, T., et al. (2017). Let-7 and MicroRNA-148 regulate parathy-roid hormone levels in secondary hyperpara-thyroidism. *J. Am. Soc. Nephrol.* 28, 2353–2363. doi:10.1681/ASN.2016050585

Shimizu, I., and Minamino, T. (2016). Physiological and pathological cardiac hypertrophy. *J. Mol. Cell Cardiol.* 97, 245–262. doi:10.1016/j.yjmcc.2016.06.001

Sun, W. L., Wang, N., and Xu, Y. (2018). Impact of miR-302b on calcium-phosphorus metabolism and vascular calcification of rats with chronic renal failure by regulating BMP-2/runx2/osterix signaling pathway. *Arch. Med. Res.* 49 (3), 164–171. doi:10.1016/j.arcmed.2018.08.002

Tian, C., Hu, G., Gao, L., Hackfort, B. T., and Zucker, I. H. (2020). Extracellular vesicular MicroRNA-27a* contributes to cardiac hypertrophy in chronic heart failure. *J. Mol. Cell Cardiol.* 143, 120–131. doi:10.1016/j.yjmcc.2020.04.032

Viegas, C., Araújo, N., Marreiros, C., and Simes, D. (2019). The interplaybetween mineral metabolism, vascular calcification and inflamma-tion in Chronic Kidney Disease (CKD): challenging old conceptswith new facts. *Aging* 11, 4274–4299. doi:10.18632/aging.102046

Wang, L., Xu, X., Zhang, M., Hu, C., Li, C., et al. (2023). Prevalence of chronic kidney disease in China: results from the sixth China chronic disease and risk factor surveillance. *JAMA Intern. Med.* 183, 298–310. doi:10.1001/jamainternmed.2022.6817

Wang, X., and Shapiro, J. I. (2019). Evolving concepts in the pathogenesis of uraemic cardiomyopathy. *Nat. Rev. Nephrol.* 15 (3), 159–175. doi:10.1038/s41581-018-0101-8

Wiese, C. B., Zhong, J., Xu, Z. Q., Zhang, Y., Ramirez Solano, M. A., Zhu, W., et al. (2019). Dual inhibition of endothelial miR-92a-3p and miR-489-3p reduces renal injury-associated atherosclerosis. *Atherosclerosis* 282, 121–131. doi:10.1016/j.atherosclerosis.2019.01.023

Xiao, Y., Zhao, J., Tuazon, J. P., Borlongan, C. V., and Yu, G. (2019). MicroRNA-133a and myocardial infarction. *Cell Transpl.* 28 (7), 831–838. doi:10.1177/0963689719843806

Zhang, H., Chen, J., Shen, Z., Gu, Y., Xu, L., Hu, J., et al. (2018). Indoxyl sulfate accelerates vascular smooth muscle cell calcification via microRNA-29b dependent regulation of Wnt/β-catenin signaling. *Toxicol. Lett.* 284, 29–36. doi:10.1016/j.toxlet.2017.11.033

Zhang, Y. X., Tang, R. N., Wang, L. T., and Liu, B. C. (2021). Role of crosstalk between endothelial cells and smooth muscle cells in vascular calcification in chronic kidney disease. *Cell Prolif.* 54 (3), e12980. doi:10.1111/cpr.12980

Zoccali, C., Moissl, U., Chazot, C., Mallamaci, F., Tripepi, G., Arkossy, O., et al. (2017). Chronic fluid overload and mortality in ESRD. *J. Am. Soc. Nephrol.* 28 (8), 2491–2497. doi:10.1681/ASN.2016121341

frontiers | Frontiers in Physiology

TYPE Original Research
PUBLISHED 04 December 2023
DOI 10.3389/fphys.2023.1273286

OPEN ACCESS

EDITED BY
Youfei Guan,
Dalian Medical University, China

REVIEWED BY
Asmaa T. Y. Kishawy,
Other, Egypt
Koushik Das,
Belda College, India

*CORRESPONDENCE
Mahr Un Nisa,
linknisa@gcuf.edu.pk
Muhammad Abdul Rahim,
abdul.rahim@gcuf.edu.pk
Fahad Al-Asmari,
falasmari@kfu.edu.sa
Nazir Ahmad,
drnazirahmad@gcuf.edu.pk

RECEIVED 05 August 2023
ACCEPTED 13 November 2023
PUBLISHED 04 December 2023

CITATION
Umer M, Nisa MU, Ahmad N, Rahim MA and Al-Asmari F (2023), Effects of different levels of dried onion powder on nutrient digestibility, biochemical parameters, and nitrogen balance in Wistar albino rats with induced hyperuricemia.
Front. Physiol. 14:1273286.
doi: 10.3389/fphys.2023.1273286

Effects of different levels of dried onion powder on nutrient digestibility, biochemical parameters, and nitrogen balance in Wistar albino rats with induced hyperuricemia

Muhammad Umer[1], Mahr Un Nisa[1]*, Nazir Ahmad[1]*, Muhammad Abdul Rahim[2,3]* and Fahad Al-Asmari[4]*

[1]Department of Nutritional Sciences, Faculty of Medical Sciences, Government College University, Faisalabad, Punjab, Pakistan, [2]Department of Food Science, Faculty of Life Sciences, Government College University, Faisalabad, Punjab, Pakistan, [3]Department of Food Science and Nutrition, Faculty of Medicine and Allied Health Sciences, Times Institute, Multan, Pakistan, [4]Department of Food and Nutrition Sciences, College of Agricultural and Food Sciences, King Faisal University, Al-Ahsa, Saudi Arabia

Introduction: Onions (*Allium cepa* L.) are excellent sources of bioactive compounds and phytochemicals such as allicin, quercetin, fisetin, and other sulfurous compounds. Therefore, our study aimed to investigate the effects of dried onion powder on growth performance, nitrogen balance, and biochemical parameters in Wistar albino rats with induced hyperuricemia.

Methods: A total of 24 rats were randomly divided into four groups, with six in each group: HU (positive control) and HOT_1, HOT_2, and HOT_3 groups, which received a diet containing onion powder at concentrations of 11.13, 14.84, and 18.61 g/100 g, respectively. Hyperuricemia was induced in rats by administering a new formulation intraperitoneally (250 mg/kg potassium oxonate) and orally (40 mg/kg potassium bromate) daily for 14 days. After confirmation of hyperuricemia induction, rats were fed with onion-treated diets with various concentrations of quercetin for 21 days.

Results: Significant decreases ($p \leq 0.05$) in serum uric acid, alanine aminotransferase, aspartate aminotransferase, alkaline phosphatase, total bilirubin, total cholesterol, and low-density lipoprotein were observed. An increasing trend ($p \leq 0.05$) in the levels of hemoglobin (Hb), white blood cell (WBC), red blood cell (RBC), and platelet count was observed. An improvement in the levels of serum high-density lipoprotein, triglycerides, blood urea nitrogen, serum creatinine, serum total protein and neutrophils, lymphocytes, and monocytes was observed. A positive progress ($p \leq 0.05$) was observed in growth performance and nutrient digestibility.

Conclusion: In conclusion, a significantly lower uric acid level was observed in rats fed with HOT_2 diet. Based on the ratio of the surface area (human/rat), the best recommended dose of onion for the incidence and prevention of hyperuricemia is 189.95 g, corresponding to the dose of 204 mg/day of quercetin in humans.

KEYWORDS

onion, quercetin, hyperuricemia, growth performance, nitrogen balance, nutrient digestibility

1 Introduction

Diet plays an important role in maintaining health by reducing the incidence of metabolic disorders (Jiang et al., 2021). Hyperuricemia is one of the metabolic disorders, which might occur due to the high level of purine and fructose and less water intake. Hyperuricemia is characterized by the elevated levels of serum uric acid, affecting 5%–30% of the population with increasing number of cases day by day (George and Minter, 2022). A recent study has shown an increase in the occurrence of hyperuricemia in Pakistan along with the burden of metabolic syndrome, weight gain, ischemic heart, and renal diseases (Qudwai and Jawaid, 2017). The most commonly considered method to control this disease is to inhibit the production of uric acid. Xanthine oxidase is a key enzyme found in the liver, and it is important for the catabolism of purines. It catalyzes the oxidation of hypoxanthine to xanthine and xanthine to uric acid. Liver xanthine dehydrogenase (XDH) is converted into xanthine oxidase (XO), and then XO catalyzes the *de novo* synthesis of uric acid; this conversion leads to the formation of superoxide anions and hydrogen peroxide in parallel to the synthesis of uric acid (Maia et al., 2007). To control this disease, the most commonly considered method involves reducing the production of uric acid by inhibiting XO in the liver. Most commonly used medicinal treatments include allopurinol and febuxostat (Fels and Sundy, 2008). Allopurinol is also an XO inhibitor in present clinical conditions. However, some adverse effects of allopurinol, such as hepatitis, nephropathy, allergic reactions, and bone marrow suppression, have been reported (Fam, 2003). Therefore, there is a need to discover alternatives to xanthine oxidase inhibitors to reduce the risk of hyperuricemia (Nguyen et al., 2004; Wang et al., 2004; Strazzullo and Puig, 2007). Xanthine oxidase is a very important enzyme that has been inhibited by various phenolic compounds (Potapovich and Kostyuk, 2003). Among them, flavonoids are a group of phenolic compounds that are present in many food plants, including aromatic plants such as onions (*Allium cepa* Liliaceae) (Kinoshita et al., 2006). Red onions contain a high level of quercetin, which is a major component of phenolic compounds, along with some flavones, flavanones, isoflavones, catechins, flavanonols, anthocyanidins, and flavonols (Pérez-Gregorio et al., 2010; Arshad et al., 2017). They can help reduce uric acid production by inhibiting the xanthine oxidase enzyme in the liver. Due to the high availability of quercetin in onions, there is a need to recommend its proper amount in the diet of patients with hyperuricemia to reduce their uric acid levels (Miean and Mohamed, 2001; Teyssier et al., 2001). The objective of this study was to use onion powder as a dietary source to reduce uric acid levels in hyperuricemia-induced male rats. Furthermore, feed and water intake, nutrient digestibility, nitrogen balance, body weight, serum biochemical parameters, and hematology in the rats were also studied.

2 Materials and methods

2.1 Reagents and chemicals

Potassium oxonate (PO) was purchased from Sigma-Aldrich Chemicals. Potassium bromate ($KBrO_3$) in the crystalline form was provided by GlaxoSmithKline, Islamabad, Pakistan.

2.2 Experimental supplement

Healthy and high-peak-seasoned red onions were purchased from the local market, cut into small pieces, and dried in a hot air oven at 65°C for 24 h. Dried onions were ground into a fine powder using an electrical lab grinder and stored in plastic bags at 4°C until further use (Arslan and Özcan, 2010).

2.3 Composition of the diet

The proximate composition of feed and feces was determined using the standard method of AOAC (AOAC, 2006). The diet was isocaloric and isonitrogenous according to the given formulation, as shown in Table 1. In this study, diet was formulated according to the American Institute of Nutrition AIN-93G for the determination of nitrogen metabolism. It contained 3,649.76 kcal/1,000 g energy, as shown in Table 1, including carbohydrates 535.44 g (535.44 × 4 = 2,141.76 kcal), protein 226.97 g (226.97 × 4 = 907.88 kcal), and fats 66.68 g (66.68 × 9 = 600.12 kcal). Therefore, the sum of the total energy from all the nutrients was 2,141.76 + 907.88 + 600.12 = 3,649.76 kcal/kg.

Diet formulation was based on gross energy and ingredients, and nutritional information was sponsored and provided by Refhan Maize and Mukhtar Feeds Ltd. A measure of 100 g of feed was mixed with water and onion powder to make diet pellets. Further proximate analysis was conducted on the resulting feed.

2.4 Study design and animals

The study was conducted *in vivo* with the collaboration of the Department of Nutritional Sciences and Department of Physiology at Government College University Faisalabad, Punjab, Pakistan. All procedures were performed according to the guidelines for the management of laboratory animals (Wade, 1978). The study was

10.3389/fphys.2023.1273286

TABLE 1 Food ingredients and their estimated nutritive values.

Ingredient (g)	HU	Carbohydrate	Protein	Fat	Total gross energy
Corn starch	154.94	152.94	—	—	—
Maize	111.91	78.44	8.95	4.81	—
Dextrose	152.94	152.94	—	—	—
Corn oil/soybean oil	52.22	—	—	52.22	—
Soybean meal	410.33	125.56	180.54	6.97	—
Canola meal	82.06	25.60	37.48	2.68	—
L-Lysine	1.57	—	—	—	—
DL-Methionine	0.64	—	—	—	—
Tryptophan	0.64	—	—	—	—
Threonine	0.91	—	—	—	—
AIN-93-MX mineral mix	24.5	—	—	—	—
AIN-93-vitamin mix	7	—	—	—	—
tert-Butylhydroquinone (TBHQ)	0.005	—	—	—	—
Total	1,000	535.44	226.97	66.68	—
Total gross energy (kcal/kg)	—	2,141.76	907.88	600.12	3,649.76
CP%	—	—	22.69	—	—

Chemical composition of diets after the addition of various levels of onion powder				
Diet	HU	HOT_1	HOT_2	HOT_3
Onion powder (g/100 g feed)	—	11.13 (0.75 mg/kg)	14.84 (0.100 mg/kg)	18.61 (0.125 mg/kg)
Nutritive value feed (%)				
Dry matter	68.25	66	63	68.72
Crude protein	18.54	18.3	18.4	18.1
Crude fiber	4.5	5.1	4.42	4.46
Ether extract	5.8	5.7	5.9	6
Ash	6	5.8	5.6	5.4
Moisture	31.75	33	37	31.28
NFE	33.41	32.1	28.68	34.76

HU, hyperuricemia; HOT_1, hyperuricemia onion treatment 1; HOT_2, hyperuricemia onion treatment 2; HOT_3, hyperuricemia onion treatment 3; NFE, nitrogen-free extract.

approved by the Animal Ethical Committee of Government College University Faisalabad, Pakistan (Wide Ref. No. GCUF/ERC/85). Twenty-four adult male Wistar albino rats weighing 180 ± 5 g were housed in the animal laboratory at a temperature of 25°C ± 5°C and humidity of 45%–55%. The rats were randomly divided into four groups based on the diets containing different levels of onion powder: HU (without onion) and HOT_1, HOT_2, and HOT_3 groups treated with doses of onion of 11.13, 14.84, and 18.61 g/100 gm feed corresponding to the concentrations of quercetin of 0.075, 0.100, and 0.125 mg/kg, respectively. Each group comprised six rats, and each group was further divided into two subgroups to ethically control the rats. Each subgroup was fed 100 g diet daily for 3 weeks.

2.5 Induction of hyperuricemia in rats

To induce hyperuricemia, a uricase inhibitor called PO (also known as potassium azaorotate, potassium otastat, or oteracil potassium) was used. A dose of 250 mg/kg was prepared in 1 mL of 0.9% saline solution and administered intraperitoneally daily for 14 days. This was done to increase the activity of the XO enzyme and was based on the research conducted by Haidari et al. (2008), Sarvaiya et al. (2015), and Yiying et al. (2016). To further induce the degenerative activity of renal cells and mildly increase the activity of XO, $KBrO_3$ was administered orally at 40 mg/kg. The goal was to increase the level of uric acid in serum, according to Kermani et al. (2020).

2.6 Evaluation of growth performance and nutrient digestibility

The growth performance parameters and nutrient digestibility were determined according to the following Eqs 1–3 (Nisa et al., 2006; Shi et al., 2015; Naeem et al., 2023). We considered last 7 days as the collection period. Feces were composited, weighed, and stored at −20°C for further analysis. The data were obtained using the following equations:

$$FCR\ (\%) = \frac{\text{Feed Intake}}{\text{Body Weight Gain}}, \quad (1)$$

$$FER = \frac{Body\ Weight\ Gain}{Feed\ Intake}, \quad (2)$$

$$Digestibility = \frac{Nutrient\ Intake - Nutrient\ in\ feces}{Nutrient\ Intake} \times 100. \quad (3)$$

2.7 Blood collection

At the end of the study, all rats were sacrificed under anesthesia. Blood was collected from the neck area using a surgical blade and preserved in ethylenediaminetetraacetic acid (EDTA) tubes. After centrifuging blood samples at 5,000 rpm, serum was collected and stored at −20°C for further biochemical analysis.

2.8 Biochemical analysis

Low-density lipid (LDL) (mg/dL) was calculated using the Friedewald equation (Kaur, 2014). The levels of serum cholesterol (mg/dL), triglycerides (TG) (mg/dL), serum high-density lipid (HDL) (mg/dL), alanine aminotransferase (ALT) (U/L), aspartate aminotransferase (AST) (U/L), serum bilirubin (mg/dL), alkaline phosphatase (ALP) (U/L), total protein (g/dL), creatinine (mg/dL), urea nitrogen, and uric acid (mg/dL) were determined using the Cobas E311 method based on the principle of a spectrophotometer using commercially available kits (Randie Little, 2016). Uric acid kit (CAT No.: UA 121120) (BioMed Diagnostics) was provided by the Department of Nutritional Sciences. The hemoglobin level (Hb) (g/dL); red blood cell (RBC) count ($\times 10^6$ µL); white blood cell (WBC) count ($\times 10^3$ µL); monocyte, lymphocyte, neutrophil (%), and platelet count ($\times 10^5$/µL) were determined using Mindray BC-6200 based on the principle of electrical impedance, flow cytometry, and light scattering (Kulik et al., 2021; Rahim et al., 2023).

2.9 Nitrogen balance study

For studying nitrogen balance in rats, urine was collected for 24 h in the following time periods: 6:00 a.m., 8:00 a.m., 10:00 a.m., 12:00 p.m., 2:00 p.m., 4:00 p.m., 6:00 p.m., 8:00 p.m., 10:00 p.m., 12:00 a.m., 2:00 a.m., and 4:00 a.m. This method was adopted after considerable observations in our laboratory. Urine was collected using the palpation and contraction technique, as discussed by Chew and Chua (2003). To perform the procedure, first hold the rat's tail with the left hand, palpating its lower back near the bladder with the forefinger and middle finger of the other hand and then applying pressure by massaging and rubbing up and down both sides of the lower back near the tail. As the rat began to urinate, the urine was immediately collected in the Eppendorf tubes and stored at −20°C for further analysis. The percentage of nitrogen in feed, urine, and feces was evaluated using the Kjeldahl method (AOAC, 2006). Nitrogen balance involves a 24-h measurement of protein intake and an estimate of nitrogen loss. Nitrogen balance was estimated using Eq. 4:

$$\text{Nitrogen balance (mg)} = (\text{Nitrigen intake} - \text{Nitrogen in urine} - \text{Nitrogen in feces}). \quad (4)$$

2.10 Statistics

Statistical software (Statistics 8.1) was used to analyze the data using a complete randomized design. Two-way ANOVA was subjected to analyze weekly feed intake, water intake, and body weight and serum uric acid, whereas other parameters were analyzed by one-way ANOVA, followed by LSD. The level of significance was $p \leq 0.05$.

2.11 Human equivalent dose

In this study, the human equivalent dose of onion is estimated to be 189.95 g with 204 mg of quercetin based on the results, while on dry matter basis, it is 30.62 g with 222 g of quercetin (Eq. 5):

$$Human\ equivalent\ dose\left(\frac{mg}{kg}\right) = Animal\ dose \times Coversion\ factor. \quad (5)$$

3 Results

3.1 Feed intake, weight management, and FCR

Feed intake (g) significantly increased ($p \leq 0.05$) in rats that fed on HOT_1 diet followed by the HOT_3 diet, as shown in Table 2. Feed intake was found to be higher in week 1 and week 2 in HOT_1 and HOT_3 groups but lower in the HOT_2 group (191.94 ± 5.9) than that in HU (264.97 ± 8.7). In HOT_3, there was a significant difference ($p \leq 0.05$) in feed intake in week 2 compared to week 1 and week 2. Feed intake significantly increased ($p \leq 0.05$) in week 1 and week 2 in treatment groups, and this might be due to the compensatory growth mechanism. Water intake was significantly increased ($p \leq 0.05$) from week 1 (158.02 ± 12.49 and 170.83 ± 10.98) to week 3 (184.74 ± 9.62 and 185.82 ± 10.29) in rats that fed on HOT_1 and HOT_3 diets compared to the HU diet in week 1 (154.46 ± 8.93) to week 3 (125.63 ± 10.09). According to Table 3, the HOT_2 treatment group did not show an increasing trend of water intake, and their results are non-significant to HU. Average gain ($p \leq 0.05$) in body weight (BW) was observed in rats that fed on HU (20.72 ± 0.05 g) and HOT_2 (22.33 ± 0.05 g) diets. Significant lower ($p \leq 0.05$) BW (18.01 ± 0.05 g and 18.93 ± 0.05 g) was observed in rats that fed on HOT_3 and HOT_1 diets, respectively (Table 4). FCR and FER values were significantly

10.3389/fphys.2023.1273286

TABLE 2 Effect of onion on feed intake (gram) in 3 weeks.

Duration of feeding	Treatments			
	HU	HOT_1	HOT_2	HOT_3
Week 1	264.97 ± 8.7[a]	245.26 ± 6.68[a]	214.67 ± 7.47[a]	235.94 ± 6.36[b]
Week 2	235.27 ± 7.29[b]	249.52 ± 7.98[a]	191.94 ± 5.9[b]	263.03 ± 7.34[a]
Week 3	234.44 ± 6.61[b]	243.85 ± 6.61[a]	205.47 ± 8.22[a]	233.08 ± 5.71[b]
Total	734.78 ± 0.1[b]	738.67 ± 0.14[a]	612.11 ± 0.09[d]	732.12 ± 0.1[c]

HU, hyperuricemia; HOT_1, hyperuricemia onion treatment 1; HOT_2, hyperuricemia onion treatment 2; HOT_3, hyperuricemia onion treatment 3.

TABLE 3 Effect of onion on water intake (mL) in 3 weeks.

Duration of feeding	Treatments			
	HU	HOT_1	HOT_2	HOT_3
Week 1	154.46 ± 8.93[a]	158.02 ± 12.49[b]	166.31 ± 12.52[a]	170.83 ± 10.98[a]
Week 2	124.69 ± 8.60[b]	178.97 ± 9.51[a]	117.62 ± 12.79[b]	171.26 ± 12.99[a]
Week 3	125.63 ± 10.09[b]	184.74 ± 9.62[a]	125.72 ± 14.04[b]	185.82 ± 10.29[a]
Total	404.80 ± 0.12[d]	521.77 ± 0.13[b]	409.69 ± 0.13[c]	527.91 ± 0.075[a]

HU, hyperuricemia; HOT_1, hyperuricemia onion treatment 1; HOT_2, hyperuricemia onion treatment 2; HOT_3, hyperuricemia onion treatment 3.

TABLE 4 Effect of onion on body weight (grams).

Group	HU	HOT_1	HOT_2	HOT_3
Initial body weight (before treatment)	179.32 ± 0.23[c]	180.30 ± 0.24[b]	180.81 ± 0.15[a]	180.90 ± 0.08[a]
Final body weight (after treatment)	200.04 ± 0.23[b]	199.23 ± 0.26[c]	203.14 ± 0.21[a]	198.92 ± 0.14[c]
Average body weight gain	20.72 ± 0.05[b]	18.93 ± 0.05[c]	22.33 ± 0.05[a]	18.01 ± 0.05[d]

HU, hyperuricemia; HOT_1, hyperuricemia onion treatment 1; HOT_2, hyperuricemia onion treatment 2; HOT_3, hyperuricemia onion treatment 3.

TABLE 5 Effect of onion on feed conversion and feed efficiency ratios (%).

Group	HU	HOT_1	HOT_2	HOT_3
Total feed intake in 3 weeks (g)	734.78 ± 0.1[b]	738.67 ± 0.14[a]	612.11 ± 0.09[d]	732.12 ± 0.1[c]
Total weight gain in 3 weeks (g)	20.72 ± 0.05[b]	18.93 ± 0.05[c]	22.33 ± 0.05[a]	18.01 ± 0.05[d]
FCR (%)	35.528 ± 0.18[c]	39.085 ± 0.17[b]	27.458 ± 0.14[d]	40.683 ± 0.12[a]
FER	0.0300 ± 0.009[a]	0.0278 ± 0.008[a]	0.0388 ± 0.009[a]	0.0263 ± 0.008[a]

FCR, feed conversion ratio; FER, feed efficiency ratio; HU, hyperuricemia; HOT_1, hyperuricemia onion treatment 1; HOT_2, hyperuricemia onion treatment 2; HOT_3, hyperuricemia onion treatment 3.

improved in rats that fed on HOT_2 diet followed by the HOT_1 diet, which means that rats utilized the feed efficiently and it has positively influenced the body weight compared to HU (Table 5).

3.2 Nutrient intake (gm)

Higher values of DM intake (22.51 ± 0.14 and 22.47 ± 0.20) were observed in rats that fed on HOT_3 and HOT_2 diets, and lower DM intake was observed in rats that fed on HOT_1 (17.60 ± 0.14) than HU (22.05 ± 0.11). Higher CP intake (6.27 ± 0.20) was observed in rats that fed on HOT_1 diet than HOT_2 (5.18 ± 0.17), HOT_3 (5.95 ± 0.14), and HU (6.08 ± 0.23). A similar trend followed in CF intake, and higher (1.78 ± 0.10) fiber intake was observed in rats that fed on HOT_1 diet than in the other treatment groups. Ether extract (EE) intake was found to be higher (2.00 ± 0.13 and 1.95 ± 0.07) in rats that fed on HOT_3 and HOT_1 diets than in HOT_2 (1.69 ± 0.12) and HU (1.91 ± 0.14). Ash intake was found to be higher (2.02 ± 0.10) in

10.3389/fphys.2023.1273286

TABLE 6 Effect of onion on nutrient intake (grams).

Group	HU	HOT_1	HOT_2	HOT_3
Dry matter	22.05 ± 0.11^{b}	22.47 ± 0.20^{a}	17.60 ± 0.14^{c}	22.51 ± 0.14^{a}
Crude protein	6.08 ± 0.23^{ab}	6.27 ± 0.20^{a}	5.18 ± 0.17^{c}	5.95 ± 0.14^{b}
Crude fiber	1.51 ± 0.13^{b}	1.78 ± 0.10^{a}	1.25 ± 0.18^{c}	1.49 ± 0.12^{b}
Ether extract	1.91 ± 0.14^{a}	1.95 ± 0.07^{a}	1.69 ± 0.12^{b}	2.00 ± 0.13^{a}
Ash	1.97 ± 0.07^{ab}	2.02 ± 0.10^{a}	1.60 ± 0.14^{c}	1.81 ± 0.14^{b}

HU, hyperuricemia; HOT_1, hyperuricemia onion treatment 1; HOT_2, hyperuricemia onion treatment 2; HOT_3, hyperuricemia onion treatment 3.

TABLE 7 Effect of onion on nutrient digestibility (%).

Nutrient	HU	HOT_1	HOT_2	HOT_3
Dry matter	92.51 ± 0.27^{b}	90.81 ± 0.12^{c}	90.44 ± 0.30^{c}	93.47 ± 0.35^{a}
Crude protein	91.30 ± 0.27^{b}	91.31 ± 0.18^{b}	91.19 ± 0.26^{b}	92.55 ± 0.25^{a}
Crude fiber	89.14 ± 0.37^{b}	89.08 ± 0.29^{b}	88.60 ± 0.29^{c}	91.15 ± 0.29^{a}
Ether extract	89.32 ± 0.23^{b}	89.51 ± 0.32^{b}	89.44 ± 0.21^{b}	90.56 ± 0.23^{a}
Ash	89.65 ± 0.19^{b}	89.43 ± 0.31^{b}	88.88 ± 0.24^{c}	91.23 ± 0.27^{a}
NFE	94.90 ± 0.20^{a}	91.80 ± 0.17^{b}	91.13 ± 0.35^{c}	94.98 ± 0.14^{a}

HU, hyperuricemia; HOT_1, hyperuricemia onion treatment 1; HOT_2, hyperuricemia onion treatment 2; HOT_3, hyperuricemia onion treatment 3; NFE, nitrogen free extract.

rats that fed on HOT_1 diet than in HOT_2 (1.60 ± 0.14), HOT_3 (1.81 ± 0.14), and HU (1.97 ± 0.07) diets (Table 6).

3.3 Nutrient digestibility (%)

Significant DM digestibility was found to be higher ($p \leq 0.05$) in rats that fed on HOT_3 (93.47 ± 0.35) and HU (92.51 ± 0.27) diets than in HOT_2 (90.44 ± 0.30) and HOT_1 (90.81 ± 0.12) diets. Similar trend in the digestibility of CP, ash, and nitrogen-free extract (NFE) was observed to be higher ($p \leq 0.05$) in HOT_3 and HU diets than the other groups. Higher (91.15% ± 0.29%) and lower (89.08 ± 0.29) CF digestibility was observed in HOT_3 and HOT_1 diets compared to the HOT_2 (88.60 ± 0.29) and HU (89.14 ± 0.37). EE digestibility was significantly improved ($p \leq 0.05$) in rats that fed on HOT_3 (90.56% ± 0.23%), HOT_1 (89.51 ± 0.32), and HOT_2 (89.44 ± 0.21) diets compared to HU (89.32 ± 0.23) (Table 7).

3.4 Uric acid and renal and liver functions

Serum uric acid was significantly induced ($p \leq 0.05$) in rats, and higher uric acid levels were found at day 14 in the treatment groups. The latest changes are discussed in this section. Uric acid was successfully induced ($p \leq 0.05$) in all the treatment groups, and it was found to be higher (4.80 ± 0.12 mg/dL and 4.20 ± 0.36 mg/dL) in rats that fed on the HOT_3 and HOT_1 diets on day 14, respectively. The treatment period started from day 14 to day 28. The serum uric acid levels significantly decreased (3.01 ± 0.54 mg/dL and 3.21 ± 0.11 mg/dL) in rats that fed on HOT_1 and HOT_3 diets, respectively. To explore the further efficacy of dried onion, the treatment period was extended until day 35, and the levels of serum uric acid were significantly decreased ($p \leq 0.05$) (1.53 ± 0.08 mg/dL and 1.81 ± 0.07 mg/dL) in rats that fed on HOT_2 and HOT_3 diets, respectively, compared to HU (4.31 ± 0.03 mg/dL), as shown in (Table 8). Significantly lower levels of creatinine (0.70 ± 0.2 mg/dL and 0.44 ± 0.05 mg/dL) were observed in rats that fed on HOT_2 and HOT_3 diets compared to HU. Serum blood urea nitrogen (BUN) was found to be lower (32.49 ± 4.69 mg/dL and 33.64 ± 2.12 mg/dL) in rats that fed on HOT_3 and HOT_2 diets than the rats that fed on HOT_1 (45.66 ± 4.16 mg/dL) and HU (35.33 ± 5.50 mg/dL) diets (Table 9). Serum ALT, AST, and ALP (U/L) were significantly ($p \leq 0.05$) decreased in rats that fed on onion diets. A decreasing trend ($p \leq 0.05$) in bilirubin levels (1.49 ± 0.14 mg/dL and 1.74 ± 0.12 mg/dL) was observed in rats that fed on HOT_3 and HOT_2 diets than HOT_1 (3.94 ± 0.21 mg/dL) and HU (3.76 ± 0.55 mg/dL) diets (Table 10).

3.5 Serum total protein and lipid profile

Significantly improved serum total protein levels (6.85 ± 0.07 mg/dL and 6.86 ± 0.10 mg/dL) were observed in rats that fed on HOT_2 and HOT_3 diets compared to HOT_1 (6.76 ± 0.06 mg/dL) and HU (6.78 ± 0.16 mg/dL) diets (Table 11). In serum total cholesterol, LDL was significantly reduced ($p \leq 0.05$) in rats that fed on onion-enriched diets compared to HU. The level of HDL did not increase ($p \leq 0.05$) in rats that fed on HOT_3 (18.75 ± 2.18 mg/dL) and HOT_2 (24.42 ± 2.63 mg/dL), but HOT_1 (30.10 ± 2.11 mg/dL) had not differed significantly ($p \geq 0.05$) compared to HU (30.70 ± 2.52 mg/dL) (Table 12).

TABLE 8 Effect of onion on the uric acid level (mg/dL).

Day	Treatments			
	HU	HOT_1	HOT_2	HOT_3
Day 0	0.95 ± 0.03^{d}	0.82 ± 0.065^{c}	0.82 ± 0.08^{d}	0.90 ± 0.05^{d}
Day 14	4.05 ± 0.03^{c}	4.20 ± 0.36^{a}	4.13 ± 0.04^{a}	4.80 ± 0.12^{a}
Day 28	4.20 ± 0.06^{b}	3.01 ± 0.54^{b}	3.52 ± 0.06^{b}	3.21 ± 0.11^{b}
Day 35	4.31 ± 0.03^{a}	2.78 ± 0.58^{b}	1.53 ± 0.08^{c}	1.81 ± 0.07^{c}

HU, hyperuricemia; HOT_1, hyperuricemia onion treatment 1; HOT_2, hyperuricemia onion treatment 2; HOT_3, hyperuricemia onion treatment 3.

TABLE 9 Effect of onion on renal function (mg/dL).

Treatment	HU	HOT_1	HOT_2	HOT_3
Creatinine	1.43 ± 0.15^{a}	0.73 ± 0.15^{bc}	0.70 ± 0.2^{bc}	0.44 ± 0.05^{d}
BUN	35.33 ± 5.50^{b}	45.66 ± 4.16^{a}	33.64 ± 2.12^{b}	32.49 ± 4.69^{b}

HU, hyperuricemia; HOT_1, hyperuricemia onion treatment 1; HOT_2, hyperuricemia onion treatment 2; HOT_3, hyperuricemia onion treatment 3; BUN, blood urea nitrogen.

TABLE 10 Effect of onion on liver function.

Group	HU	HOT_1	HOT_2	HOT_3
ALT (U/L)	238.67 ± 8.02^{a}	119.33 ± 12.05^{c}	54.463 ± 1.56^{e}	84.62 ± 3.21^{d}
AST (U/L)	352.77 ± 10.52^{a}	125.64 ± 5.75^{bc}	82.72 ± 10.53^{c}	104.71 ± 14.20^{bc}
Total bilirubin (mg/dL)	3.76 ± 0.55^{b}	3.94 ± 0.21^{b}	1.49 ± 0.14^{c}	1.74 ± 0.12^{c}
ALP (U/L)	385.33 ± 10.06^{a}	241.33 ± 20.55^{d}	160.00 ± 20.29^{e}	164.33 ± 19.00^{e}

ALT, alanine aminotransferase; AST, aspartate aminotransferase; ALP, alkaline phosphatase; HU, hyperuricemia; HOT_1, hyperuricemia onion treatment 1; HOT_2, hyperuricemia onion treatment 2; HOT_3, hyperuricemia onion treatment 3.

TABLE 11 Effect of onion on serum total protein.

Group	HU	HOT_1	HOT_2	HOT_3
Total protein (g/dL)	6.78 ± 0.16^{b}	6.76 ± 0.06^{b}	6.85 ± 0.07^{ab}	6.86 ± 0.10^{ab}

HU, hyperuricemia; HOT_1, hyperuricemia onion treatment 1; HOT_2, hyperuricemia onion treatment 2; HOT_3, hyperuricemia onion treatment 3.

TABLE 12 Effect of onion on the lipid profile (mg/dL).

Treatment	HU	HOT_1	HOT_2	HOT_3
Cholesterol	136.33 ± 5.68^{a}	94.08 ± 4.34^{cd}	87.69 ± 1.55^{d}	134.67 ± 14.57^{a}
HDL	30.70 ± 2.52^{a}	30.10 ± 2.11^{a}	24.42 ± 2.63^{b}	18.75 ± 2.18^{c}
Triglycerides	165.00 ± 9.53^{c}	82.66 ± 19.13^{e}	134.00 ± 8.18^{d}	187.67 ± 16.86^{bc}
LDL	72.63 ± 9.77^{a}	47.44 ± 4.38^{bc}	36.47 ± 2.96^{bc}	78.38 ± 10.90^{a}

HDL, high-density lipid; LDL, low-density lipids; HU, hyperuricemia; HOT_1, hyperuricemia onion treatment 1; HOT_2, hyperuricemia onion treatment 2; HOT_3, hyperuricemia onion treatment 3.

3.6 Effects of onions on body immunity and hematology

Higher WBC count was observed in rats that fed on onion-containing diets; however, HOT_1 had shown significantly higher ($15.89 \pm 0.27 \times 10^3$ µL) WBC count than other treatment groups. Significant improvement ($p \leq 0.05$) was observed in neutrophil and lymphocyte percentages among onion-treated groups compared to HU. Monocytes were considerably found to be higher in rats that fed on HOT_1 (8.70% ± 0.2%) and HOT_2 (8.63% ± 0.20%) diets than HU.

TABLE 13 Effect of onion on body immunity and hematology.

Group	HU	HOT_1	HOT_2	HOT_3
White blood cell count ($\times 10^3$ µL)	14.12 ± 0.22^{e}	15.89 ± 0.27^{b}	15.41 ± 0.22^{cd}	15.82 ± 0.15^{bc}
Neutrophils %	0.76 ± 0.15^{d}	4.50 ± 0.3^{a}	4.31 ± 0.19^{a}	4.17 ± 0.16^{a}
Lymphocytes %	90.067 ± 1.00^{b}	79.41 ± 1.68^{c}	102.52 ± 4.09^{a}	83.40 ± 0.92^{c}
Monocytes %	8.36 ± 0.25^{ab}	8.70 ± 0.2^{a}	8.63 ± 0.20^{ab}	8.26 ± 0.30^{b}
RBC ($\times 10^6$ µL)	6.99 ± 0.07^{abc}	6.35 ± 0.09^{e}	7.21 ± 0.22^{a}	6.82 ± 0.10^{c}
Hb (g/dL)	12.92 ± 0.13^{d}	13.32 ± 0.06^{bcd}	13.23 ± 0.25^{cd}	13.31 ± 0.44^{bcd}
Platelet (PLT) ($\times 10^5$/µL)	574.33 ± 12.22^{e}	682.33 ± 30.27^{c}	642.00 ± 17.08^{d}	665.67 ± 8.50^{cd}

RBC, red blood cell; HB, hemoglobin; HU, hyperuricemia; HOT_1, hyperuricemia onion treatment 1; HOT_2, hyperuricemia onion treatment 2; HOT_3, hyperuricemia onion treatment 3.

TABLE 14 Effect of onion on nitrogen balance.

Parameters (mg/day)	HU	HOT_1	HOT_2	HOT_3
N-intake	0.961 ± 0.01^{b}	0.99 ± 0.004^{a}	0.82 ± 0.01^{c}	0.94 ± 0.01^{b}
Urinary-N	0.140 ± 0.007^{a}	0.134 ± 0.009^{ab}	0.138 ± 0.008^{a}	0.122 ± 0.009^{b}
Fecal-N	0.336 ± 0.005^{a}	0.340 ± 0.01^{a}	0.334 ± 0.007^{a}	0.345 ± 0.006^{a}
N-balance	0.484 ± 0.001^{b}	0.521 ± 0.01^{a}	0.353 ± 0.004^{c}	0.480 ± 0.006^{b}

HU, hyperuricemia; HOT_1, hyperuricemia onion treatment 1; HOT_2, hyperuricemia onion treatment 2; HOT_3, hyperuricemia onion treatment 3.

The RBC count was significantly found to be higher ($p \leq 0.05$) in rats that fed on HOT_2 ($7.21 \pm 0.22 \times 10^6$µL) than those in the other groups. Higher (13.32 ± 0.06 g/dL) and lower (13.23 ± 0.25 g/dL) Hb levels were observed in rats that fed on onion-treated diets compared to the other diets. Similarly, in platelet count, onion-enriched diets had shown an improvement compared to HU. It was significantly improved ($p \leq 0.05$) in onion-supplemented diets, and a higher value ($682.33 \pm 30.27 \times 10^5$/µL) of platelet count was observed in rats that fed on HOT_1 diet compared to other treatment groups (Table 13).

3.7 Effects of onion on nitrogen balance

Positive nitrogen balance (0.521 ± 0.01 mg/day) was observed ($p \leq 0.05$) in rats that fed on the HOT_1 diet, but HOT_2 diet did not show any improvement in nitrogen balance. HOT_3 (0.480 ± 0.006 mg/day) had shown non-significant ($p \geq 0.05$) results in the nitrogen balance study compared to HU (0.484 ± 0.001 mg/day) (Table 14).

4 Discussion

Hyperuricemia is a condition where uric acid levels in the body are imbalanced, leading to joint pain and kidney problems. Drugs like allopurinol are used to treat hyperuricemia , but natural medicinal plants are being researched as a potential cure. The groups fed with onions showed a significant improvement in their feed intake (g) compared to the positive control group (HU). After the adaptation period, the rats' feed intake improved due to the addition of onions in their diet, which attracted more attention. According to Table 2, feed intake was lowered during the third week due to the compensatory growth mechanism. However, feed intake was improved until the third week in HOT_2. Onions contain fructooligosaccharide and inulin, which are fibers that aid in digestion and absorption by increasing the activity of healthy bacteria in the gut. Additionally, onions contain essential vitamins and minerals, such as vitamin C, vitamin B6, potassium, and folate, which contribute to animal health and growth performance (Fernández-Jalao et al., 2021; Rahim et al., 2021). Onions also enhance feed intake by reducing inflammation in gastrointestinal lining (Sangpreecha et al., 2023). Similar studies have shown that feed intake is improved in broiler chicks when fed on 100 mg of onion powder in water (Aji et al., 2011). The antifungal, anti-inflammatory, and antibacterial properties of onions also improve digestion and absorption by halting the activity of pathogenic microbes and enhancing the activity of commensal microbes (Farahani et al., 2015). However, Al-Homidan (2005) observed that 2% onion powder did not impact the feed intake, and the addition of 6% onion to the diet decreased feed intake in broilers. During the experimental period, water intake was also observed, which is influenced by the presence of fiber and protein digestion and absorption activities in the body. Weekly water intake (mL) in HU was significantly decreased as a result of degenerative changes produced by PO and potassium bromate (Table 3). Water intake was observed to be higher in rats fed with onion diets, which may be associated with their higher protein and fiber intake. Similar results of high water intake were also observed by Ulger and Cakiroglu (2020), who provided 5% lyophilized and furnaced onion to diabetic rats.

In the experimental period, higher BW was observed in induced rats than other studies where BW was reduced by the administration of PO and potassium bromate. It had been observed that despite the adverse effects of PO and potassium bromate (Ajarem et al., 2016;

Al-Masri, 2016; Park et al., 2018), BW was increased within the treatment groups, and this might be due to a high protein diet and high feed intake. As shown in Table 4, fluctuation in BW observed in rats that fed on onion-enriched diets may be due to the presence of quercetin, rutin, sulfur, and phenolic compounds, and these compounds have antioxidant and anti-inflammatory effects on the body (Slimestad et al., 2007). Al-Masri, (2016) proposed that BW decreased in rats fed with 2% PO for 6 weeks. Elberry et al. (2014) explored the antioxidant and antimicrobial effects of onions that influence gain in body weight. Similarly, Goodarzi et al. (2014) also found BW gain in broiler chicks that fed on diet containing 3% onion bulbs. Hassan et al. (2018) also found a positive impact on BW in female Ross-308 broiler chicks that were provided rutin at various levels. Rutin is a subtype of quercetin and has antioxidant and anti-inflammatory properties.

Feed conversion and feed efficiency ratios are the indications of growth performance parameters, feed conversion ratio is feed intake per body weight gain, and feed efficiency is the body weight gain per feed intake. An improvement in values of FCR and FER were observed among the rats fed with onion diets, and this positive influence was associated with the concentration of protein available from the diet. According to Table 5, HOT_2 showed greater improvement in FCR (%) and FER than the other treatment groups. This could be because onions have antibacterial properties that prevent harmful pathogens from multiplying while also widening the intestinal surface to aid in amino acid absorption. Goodarzi et al. (2014) and Bedford (2000) found that herbs and phytogenic compounds were more effective at controlling harmful bacteria in chick guts than antibiotics. Onions contain other beneficial compounds, such as polyphenols, terpenoids, polypeptides, lectins, alkalis, and essential oils, which also positively impact digestion, leading to improved FCR and FER values. However, Rohn et al. (2002) and Swieca et al. (2013) found that flavonoids can interact with nutrients and reduce the activity of digestive enzymes, resulting in no improvement in FCR and FER values.

Nutrient intake is a critical factor that both humans and animals must prioritize. It is essential for fulfilling energy needs, supporting growth and maintenance, boosting immunity, promoting reproduction, and preventing diseases. Therefore, consuming necessary nutrients is crucial for various physiological functions. The rats that fed on HOT_1 and HOT_3 diets showed a significantly higher intake of DM and EE (g) than those in the HU group, with HOT_1 demonstrating a higher intake of CP, CF, and ash, as shown in Table 6. The difference in nutrient intake among the treatment groups could be attributed to high feed intake, nutrient digestibility, anti-quality compounds in onions, and onion-to-feed ratio. Aditya et al. (2017) attribute the positive impact of onion and quercetin on nutrient intake to their antioxidant, anti-inflammatory, and prebiotic properties.

Apparent nutrient digestibility describes the status of ingested nutrients in the body. It showed the difference between the amount of feed consumption, feed utilization, and nutrients present in the feces. It is shown in general terms, including DM, CP, EE, NFE (carbohydrates), and ash digestibilities. It also revealed the digestibility of energy and nitrogen in the diet and feces. In the present trial, CP and EE digestibility was found to be higher in HOT_1 and HOT_3 groups than HOT_2 and HU groups. Significantly higher DM, CF, ash, and NFE digestibility was observed in rats that fed on HOT_3 diet compared with HOT_1, HOT_2, and HU diets. A variation in digestibility among the groups may occur due to the higher feed and nutrient intake. HOT_2 had shown lower CP and EE digestibility due to the less feed intake and associated with the compensatory growth mechanism, as previously discussed in feed intake in Table 7. Onions contain nutrients such as protein, fat, fiber, vitamins, and minerals that facilitate digestion and absorption (Mitra et al., 2012). Quercetin acts as a growth promoter and improves the digestion system functionality by enhancing the activity of commensal microbes (Saeed et al., 2017). In the same manner, onions improve the activity of digestive enzymes and plays a role as a prebiotic due to soluble fiber contents like inulin and fructooligosaccharides (Gibson, 1998; Binaii et al., 2014; Safari et al., 2014; Mousavi et al., 2016). In contrast to our findings, another study reported the beneficial effects of onions, including increasing the nutrient digestibility and promoting the growth and development in the body by creating a balance in the gut microbiota. In the colon, beneficial microbes significantly enhance the fermentation of fiber content and produce short-chain fatty acids that comply with the energy needs of the body (Nakano, 2007; Ye et al., 2011).

Hyperuricemia is linked to various medical disorders in the body, such as joint pain, renal stones, and inflammation. During the breakdown of purine and pyrimidines, XO) plays an important role in catalyzing the production of uric acid by the conversion of hypoxanthine to xanthine and uric acid. Potassium oxonate (a uricase inhibitor) enhances XO activity and synthesizes uric acid in the body. This study presented that the levels of serum uric acid were significantly lower in rats that fed on HOT_2 and HOT_3 diets, as shown in Table 8. Onions have a higher capacity to reduce serum uric acid levels than quercetin aglycone alone. This could be due to flavonoids in onions having higher intestinal absorption and bioavailability than quercetin (Hertog et al., 1992; Haidari et al., 2008). In the present investigation, onion as a whole food having various concentrations of quercetin was explored for its potent effect to reduce uric acid levels. Contrary to the statement made previously, Zhu et al. (2004) conducted an experiment that administered *Biota orientalis* (BO) extract, quercetin, and rutin at a 100 mg/kg level to hyperuricemia-induced mice. Both substances demonstrated potential effects in reducing serum uric acid levels, with BO extract surpassing the positive control in effectiveness. The result suggests that quercetin and rutin have the ability to bind to XO and regulate serum uric acid levels. Quercetin also regulates the organic anion transporters (mOAT1) responsible for the absorption and excretion of uric acid in the kidney's proximal tubules. In comparison to the previous study, quercetin was found to reduce uric acid levels by increasing the expression of mOAT1 in fructose-induced rats (Hu et al., 2009; Hu et al., 2012). The expression of mOAT1 facilitates the removal of uric acid from the body (Hong et al., 2007). However, it is worth noting that the intake of flavonoids in food and supplements may sometimes interfere with the expression of mOAT (Wong et al., 2011). This may form a link among the onion-treated groups, which did not show a higher effect on serum uric acid levels. In another *in vitro* study, red onion polyphenols hold more promising antioxidant and XO inhibition activities. According to the previous results, polyphenols in red onions had high antioxidant activity, and they restricted the XO

inhibition activity up to IC_{50} 17.36 mg/mL (Ouyang et al., 2018). Another study conducted by Mo et al. (2007) evaluated the hypouricemic effects of 15 dietary flavonoids, namely, quercetin, morin, myricetin, kaempferol, icariin, apigenin, luteolin, baicalin, silibinin, naringenin, formononetin, genistein, puerarin, daidzin, and naringin dihydrochalcone. Hyperuricemia was induced with intraperitoneal injection of PO, and after 1 h, tested flavonoids and allopurinol were administered orally for 3 days. Quercetin, myricetin, morin, puerarin, and kaempferol at the level of 50 and 100 mg/kg had shown a decreasing trend in the liver XO activity and also elicited a declining effect in serum uric acid levels.

Reports indicate that biochemical and morphological changes occur after the adverse effects of PO and potassium bromate induction (Ahmed et al., 2016; Vijeesh et al., 2022). Induction with PO and potassium bromate may have adversely affected the renal function by changing renal parameters, and it adversely affects the renal parenchyma and decreases the glomerular filtration rate (Khan et al., 2003). If the kidney glomerular filtration rate decreases, then it means kidneys are not in a position to filter the waste materials from the body resulting in many complications. An increase in creatinine and BUN truly shows the decrease in the glomerular filtration rate resulting from morphological and structural changes in the renal tubules (Gowda et al., 2010). According to Table 9, our findings showed that the renal parameters were attenuated, which can be attributed to onion's anti-inflammatory and antioxidant activities. The increased serum uric acid level and reactive oxygen species (ROS) production may have resulted from the degradation of purine and pyrimidines and an increase in the activity of XO. Quercetin in the onion may have the capacity to bind to XO and decrease the synthesis of uric acid in the body (Mohamed and Saddek, 2019). Onions enhanced the antioxidant status and restored the renal parameters that had been approved in the study conducted by Rahmat et al. (2019), who provided 5 g/kg/day onion to the hyperuricemic rats. Quercetin lowers the harmful effects by scavenging free radicals and inhibiting lipid peroxidation and XO enzyme activity (Frankel et al., 1993). Flavonoids are found in various fruits and vegetables which hold antioxidant activity, and they are widely distributed into various groups and categories according to their chemical structures and therapeutic values. Quercetin significantly attenuated the renal morphology and function by increasing the glomerular filtration rate. It might be due to the anti-inflammatory activity of quercetin (Gomes et al., 2014; Tang et al., 2020).

In this study, HOT_2 and HOT_3 significantly reduced the levels of ALT, AST, ALP, and total bilirubin, as shown in Table 10. Onion contains numerous functional compounds, such as quercetin and sulfur. It attenuates the liver enzymes by protecting the liver cell from oxidative stress and inflammation. Quercetin in the onion scavenges free radicals and protects the cells from lipid peroxidation. Lipid peroxidation is the chain of reactions that causes oxidative damage to the cell layer of the liver. Most often, the phospholipid layer of the cell gets damaged due to lipid peroxidation. When onion and quercetin are added to the diet, it lowers the lipid levels in the liver along with improvement in BW, which results in a decrease in liver enzymes. Onion contains fiber, sulfur compounds, and flavonoids that have shown good results compared to quercetin alone (Lee et al., 2008). There are various health benefits of onions that have been reported, including antibacterial, antifungal, anti-atherosclerotic, hypolipidemic, antihypertensive, hypoglycemic, anti-inflammatory, and antioxidant properties. These therapeutic effects have directly or indirectly improved liver morphology and functions (Ozougwu et al., 2008; Eyo et al., 2011; Ozougwu, 2011). From the diseased liver or fatty liver, enzymes ooze out from the cell into the serum. Kuo et al. (2012) induced hyperuricemia in rats with an intraperitoneal injection of potassium oxonate at 280 mg/kg for 1 week. *Hibiscus sabdariffa* L. provided at the level of 1%, 2%, and 5% in the diet significantly attenuated the levels of uric acid, ALT, and AST. Both are important enzymes that are present in the cytoplasm and mitochondria of the liver (Amacher, 1998). Ozer et al. (2008) also investigated the mechanism of liver damage and injury. Bilirubin is the end product of RBCs and is mostly found in the liver, bile, intestine, and spleen, whereas ALP and ?-GT are found in the cell membrane (Ramaiah, 2007). Our study was correlated with the study conducted by de David et al. (2011) and Mishra et al. (2013), who found quercetin's capacity to reverse the levels of bilirubin, ALT, AST, ALP, and ?-GT attributed to its hepatoprotective effect. In another study, quercetin at 20 mg/kg provided to the rats had protected the rats from melphalan (MPLN)-induced toxicity. It may be attributed to anti-inflammatory and antioxidant activity of quercetin (Olayinka et al., 2014). Table 11 shows that with the improvement in the functioning of the liver, serum total protein also improved among the rats that fed on onion-treated diets (Karakilcik et al., 2004).

The high levels of uric acid induce gluconeogenesis in the liver, stimulating adenosine monophosphate dehydrogenase, lowering the activity of adenosine monophosphate kinase, and causing a disturbance in lipid metabolism that can lead to hepatic lipogenesis (Cicerchi et al., 2014; Lanaspa et al., 2015). Table 12 shows that rats that fed on HOT_1 and HOT_2 diets experienced a greater decrease in lipid levels than those fed on HOT_3 diet due to the higher feed intake and onion-to-feed ratio in HOT_1 and HOT_2 diets. Onions contain various sulfur compounds, such as s-methyl cysteine, that can increase HDL levels and lower LDL levels, triglycerides, and HMG CoA reductase activity (Thomas et al., 2015). Onions significantly reduced lipid levels in streptozotocin-induced diabetic rats due to the presence of allyl propyl disulfide (Ozougwu, 2011). However, rats that fed on high-cholesterol diet with 10% onion powder did not show any changes in total cholesterol, LDL, or triglyceride levels (González-Peña et al., 2014). Quercetin restricts the working of lipase enzymes and lowers *de novo* lipid synthesis in the liver, as found in the study conducted by Gnoni et al. (2009). Rutin (quercetin-3-rutinoside), a subtype of quercetin found in various plants and fruits, also reduces lipid levels by restricting the activity of the PPAR enzyme in the liver, which is important for lipid synthesis (Ahmadipour et al., 2015). In rabbits that fed on a high-fat diet, quercetin had a positive effect on the lipid profile (Juzwiak et al., 2005).

The experimental studies that have been accomplished to study the organism status and conditions are adopted according to the laboratory protocols. Various biochemical and hematological tests are performed to explore the status of disease, and new therapeutic strategies are developed and validated using the scientific studies. The present research has been conducted to explore the negative effect of PO and potassium bromate on the hematological parameters and to find out the effect of onion powder on the hematological values in hyperuricemia-induced albino rats.

According to the study results, the levels of WBCs, RBCs, and Hb were significantly improved in rats that fed on the HOT_1, HOT_2, and HOT_3 diets compared to HU, as shown in Table 13. This may be attributed to antioxidant, anti-inflammatory, and antibacterial activities of onions. Some other contributing factors include higher CP intake and digestibility as well as an increase in the synthesis of serum protein in the liver. The most important function of the liver is to maintain hemopoiesis and the formation of coagulation proteins. Disturbance in the liver functions and morphology might have led to the disturbance in the hematological parameters. Higher intake of protein may improve the immunological response and hematological values in the body. Serum parameters such as RBC, WBC, and platelet count have been indicated as essential biomarkers in various clinical conditions. Due to the different morphological structures and shape of RBCs, they play an important role in transporting oxygen and nutrients to all parts of the body (Barbalato and Pillarisetty, 2020). Ufele et al. (2008) found positive variations in RBC levels in mice that fed on plant-based protein (soybean and corn meal). Similarly, higher RBCs were found due to the bioavailability of animal protein than plant-based protein (Aguirre et al., 1959). Contrary to this study, Kim et al. (2014) reported a decrease in WBC count upon providing a high level of plant-based protein. WBC count has been known for their active role in immunity, including innate and humoral immune response. They are also called leukocytes. They encounter foreign substances and protect the body from harmful exposure to infectious substances (Ashton, 2007; Tigner et al., 2021). Platelet count play an important role in maintaining the level of blood through the activation of blood clotting factors in various type of vascular injury (Fountain and Lappin, 2020). The diet composition contains more protein content from the soybean meal, and its bioavailability is 70% compared to 86% animal protein. Animal proteins such as those present in meat, poultry, fish, and dairy products are more abundant in the heme-iron, which is readily absorbed by the body compared with the plant-based protein. Plant protein contains non-heme-iron, which has a less absorption level, such as legumes, fortified cereals, and leafy greens. However, it has a positive effect on hematological values. The levels of WBC and RBC count were shown to be improved in the study conducted by Akrami et al. (2013), who provided 1% onion powder to the fish. Quercetin in the onion has anti-inflammatory and immune-boosting activity. Feeding onion to grass carp resulted in an improvement in the Hb level, WBC count, and RBC count, and it also revealed onion's immunomodulating and antibacterial activity. Lymphocyte and neutrophil levels were found to be non-significant in onion-treated groups but found to be higher compared with HU. Monocytes also significantly improved in the rats that fed on onion diets (Gholipour Kanani et al., 2014). Keskin et al. (2016) and Aguirre et al. (2011) reported that RBC count was increased by the supplementation of quercetin. Quercetin in the onion reduces the inflammation in the body and protects RBCs from free radicals by increasing their oxygen-carrying capacity. Nazima et al. (2016) also highlighted the positive effect of quercetin on hematological values and explored its protective effect on erythrocyte cell membranes from free radical exposure. Similarly, positive effects on hematological parameters had been studied in rats that fed on diets treated with garlic and onion powders (Kalyankar et al., 2013). In another study, quercetin injected intraperitoneally at a level of 50 mg/kg produced a positive effect on the level of hemoglobin, RBC, WBC, and platelet count. Quercetin also attenuated the hematological parameters that were observed in rats with furan- and cadmium-induced toxicity (Alam et al., 2017; Donmez et al., 2019). This might be due to antioxidant and anti-inflammatory effects of quercetin (Karimi et al., 2021).

Nitrogen balance is investigated in animals or humans to sort out the balance between nitrogen intake and nitrogen excretion from the body. It is an important part of the nutrition research and mechanism to assess an individual's protein metabolism and overall nutritional status. For this purpose, investigation of nitrogen balance had been performed in this study, and it showed that rats that fed on HOT_1 diet had shown positive nitrogen balance; however, a non-significant result was observed in rats that fed on HU and HOT_3 diets. The groups that showed positive nitrogen balance could be due to the increase in their feed intake, CP intake, and digestibility. These parameters were not positive in HOT_2 resulting in negative nitrogen balance, as shown in Table 14. Essential oils in onion and garlic reduce ruminal NH3-N concentration and increase protein availability in the intestine. Therefore, when protein deamination stopped in the rumen, the ammonia level decreased, allowing ruminants to have higher amino acid availability in the small intestine. Onions have free radical scavenging and anti-inflammatory activity that restricts degenerative changes in the body. Morshedy et al. (2021) provided rocket seed oil (*Eruca sativa* Mill.) and wheat germ oil to rabbits. A mixture of both oils enhanced nitrogen absorption and reduced nitrogen excretion. Quercetin and diallyl disulfide in the onion increase the digestion of protein and promote the growth of friendly microbes in the gut. Kamruzzaman et al. (2011) also reported the positive effect of garlic on nitrogen retention. This effect could be due to the upregulation of the proteolytic enzyme activity in sheep's rumen and inhibition of ammonia nitrogen deamination. Similarly, according to the work of Nisa et al. (2006), the slower release of N attached to fiber synchronized with fiber fermentation and its utilization by the ruminal microbes, preventing loss. Fiber facilitates the fermentation activities in the gut. It also produces short-chain fatty acids (SCFAs) that provide energy and strength to the intestinal lining for better digestion and absorption. Herbal supplements may retain more nitrogen in the gut and facilitate protein digestion by enhancing the activity of the protease. This could be possible due to the antibacterial activity of the herbal supplement. The higher level of 1.5 kg/ton has shown a positive nitrogen balance compared with other treatments (Saleh et al., 2018). So onion and quercetin regulated the protein metabolism and showed a positive influence on the retention of protein in the body.

5 Conclusion

The results showed that HOT_2, a diet containing onion powder (14.84 g/100 g feed) corresponding to the quercetin content of 0.100 mg/kg, had shown strong anti-hyperuricemia potential which generated a healthy and favorable effect on the serum and hematological traits. Rats that fed on HOT_1 (11.13 g/100 feed) diet corresponding to the quercetin content of 0.075 mg/kg had shown promising effects on nutrient intake and digestibility, feed intake, body weight, and nitrogen balance in hyperuricemia-induced male Wistar albino rats. Therefore, onion has a protective and therapeutic potential for the cure of various ailments, and it might be used for

the occurrence and treatment of hyperuricemia and related disorders.

Data availability statement

The raw data supporting the conclusion of this article will be made available by the authors, without undue reservation.

Ethics statement

The animal study was approved by the Animal Ethical Committee of Government College University Faisalabad, Pakistan (Wide Ref. No. GCUF/ERC/85). The study was conducted in accordance with the local legislation and institutional requirements.

Author contributions

MU: writing–original draft. MUN: supervision and writing–review and editing. NA: conceptualization and writing–original draft. MAR: visualization and writing–review and editing. FA: funding acquisition and writing–review and editing.

Funding

The author(s) declare that financial support was received for the research, authorship, and/or publication of this article. This work was supported by the Deanship of Scientific Research, Vice Presidency for Graduate Studies and Scientific Research, King Faisal University, Saudi Arabia (Grant No. 3889).

Acknowledgments

The authors would like to thank the Library Department, Government College University Faisalabad (GCUF), and IT Department, Higher Education Commission (HEC, Islamabad) for access to journals, books, and valuable databases. The research was completed after using the available resources in the department and university.

Conflict of interest

The authors declare that the research was conducted in the absence of any commercial or financial relationships that could be construed as a potential conflict of interest.

Publisher's note

All claims expressed in this article are solely those of the authors and do not necessarily represent those of their affiliated organizations, or those of the publisher, the editors, and the reviewers. Any product that may be evaluated in this article, or claim that may be made by its manufacturer, is not guaranteed or endorsed by the publisher.

References

Aditya, S., Ahammed, M., Jang, S. H., and Ohh, S. J. (2017). Effects of dietary onion (Allium cepa) extract supplementation on performance, apparent total tract retention of nutrients, blood profile and meat quality of broiler chicks. *Asian-australas. J. Anim. Sci.* 30, 229–235. doi:10.5713/ajas.16.0553

Aguirre, F., Scrimshaw, N. S., Munoz, J. A., and Cabezas, A. (1959). The effect of supplements of animal and vegetable protein, vitamin B12, and aureomycin on haematological values in central American school children. *Bol. Oficina Sanit. Panam.* 4, 162–169.

Aguirre, L., Arias, N., Teresa Macarulla, M., Gracia, A., and Portillo, P. M. (2011). Beneficial effects of quercetin on obesity and diabetes. *Open Nutraceuticals J.* 4 (1), 189–198. doi:10.2174/1876396001104010189

Ahmadipour, B., Hassanpour, H., Rafiei, F., and Khajali, F. (2015). Antioxidative, antihyperlipidemic, and growth-promoting effects of Kelussia odoratissima in meat-type chickens. *Poult. Sci. J.* 3 (1), 37–46. doi:10.22069/psj.2015.2326

Ahmed, W. E., Ali, E., and Osman, I. (2016). Biochemical and histopathological changes in potassium bromate-fed rats. *Int. J. Sci. Res.* 5 (11), 123–126. doi:10.21275/ART20161489

Ajarem, J., Altoom, N. G., Allam, A. A., Maodaa, S. N., Abdel-Maksoud, M. A., and Chow, B. K. (2016). Oral administration of potassium bromate induces neurobehavioral changes, alters cerebral neurotransmitters level and impairs brain tissue of swiss mice. *Behav. Brain Funct.* 12, 14–10. doi:10.1186/s12993-016-0098-8

Aji, S. B., Ignatius, K., Ado, A. A., Nahu, J. B., Abdulkarim, A., Aliyu, U., et al. (2011). Effects of feeding onion (Allium cepa) and garlic (allium sativum) on some performance characteristics of broiler chickens. *Res. J. Poult. Sci.* 4, 22–27. doi:10.3923/rjpscience.2011.22.27

Akrami, R., Iri, Y., Rostami, H. K., and Mansour, M. R. (2013). Effect of dietary supplementation of fructooligosaccharide (FOS) on growth performance, survival, lactobacillus bacterial population and hemato-immunological parameters of stellate sturgeon (*Acipenser stellatus*) juvenile. *Fish. Shellfish Immunol.* 35 (4), 1235–1239. doi:10.1016/j.fsi.2013.07.039

Alam, R. T., Zeid, E. H. A., and Imam, T. S. (2017). Protective role of quercetin against hematotoxic and immunotoxic effects of furan in rats. *Environ. Sci. Pollut. Res.* 24, 3780–3789. doi:10.1007/s11356-016-8108-9

Al-Homidan, A. (2005). Efficacy of using different sources and levels of Allium sativum and Zingiber officinale on broiler chicks performance. *Saudi J. Biol. Sci.* 12, 96–102.

Al-Masri, S. A. (2016). Beneficial role of high plant proteins in the treatment against hyperuricemia in experimental rats. *JAPS J. Anim. Plant Sci.* 26 (3).

Amacher, D. E. (1998). Serum transaminase elevations as indicators of hepatic injury following the administration of drugs. *Regul. Toxicol. Pharmacol.* 27 (2), 119–130. doi:10.1006/rtph.1998.1201

AOAC (2006). *Official methods of analysis*. 18th Edn. Gaithersburg, MD, USA: Association of Official Analytical Chemists.

Arshad, M. S., Sohaib, M., Nadeem, M., Saeed, F., Imran, A., Javed, A., et al. (2017). Status and trends of nutraceuticals from onion and onion by-products: a critical review. *Cogent Food Agric.* 3, 1280254. doi:10.1080/23311932.2017.1280254

Arslan, D., and Özcan, M. M. (2010). Study the effect of sun, oven and microwave drying on quality of onion slices. *LWT - Food Sci.* 43 (7), 1121–1127. doi:10.1016/j.lwt.2010.02.019

Ashton, N. (2007). Physiology of red and white blood cells. *Anaesth. Intensive Care Med.* 8 (5), 203–208. doi:10.1016/j.mpaic.2007.02.003

Barbalato, L., and Pillarisetty, L. S. (2020). "Histology, red blood cell," in *StatPearls*. Treasure Island, FL: StatPearls Publishing.

Bedford, M. (2000). Removal of antibiotic growth promoters from poultry diets: implications and strategies to minimise subsequent problems. *Worlds Poult. Sci. J.* 56 (4), 347–365. doi:10.1079/WPS20000024

Binaii, M., Ghiasi, M., Farabi, S. M. V., Pourgholam, R., Fazli, H., Safari, R., et al. (2014). Biochemical and hemato-immunological parameters in juvenile beluga (*Huso huso*) following the diet supplemented with nettle (Urtica dioica). *Fish. Shellfish Immunol.* 36 (1), 46–51. doi:10.1016/j.fsi.2013.10.001

Chew, J. L., and Chua, K. Y. (2003). Collection of mouse urine for bioassays. *Lab. Anim.* 32 (7), 48–50. doi:10.1038/laban0803-48

Cicerchi, C., Li, N., Kratzer, J., Garcia, G., Roncal-Jimenez, C. A., Tanabe, K., et al. (2014). Uric acid-dependent inhibition of AMP kinase induces hepatic glucose

production in diabetes and starvation: evolutionary implications of the uricase loss in hominids. *J. Faseb.* 28 (8), 3339–3350. doi:10.1096/fj.13-243634

de David, C., Rodrigues, G., Bona, S., Meurer, L., Gonzalez-Gallego, J., Tunon, M. J., et al. (2011). Role of quercetin in preventing thioacetamide-induced liver injury in rats. *Toxicol. Pathol.* 39 (6), 949–957. doi:10.1177/0192623311418680

Donmez, H., Donmez, N., Kısadere, I., and Undag, I. (2019). Protective effect of quercetin on some hematological parameters in rats exposed to cadmium. *Biotech. Histochem.* 94 (5), 381–386. doi:10.1080/10520295.2019.1574027

Elberry, A. A., Mufti, S., Al-Maghrabi, J., Abdel Sattar, E., Ghareib, S. A., Mosli, H. A., et al. (2014). Immunomodulatory effect of red onion (Allium cepa Linn) scale extract on experimentally induced atypical prostatic hyperplasia in Wistar rats. *Mediat. Inflamm.* 640746, 640746–640813. doi:10.1155/2014/640746

Eyo, J. E., Ozougwu, J. C., and Echi, P. C. (2011). Hypoglycaemic effects of Allium cepa, Allium sativum and Zingiber officinale aqueous extracts on alloxan-induced diabetic Rattus novergicus. *Med. J. Islam World Acad. Sci.* 19 (3), 121–126.

Fam, A. (2003). Alternative urate-lowering drugs and the management of hyperuricemia in allopurinol-intolerant patients. *Int. J. Adv. Rheumatol.* (1), 122–130.

Farahani, M., Goodarzi, M., and Nanekarani, S. (2015). The effects of aqueous extract of onion on performance and some blood biochemical parameters of the Cobb and Ross broilers. *Int. J. Adv. Biol. Biomed. Res.* 3 (4), 370–377. doi:10.18869/IJABBR.2015.370

Fels, E., and Sundy, J. S. (2008). Refractory gout: what is it and what to do about it? *Curr. Opin. Rheumatol.* 20 (2), 198–202. doi:10.1097/BOR.0b013e3282f4eff5

Fernández-Jalao, I., Balderas, C., Calvo, M. V., Fontecha, J., Sánchez-Moreno, C., and De Ancos, B. (2021). Impact of high-pressure processed onion on colonic metabolism using a dynamic gastrointestinal digestion simulator. *Metabolites* 11 (5), 262. doi:10.3390/metabo11050262

Fountain, J. H., and Lappin, S. L. (2020). "Physiology, platelet," in *StatPearls*. Treasure Island, FL: StatPearls Publishing.

Frankel, E., German, J., Kinsella, J., Parks, E., and Kanner, J. (1993). Inhibition of oxidation of human low-density lipoprotein by phenolic substances in red wine. *Lancet* 341 (8843), 454–457. doi:10.1016/0140-6736(93)90206-V

George, C., and Minter, D. A. (2022). "Hyperuricemia," in *StatPearls*. Treasure Island, FL: StatPearls Publishing.

Gholipour Kanani, H., Nobahar, Z., Kakoolaki, S., and Jafarian, H. (2014). Effect of ginger-and garlic-supplemented diet on growth performance, some hematological parameters and immune responses in juvenile *Huso huso*. *Fish. Physiol. Biochem.* 40, 481–490. doi:10.1007/s10695-013-9859-6

Gibson, G. R. (1998). Dietary modulation of the human gut microflora using prebiotics. *Br. J. Nutr.* 80 (S2), S209–S212. doi:10.1017/S0007114500006048

Gnoni, G., Paglialonga, G., and Siculella, L. (2009). Quercetin inhibits fatty acid and triacylglycerol synthesis in rat-liver cells. *Eur. J. Clin. Invest.* 39 (9), 761–768. doi:10.1111/j.1365-2362.2009.02167.x

Gomes, I. B., Porto, M. L., Santos, M. C. L., Campagnaro, B. P., Pereira, T., Meyrelles, S. S., et al. (2014). Renoprotective, anti-oxidative and anti-apoptotic effects of oral low-dose quercetin in the C57BL/6J model of diabetic nephropathy. *Lipids Health Dis.* 13 (1), 184–210. doi:10.1186/1476-511X-13-184

González-Peña, D., Angulo, J., Vallejo, S., Colina-Coca, C., de Ancos, B., Sánchez-Ferrer, C. F., et al. (2014). High-cholesterol diet enriched with onion affects endothelium-dependent relaxation and NADPH oxidase activity in mesenteric microvessels from Wistar rats. *Nutr. Metab.* 11 (1), 57–11. doi:10.1186/1743-7075-11-57

Goodarzi, M., Nanekarani, S., and Landy, N. (2014). Effect of dietary supplementation with onion (Allium cepa L.) on performance, carcass traits and intestinal microflora composition in broiler chickens. *Asian. pac. J. Trop. Med.* 4, S297–S301. doi:10.1016/s2222-1808(14)60459-x

Gowda, S., Desai, P. B., Kulkarni, S. S., Hull, V. V., Math, A. A., and Vernekar, S. N. (2010). Markers of renal function tests. *N. Am. J. Med. Sci.* 2 (4), 170–173.

Haidari, F., Rashidi, M. R., Eshraghian, M. R., Mahboob, S. A., Shahi, M. M., and Keshavarz, S. A. (2008). Hypouricemic and antioxidant activities of Allium cepa Lilliaceae and quercetin in normal and hyperuricemic rats. *J. Saudi Med.* 29 (11), 1573–1579.

Hassan, F. A., Roushdy, E. M., Kishawy, A. T., Zaglool, A. W., Tukur, H. A., and Saadeldin, I. M. (2018). Growth performance, antioxidant capacity, lipid-related transcript expression and the economics of broiler chickens fed different levels of rutin. *Animals* 9 (1), 7. doi:10.3390/ani9010007

Hertog, M. G., Hollman, P. C., and Katan, M. B. (1992). Content of potentially anticarcinogenic flavonoids of 28 vegetables and 9 fruits commonly consumed in The Netherlands. *J. Agric. Food Chem.* 40 (12), 2379–2383. doi:10.1021/jf00024a011

Hong, S. S., Seo, K., Lim, S. C., and Han, H. K. (2007). Interaction characteristics of flavonoids with human organic anion transporter 1 (hOAT1) and 3 (hOAT3). *Pharmacol. Res.* 56 (6), 468–473. doi:10.1016/j.phrs.2007.08.007

Hu, Q. H., Wang, C., Li, J. M., Zhang, D. M., and Kong, L. D. (2009). Allopurinol, rutin, and quercetin attenuate hyperuricemia and renal dysfunction in rats induced by fructose intake: renal organic ion transporter involvement. *Am. J. Physiol. Ren. Physiol.* 297 (4), F1080–F1091. doi:10.1152/ajprenal.90767.2008

Hu, Q. H., Zhang, X., Wang, X., Jiao, R. Q., and Kong, L. D. (2012). Quercetin regulates organic ion transporter and uromodulin expression and improves renal function in hyperuricemic mice. *Eur. J. Nutr.* 51, 593–606. doi:10.1007/s00394-011-0243-y

Jiang, S., Liu, H., and Li, C. (2021). Dietary regulation of oxidative stress in chronic metabolic diseases. *Foods* 10 (8), 1854. doi:10.3390/foods10081854

Juzwiak, S., Wójcicki, J., Mokrzycki, K., Marchlewicz, M., Białecka, M., Wenda-Różewicka, L., et al. (2005). Effect of quercetin on experimental hyperlipidemia and atherosclerosis in rabbits. *Pharmacol. Rep.* 57 (57), 604–609.

Kalyankar, A., Gupta, R., Bansal, N., Sabhlok, V., and Singh, D. (2013). Effect of garlic (allium sativum) against aeromonas hydrophila and health management of swordtail, Xiphophorus helleri. *J. Environ. Sustain. JESS* 1 (2), 41–48.

Kamruzzaman, M., Torita, A., Sako, Y., Al-Mamun, M., and Sano, H. (2011). Effects of feeding garlic stem and leaf silage on rates of plasma leucine turnover, whole body protein synthesis and degradation in sheep. *Small Rumin. Res.* 99 (1), 37–43. doi:10.1016/j.smallrumres.2011.03.052

Karakilcik, A. Z., Zerin, M., Arslan, O., Nazligul, Y., and Vural, H. (2004). Effects of vitamin C and E on liver enzymes and biochemical parameters of rabbits exposed to aflatoxin B1. *Vet. Hum. Toxicol.* 46 (4), 190–192.

Karimi, A., Naeini, F., Azar, V. A., Hasanzadeh, M., Ostadrahimi, A., Niazkar, H. R., et al. (2021). A comprehensive systematic review of the therapeutic effects and mechanisms of action of quercetin in sepsis. *Phytomedicine* 86, 153567. doi:10.1016/j.phymed.2021.153567

Kaur, J. (2014). Use of friedewald equation for dyslipidemia in metabolic syndrome. *Age* 58, 36–02. doi:10.14419/ijm.v2i1.2370

Kermani, N. M., Abushofa, F. A., Aldaek, A. M., and Jaat, F. (2020). Protective effect of Allium cepa L. (onion) against potassium bromate-induced hematological, biochemical and histopathological alterations in rats. *Int. J. Innov. Sci. Res. Technol.* 5 (11), 201–207.

Keskin, E., Dönmez, N., Kiliçarslan, G., and Kandır, S. (2016). Beneficial effect of quercetin on some haematological parameters in streptozotocin-induced diabetic rats. *Bull. Env. Pharmacol. Life Sci.* 5 (6), 65–68.

Khan, N., Sharma, S., and Sultana, S. (2003). Nigella sativa (black cumin) ameliorates potassium bromate-induced early events of carcinogenesis: diminution of oxidative stress. *Hum. Exp. Toxicol.* 22 (4), 193–203. doi:10.1191/0960327103ht349oa

Kim, K. O., Park, H., Chun, M., and Kim, H. S. (2014). Immunomodulatory effects of high-protein diet with resveratrol supplementation on radiation-induced acute-phase inflammation in rats. *J. Med. Food.* 17 (9), 963–971. doi:10.1089/jmf.2013.2976

Kinoshita, T., Lepp, Z., Kawai, Y., Terao, J., and Chuman, H. (2006). An integrated database of flavonoids. *Biofactors* 26 (3), 179–188. doi:10.1002/biof.5520260303

Kulik, K., Kwiecień, I., Chełstowska, B., Rutkowska, E., and Rzepecki, P. (2021). Evaluation and comparison of the new Mindray BC-6200 hematology analyzer with ADVIA 2120i. *Int. J. Lab. Hematol.* 43 (3), 395–402. doi:10.1111/ijlh.13418

Kuo, C. Y., Kao, E. S., Chan, K. C., Lee, H. J., Huang, T. F., and Wang, C. J. (2012). Hibiscus sabdariffa L. extracts reduce serum uric acid levels in oxonate-induced rats. *J. Funct. Foods.* 4 (1), 375–381. doi:10.1016/j.jff.2012.01.007

Lanaspa, M. A., Epperson, L. E., Li, N., Cicerchi, C., Garcia, G. E., Roncal-Jimenez, C. A., et al. (2015). Opposing activity changes in AMP deaminase and AMP-activated protein kinase in the hibernating ground squirrel. *PLoS One* 10 (4), e0123509. doi:10.1371/journal.pone.0123509

Lee, K. H., Kim, Y. H., Park, E. J., and Hwang, H. J. (2008). Effect of onion powder supplementation on lipid metabolism in high fat-cholesterol fed SD Rats. *Prev. Nutr. Food. Sci.* 13 (2), 71–76. doi:10.3746/jfn.2008.13.2.071

Maia, L., Duarte, R. O., Ponces-Freire, A., Moura, J. J., and Mira, L. (2007). NADH oxidase activity of rat and human liver xanthine oxidoreductase: potential role in superoxide production. *J. Biol. Inorg. Chem.* 12, 777–787. doi:10.1007/s00775-007-0229-7

Miean, K. H., and Mohamed, S. (2001). Flavonoid (myricetin, quercetin, kaempferol, luteolin, and apigenin) content of edible tropical plants. *J. Agric. Food Chem.* 49 (6), 3106–3112. doi:10.1021/jf000892m

Mishra, S. K., Singh, P., and Rath, S. K. (2013). Protective effect of quercetin on chloroquine-induced oxidative stress and hepatotoxicity in mice. *Malar. Res. Treat.* 2013, 1–10. Article ID. 141734. doi:10.1155/2013/141734

Mitra, J., Shrivastava, S. A., and Rao, P. (2012). Onion dehydration: a review. *J. Food Sci. Technol.* 49, 267–277. doi:10.1007/s13197-011-0369-1

Mo, S. F., Zhou, F., Lv, Y. Z., Hu, Q. H., Zhang, D. M., and Kong, L. D. (2007). Hypouricemic action of selected flavonoids in mice: structure–activity relationships. *Biol. Pharm. Bull.* 30 (8), 1551–1556. doi:10.1248/bpb.30.1551

Mohamed, E. A. K., and saddek, E. A. (2019). The protective effect of taurine and/or vanillin against renal, testicular, and hematological alterations induced by potassium bromate toxicity in rats. *J. Basic Appl. Zool.* 80 (1), 3–11. doi:10.1186/s41936-018-0070-2

Morshedy, S. A., Abdelmodather, A. M., Basyony, M. M., Zahran, S. A., and Hassan, M. A. (2021). Effects of rocket seed oil, wheat germ oil, and their mixture on growth performance, feed utilization, digestibility, redox status, and meat fatty acid profile of growing rabbits. *Agriculture* 11 (7), 662. doi:10.3390/agriculture11070662

Mousavi, E., Mohammadiazarm, H., Mousavi, S. M., and Ghatrami, E. R. (2016). Effects of inulin, savory and onion powders in diet of juveniles carp *Cyprinus carpio*

(Linnaeus 1758) on gut micro flora, immune response and blood biochemical parameters. *Turk. J. Fish. Aquat. Sci.* 16 (4), 831–838. doi:10.4194/1303-2712-v16_4_09

Naeem, M., Rahim, M. A., Nisa, M. U., Khalid, K., Ahmad, N., Khalid, N., et al. (2023). Digestibility, intake, and growth performance of egg protein replaced with vegetable protein in weaning food. *Cogent Food & Agric.* 9 (1), 2258800. doi:10.1080/23311932.2023.2258800

Nakano, T. (2007). *Dietary supplements for the health and quality of cultured fish. III*. USA: CAB International., 86–109.

Nazima, B., Manoharan, V., and Miltonprabu, S. (2016). Oxidative stress induced by cadmium in the plasma, erythrocytes and lymphocytes of rats: attenuation by grape seed proanthocyanidins. *Hum. Exp. Toxicol.* 35 (4), 428–447. doi:10.1177/0960327115591376

Nguyen, M. T. T., Awale, S., Tezuka, Y., Le Tran, Q., Watanabe, H., and Kadota, S. (2004). Xanthine oxidase inhibitory activity of Vietnamese medicinal plants. *Biol. Pharm. Bull.* 27 (9), 1414–1421. doi:10.1248/bpb.27.1414

Nisa, M.-u., Khan, M. A., Sarwar, M., Lee, W. S., Lee, H. J., Ki, K. S., et al. (2006). Influence of corn steep liquor on feeding value of urea treated wheat straw in buffaloes fed at restricted diets. *Asian-australas. J. Anim. Sci.* 19 (11), 1610–1616. doi:10.5713/ajas.2006.1610

Olayinka, E. T., Ore, A., Ola, O. S., and Adeyemo, O. A. (2014). Protective effect of quercetin on melphalan-induced oxidative stress and impaired renal and hepatic functions in rat. *Chemother. Res. Pract.* 2014, 936526–936528. Article ID. 936526. doi:10.1155/2014/936526

Ouyang, H., Hou, K., Peng, W., Liu, Z., and Deng, H. (2018). Antioxidant and xanthine oxidase inhibitory activities of total polyphenols from onion. *Saudi J. Biol. Sci.* 25 (7), 1509–1513. doi:10.1016/j.sjbs.2017.08.005

Ozer, J., Ratner, M., Shaw, M., Bailey, W., and Schomaker, S. (2008). The current state of serum biomarkers of hepatotoxicity. *Toxicology* 245 (3), 194–205. doi:10.1016/j.tox.2007.11.021

Ozougwu, J. C. (2011). Anti-diabetic effects of Allium cepa (onions) aqueous extracts on alloxan-induced diabetic Rattus novergicus. *J. Med. Plant Res.* 5 (7), 1134–1139.

Ozougwu, J. C., Nwachi, U. E., and Eyo, J. E. (2008). Comparative hypolipidaemic effects of Allium cepa, Allium sativum and Zingiber officinale aqueous extracts on alloxan-induced diabetic Rattus novergicus. *Bio-Research* 6 (2), 384–391. doi:10.4314/br.v6i2.28672

Park, J. E., Yeom, Z., Park, K. T., Han, E. H., Yu, H. J., Kang, H. S., et al. (2018). Hypouricemic effect of ethanol extract of Aster glehni leaves in potassium oxonate-induced hyperuricemic rats. *Clin. Nutr. Res.* 7 (2), 126–135. doi:10.7762/cnr.2018.7.2.126

Pérez-Gregorio, R. M., García-Falcón, M. S., Simal-Gándara, J., Rodrigues, A. S., and Almeida, D. P. (2010). Identification and quantification of flavonoids in traditional cultivars of red and white onions at harvest. *J. Food Compos. Anal.* 23, 592–598. doi:10.1016/j.jfca.2009.08.013

Potapovich, A., and Kostyuk, V. (2003). Comparative study of antioxidant properties and cytoprotective activity of flavonoids. *Biochem.* 68, 514–519. doi:10.1023/A:1023947424341

Qudwai, W., and Jawaid, M. (2017). Frequency of uric acid levels symptomatic and asymptomatic hyperuricemia among the Pakistani population. *Mid. East. J. Fam. Med.* 15, 52–57.

Rahim, M. A., Naeem, M., Khalid, K., Imran, M., Khan, M. K., Khan, M. I., et al. (2023). Effects of different levels of egg protein replacement in weaned diets on hematology, kidney functions, and immunity biomarkers. *Food Sci. Nutr.* 11 (4), 1747–1754. doi:10.1002/fsn3.3204

Rahim, M. A., Saeed, F., Khalid, W., Hussain, M., and Anjum, F. M. (2021). Functional and nutraceutical properties of fructo-oligosaccharides derivatives: a review. *Int. J. Food Prop.* 24 (1), 1588–1602. doi:10.1080/10942912.2021.1986520

Rahmat, R. F., Adnan, S., Anugrahwaty, R., Alami, E. P. S., and Siregar, B. (2019). Red onion growth monitoring system in hydroponics environment. *J. Phys.* 1235 (1), 012117. doi:10.1088/1742-6596/1235/1/012117

Ramaiah, S. K. (2007). A toxicologist guide to the diagnostic interpretation of hepatic biochemical parameters. *Food Chem. Toxicol.* 45 (9), 1551–1557. doi:10.1016/j.fct.2007.06.007

Randie Little (2016). *Laboratory procedure manual, roche Cobas C311 2017—standard*. Columbia, MO, US: Fasting Glucose NHANES.

Rohn, S., Rawel, H. M., and Kroll, J. (2002). Inhibitory effects of plant phenols on the activity of selected enzymes. *J. Agric. Food Chem.* 50 (12), 3566–3571. doi:10.1021/jf011714b

Saeed, M., Naveed, M., Arain, M. A., Arif, M., Abd El-Hack, M. E., Alagawany, M., et al. (2017). Quercetin: nutritional and beneficial effects in poultry. *Worlds Poult. Sci. J.* 73 (2), 355–364. doi:10.1017/S004393391700023X

Safari, O., Shahsavani, D., Paolucci, M., and Atash, M. M. S. (2014). Single or combined effects of fructo-and mannan oligosaccharide supplements on the growth performance, nutrient digestibility, immune responses and stress resistance of juvenile narrow clawed crayfish, Astacus leptodactylus leptodactylus Eschscholtz, 1823. *Aquaculture* 432, 192–203. doi:10.1016/j.aquaculture.2014.05.012

Saleh, A. A., Ebeid, T. A., and Abudabos, A. M. (2018). Effect of dietary phytogenics (herbal mixture) supplementation on growth performance, nutrient utilization, antioxidative properties, and immune response in broilers. *Environ. Sci. Pollut. Res. Int.* 25 (15), 14606–14613. doi:10.1007/s11356-018-1685-z

Sangpreecha, N., Chanmuang, S., Park, K. H., Sangar, M., Sharma, D., Song, D., et al. (2023). Effects of fermented onion on gut health in dextran sodium sulfate (DSS)-Induced inflammatory bowel disease (IBD) rats. *Appl. Sci.* 13 (3), 1590. doi:10.3390/app13031590

Sarvaiya, V. N., Sadariya, K. A., Pancha, P. G., Thaker, A. M., Patel, A. C., and Prajapati, A. S. (2015). Evaluation of antigout activity of Phyllanthus emblica fruit extracts on potassium oxonate-induced gout rat model. *Vet. World.* 8 (10), 1230–1236. doi:10.14202/vetworld.2015.1230-1236

Shi, H., Li, S., Cao, Z., Wang, Y., Alugongo, G., and Doane, P. (2015). Effects of replacing wild rye, corn silage, or corn grain with CaO-treated corn stover and dried distillers grains with solubles in lactating cow diets on performance, digestibility, and profitability. *J. Dairy Sci.* 98 (10), 7183–7193. doi:10.3168/jds.2014-9273

Slimestad, R. , Fossen, T., and Vågen, I. M. (2007). Onions: a source of unique dietary flavonoids. *J. Agric. Food Chem.* 55 (25), 10067–10080.

Strazzullo, P., and Puig, J. G. (2007). Uric acid and oxidative stress: relative impact on cardiovascular risk. *Nutr. Metab. Cardiovasc. Dis.* 17 (6), 409–414. doi:10.1016/j.numecd.2007.02.011

Świeca, M., Gawlik-Dziki, U., Dziki, D., Baraniak, B., and Czyż, J. (2013). The influence of protein–flavonoid interactions on protein digestibility *in vitro* and the antioxidant quality of breads enriched with onion skin. *Food Chem.* 141 (1), 451–458. doi:10.1016/j.foodchem.2013.03.048

Tang, L., Li, K., Zhang, Y., Li, H., Li, A., Xu, Y., et al. (2020). Quercetin liposomes ameliorate streptozotocin-induced diabetic nephropathy in diabetic rats. *Sci. Rep.* 10 (1), 2440. doi:10.1038/s41598-020-59411-7

Teyssier, C., Amiot, M.-J., Mondy, N., Auger, J., Kahane, R., and Siess, M.-H. (2001). Effect of onion consumption by rats on hepatic drug-metabolizing enzymes. *Food Chem. Toxicol.* 39 (10), 981–987. doi:10.1016/S0278-6915(01)00056-4

Thomas, S., Senthilkumar, G. P., Sivaraman, K., Bobby, Z., Paneerselvam, S., and Harichandrakumar, K. T. (2015). Effect of smethyl-L-cysteine on oxidative stress, inflammation and insulin resistance in male Wistar rats fed with high fructose diet. *Iran. J. Med. Sci.* 40 (1), 45–50.

Tigner, A., Ibrahim, S. A., and Murray, I. (2021). "Histology, white blood cell," in *StatPearls*. Treasure Island, FL: StatPearls Publishing.

Ufele, A. N., Mgbenka, B. O., and Ude, J. F. (2008). Effect of nutrition on the red blood cells of trypanosome-infected female rats. *Anim. Res. Int.* 5 (1), 816–818. doi:10.4314/ari.v5i1.48720

Ülger, T. G., and Çakiroglu, F. P. (2020). The effects of onion (Allium cepa L.) dried by different heat treatments on plasma lipid profile and fasting blood glucose level in diabetic rats. *Avicenna J. Phytomed* 10 (4), 325–333.

Vijeesh, V., Vysakh, A., Jisha, N., and Latha, M. S. (2022). Malic acid attenuates potassium oxonate induced gouty inflammation in wistar rat. *Biointerface Res. Appl. Chem.* 12 (2), 1682–1691. doi:10.33263/BRIAC122.16821691

Wade, N. (1978). A new militancy in England. *Science* 199 (4326), 279. doi:10.1126/science.199.4326.279.a

Wang, Y., Zhu, J. X., Kong, L. D., Yang, C., Cheng, C. H. K., and Zhang, X. (2004). Administration of procyanidins from grape seeds reduces serum uric acid levels and decreases hepatic xanthine dehydrogenase/oxidase activities in oxonate-treated mice. *Basic Clin. Pharmacol. Toxicol.* 94 (5), 232–237. doi:10.1111/j.1742-7843.2004.pto940506.x

Wong, C. C., Botting, N. P., Orfila, C., Al-Maharik, N., and Williamson, G. (2011). Flavonoid conjugates interact with organic anion transporters (OATs) and attenuate cytotoxicity of adefovir mediated by organic anion transporter 1 (OAT1/SLC22A6). *Biochem. Pharmacol.* 81 (7), 942–949. doi:10.1016/j.bcp.2011.01.004

Ye, J. D., Wang, K., Li, F. D., and Sun, Y. Z. (2011). Single or combined effects of fructo- and mannan oligosaccharide supplements and Bacillus clausii on the growth, feed utilization, body composition, digestive enzyme activity, innate immune response and lipid metabolism of the Japanese flounder Paralichth: dietary benefits of FOS, MOS and B. clausii in the Japanese flounder. *Aquac. Nutr.* 17 (4), e902–e911. doi:10.1111/j.1365-2095.2011.00863.x

Yiying, K., Yongfang, L., Husai, M., Wangyu, L., Ruilian, L., and Zhancui, D. (2016). Uric acid lowering effect of Tibetan Medicine RuPeng15 powder in animal models of hyperuricemia. *J. Tradit. Chin. Med.* 36 (2), 205–210. doi:10.1016/S0254-6272(16)30028-0

Zhu, J. X., Wang, Y., Kong, L. D., Yang, C., and Zhang, X. (2004). Effects of Biota orientalis extract and its flavonoid constituents, quercetin and rutin on serum uric acid levels in oxonate-induced mice and xanthine dehydrogenase and xanthine oxidase activities in mouse liver. *J. Ethnopharmacol.* 93 (1), 133–140. doi:10.1016/j.jep.2004.03.037

frontiers | Frontiers in Physiology

TYPE Systematic Review
PUBLISHED 09 January 2024
DOI 10.3389/fphys.2023.1293402

OPEN ACCESS

EDITED BY
Xiaoyan Zhang,
East China Normal University, China

REVIEWED BY
Miha Arnol,
University Medical Centre Ljubljana, Slovenia
Liang Zhu,
Dalian Medical University, China

*CORRESPONDENCE
Liang Wei,
lweimd@uestc.edu.cn

†These authors have contributed equally to this work

RECEIVED 13 September 2023
ACCEPTED 26 December 2023
PUBLISHED 09 January 2024

CITATION
Yang H, Wang D, Sun X, Wang H, Lan Y and Wei L (2024), Diagnostic performance of GcfDNA in kidney allograft rejection: a meta-analysis. *Front. Physiol.* 14:1293402. doi: 10.3389/fphys.2023.1293402

Diagnostic performance of GcfDNA in kidney allograft rejection: a meta-analysis

Hongji Yang[1,2†], Duo Wang[1†], Xin Sun[3], Hailian Wang[1,2], Yang Lan[1] and Liang Wei[1,2*†]

[1]Clinical Immunology Translational Medicine Key Laboratory of Sichuan Province, Sichuan Provincial People's Hospital, School of Medicine, University of Electronic Science and Technology of China, Chengdu, China, [2]Transplantation Center, Sichuan Provincial People's Hospital, School of Medicine, University of Electronic Science and Technology of China, Chengdu, China, [3]Chinese Evidence-Based Medicine Center and Chinese Cochrane Center, West China Hospital, Sichuan University, Chengdu, China

In this comprehensive meta-analysis, our objective was to evaluate the diagnostic utility of graft-derived cell-free DNA (GcfDNA) in kidney allograft rejection and explore associated factors. We conducted a thorough search of PubMed, Embase, and the Cochrane Library databases, spanning from their inception to September 2022. Statistical analysis was executed utilizing Stata 15, Meta-DiSc 1.4, and Review Manager 5.4 software. The combined pooled sensitivity, specificity, positive likelihood ratio (PLR), negative likelihood ratio (NLR), diagnostic odds ratio (DOR), and the area under the summary receiver operating characteristics (SROC) curve from the synthesis of findings across ten studies were as follows: 0.75 (0.67–0.81), 0.78 (0.72–0.83), 3.36 (2.89–4.35), 0.32 (0.24–0.44), 8.77 (4.34–17.74), and 0.83 (0.80–0.86), respectively. Among the ten studies primarily focused on GcfDNA's diagnostic potential for antibody-mediated rejection (ABMR), the optimal cut-off threshold demonstrated substantial diagnostic efficacy, with pooled sensitivity, specificity, positive likelihood ratio, negative likelihood ratio, DOR, and area under the summary receiver operating characteristics curve values of 0.83 (0.74–0.89), 0.75 (0.70–0.80), 3.37 (2.64–4.30), 0.23 (0.15–0.36), 14.65 (7.94–27.03), and 0.85 (0.82–0.88), respectively. These results underscore the high diagnostic accuracy of GcfDNA in detecting rejection. Furthermore, the optimal cut-off threshold proves effective in diagnosing ABMR, while a 1% threshold remains a robust diagnostic criterion for rejection. Notably, for ABMR diagnosis, droplet digital PCR digital droplet polymerase chain reaction emerges as a superior method in terms of accuracy when compared to other techniques. Nonetheless, further research is warranted to substantiate these findings.

KEYWORDS

graft-derived cell-free DNA, kidney transplantation, diagnostic performance, rejection, meta-analysis

Introduction

Kidney transplantation stands as the most effective remedy for individuals afflicted by end-stage kidney disease. Despite significant advancements in graft survival, allograft rejection persists as a formidable challenge. Notably, in United States and numerous other nations, acute rejection within the first year post-kidney transplantation occurs in

approximately 12% of cases (McDonald, 2015; Hart et al., 2021). Among adult recipients, the incidence rate of acute kidney allograft rejection (AR) hovers around 7.8% (Wolfe et al., 1999; Hart et al., 2019). Thus, early diagnosis holds pivotal clinical significance. However, contemporary methods for monitoring allograft injury, including markers such as serum creatinine, urinary protein, urinalysis, donor-specific antibodies, and BK virus surveillance, are encumbered by limitations in sensitivity and specificity (Schinstock et al., 2017; Cheungpasitporn et al., 2018; Leeaphorn et al., 2020). Serum creatinine, although a sensitive marker for evaluating glomerular filtration rate (GFR), lacks the requisite sensitivity and specificity for diagnosing allograft rejection, and monitoring its trends offers meager predictive value for detecting active rejection. Kidney needle biopsy, the gold standard for diagnosing rejection, proves unsuitable for frequent monitoring owing to its invasive nature and potential complications, such as gross hematuria and hematoma (Schwarz et al., 2005; Redfield et al., 2016). It was reported that up to 25% of biopsies yield an inadequate specimen (Oellerich et al., 2021). A study has suggested that performing protocol biopsies yields no significant benefits in terms of rejection rates, graft survival, or kidney function within the first 12 months post-transplant (Redfield et al., 2016). Due to complications, sampling error and variability in the interpretation of histological findings, rejection reactions with negative biopsy results may occur. One study showed "biopsynegative" rejection occurs in up to 20% of patients (Miller et al., 2013; Moein et al., 2023). Therefore, the quest for noninvasive diagnostic biomarkers boasting high sensitivity and specificity to facilitate optimal management of kidney transplant patients is of paramount importance.

Allograft transplantation exhibits unique allogenic genomic characteristics and can be conceived of as genomic transplantation. The investigation into plasma donor DNA as a potential biomarker of rejection dates back to 1998. Graft-derived cell-free DNA (GcfDNA), emanating from the necrotic or apoptotic cells of transplanted organs, emerges as a potential universal noninvasive biomarker for assessing allograft health (Lo et al., 1998). During periods of stable graft function, GcfDNA circulates at low levels. However, in cases of injury, including rejection, significantly elevated levels of GcfDNA are released into the bloodstream, signifying organ damage in solid organ transplantation. The quantification of GcfDNA can be accomplished through next-generation sequencing (NGS) or droplet digital PCR (ddPCR) and can be expressed either as GcfDNA percentage (GcfDNA/total cfDNA) or via absolute quantification in copies per milliliter (Di et al., 2021).

The gradual application of GcfDNA to clinical practice has been facilitated by the advancement of molecular detection technology (Oellerich et al., 2021). While most studies have uncovered associations between GcfDNA levels and the presence of acute rejection, a minority have failed to establish such correlations (Bromberg et al., 2017; Mayer et al., 2022). Moreover, the optimal threshold for distinguishing between rejection and non-rejection varies among studies. Although 1.0% serves as the threshold in the majority of GcfDNA investigations, some studies utilize the optimal cut-off threshold for this differentiation. Another study suggests that a lower threshold such as 0.5% may be more appropriate if a threshold is to be used (Stites et al., 2020). Furthermore, various factors, including disparities in testing methods, types of sampling tubes, and ethnicity, exert an influence on the outcomes of GcfDNA testing. Consequently, further exploration is warranted to enhance post-transplantation monitoring, curtail premature graft loss, and improve patient survival. The objective of this meta-analysis is to assess the diagnostic performance of GcfDNA as a biomarker for kidney transplant rejection. We also compared the diagnostic performance under different thresholds (1.0%/optimal cut-off threshold) and different detection methods.

Materials and methods

Search strategy

We conducted a comprehensive search of the PubMed, EMBASE, and Cochrane Library databases from their inception up to 30 September 2022. Retrieval was based on a combination of subject words and free words. The search terms encompassed "Donor-derived cell-free DNA," "dd-cfDNA," "Graft-derived cell-free DNA," "GcfDNA," "Kidney," "Renal," and "Transplantation." These terms were utilized as either keywords or Medical Subject Headings (MeSH) terms, and different combinations of these terms were searched using Boolean operators "AND" and "OR." Subsequently, two independent investigators (HLW and YL) conducted a secondary search of eligible studies. In cases of disagreement, consensus was reached through negotiation. The detailed search strategy is available in the Supplementary Material S1.

Selection criteria

Following the predefined inclusion and exclusion criteria, investigators (HLW and YL) evaluated potentially relevant articles, with any discrepancies resolved by another reviewer (LW). The inclusion criteria were as follows: 1) Published studies on the use of GcfDNA for adjunctive diagnosis of rejection in kidney transplant recipients; 2) The study subjects were first-time kidney transplant recipients; 3) All episodes of rejection were confirmed by biopsy and scored using the Banff criteria; 4) The studies reported outcome indicators in the form of four-grid diagnostic tables, which could be extracted directly or indirectly. The exclusion criteria comprised: 1) Duplicate publications; 2) Reviews, conference abstracts, editorials, and case reports; 3) Animal experiments; 4) Studies involving recipients of multiorgan transplants or retransplants; 5) Studies with unavailable or incomplete data required for reconstructing a four-grid diagnostic table.

Data extraction and quality assessment

Two independent investigators (HLW and YL) extracted relevant information, including general and clinical details from the literature (first author, publication year, country, type of rejection, study duration, study design, GcfDNA detection technology, and patient age), as well as diagnostic parameters from the literature (area under the curve [AUC], sensitivity, specificity, true positive [TP], false positive [FP], false negative [FN], true negative [TN], positive predictive value [PPV], and negative predictive value [NPV]). Quality assessment was conducted using the QUADAS-2 scale by two investigators (HLW and YL), with discrepancies resolved by a third investigator (LW) (Whiting et al., 2011).

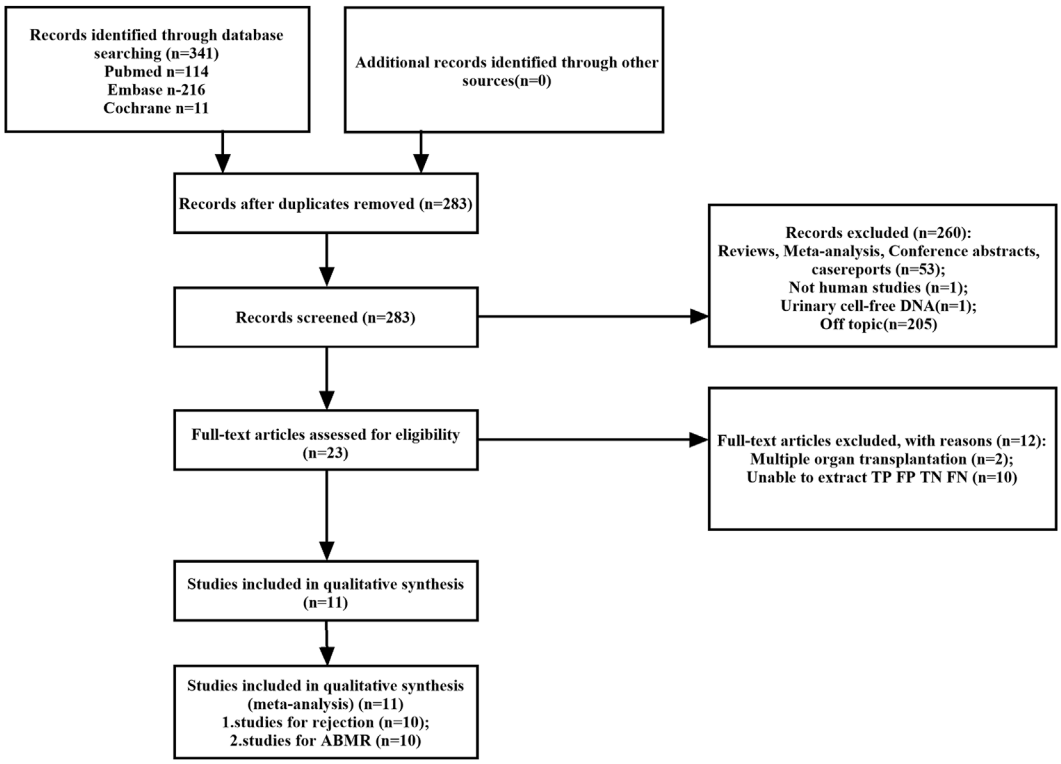

FIGURE 1
Flowchart detailing the study selection process. 11 studies that met the inclusion criteria were finally included. FN, false negative; FP, false positive; TN, true negative; TP, true positive.

Statistical analysis

Data on TP, FP, TN, and FN were extracted from the included studies to establish the four values for a diagnostic 2 × 2 contingency table. We used Spearman rank correlation, Cochran's Q test, Higgins' I^2 test, and forest plots to evaluate both the threshold and non-threshold sources of heterogeneity. In general, we graded the degree of heterogeneity as low ($I^2 < 25\%$), moderate ($25\% < I^2 < 75\%$), or high ($I^2 > 75\%$) (Whiting et al., 2011). A random-effects model was employed if evidence of non-threshold effect was present. Subgroup analyses and Meta-regression were used to explore the sources of heterogeneity. Publication bias was assessed using Deeks funnel plot asymmetry test. A significance level of $p < 0.05$ was considered statistically significant. Statistical analyses were performed using Stata 15.1, Review Manager 5.4, and Meta-DiSc 1.4 (Higgins et al., 2003; Zamora et al., 2006).

Results

Literature search

A total of 341 potentially relevant studies were initially identified across the three databases. Following a comprehensive review of the full-text literature, we ultimately included 11 studies, comprising 1,248 patients, for systematic review and meta-analysis (Figure 1) (Bloom et al., 2017; Jordan et al., 2018; Sigdel et al., 2018; Huang et al., 2019; Oellerich et al., 2019; Whitlam et al., 2019; Gielis et al., 2020; Zhang et al., 2020; Puliyanda et al., 2021; Bu et al., 2022; Verhoeven et al., 2022). Detailed information pertaining to these 11 studies can be found in Supplementary Table S1. Our research encompassed studies conducted on four continents and in six different countries, including the United States ($n = 5$), Australia ($n = 1$), Belgium ($n = 1$), China ($n = 1$), Germany ($n = 1$), and the Netherlands ($n = 1$). GcfDNA content was assessed using either Next-Generation Sequencing (NGS) technology ($n = 7$) or Droplet Digital Polymerase Chain Reaction (dd-PCR) technology ($n = 3$). The study populations ranged in size from 37 to 203 patients, with an average age spanning 10–60 years. Diagnostic parameters from the literature are presented in Supplementary Table S2. Notably, there was no unified threshold for diagnosing rejection, with approximately half of the studies employing a 1% threshold. Among the included literature, 10 studies aimed to distinguish between rejection and non-rejection reactions, while 10 studies focused on diagnosing Antibody-Mediated Rejection (ABMR). Nine studies used a 1% threshold, two used a 0.5% threshold, and the remainder applied optimal cut-off thresholds tailored to each study. Separate meta-analyses were conducted for rejection and ABMR due to variations in research focus and the pathological classification of rejection.

Data characteristics and quality assessment

Based on the QUADAS-2 assessment, Supplementary Figure S1 illustrates the quality and applicability evaluations of the 11 included studies. All of the studies met four or more of the seven criteria,

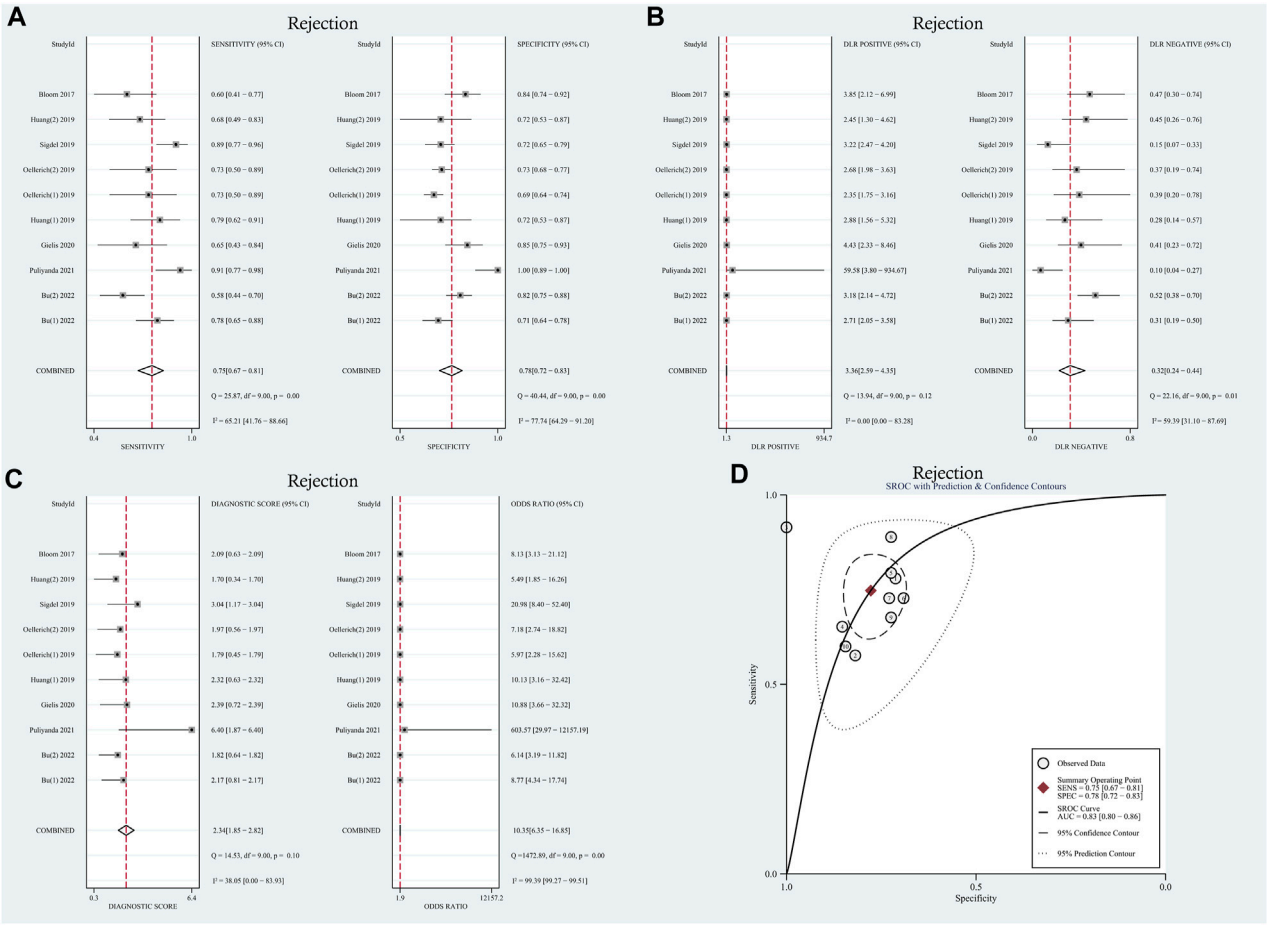

FIGURE 2
Diagnostic accuracy of GcfDNA in rejection. **(A)** Forest plots of sensitivity and specificity for GcfDNA in diagnosis. **(B)** Forest plots of the positive likelihood ratio and negative likelihood ratio in diagnosis. **(C)** Forest plots of the diagnostic odds ratio in diagnosis. **(D)** SROC curve of GcfDNA. The SROC curve analysis of the GcfDNA test accuracy in rejection diagnosis revealed an AUC of 0.83.

indicating an overall acceptable quality level for the included studies. Nevertheless, two studies were non-consecutively enrolled and exhibited unclear inclusion and exclusion criteria. One study established a preset threshold and assessed the results against known reference standards. Moreover, two studies did not include all patients in the analysis. Concerning the inclusion of patients in the applicability analysis, two studies were categorized as "of high concern" due to a lack of detailed demographic characteristic descriptions, and one study was classified as "of unknown concern".

Results of the meta-analysis

Rejection

Heterogeneity analysis

Moderate levels of heterogeneity were observed and assessed using the random-effects model ($I^2 > 50\%$) (Higgins and Green, 2011). In the entire cohorts, the results were as follows: pooled sensitivity, 0.75 (95% CI: 0.67–0.81, $I^2 = 65.21\%$); pooled specificity, 0.78 (95% CI: 0.72–0.83, $I^2 = 77.74\%$); pooled PLR, 3.36 (95% CI: 2.59–4.35, $I^2 = 0.00$); pooled NLR, 0.32 (95% CI: 0.24–0.44, $I^2 = 59.39$); DOR, 8.77 (95% CI: 4.34–17.74, $I^2 = 99.39$); AUC, 0.83 (95% CI: 0.80–0.86). Forest plots and summary receiver operating characteristics (SROC) curves are presented in Figure 2. To assess the presence of a threshold effect, the Spearman rank correlation coefficient was calculated, yielding a value of 0.24 ($p = 0.53$). Notably, the scatter plots did not exhibit the characteristic "shoulder-arms" pattern on the SROC curve, suggesting an absence of a threshold effect.

Meta-regression analysis and subgroup analysis

To explore potential sources of heterogeneity within the included studies, we conducted both meta-regression analysis and subgroup analysis. Covariates such as study design, research center, research region, number of patients, and sampling tube were included in the meta-regression analysis. However, as summarized in Table 1, it was determined that none of these covariates could sufficiently account for the observed heterogeneity ($p > 0.05$), with the exception of the sampling tube, which demonstrated a significant contribution to the overall

TABLE 1 Result of univariate meta-regression analysis diagnostic odd ratio.

Type	Var	*p*-value	RDOR	95% CI
Rejection	Design	0.41	0.51	0.05–4.92
	Center	0.06	0.01	0.00–1.24
	Continent	0.57	1.22	0.55–2.70
	Quality	0.88	1.08	0.23–5.15
	Tube	0.05	248.68	0.82–7,583.12
ABMR	Design	0.56	0.72	0.18–2.18
	Center	0.51	0.68	0.16–2.82
	Continent	0.22	0.53	0.17–1.69
	Quality	0.09	0.37	0.11–1.22
	Tube	0.86	1.12	0.23–5.38

Relative diagnostic odds ratio (RDOR).

heterogeneity (Relative Diagnostic Odds Ratio [RDOR] = 248.68, p = 0.05). Given the lack of a standardized testing method and diagnostic threshold across the studies, we performed a subgroup analysis based on threshold levels and detection methods, as detailed in Table 2. The pooled sensitivity and specificity of 6 tests using the NGS detection method were 0.72 (95% CI: 0.66–0.77), 0.79 (95% CI: 0.75–0.82). Two tests used the detection method of dd-PCR, the pooled sensitivity was 0.73 (95% CI: 0.57–0.85) and the pooled specificity was 0.71 (95% CI: 0.68–0.74), respectively. Two tests used the detection method of mmPCR-NGS, the pooled sensitivity and specificity were 0.82 (95% CI: 0.71–0.90), 0.76 (95% CI: 0.70–0.82). Regarding the diagnostic threshold, 1% was employed in 5 tests, while the remaining 5 tests used optimal cut-off thresholds. The pooled sensitivity and specificity were 0.73 (95% CI: 0.67–0.79), 0.80 (95% CI: 0.76–0.83); 0.75 (95% CI: 0.68–0.82), 0.72 (95% CI: 0.69–0.75), respectively.

Sensitivity analysis

We conducted a sensitivity analysis to assess the impact of each individual study on the overall outcomes of the meta-analysis. The results of this analysis, presented in Supplementary Figure S2A, suggest that the stability and reliability of the included literature were acceptable.

Differential diagnostic value of GcfDNA

A random-effects model was used for the meta-analysis of included studies. Results showed a pooled sensitivity of 0.75 (95% CI: 0.67–0.81), pooled specificity of 0.78 (95% CI: 0.72–0.83), pooled positive likelihood ratio (PLR) of 3.36 (95% CI: 2.59–4.35), pooled negative likelihood ratio (NLR) of 0.32 (95% CI: 0.24–0.44), diagnostic odds ratio (DOR) of 8.77 (95% CI: 4.34–17.74). Hierarchical summary receiver operating characteristic (HSROC) curves are shown in Supplementary

TABLE 2 Assessment of diagnostic accuracy and heterogeneity in subgroup analysis.

Type	Parameter	Category	Number of studies	Sensitivity (95%CI)	Specificity (95%CI)	PLR(95% CI)	NLR(95% CI)	DOR (95% CI)
Rejection	All		10	0.75 (0.67–0.81)	0.78 (0.72–0.83)	3.36 (2.59–4.35)	0.32 (0.24–0.44)	8.77 (4.34–17.74)
	Method	NGS	6	0.72 (0.66–0.77)	0.79 (0.75–0.82)	2.98 (2.26–3.92)	0.37 (0.26–0.52)	8.23 (4.70–14.42)
		dd-PCR	2	0.73 (0.57–0.85)	0.71 (0.68–0.74)	2.47 (2.00–3.01)	0.40 (0.25–0.63)	6.21 (3.21–12.02)
		mmPCR-NGS	2	0.82 (0.71–0.90)	0.76 (0.70–0.82)	3.32 (2.60–4.24)	0.27 (0.10–0.72)	14.89 (7.54–29.43)
	Threshold	1%	5	0.73 (0.67–0.79)	0.80 (0.76–0.83)	3.22 (2.35–4.40)	0.32 (0.19–0.55)	10.93 (4.65–25.70)
		Optimal cut-off threshold	5	0.75 (0.68–0.82)	0.72 (0.69–0.75)	2.65 (2.26–3.09)	0.36 (0.28–0.47)	7.83 (5.21–11.76)
ABMR	All		10	0.83 (0.74–0.89)	0.75 (0.70–0.80)	3.37 (2.64–4.30)	0.23 (0.15–0.36)	14.65 (7.94–27.03)
	Method	NGS	7	0.79 (0.72–0.84)	0.74 (0.70–0.77)	3.15 (2.36–4.20)	0.33 (0.22–0.47)	10.28 (5.67–18.65)
		dd-PCR	3	0.85 (0.71–0.94)	0.75 (0.63–0.84)	3.04 (2.03–4.54)	0.25 (0.13–0.46)	12.77 (5.14–31.71)
	Threshold	1%	5	0.76 (0.67–0.83)	0.78 (0.74–0.83)	3.32 (2.57–4.29)	0.33 (0.22–0.48)	10.13 (5.76–17.81)
		Optimal cut-off threshold	5	0.85 (0.76–0.91)	0.68 (0.62–0.73)	2.89 (2.01–4.14)	0.29 (0.18–0.48)	11.19 (4.62–27.09)

Next-generation sequencing (NGS); digital droplet polymerase chain reaction (ddPCR); antibody-mediated rejection (ABMR).

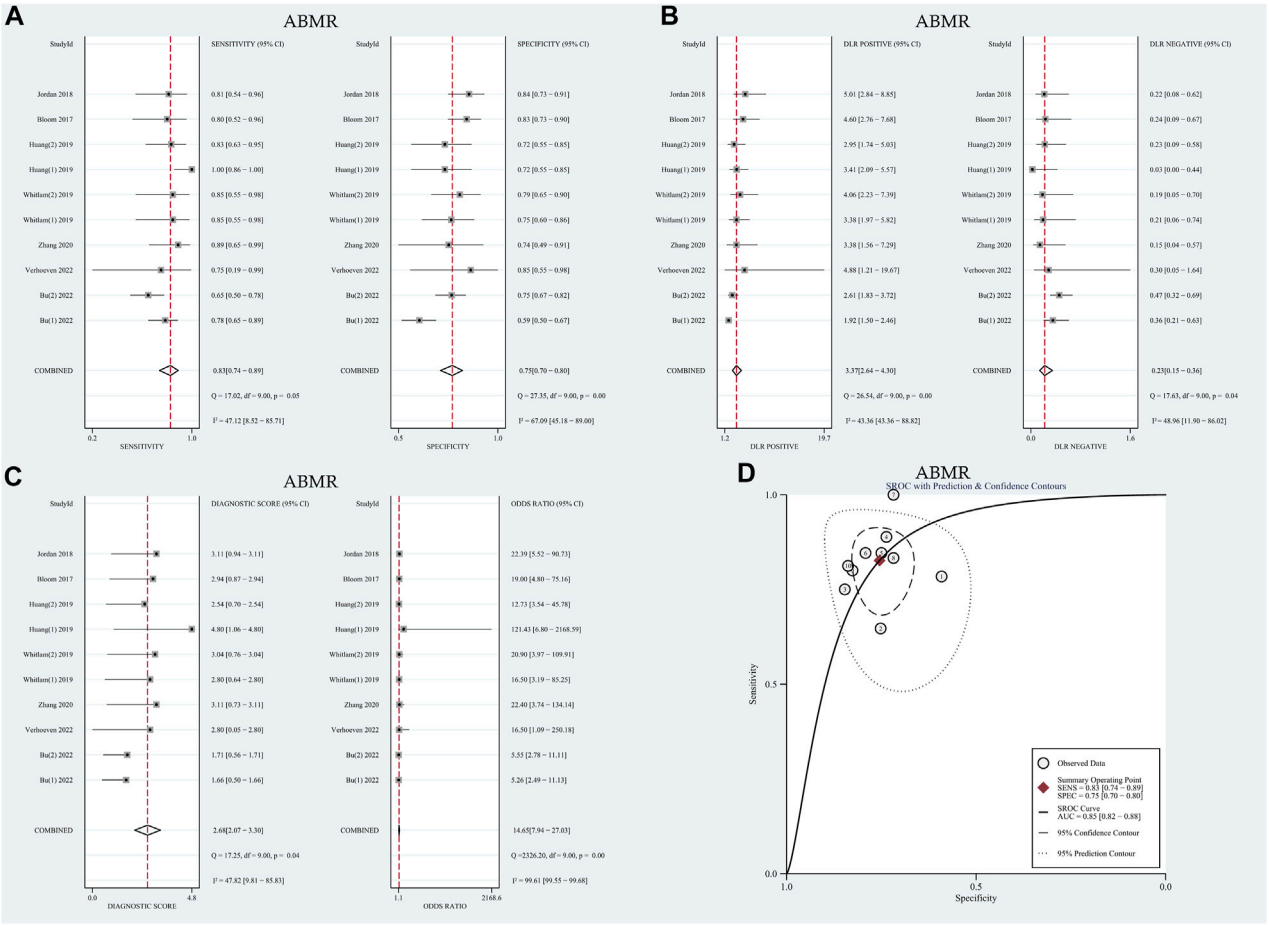

FIGURE 3
Diagnostic accuracy of GcfDNA in ABMR. **(A)** Forest plots of sensitivity and specificity for GcfDNA in diagnosis. **(B)** Forest plots of the positive likelihood ratio and negative likelihood ratio in diagnosis. **(C)** Forest plots of the diagnostic odds ratio in diagnosis. **(D)** SROC curve of GcfDNA. The SROC curve analysis of the GcfDNA test accuracy in rejection diagnosis revealed an AUC of 0.84.

Figure S3A. The estimated value of β was −0.25 (95% CI: 1.39–0.89), and the value of z and the *p*-value were −0.43 and 0.67 separately, indicates that the SROC curve was symmetric. The diagnostic accuracy of GcfDNA was 0.83, $p < 0.05$. Based on the aforementioned data, it can be concluded that GcfDNA exhibits favorable sensitivity and specificity for the early diagnosis of rejection, substantiating its diagnostic value. These results collectively suggest that GcfDNA demonstrates acceptable diagnostic performance for the detection of rejection. Furthermore, an assessment of publication bias in the selected studies was conducted using the Deeks' funnel plot asymmetry test (Supplementary Figure S4A), which did not indicate any significant publication bias ($p = 0.59$).

ABMR

Heterogeneity analysis

The I^2 values for sensitivity and specificity were found to be 47.12% and 67.09% ($p < 0.01$), respectively. These values suggest moderate levels of heterogeneity, leading to the calculation of sensitivity and specificity using the random effects model. The pooled sensitivity and specificity were determined to be 0.83 (95% CI: 0.74–0.89) and 0.75 (95% CI: 0.70–0.80), respectively. Furthermore, the pooled positive likelihood ratio (PLR), negative likelihood ratio (NLR), and diagnostic odds ratio (DOR) were calculated as 3.37 (95% CI: 2.64–4.30), 0.23 (95% CI: 0.15–0.36), and 14.65 (95% CI: 7.94–27.03), respectively. The AUC in the SROC curve was determined to be 0.85 (95% CI: 0.82–0.88), as illustrated in Figure 3. Similarly, there was no threshold effect: the spearman correlation coefficient was 0.319 ($p = 0.40$) and the scatter plots did not appear as "shoulder-arms" in the image formed on the SROC curve.

Meta-regression analysis and subgroup analysis

Similarly, meta-regression and subgroup analysis were conducted to further explore potential sources of heterogeneity. As summarized in Table 1, it was observed that none of the covariates could account for the observed heterogeneity ($p > 0.05$). Subsequently, subgroup analysis was carried out based on threshold levels and detection methods, as detailed in Table 2. For

the 7 tests utilizing the NGS detection method, the pooled sensitivity and specificity were determined to be 0.79 (95% CI: 0.72–0.84) and 0.74 (95% CI: 0.70–0.77), respectively. On the other hand, among the 3 tests employing the dd-PCR detection method, the pooled sensitivity was 0.85 (95% CI: 0.71–0.94), and the pooled specificity was 0.75 (95% CI: 0.63–0.84).

Sensitivity analysis

The results of the sensitivity analysis demonstrated the overall stability of the included literature, as illustrated in Supplementary Figure S2B.

Differential diagnostic value of GcfDNA

The meta-analysis, conducted using a random-effects model, revealed that the combined pooled sensitivity, specificity, PLR, NLR, DOR, and the area under the SROC curve of the 10 tests were 0.83 (95% CI: 0.74–0.89), 0.75 (95% CI: 0.70–0.80), 3.37 (95% CI: 2.64–4.30), 0.23 (95% CI: 0.15–0.36), 14.65 (95% CI: 7.94–27.03), and 0.85 (95% CI: 0.82–0.88), respectively, as depicted in Figure 3. The HSROC curves are presented in Supplementary Figure S3B. The estimated value of β was −0.39 (95% CI: 1.61–0.84), with the corresponding values of z and P being −0.62 and 0.54, respectively, indicating a symmetric SROC curve. The diagnostic accuracy of GcfDNA was 0.85, with $p < 0.05$. Therefore, it can be concluded that GcfDNA exhibits excellent discriminatory value for ABMR. The assessment of publication bias using the Deeks funnel plot indicated no significant publication bias ($p = 0.07$), as shown in Supplementary Figure S4B.

Discussion

GcfDNA, as an emerging biomarker, holds significant clinical relevance for the early prediction of rejection (Lo et al., 1998). Nevertheless, several critical issues warrant discussion, primarily pertaining to diagnostic thresholds and detection methods. In this meta-analysis, we offer comprehensive insights into the distinctive diagnostic value of GcfDNA concerning kidney allograft rejection and ABMR.

This comprehensive meta-analysis encompassed 20 tests conducted between 2017 and 2022, collectively involving 1,248 patients. Our findings reveal that GcfDNA exhibits comparable diagnostic accuracy for both rejection and ABMR scenarios. Specifically, the pooled sensitivity, specificity, and the area under the SROC curve were 0.75 (95% CI: 0.67–0.81), 0.78 (95% CI: 0.72–0.83), and 0.83 (95% CI: 0.80–0.86) for rejection, and 0.83 (95% CI: 0.74–0.89), 0.75 (95% CI: 0.70–0.80), and 0.85 (95% CI: 0.82–0.88) for ABMR, respectively. The diagnostic sensitivity of ABMR alone is higher, which confirms the research of Bloom et al. (2017). Taking a step furtherGcfDNA elevation has often been demonstrated in patients with ABMR, its association with TCMR is less clear (Agbor-Enoh et al., 2018; Agbor-Enoh, 2019; Wijtvliet et al., 2020). One possible explanation is that microvascular injury is the main pathological change of ABMR, while TCMR is characterized by interstitial inflammation and tubulitis, only the higher-level classification releases GcfDNA (Haas et al., 2018). Therefore only a small increase in GcfDNA levels was observed in patients with TCMR (Bloom et al., 2017). This may account for the limited sensitivity of GcfDNA in identifying TCMR. However, the conclusion remains inconclusive. In recipients with acute rejection or without rejection, the GcfDNA (%) detected by short amplicons (86–128 bp) was significantly higher than that quantified with long amplicons (106–156 bp). In the study by Huang et al., the median GcfDNA (%) in patients with TCMR measured using the Allosure detection method was even lower than that of patients without rejection (0.27% vs. 0.38%). The amplicon length was 100–130 bp (Huang et al., 2019). Sigdel et al. successfully used the multiplex PCR NGS methodology to detect plasma dd-cfDNA elevations in patients with TCMR (Sigdel et al., 2018). A group also observed an increase in GcfDNA levels of patients with TCMR through ddPCR detection. In order to correct each sample for its individual mean fragment length a ddPCR assay using amplicons of two different lengths (94 bp and 249 bp) was developed (Oellerich et al., 2019). This seems to implicate that the research results are influenced by the quantification methodology used (Dauber et al., 2020). Further research is required to test this hypothesis. As mentioned above, there are still many questions about the identification of TCMR using GcfDNA, and more research on TCMR related analysis is needed for further analysis.

It is important to note that a moderate level of heterogeneity was observed in sensitivity and specificity across the included studies. To identify potential sources of this heterogeneity, we conducted meta-regression analyses, taking into account various factors such as study design, research center, research region, number of patients, and the type of collection tube utilized. Unfortunately, the meta-regression did not provide clear insights into the origins of this heterogeneity. Notably, among the covariates studied, the type of collection tube appeared to contribute the most to the observed heterogeneity. In detail, the tube yielded maximal RDOR value and minimal p-value among all covariates. It is crucial to emphasize that the choice of collection tubes employed by different research centers has not been standardized. Maintaining sample stability is paramount to ensure accurate cfDNA analysis. Furthermore, the rupture of white blood cells (WBCs) within the collection tube can lead to the release of cfDNA, resulting in an elevated DNA background that may impact cfDNA detection results. Streck tubes, designed to stabilize blood cells and prevent hemolysis and WBC degradation over time, offer a solution to this issue. Research by Nikolaev et al. demonstrated that cfDNA in blood samples stored in EDTA tubes becomes contaminated with DNA fragments from lysed leukocytes after 16 h at room temperature, whereas samples stored in Streck tubes remain uncontaminated for at least 7 days (Nikolaev et al., 2018). This underscores the importance of using Streck tubes to prevent leukocyte lysis and maintain the stability of blood samples (Lam et al., 2004; Medina Diaz et al., 2016; Di et al., 2021).

We subsequently conducted a subgroup analysis, stratifying the data based on threshold levels and detection methods, in an effort to discern the origin of the observed heterogeneity. Our findings reveal intriguing insights into the impact of different thresholds and detection methods on diagnostic performance. For the diagnosis of rejection, the specificity associated with the 1% threshold was notably higher (0.80) compared to the optimal cut-off threshold

(0.72). Moreover, the corresponding DOR value was also higher at 10.93. It is worth highlighting that approximately half of the studies included in our analysis employed the 1% threshold as the criterion for diagnosing rejection, while the remaining studies opted for the optimal cut-off threshold. The question of whether the 1% threshold can be universally adopted as the standard for diagnosing rejection remains open for further verification. Conversely, in the context of diagnosing ABMR, the optimal cut-off threshold exhibited superior sensitivity (0.85 vs. 0.75) and a higher DOR value (11.19 vs. 8.88) when compared to the 1% threshold. These findings align with a study conducted by Huang et al., which reported higher sensitivity (100% vs. 83.3%), specificity (71.8% vs. 71.8%), PPV (68.6% vs. 64.5%), and NPV (100% vs. 87.5%) for the optimal cut-off threshold when compared to the 1% threshold (Huang et al., 2019). These results underscore the importance of carefully considering the threshold level when utilizing GcfDNA for diagnosing rejection and ABMR in kidney transplant recipients, as it can significantly impact the diagnostic accuracy and clinical utility of this biomarker. Further research and standardization efforts are warranted to establish the most appropriate thresholds for different clinical scenarios.

Two distinct methods are employed for establishing the cut-off threshold of GcfDNA: percentage or copy quantity. The GcfDNA percentage signifies the relative proportion of graft cfDNA in plasma, calculated as the ratio of graft cfDNA to total cfDNA. It is important to note that the majority of cfDNA originates from circulating WBCs, and the GcfDNA percentage may be influenced by fluctuations in both graft and recipient cfDNA levels. These fluctuations can arise due to various factors such as graft quality, leukopenia, leukocytosis, among others (Sun et al., 2015; Schütz et al., 2017). A notable study conducted by Oellerich et al. yielded intriguing insights into the quantification methods for GcfDNA thresholds. They observed that the diagnostic accuracy, as measured by the Area Under the Curve (AUC), of absolute quantification in distinguishing acute rejection confirmed by biopsy (AUC = 0.83) was significantly superior to that of GcfDNA percentage (AUC = 0.73), with a statistically significant difference ($p < 0.01$) (Oellerich et al., 2019). These findings suggest that absolute quantification of GcfDNA holds promising potential as a more accurate and reliable method for diagnostic purposes. The choice between GcfDNA percentage and absolute quantification for establishing thresholds warrants careful consideration, as it can significantly impact the diagnostic precision and clinical utility of GcfDNA in assessing kidney transplant rejection. Further research and consensus-building efforts are essential to determine the most appropriate quantification method for different clinical scenarios.

Notably, the detection method mmPCR-NGS exhibited a higher pooled sensitivity compared to NGS and ddPCR, boasting a sensitivity rate of 0.82. Furthermore, the Diagnostic Odds Ratio (DOR) associated with mmPCR-NGS was the most favorable among the three methods, with a DOR of 14.89. This suggests that the utilization of Multiplex PCR for detecting Single Nucleotide Polymorphisms (SNPs) in conjunction with NGS can yield more precise and sensitive results. This combination has previously been employed successfully by Enyedi et al. in the more accurate detection of BRCA1 and BRCA2 genes (Enyedi et al., 2016). When diagnosing ABMR, ddPCR demonstrated superior sensitivity, specificity, and DOR values. But due to a smaller number of studies and patients, more studies and further laboratory studies may be needed to confirm this phenomenon. It is worth mentioning that similar performance metrics have been reported for ddPCR and NGS methods (Oellerich et al., 2020). Moreover, ddPCR offers a much broader linear quantifiable range, spanning from 0.15% to 99.9%, in contrast to the more limited range of targeted NGS, which typically spans from 0.20% to 20%. (Basu, 2017; Oellerich et al., 2020). In terms of application, if GcfDNA is used as an indicator for long-term monitoring of grafts, NGS is clearly expensive (Watkins and Charames, 2018) and time-consuming (2-3days vs. 1d), although there are 3 commercially available tests (AlloSure Kidney, TRAC Kidney, and Prospera). However, so far, the validation of these methods has been limited, and caution should be exercised when using liquid biopsy results to guide clinical practices (Whitlam et al., 2019).

There are limitations within this meta-analysis, and the results should be interpreted with caution. First, in order to improve the quality of the literature, some data such as conference abstracts, case studies, and other unpublished literature were excluded. All of these inevitably increase publication bias to a certain extent. Second, the overall sample size included in the study was small, limiting the interpretation of the results. Heterogeneity was observed in the pooled sensitivity and specificity of rejection and ABMR analysis, although meta-regression analysis and subgroup analysis were conducted to explore potential sources of heterogeneity before conducting the meta-analysis.

Conclusion

In summary, the collective findings underscore the substantial diagnostic potential of GcfDNA as a biomarker for discriminating between rejection and Antibody-Mediated Rejection (ABMR) in kidney transplant recipients. Notably, the optimal cut-off threshold exhibits a particularly favorable diagnostic performance in the context of ABMR diagnosis. Furthermore, it is worth highlighting that the accuracy of the ddPCR detection method in diagnosing ABMR surpasses that of Next-Generation Sequencing (NGS). However, it is imperative to acknowledge that further extensive and comprehensive studies are warranted to corroborate and build upon these observations.

These results hold significant promise and implications for the field of kidney transplantation, potentially offering improved diagnostic capabilities and guiding more tailored therapeutic interventions. Nevertheless, the ongoing pursuit of robust and validated methodologies remains paramount to harness the full potential of GcfDNA as a diagnostic tool in this context.

Data availability statement

The original contributions presented in the study are included in the article/Supplementary Material, further inquiries can be directed to the corresponding author.

Author contributions

HY: Writing–original draft. DW: Writing–review and editing. XS: Writing–review and editing. HW: Writing–review and

editing. YL: Writing–review and editing. LW: Writing–review and editing.

Funding

The author(s) declare financial support was received for the research, authorship, and/or publication of this article. This work was supported by Sichuan Provincial People's Hospital (2020LZ03), China and University of Electronic Science and Technology of China and Sichuan Provincial People's Hospital (ZYGX2021YGLH210), China and Chengdu Science and Technology Project (2022-YF09-00032-SN).

Acknowledgments

We would like to thank Sichuan Provincial People's Hospital, China and University of Electronic Science and Technology of China and Sichuan Provincial People's Hospital for their assistance with this study.

Conflict of interest

The authors declare that the research was conducted in the absence of any commercial or financial relationships that could be construed as a potential conflict of interest.

Publisher's note

Supplementary material

The Supplementary Material for this article can be found online at: https://www.frontiersin.org/articles/10.3389/fphys.2023.1293402/full#supplementary-material

References

Agbor-Enoh, S. (2019). 2018 ATS BEAR cage winning proposal: cell-free DNA to improve lung transplant outcomes. *Am. J. Respir. Crit. Care Med.* 199, 1058–1060. doi:10.1164/rccm.201902-0458ED

Agbor-Enoh, S., Jackson, A. M., Tunc, I., Berry, G. J., Cochrane, A., Grimm, D., et al. (2018). Late manifestation of alloantibody-associated injury and clinical pulmonary antibody-mediated rejection: evidence from cell-free DNA analysis. *J. Heart Lung Transpl.* 37, 925–932. doi:10.1016/j.healun.2018.01.1305

Basu, A. S. (2017). Digital assays Part I: partitioning statistics and digital PCR. *SLAS Technol.* 22, 369–386. doi:10.1177/2472630317705680

Bloom, R. D., Bromberg, J. S., Poggio, E. D., Bunnapradist, S., Langone, A. J., Sood, P., et al. (2017). Cell-free DNA and active rejection in kidney allografts. *J. Am. Soc. Nephrol.* 28, 2221–2232. doi:10.1681/ASN.2016091034

Bromberg, J. S., Brennan, D. C., Poggio, E., Bunnapradist, S., Langone, A., Sood, P., et al. (2017). Biological variation of donor-derived cell-free DNA in renal transplant recipients: clinical implications. *J. Appl. Lab. Med.* 2, 309–321. doi:10.1373/jalm.2016.022731

Bu, L., Gupta, G., Pai, A., Anand, S., Stites, E., Moinuddin, I., et al. (2022). Clinical outcomes from the assessing donor-derived cell-free DNA monitoring insights of kidney allografts with longitudinal surveillance (ADMIRAL) study. *Kidney Int.* 101, 793–803. doi:10.1016/j.kint.2021.11.034

Cheungpasitporn, W., Kremers, W. K., Lorenz, E., Amer, H., Cosio, F. G., Stegall, M. D., et al. (2018). *De novo* donor-specific antibody following BK nephropathy: the incidence and association with antibody-mediated rejection. *Clin. Transpl.* 32, e13194. doi:10.1111/ctr.13194

Dauber, E. M., Kollmann, D., Kozakowski, N., Rasoul-Rockenschaub, S., Soliman, T., Berlakovich, G. A., et al. (2020). Quantitative PCR of INDELs to measure donor-derived cell-free DNA-a potential method to detect acute rejection in kidney transplantation: a pilot study. *Transpl. Int.* 33 (3), 298–309. doi:10.1111/tri.13554

Di, W., Ran, Q., Yang, H., Lu, J., Hou, Y., Wang, X., et al. (2021). Use of graft-derived cell-free DNA as a novel biomarker to predict allograft function after kidney transplantation. *Int. J. Urol.* 28 (10), 1019–1025. doi:10.1111/iju.14638

Enyedi, M. Z., Jaksa, G., Pintér, L., Sükösd, F., Gyuris, Z., Hajdu, A., et al. (2016). Simultaneous detection of BRCA mutations and large genomic rearrangements in germline DNA and FFPE tumor samples. *Oncotarget* 7, 61845–61859. doi:10.18632/oncotarget.11259

Gielis, E. M., Ledeganck, K. J., Dendooven, A., Meysman, P., Beirnaert, C., Laukens, K., et al. (2020). The use of plasma donor-derived, cell-free DNA to monitor acute rejection after kidney transplantation. *Nephrol. Dial. Transpl.* 35, 714–721. doi:10.1093/ndt/gfz091

Haas, M., Loupy, A., Lefaucheur, C., Roufosse, C., Glotz, D., Seron, D., et al. (2018). The Banff 2017 Kidney Meeting Report: revised diagnostic criteria for chronic active T cell-mediated rejection, antibody-mediated rejection, and prospects for integrative endpoints for next-generation clinical trials. *Am. J. Transpl.* 18, 293–307. doi:10.1111/ajt.14625

Hart, A., Lentine, K. L., Smith, J. M., Miller, J. M., Skeans, M. A., Prentice, M., et al. (2021). OPTN/SRTR 2019 annual data report: kidney. *Am. J. Transpl.* 21 (2), 21–137. doi:10.1111/ajt.16502

Hart, A., Smith, J. M., Skeans, M. A., Gustafson, S. K., Wilk, A. R., Castro, S., et al. (2019). OPTN/SRTR 2017 annual data report: kidney. *Am. J. Transpl.* 19 (2), 19–123. doi:10.1111/ajt.15274

Higgins, J., and Green, S. (2011). "Chapter 8: assessing risk of bias in included studies," in *Cochrane handbook for systematic reviews of interventions version 5.1.0* (United States: Wiley Press).

Higgins, J. P., Thompson, S. G., Deeks, J. J., and Altman, D. G. (2003). Measuring inconsistency in meta-analyses. *BMJ* 327, 557–560. doi:10.1136/bmj.327.7414.557

Huang, E., Sethi, S., Peng, A., Najjar, R., Mirocha, J., Haas, M., et al. (2019). Early clinical experience using donor-derived cell-free DNA to detect rejection in kidney transplant recipients. *Am. J. Transpl.* 19, 1663–1670. doi:10.1111/ajt.15289

Jordan, S. C., Bunnapradist, S., Bromberg, J. S., Langone, A. J., Hiller, D., Yee, J. P., et al. (2018). Donor-derived cell-free DNA identifies antibody-mediated rejection in donor specific antibody positive kidney transplant recipients. *Transpl. Direct* 4 (9), e379. doi:10.1097/TXD.0000000000000821

Lam, N. Y., Rainer, T. H., Chiu, R. W., and Lo, Y. M. D. (2004). EDTA is a better anticoagulant than heparin or citrate for delayed blood processing for plasma DNA analysis. *Clin. Chem.* 50, 256–257. doi:10.1373/clinchem.2003.026013

Leeaphorn, N., Thongprayoon, C., Chon, W. J., Cummings, L. S., Mao, M. A., and Cheungpasitporn, W. (2020). Outcomes of kidney retransplantation after graft loss as a result of BK virus nephropathy in the era of newer immunosuppressant agents. *Am. J. Transpl.* 20, 1334–1340. doi:10.1111/ajt.15723

Lo, Y. M., Tein, M. S., Pang, C. C., Yeung, C. K., Tong, K. L., and Hjelm, N. M. (1998). Presence of donor-specific DNA in plasma of kidney and liver-transplant recipients. *Lancet* 351, 1329–1330. doi:10.1016/s0140-6736(05)79055-3

Mayer, K. A., Omic, H., Weseslindtner, L., Doberer, K., Reindl-Schwaighofer, R., Viard, T., et al. (2022). Levels of donor-derived cell-free DNA and chemokines in BK polyomavirus-associated nephropathy. *Clin. Transpl.* 36, e14785. doi:10.1111/ctr.14785

McDonald, S. P. (2015). Australia and New Zealand dialysis and transplant registry. *Kidney Int. Suppl.* 5, 39–44. doi:10.1038/kisup.2015.8

Medina Diaz, I., Nocon, A., Mehnert, D. H., Fredebohm, J., Diehl, F., and Holtrup, F. (2016). Performance of Streck cfDNA blood collection tubes for liquid biopsy testing. *PLoS One* 11, e0166354. doi:10.1371/journal.pone.0166354

Miller, C. A., Fildes, J. E., Ray, S. G., Doran, H., Yonan, N., Williams, S. G., et al. (2013). Non-invasive approaches for the diagnosis of acute cardiac allograft rejection. *Heart* 99, 445–453. doi:10.1136/heartjnl-2012-302759

Moein, M., Papa, S., Ortiz, N., and Saidi, R. (2023). Protocol biopsy after kidney transplant: clinical application and efficacy to detect allograft rejection. *Cureus* 15, e34505. doi:10.7759/cureus.34505

Nikolaev, S., Lemmens, L., Koessler, T., Blouin, J. L., and Nouspikel, T. (2018). Circulating tumoral DNA: preanalytical validation and quality control in a diagnostic laboratory. *Anal. Biochem.* 542, 34–39. doi:10.1016/j.ab.2017.11.004

Oellerich, M., Christenson, R. H., Beck, J., Schütz, E., Sherwood, K., Price, C. P., et al. (2020). Donor-derived cell-free dna testing in solid organ transplantation: a value proposition. *J. Appl. Lab. Med.* 5, 993–1004. doi:10.1093/jalm/jfaa062

Oellerich, M., Sherwood, K., Keown, P., Schütz, E., Beck, J., Stegbauer, J., et al. (2021). Liquid biopsies: donor-derived cell-free DNA for the detection of kidney allograft injury. *Nat. Rev. Nephrol.* 17, 591–603. doi:10.1038/s41581-021-00428-0

Oellerich, M., Shipkova, M., Asendorf, T., Walson, P. D., Schauerte, V., Mettenmeyer, N., et al. (2019). Absolute quantification of donor-derived cell-free DNA as a marker of rejection and graft injury in kidney transplantation: results from a prospective observational study. *Am. J. Transpl.* 19, 3087–3099. doi:10.1111/ajt.15416

Puliyanda, D. P., Swinford, R., Pizzo, H., Garrison, J., De Golovine, A. M., and Jordan, S. C. (2021). Donor-derived cell-free DNA (dd-cfDNA) for detection of allograft rejection in pediatric kidney transplants. *Pediatr. Transpl.* 25, e13850. doi:10.1111/petr.13850

Redfield, R. R., McCune, K. R., Rao, A., Sadowski, E., Hanson, M., Kolterman, A. J., et al. (2016). Nature, timing, and severity of complications from ultrasound-guided percutaneous renal transplant biopsy. *Transpl. Int.* 29, 167–172. doi:10.1111/tri.12660

Schinstock, C. A., Gandhi, M., Cheungpasitporn, W., Mitema, D., Prieto, M., Dean, P., et al. (2017). Kidney transplant with low levels of DSA or low positive B-flow crossmatch: an underappreciated option for highly sensitized transplant candidates. *Transplantation* 101, 2429–2439. doi:10.1097/TP.0000000000001619

Schütz, E., Fischer, A., Beck, J., Harden, M., Koch, M., Wuensch, T., et al. (2017). Graft-derived cell-free DNA, a noninvasive early rejection and graft damage marker in liver transplantation: a prospective, observational, multicenter cohort study. *PLoS Med.* 14, e1002286. doi:10.1371/journal.pmed.1002286

Schwarz, A., Gwinner, W., Hiss, M., Radermacher, J., Mengel, M., and Haller, H. (2005). Safety and adequacy of renal transplant protocol biopsies. *Am. J. Transpl.* 5, 1992–1996. doi:10.1111/j.1600-6143.2005.00988.x

Sigdel, T. K., Archila, F. A., Constantin, T., Prins, S. A., Liberto, J., Damm, I., et al. (2018). Optimizing detection of kidney transplant injury by assessment of donor-derived cell-free DNA via massively multiplex PCR. *J. Clin. Med.* 8, 19. doi:10.3390/jcm8010019

Stites, E., Kumar, D., Olaitan, O., John Swanson, S., Leca, N., Weir, M., et al. (2020). High levels of dd-cfDNA identify patients with TCMR 1A and borderline allograft rejection at elevated risk of graft injury. *Am. J. Transpl.* 20, 2491–2498. doi:10.1111/ajt.15822

Sun, K., Jiang, P., Chan, K. C., Wong, J., Cheng, Y. K. Y., Liang, R. H. S., et al. (2015). Plasma DNA tissue mapping by genome-wide methylation sequencing for noninvasive prenatal, cancer, and transplantation assessments. *Proc. Natl. Acad. Sci. U. S. A.* 112, E5503–E5512. doi:10.1073/pnas.1508736112

Verhoeven, JGHP, Boer, K., Peeters, A. M. A., Clahsen-van Groningen, M. C., Roodnat, J. I., van de Wetering, J., et al. (2022). A novel high-throughput droplet digital PCR-based indel quantification method for the detection of circulating donor-derived cell-free DNA after kidney transplantation. *Transplantation* 106, 1777–1786. doi:10.1097/TP.0000000000004078

Watkins, N. A., and Charames, G. S. (2018). Implementing next-generation sequencing in clinical practice. *J. Appl. Lab. Med.* 3, 338–341. doi:10.1373/jalm.2017.025791

Whiting, P. F., Rutjes, A. W., Westwood, M. E., Mallett, S., Deeks, J. J., Reitsma, J. B., et al. (2011). QUADAS-2: a revised tool for the quality assessment of diagnostic accuracy studies. *Ann. Intern Med.* 155, 529–536. doi:10.7326/0003-4819-155-8-201110180-00009

Whitlam, J. B., Ling, L., Skene, A., Kanellis, J., Ierino, F. L., Slater, H. R., et al. (2019). Diagnostic application of kidney allograft-derived absolute cell-free DNA levels during transplant dysfunction. *Am. J. Transpl.* 19, 1037–1049. doi:10.1111/ajt.15142

Wijtvliet, VPWM, Plaeke, P., Abrams, S., Hens, N., Gielis, E. M., Hellemans, R., et al. (2020). Donor-derived cell-free DNA as a biomarker for rejection after kidney transplantation: a systematic review and meta-analysis. *Transpl. Int.* 33, 1626–1642. doi:10.1111/tri.13753

Wolfe, R. A., Ashby, V. B., Milford, E. L., Ojo, A. O., Ettenger, R. E., Agodoa, L. Y., et al. (1999). Comparison of mortality in all patients on dialysis, patients on dialysis awaiting transplantation, and recipients of a first cadaveric transplant. *N. Engl. J. Med.* 41, 1725–1730. doi:10.1056/NEJM199912023412303

Zamora, J., Abraira, V., Muriel, A., Khan, K., and Coomarasamy, A. (2006). Meta-DiSc: a software for meta-analysis of test accuracy data. *BMC Med. Res. Methodol.* 6, 31. doi:10.1186/1471-2288-6-31

Zhang, H., Zheng, C., Li, X., Fu, Q., Li, J., Su, Q., et al. (2020). Diagnostic performance of donor-derived plasma cell-free dna fraction for antibody-mediated rejection in post renal transplant recipients: a prospective observational study. *Front. Immunol.* 11, 342. doi:10.3389/fimmu.2020.00342

frontiers | Frontiers in Physiology

TYPE Original Research
PUBLISHED 15 February 2024
DOI 10.3389/fphys.2024.1300667

OPEN ACCESS

EDITED BY
Carolyn Mary Ecelbarger,
Georgetown University, United States

REVIEWED BY
Marcela Sorelli Carneiro-Ramos,
Federal University of ABC, Brazil
Victor Babich,
Mercy College of Health Sciences, United States

*CORRESPONDENCE
Xiaoming Zhou,
xiaoming.zhou@usuhs.edu

RECEIVED 23 September 2023
ACCEPTED 26 January 2024
PUBLISHED 15 February 2024

CITATION
Packialakshmi B, Limerick E, Ackerman HC, Lin X, Nekhai S, Oliver JD III, Stewart IJ, Knepper MA, Fitzhugh C and Zhou X (2024), Proteomic analyses of urinary exosomes identify novel potential biomarkers for early diagnosis of sickle cell nephropathy, a sex-based study.
Front. Physiol. 15:1300667.
doi: 10.3389/fphys.2024.1300667

Proteomic analyses of urinary exosomes identify novel potential biomarkers for early diagnosis of sickle cell nephropathy, a sex-based study

Balamurugan Packialakshmi[1], Emily Limerick[2], Hans C. Ackerman[3], Xionghao Lin[4], Sergei Nekhai[4], James D. Oliver III[1,5], Ian J. Stewart[1], Mark A. Knepper[6], Courtney Fitzhugh[2] and Xiaoming Zhou[1]*

[1]Department of Medicine, Uniformed Services University of Health Sciences, Bethesda, MD, United States, [2]Cellular and Molecular Therapeutic Branch, National Heart Lung and Blood Institute, Bethesda, MD, United States, [3]Physiology Unit, Laboratory of Malaria and Vector Research, National Institute of Allergy and Infectious Diseases, Rockville, MD, United States, [4]Department of Medicine, Howard University, Washington, DC, United States, [5]Nephrology Service, Walter Reed National Military Medical Center, Bethesda, MD, United States, [6]System Biology Center, National Heart Lung and Blood Institute, Bethesda, MD, United States

Sickle cell nephropathy (SCN) is a leading cause of morbidity and mortality in sickle cell disease (SCD). Early intervention is crucial for mitigating its effects. However, current diagnostic methods rely on generic tests and may not detect SCN until irreversible renal damage occurs. Therefore, specific biomarkers for early diagnosis of SCN are needed. Urinary exosomes, membrane-bound vesicles secreted by renal podocytes and epithelial cells, contain both common and cell type-specific membrane and cytosolic proteins, reflecting the physiologic and pathophysiologic states of the kidney. Using proteomics, we analyzed the proteomes of urinary exosomes from humanized SCD mice at 2 months (without albuminuria) and 4 months (with albuminuria) of age. Excretion of 164 proteins were significantly increased and 176 proteins was significantly decreased in the exosomes when mice developed albuminuria. Based on the relevance to SCD, chronic kidney disease and Western blot confirmation in mice, we analyzed protein abundance of heparanase, cathepsin C, α2-macroglobulin and sarcoplasmic endoplasmic Ca^{2+} ATPase-3 (SERCA3) in the urinary exosomes and urine of 18 SCD subjects without albuminuria and 12 subjects with albuminuria using Western blot analyses. Both male and female subjects increased or tended to increase the excretion of these proteins in their urinary exosomes upon developing albuminuria, but female subjects demonstrated stronger correlations between the excretion of these proteins and urine albumin creatinine ratio (UACR) compared to male subjects. In contrast,

Abbreviations: A2M, α2-macroglobulin; CATC, cathepsin C; H & E, hematoxylin-eosin; FITC, fluorescein isothiocyanate; GFR, glomerular filtration rate; eGFR, estimated glomerular filtration rate; HPSE, heparanase; KIM-1, kidney injury molecule-1; LC-MS/MS, liquid chromatography-tandem mass spectrometry; MTC, Masson's trichrome; SCD, sickle cell disease; SCN, sickle cell disease-induced nephropathy; SERCA3, sarcoplasmic endoplasmic Ca^{2+} ATPase-3; SHP-1, SH2-domain-containing protein tyrosine phosphatase-1; THP, Tamm-Horsfall protein; tGFR, transcutaneous glomerular filtration rate; UACR, urine albumin creatinine ratio.

exosomal excretion of Tamm-Horsfall protein, β-actin and SHP-1 was independent of albuminuria. These findings provide a foundation for a time-course study to determine whether increases in the levels of these proteins precede the onset of albuminuria in patients, which will help determine the potential of these proteins as biomarkers for early detection of SCN.

KEYWORDS

heparanase, cathepsin C, α2-macroglobulin, sarcoplasmic endoplasmic Ca^{2+} ATPase-3, albuminuria, sex difference, chronic kidney disease, gender difference

Introduction

Sickle cell disease (SCD) is a hereditary blood disorder characterized by a mutation of glutamic acid to valine in both chains of β-globin. This genetic alteration leads to the pathologic polymerization of hemoglobin, resulting in the deformation of red blood cells. As a consequence, these cells become rigid and encounter difficulty passing through narrow blood vessels. This process leads to various complications in renal tissues, including ischemia, vasoconstriction, infarction, inflammation, and the activation of platelets and coagulation (Becker, 2011; Nath and Hebbel, 2015; Ataga et al., 2022). Approximately 40% of SCD patients develop sickle cell nephropathy (SCN) (Becker, 2011). In these cases, SCD significantly alters kidney structure and disrupts nearly all major renal physiological processes (Becker, 2011; Nath and Hebbel, 2015; Ataga et al., 2022). Moreover, approximately 4%–18% of SCD patients progress to end-stage kidney disease (ESKD), necessitating treatments such as dialysis or kidney transplantation (Becker, 2011). Unfortunately, the average survival rate following the onset of ESKD is only 4 years, and a substantial 40% of SCD patients on dialysis succumb within 20 months (Becker, 2011).

Sickle cell nephropathy is a progressive condition. Patients with SCD develop urinary concentration defects, increased glomerular filtration rate (GFR) and hematuria as early as infancy. With increasing age, some patients may develop micro-albuminuria and then macro-albuminuria, leading to ESKD (Becker, 2011; Nath and Hebbel, 2015; Wang et al., 2019). In the progression of SCN, a sex difference is observed. Both adult and pediatric male patients exhibit a more rapid decline in estimated GFR compared to their female counterparts (Kasztan et al., 2020; Ataga et al., 2023). Early interventions may help prevent or mitigate SCN, as demonstrated by successful early interventions for diabetic nephropathy (Molitch et al., 2004). The current diagnosis of SCN relies on tests, such as serum creatinine levels and urine albumin excretion, which may manifest too late for optimal interventions and management (Voskaridou et al., 2006; Sundaram et al., 2011). To address this problem, researchers have explored novel biomarkers in the blood and urine for early detection of SCN. Some of the potential biomarkers reported include kidney injury molecule-1 (KIM-1), N-acetyl-β-D-glucosaminidase, endothelin-1, TGF-β1, soluble urokinase-type plasminogen activator receptor, urinary macrophage stimulating protein, plasma and urinary orosomucoid, and ceruloplasmin (Voskaridou, Terpos, Michail, Hantzi, Anagnostopoulos, Margeli, Simirloglou, Loukopoulos and Papassotiriou, 2006; Mohtat et al., 2011; Sundaram, Bennett, Wilhelm, Kim, Atweh, Devarajan and Malik, 2011; Jerebtsova et al., 2018; Jerebtsova et al., 2020; Nekhai et al., 2021; Afangbedji et al., 2022). However, questions remain regarding the specificity and reproducibility of some of these biomarkers (Mohtat, Thomas, Du, Boakye, Moulton, Driscoll and Woroniecki, 2011; Sundaram, Bennett, Wilhelm, Kim, Atweh, Devarajan and Malik, 2011; Hamideh et al., 2014). Some of these biomarker candidates are non-specific and may increase in urine or serum as a result of damage in other organs without known renal injury (Tsai et al., 1997; Finazzi et al., 2001; Holzscheiter et al., 2014; Wasung et al., 2015). Additionally, whether sex differences affect these biomarkers remains largely unknown.

Urinary exosomes are membrane-bound vesicles secreted by renal podocytes and epithelial cells facing the urine and urinary drainage system. They contain both common and cell type-specific membrane and cytosolic proteins, providing valuable insights into the physiological and pathophysiological states of the kidney (van Balkom et al., 2011). Urinary exosomes have shown promise as a source of specific biomarkers for renal diseases (Hoorn et al., 2005). Therefore, our hypothesis was that unique protein fingerprints in urinary exosomes could predict the risk of SCN and potentially serve as biomarkers for early SCN diagnosis. To test this hypothesis, we initially compared the proteomes of urinary exosomes from the same humanized SCD mice (Townes model) when they had no albuminuria with when they developed albuminuria. We identified differentially increased proteins. Subsequently, we examined whether some of these findings could be reproduced in SCD patients, using Western blot analyses. Because sex plays a critical role in SCN, we analyzed the data separately based on sex. Our results show that when albuminuria developed, both men and women showed an increase or a tendency to increase in the release of heparanase, cathepsin C, α2-macroglobulin, and sarcoplasmic endoplasmic Ca2+ ATPase-3 (SERCA3) in their urinary exosomes. However, in women, there was a stronger correlation between the release of these proteins and the urine albumin creatinine ratio (UACR) compared to men. This data forms the basis for future studies, which will investigate if the elevation of these protein levels occurs before the onset of albuminuria.

Materials and methods

Animals

All animal procedures were approved by the Institutional Animal Care and Use Committee of the Uniformed Services University of the Health Sciences (Protocol # MED-16-978). Townes SCD mice and their heterozygous (non-SCD) controls (JAX Stock: 013071) as well as

C57BL/6 mice were purchased from The Jackson Laboratory and housed in the university vivarium on a 12:12 light:dark cycle with *ad libitum* access to regular food and water. To avoid sex bias, both male and female mice were used. Urine was collected from mice housed in metabolic cages using methods previously described (Zhou et al., 2014), and each collection vial contained a quarter of a Roche protease inhibitor cocktail tablet to prevent protein degradation. Urine samples were centrifuged at 2,000 g for 10 min at 4°C to remove debris and stored at −80°C until further analysis.

Glomerular filtration rate and urine albumin measurements

Mouse transcutaneous glomerular filtration rate (tGFR) was measured as previously described (Packialakshmi et al., 2022). Briefly, a transdermal NIC-Kidney unit with internal memory (Mannheim Pharma and Diagnostics GmbH) was mounted on the back of a mouse. Fluorescein isothiocyanate (FITC)-sinistrin (15 mg/100 g BW; dissolved in saline at 35 mg/mL, Mannheim Pharma and Diagnostics GmbH) was injected via the intraocular route 2 min after the mounting. The mouse was placed in a single cage for an hour for recording and the data was analyzed with the MPD 1.0 software (Scarfe et al., 2018). The $t^{1/2}$ value was used to calculate the tGFR. Mouse urine albumin levels were measured using the Mouse Albumin Assay Max ELISA kit (catalog # EMA3201-1 from AssayPro) according to the manufacturer's protocol.

Histology

The renal structure of humanized SCD mice was analyzed with Hematoxylin-eosin (H & E) and Masson's trichrome (MTC) staining.

Mouse urine exosomes isolation and digestion

The exosomes were extracted from the urine of 5 SCD mice (2 males and 3 females) when they were 2 and 4 months old respectively. The urine (~4 mL pooled from consecutive collections) from each mouse was thawed, mixed and followed by centrifugation at 1,000 g for 10 min at 4°C and the supernatant was again centrifuged at 17,000 g for 15 min at 4°C. The supernatant was then subjected to ultracentrifugation at 200,000 g for 60 min at 4°C to precipitate pellets. The pellets containing exosomes were treated with freshly prepared 200 mg/mL dithriothretol (DTT) in an isolation buffer (10 mM triethanolamine and 250 mM sucrose, pH 7.6 with the Roche protease inhibitor tablets) and heated for 2 min at 95°C to break down Tamm-Horsfall protein also known as uromodulin. The solution was centrifuged at 200,000 g for 60 min at 4°C. The pellets were dissolved again in the isolation buffer and centrifuged at 200,000 g for 60 min at 4°C to remove DTT (Zhou et al., 2006b). The final pellets were dissolved in ~400 µL of the isolation buffer. The exosomes were examined under an electron microscope. The protein contents of the exosomes were measured at A280 nm with a NanoDrop (ThermoFisher). The exosome samples (400 µg) were dried under speed vacuum with a DNA110 Speed Vac under no heating (Forma Scientific) and then dissolved in 6 M urea buffer (6 M urea and 50 mM Tris-HCl, pH 8.0). The samples were treated with 10 mM DTT for 60 min at 60°C and alkylated with 40 mM freshly prepared iodoacetamide (IAA). Excess IAA was neutralized with 10 mM DTT, and the samples were digested with 40 ng/µL trypsin (Pierce) at 37°C for 48 h. The digested peptides were dried and purified with C18 spin columns (Pierce) (Figure 1A).

Electron microscopy

5–10 µL of sample were applied to a standard 3 mm formvar-carbon coated grid (Electron Microscopy Sciences, Hatfield, PA) for 5 min and the excess was wicked off with a piece of filter paper. The grid was then washed very briefly on 3 drops of water to remove buffer salts. Following this, 5 µL of 2% aqueous uranyl acetate was applied to the grid for 1 min before the excess was again wicked off. The grid was then allowed to air dry for several minutes before examination in a JEOL JEM-1011 TEM (JEOL United States Inc., Peabody, MA). Images were captured using an AMT XR50S-A digital camera (Advanced Microscopy Techniques, Woburn, MA).

Liquid chromatography-tandem mass spectrometry (LC-MS/MS) and bioinformatics

The purified peptides were dried and dissolved in 50 µL of 0.1% formic acid. Aliquots of 10 µL tryptic peptides were loaded to a LC-20AD Nano HPLC system (Shimadzu Corporation, Columbia, MD, United States) coupled to LTQ XL Orbitrap mass spectrometer (Thermo Fisher Scientific) with the installed Xcalibur software (version 2.0.7, Thermo Fisher Scientific). Liquid chromatography was carried out on an in-house made Nano-HPLC column (Polymicro Technologies Inc., Phoenix, AZ, United States) packed with reverse phase PolySulfoethyl A, 5 µM, 200 Å (PolyLC Inc., Columbia, MD, United States). Full-scan mass spectra were acquired in the Orbitrap over 300–2,000 m/z with a resolution of 30,000. Three most intense ions were selected for fragmentation using collision-induced dissociation (CID). Samples from each mouse were run in triplicate. Protein identifications were carried out using Proteome Discoverer 2.3 software in combination with the SEQUEST protein database search engine. A sequential database search was performed using the Uniprot mouse database (1/23/2019, 4195 sequences) at a false discovery cut off ≤1%. Label-free quantitation was performed and the results were exported as *.xls files for analysis. Label-free quantitation was performed. The list of differentially expressed proteins were shortlisted based on p-value <0.05, unique peptide ≥1, reproducibility (must be present in all the 10 samples and their 3 replicates) and identified with medium or high confidence. The protein results were analyzed by DAVID GO for their known functions (Huang et al., 2009) (Figure 1B). A Venn Diagram was created using a free on-line program (https://venngage.com) (Figure 3B). A Vocano plot was generated with R program (https://www.r-project.org). Log2 was used as a predetermined threshold for the fold change (FC) (Figure 3C).

10.3389/fphys.2024.1300667

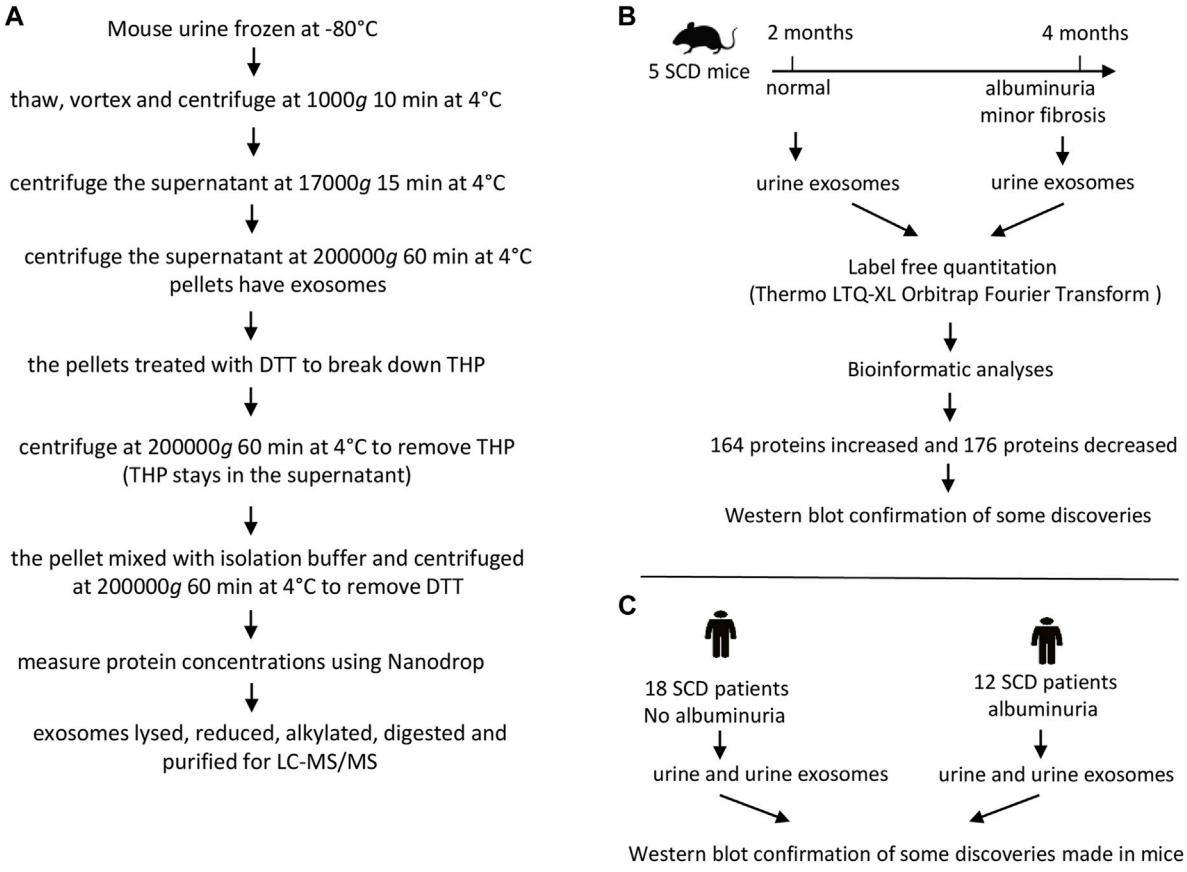

FIGURE 1
The flow charts of experimental protocol and designs. **(A)** Protocol for preparing mouse urinary exosomes for liquid chromatography-tandem mass spectrometry (LC-MS/MS). **(B)** Design for proteomic analyses of mouse urinary exosomes. **(C)** Design for Western blot analyses of human urine and urinary exosomes.

TABLE 1 Subjects' profiles.

	SCD subjects with no albuminuria	SCD subjects with albuminuria
Sample size	18	12
Male: Female	10:8	5:7
Median age (range)	32.5 (18–45)	30 (24–55)
Race	Black or African American	Black or African American (1 unknown)
Ethnicity	Not Latino or Hispanic (1 unknown)	Not Latino or Hispanic (1 unknown)
Mean Urinary Albumin Creatinine Ratio (mg/g)	7.0 ± 2.1	389.5 ± 169.2*
Mean eGFR CKD-EPI Creatinine Equation (2021) (ml/min/1.73 m2)	125.4 ± 3.2	107.4 ± 7.2*

*$p < 0.05$, unpaired t-test.

Participant enrollment and urine collection

All procedures were approved by the Institutional Review Board of National Heart Lung and Blood Institute (Clinical Trials identifier: NCT03958643). Adults with sickle cell anemia (HbSS or HbSβ^0-thalassemia) were eligible to participate. Participants were recruited from 24 May 2019 to 1 May 2021. All participants provided written informed consent. Study procedures were performed at subject's clinical baseline. Participants on stable hydroxyurea, antihypertensive medication, and/or chronic transfusion therapy were allowed to enroll. The estimated glomerular filtration rate (eGFR) was calculated based on serum cystatin C and creatinine (2021 equation). Both cystatin C and creatinine were measured in a clinical lab with cystatin C measured in a Cobas C (Roche) and creatinine measured in an Architect 39 (Abbott). Patients eGFR <60 mL/min/1.73 m^2, HIV, hepatitis B or

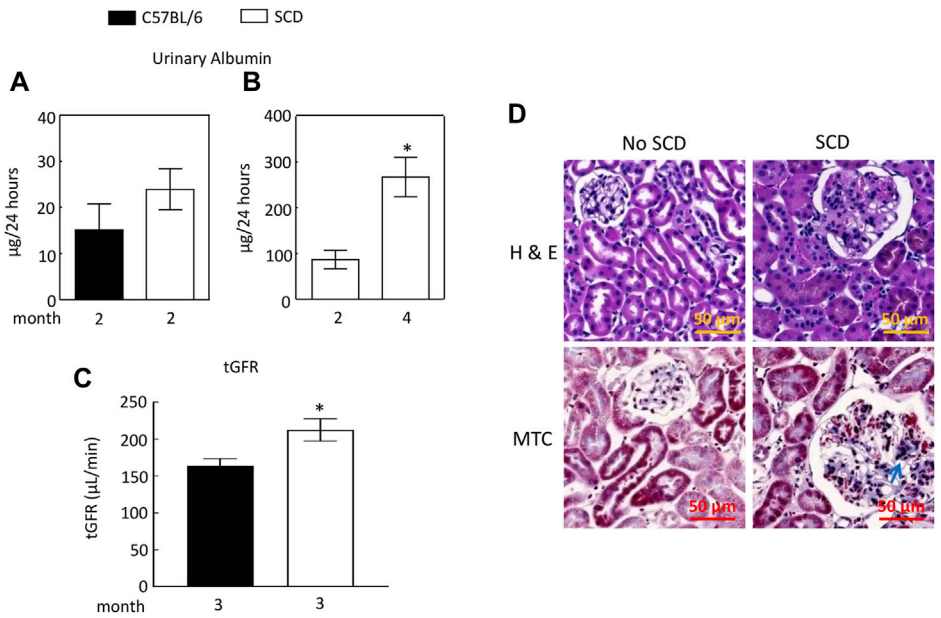

FIGURE 2
Sickle cell disease (SCD) mice have albuminuria when they reach 4 months old. **(A)** At 2 months old, there was no significant difference in urinary albumin excretion between SCD and C57BL/6 mice (n = 3, 2 males and 1 female in each strain). **(B)** By the age of 4 months, SCD mice exhibited a more than threefold increase in urinary albumin excretion compared to their levels at 2 months old (*p < 0.05, n = 5, 2 males and 3 females). It is worth noting that the disparities in urinary albumin levels observed between **(A,B)** for 2-month-old SCD mice are likely attributable to variations in measurement times and the use of different sets of SCD mice for each measurement. Urinary albumin levels were quantified using an ELISA kit (EMA3201, AssayPro). **(C)** SCD mice showed significantly elevated transcutaneous glomerular filtration rate (tGFR) compared to C57BL/6 mice (*p < 0.05, t-test, n = 5, 2 males and 3 females). The tGFR was determined by measuring the disappearance of fluorescein isothiocyanate (FITC)-sinistrin from the mouse body. **(D)** At 4 months old, SCD mice displayed enlarged glomeruli and minor fibrosis (indicated by arrows) compared to non-SCD mice (heterozygotes), as shown in representatives from three independent experiments. H & E, hematoxylin-eosin staining; MTC, Masson's trichrome staining.

C, chronic inflammatory condition, acute illness, uncontrolled hypertension, and pain crisis within 4 weeks were excluded. Subjects with nephropathy were identified by albuminuria (≥30 mg/g). Among these subjects, two had an eGFR ranging from 60 to 70 mL/min/1.73 m^2, while the remaining subjects had an eGFR greater than 90 mL/min/1.73 m^2. The second and third morning urine samples were collected from outpatient clinic patients who were then divided into those with (≥30 mg/g) and without (<30 mg/g) albuminuria (Table 1). A Roche protease inhibitor cocktail tablet was added to the urine collection container to prevent protein degradation. A total of 31 subjects were recruited, but the urine sample from one subject was not used due to technical reasons. Therefore, 18 participants without albuminuria and 12 subjects with albuminuria were included in the study (Table 1).

Participants' urine exosomes isolation for Western blot analyses

The urine (~25 mL) from each subject was thawed, mixed, and centrifuged at 1,000 g for 10 min at 4°C. The supernatant was again centrifuged at 17,000 g for 15 min at 4°C. The supernatant was then subjected to ultracentrifugation at 200,000 g for 60 min at 4°C to precipitate exosomes. The exosomes were dissolved in PBS buffer with protease inhibitor tablets and examined under an electron microscope. The protein concentrations of exosomes were estimated using the BCA method and dissolved in 4X SDS loading buffer (Figure 1C). Urine samples were directly used without any extraction. The protein concentrations in the urine were estimated using the BCA method and then dissolved in 4X SDS loading buffer as well (Figure 1C).

Western blot analysis

Equivalent amount of protein samples in the SDS loading buffer (mouse exosomes = 12 μg/lane, human urine exosomes = 20 μg/lane, human urine = 50 μg/lane) were fractionated in a 4%–12% Bis-Tris gel (ThermoFisher). Proteins in the gel were transferred to a nitrocellulose membrane and the membrane was submerged in the Odyessy blocking buffer (Li-Cor) or 5% non-fat milk in PBS for 60 min at room temperature. The membrane was probed with a primary antibody against heparanase (1:1000 dilution, Proteintech 24529-1-AP), cathepsin c (1:1000 dilution, ThermoFisher PA5-37849), α2-macroglobulin (1:1000 dilution, Proteintech 66126-1-Ig), SERCA3 (1:500 dilution, Proteintech 13619-1-AP), integrin αV (1:500 dilution, Proteintech 27096-1-1AP), podocalyxin (1:500 dilution, Proteintech 18150-1-AP), HSP27 (1:1000 dilution, Cell Signaling 2402), β-actin (1:1000 dilution Cell Signaling 3700), SHP-1 (1:500 dilution, SC-287) or Tamm-Horsfall protein (1:2500 dilution, SC-271022) at 4°C overnight. The membrane was then washed briefly and probed with a corresponding Alexa fluorophore conjugated secondary antibody at room temperature

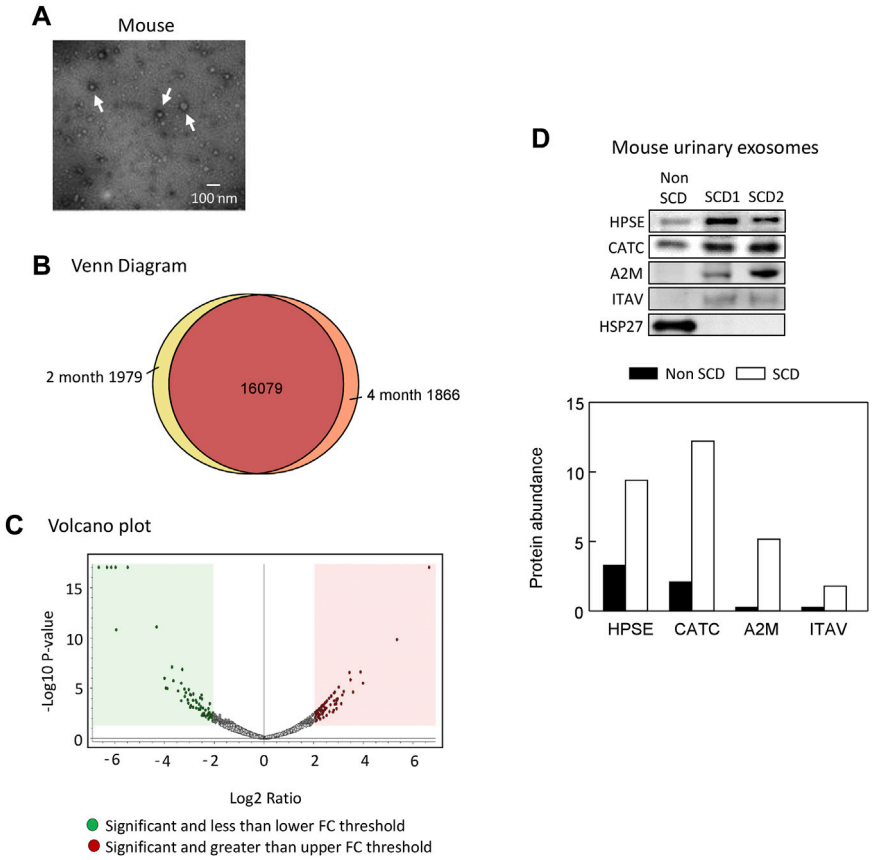

FIGURE 3
Proteomic analyses of mouse urinary exosomes. **(A)** Confirmation of urinary exosome morphology by electron microscopy. Urinary exosomes were extracted through differential centrifugation and verified using an electron microscope (JEOL JEM-1011 TEM, JEOL United States Inc., Peabody, MA). The image represents one of three independent experiments. **(B)** Venn Diagram analysis revealed that mice at 4 months old shared 16,079 peptides in their urinary exosomes with mice at 2 months old, while having 1,866 unique peptides. Conversely, mice at 2 months old also possessed 1,979 unique peptides. **(C)** A Volcano plot of 164 proteins increased and 176 protein decreased when SCD mice reached 4 month old compared with 2 month old. FC, fold change. **(D)**. Western blot analysis of protein abundance of heparanase (HPSE), cathepsin C (CATC), α2-macroglobulin (A2M), integrin αV (ITAV) and heat shock protein 27 (HSP27) in the urinary exosomes of non SCD (heterozygote) and SCD mice.

TABLE 2 Proteins shortlisted for further evaluation.

Proteins reported in the literature	Disease	References	Proteins identified in our proteomic analyses
Integrin α4β1	SCD	Lee et al. (2001)	Integrin αV
α2- macroglobulin	SCD	Makis et al. (2000)	α2-macroglobulin
iNOS	Sepsis-induced AKI	Heemskerk et al. (2006)	iNOS
Xanthine oxidase	Urinary tract infection	Ciragil et al. (2014)	Xanthine oxidase
Heparanase	Proteinuria in renal transplant patients	Shafat et al. (2012)	Heparanase
Cathepsins	SCD	Selma et al. (2022)	Cathepsin c
Collectin-12	Diabetic nephropathy	Caseiro et al. (2014)	Collectin-12
SERCA	Ischemia/reperfusion-induced heart injury	Tan et al. (2020)	SERCA3
Myosin-3	Radiation-induced nephropathy	Sharma et al. (2008)	Myosin-3

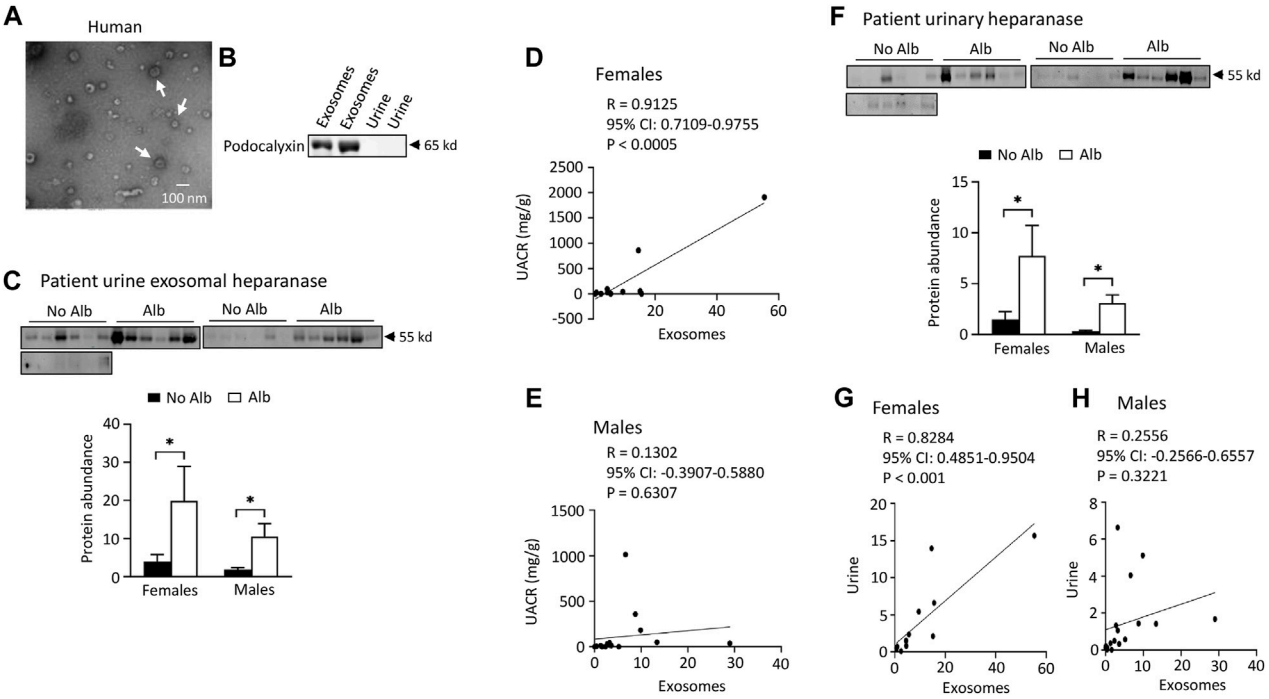

FIGURE 4
Elevated excretion levels of heparanase protein in urinary exosomes and urine are positively associated with albuminuria (Alb) in both male and female SCD subjects. However, only female subjects demonstrate stronger correlations between the excretion of urine exosomal heparanase and urine albumin creatinine ratio (UACR) and in excretion of heparanase between urinary exosomes and urine compared to male subjects. **(A)** Conformation of extraction of urinary exosomes by electron microscopy, a representative of three independent experiments. Urinary exosomes extraction and electron microscopic analysis were performed as described in Figure 3A. **(B)** Conformation of extraction of urinary exosomes by Western blot analysis. Each lane was loaded with 30 µg proteins. **(C)** Both male and female SCD subjects increased excretion of heparanase in their urine exosomes upon developing albuminuria as determined by Western blot analyses (Males: n = 10 for No Alb, n = 7 for Alb, Females: n = 8 for No Alb, n = 5 for Alb). **(D,E)** Increased excretion of heparanase in the urinary exosomes correlated with UACR only in female subjects, but not in male subjects (Pearson test, Males: n = 9 for No Alb, n = 7 for Alb, Females: n = 7 for No Alb, n = 5 for Alb). **(F)** Western blot analyses indicate that both male and female SCD subjects increased excretion of heparanase protein in their urine upon developing albuminuria (Males: n = 10 for No Alb, n = 7 for Alb, Females: n = 8 for No Alb, n = 5 for Alb). **(G,H)** Only female subjects demonstrated a good correlation in excretion of heparinase protein between urinary exosomes and urine (Pearson test, Males: n = 9 for No Alb, n = 7 for Alb, Females: n = 7 for No Alb, n = 5 for Alb). (*p < 0.05, two-tailed t-test).

for an hour. An infrared imaging scanner (Li-Cor) was used to images and analyze protein abundance.

Statistics

All data were presented as mean ± standard error (SE). Band intensity data were analyzed using an unpaired two-tailed t-test with statistical significance set at $p < 0.05$. Correlation analyses were performed using Pearson's correlation test with GraphPad Prism 10.1.2.

Results

SCD mice increase urinary excretion of albumin at 4 months old with only minor fibrosis in the renal cortex

We found that urinary excretion of albumin in SCD mice (2 males and 1 females) at 2 months old and was not significantly different from that of C57BL/6 mice (2 males and 1 females) (Figure 2A). We then used a different cohort of SCD mice (2 males and 3 females) and collected urine from each SCD mouse at this age, whose urinary excretion of albumin served as the baseline. We monitored the SCD mice urinary excretion of albumin every two to 3 weeks and found that SCD mice urinary albumin excretion rate was more than tripled when mice reached 4 months age (87 ± 20 vs. 267 ± 43 µg/24, Figure 2B). The SCD mice had a significantly higher tGFR than C57BL/6 mice (212 ± 15 vs. 164 ± 10 µL/min, Figure 2C). Histology analyses revealed that SCD mice had enlarged glomeruli compared with heterozygotes (non-SCD), a typical feature observed in both SCD mice and patients, but only had minor fibrosis when they reached 4 months old (Figure 2D).

Proteomic analyses of the mouse urinary exosomes

We extracted exosomes from 2 to 4 month old SCD mouse urine samples and confirmed their presence by electron microscopy (Figure 3A). We identified 19,924 peptides corresponding to 9,497 proteins, of which 1,979 peptides were specific to 2-month-old

10.3389/fphys.2024.1300667

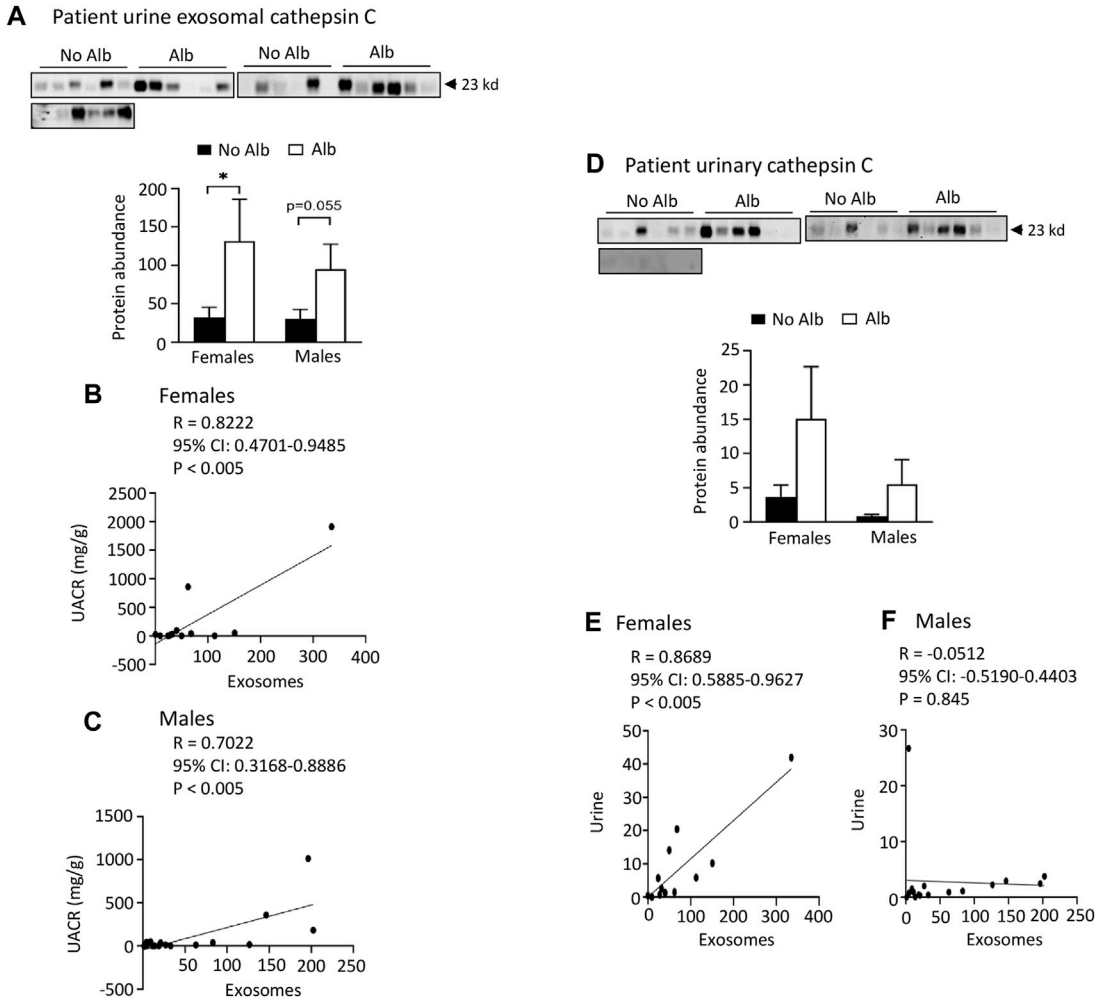

FIGURE 5
Elevated levels of cathepsin C protein excretion in both urinary exosomes and urine demonstrate a positive association with albuminuria (Alb) in male and female SCD subjects. Importantly, the correlations between urine exosomal cathepsin C excretion and the urine albumin creatinine ratio (UACR), as well as cathepsin C excretion between urinary exosomes and urine, are particularly pronounced in female subjects compared to their male counterparts. **(A)** Western blot analyses of cathepsin C in the urinary exosomes (Males: n = 10 for No Alb, n = 7 for Alb, Females: n = 8 for No Alb, n = 5 for Alb). **(B,C)** The elevated excretion of cathepsin C in urinary exosomes exhibited a stronger correlation with urine UACR in female subjects compared to male subjects (Pearson test, Males: n = 9 for No Alb, n = 7 for Alb, Females: n = 7 for No Alb, n = 5 for Alb). **(D)** Both male and female subjects with albuminuria tended to increase urinary excretion of cathepsin C as shown by Western blot analyses (Males: n = 10 for No Alb, n = 7 for Alb, Females: n = 8 for No Alb, n = 5 for Alb). **(E,F)** Increased excretion of cathepsin C in the urinary exosomes correlated with its excretion in urine in female subjects, but not in male subjects (Pearson test, Males: n = 9 for No Alb, n = 7 for Alb, Females: n = 7 for No Alb, n = 5 for Alb). (*p < 0.05, two-tailed t-test).

samples and 1,866 peptides were specific to 4-month-old samples, as shown by Venn diagram analysis (Figure 3B). The complete data was deposited into jPOST repository at the address https://repository.jpostdb.org/ with accession number PXD043401 and project number JPST002221. Label-free quantitation based on unique peptides ≥1 found in all 5 samples and 3 replicates in both groups revealed that 340 proteins were differentially secreted in the exosomes (164 increased and 176 decreased, p < 0.05, Figure 3C; Supplementary Table S1).

Short-listed 9 proteins for further analyses

We focused on the 164 significantly increased proteins, as they are easier to monitor experimentally and potentially clinically than the decreased proteins. Based on the relevance to SCD pathophysiology, kidney injury and chronic kidney disease, we shortlisted 9 proteins for further evaluation (Table 2). Western blot analysis showed that excretion of heparanase, cathepsin C, α2-macroglobulin, and integrin αV was increased in SCD mice when they were 4 months old compared with a non-SCD mouse at the same age, while HSP27 was not detectable in their urine exosomes (Figure 3D). We could not identify a reliable signal with antibodies we have against other 5 proteins.

Both male and female subjects increase or have a tendency to increase the excretion of heparanase, cathepsin C, α2-macroglobulin, and SERCA3 in their urinary exosomes upon developing albuminuria, but female subjects demonstrate stronger correlations between the excretion of these proteins and urine albumin creatinine ratio (UACR) compared to male subjects. Our ultimate objective is to identify a biomarker capable of diagnosing sickle nephropathy before the onset of albuminuria. To explore potential candidates,

10.3389/fphys.2024.1300667

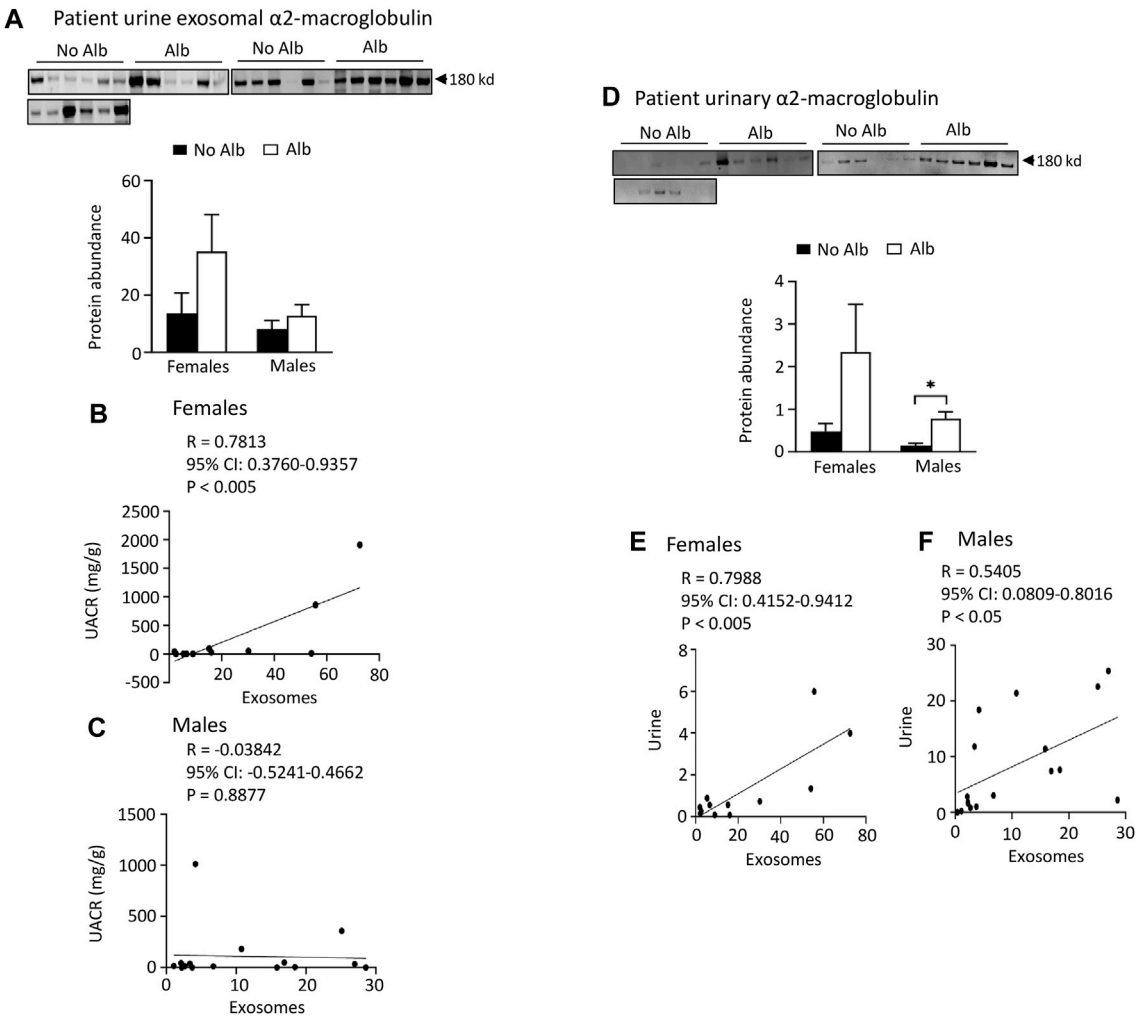

FIGURE 6
Excretion of α2-macroglobulin protein in both urinary exosomes and urine is increased in parallel with albuminuria (Alb) in male and female SCD subjects. However, female subjects exhibit better correlations between urine exosomal α2-macroglobulin excretion and the urine albumin creatinine ratio (UACR), as well as in α2-macroglobulin excretion between urinary exosomes and urine, compared to their male counterparts. **(A)** Western blot analyses of α2-macroglobulin protein in the urinary exosomes (Males: n = 10 for No Alb, n = 7 for Alb, Females: n = 8 for No Alb, n = 5 for Alb). **(B,C)** Only female subjects, but not male subjects, displayed a correlation in excretion of α2-macroglobulin in the urinary exosomes with UACR (Pearson test, Males: n = 9 for No Alb, n = 7 for Alb, Females: n = 7 for No Alb, n = 5 for Alb). **(D)** Western blot analyses of α2-macroglobulin protein in both male and female subjects' urine (Males: n = 10 for No Alb, n = 7 for Alb, Females: n = 8 for No Alb, n = 5 for Alb). **(E,F)** Increased excretion of α2-macroglobulin protein in the urinary exosomes correlated better with its excretion in urine in female subjects than in male subjects (Pearson test, Males: n = 9 for No Alb, n = 7 for Alb, Females: n = 7 for No Alb, n = 5 for Alb). (*p < 0.05, two-tailed t-test).

we investigated whether our findings from mouse urine exosomes could be replicated in the urinary exosomes of patients. Successful validation in humans would allow us to design a time-course study to assess whether these protein levels increase before the onset of albuminuria in patients. Therefore, we analyzed 18 subjects without albuminuria and 8 subjects with microalbuminuria and 4 participants with macroalbuminuria (Table 1). Among the participants, 54% were male and 97% were Black or African American (Table 1). We confirmed the isolation of exosomes with electron microscopy (Figure 4A) and Western blot analysis with an antibody against podocalyxin, a biomarker of exosomes (Figure 4B). Both male and female SCD subjects with albuminuria exhibited an increase in or a tendency to increase excretion of heparanase, cathepsin C, α2-macroglobulin, and SERCA3 in their urinary exosomes compared with subjects without albuminuria (Figures 4C-H to Figure 7). However, female subjects had better correlations of protein excretion with UACR than male subjects with Pearson correlation coefficient value 0.9125, 0.8222, 0.7813 and 0.9791, respectively. In contrast, the Pearson correlation coefficient value for males were 0.1302, 0.7022, −0.03842 and 0.0691, respectively (Figures 4C-H to Figure 7). Neither female nor male subjects showed a correlation between excretion of these proteins in the exosomes and eGFR CKD-EPI Creatinine Equation (2021) (Data not shown). We were unable to obtain a reliable signal using the antibody we have against human integrin αV.

Both male and female SCD subjects with albuminuria exhibit significantly increased or tend to excrete higher levels of heparanase, cathepsin C, and α2-macroglobulin in their urine compared to those without albuminuria, but only female subjects demonstrated superior correlations between the excretion of these proteins in urinary

10.3389/fphys.2024.1300667

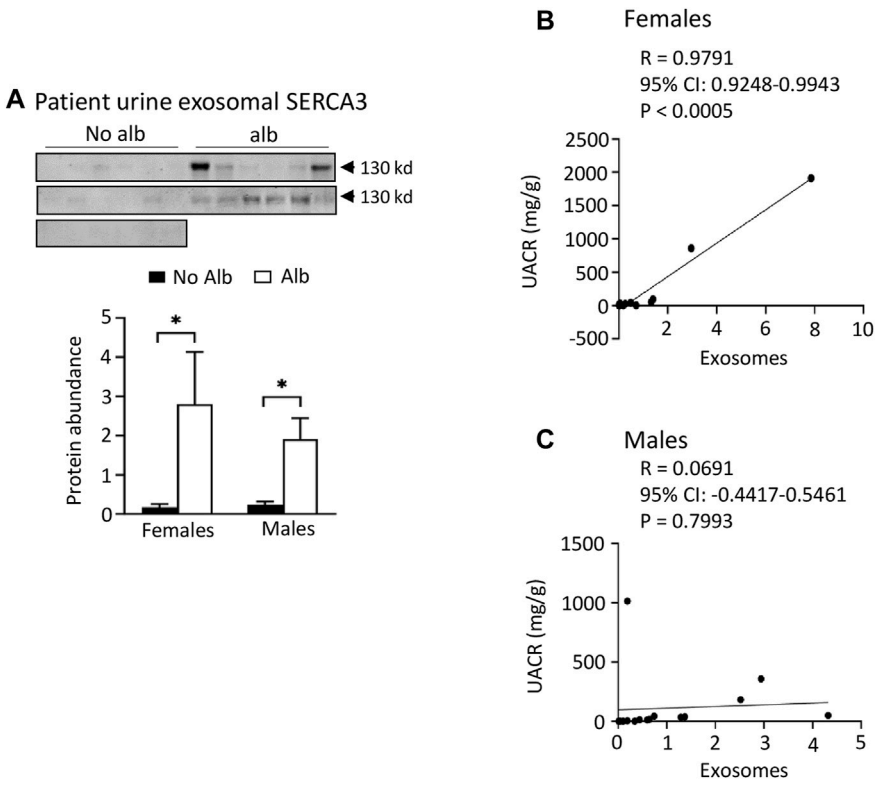

FIGURE 7
Both male and female SCD subjects with albuminuria increases excretion of SERCA3 protein in the urinary exosomes. However, only female subjects show a correlation of urine exosomal excretion of SERCA3 protein with the urine albumin creatinine ratio (UACR), whereas male subjects do not. **(A)** Western blot analyses of SERCA3 in the urinary exosomes (Males: n = 10 for No Alb, n = 7 for Alb, Females: n = 8 for No Alb, n = 5 for Alb). **(B,C)** A strong correlation between the urine exosomal excretion of SERCA3 protein and UACR was observed only in female subjects, with no such correlation found in male subjects (Pearson test, Males: n = 9 for No Alb, n = 7 for Alb, Females: n = 7 for No Alb, n = 5 for Alb). (*p < 0.05, two-tailed t-test).

exosomes and urine, in contrast to male subjects. To expedite detection, we explored whether heparanase, cathepsin C, α2-macroglobulin, and SERCA3 could be directly identified in participants' urine using Western blot analysis. In the presence of albuminuria, both male and female SCD subjects excreted significantly higher levels or exhibited a tendency to excrete more heparanase, cathepsin C, and α2-macroglobulin in their urine compared to subjects without albuminuria (Figures 4C-H to Figure 6). However, only female subjects exhibited a robust correlation of protein excretion in urine with urinary exosomes, with Pearson correlation coefficient values of 0.8284, 0.8689, and 0.7988, respectively, while the corresponding values for males were only 0.2556, −0.0512, and 0.5405 (Figures 4C-H to Figure 6). Unfortunately, the urine SERCA3 signal was too low to be considered reliable.

Neither male nor female subjects significantly increased the excretion of Tamm-Horsfall protein (THP), β-actin, or SH2-domain-containing protein tyrosine phosphatase-1 (SHP-1) in their urinary exosomes upon developing albuminuria. To examine whether the increased excretion of heparanase, cathepsin C, α2-macroglobulin and SERCA3 in SCD subjects' urinary exosomes specifically correlated with albuminuria, we examined the excretion of THP in urine exosomes and urine. The excretion of THP in both urinary exosomes and urine was unaffected by albuminuria in male or female subjects, and there was no correlation between their excretion levels in urinary exosomes and UACR with the Pearson correlation coefficient value only −0.2504 and −0.2278, respectively (Figure 8). There was a weak correlation in excretion of THP protein between urinary exosomes and urine in female subjects only, but not in male subjects with the Pearson correlation coefficient value 0.5654 and −0.0483, respectively (Figure 8). THP is almost exclusively produced by the epithelial cells lining the thick ascending limb of the loop of Henle and early distal tubules, and it does not represent the glomeruli or other segments of the nephron (Micanovic et al., 2020). Therefore, we examined the excretion of β-actin, a universally expressed protein, and SHP-1, which is expressed in the kidney cortex, outer and inner medullas (Wang et al., 2015), in the exosomes. The excretion of these two proteins in the exosomes is independent of albuminuria as well in male or female subjects (Figure 8). These findings indicate that the increased excretion of heparanase, cathepsin C, α2-macroglobulin and SERCA3 in SCD subjects' urinary exosomes specifically correlated with albuminuria.

Discussion

Exosomes are small extracellular vesicles, typically ranging from 30 to 150 nm in diameter, known for their role in intercellular communication. Urinary exosomes, originating primarily from renal epithelial cells and podocytes, provide a rich source of cellular information, emerging as promising candidates for

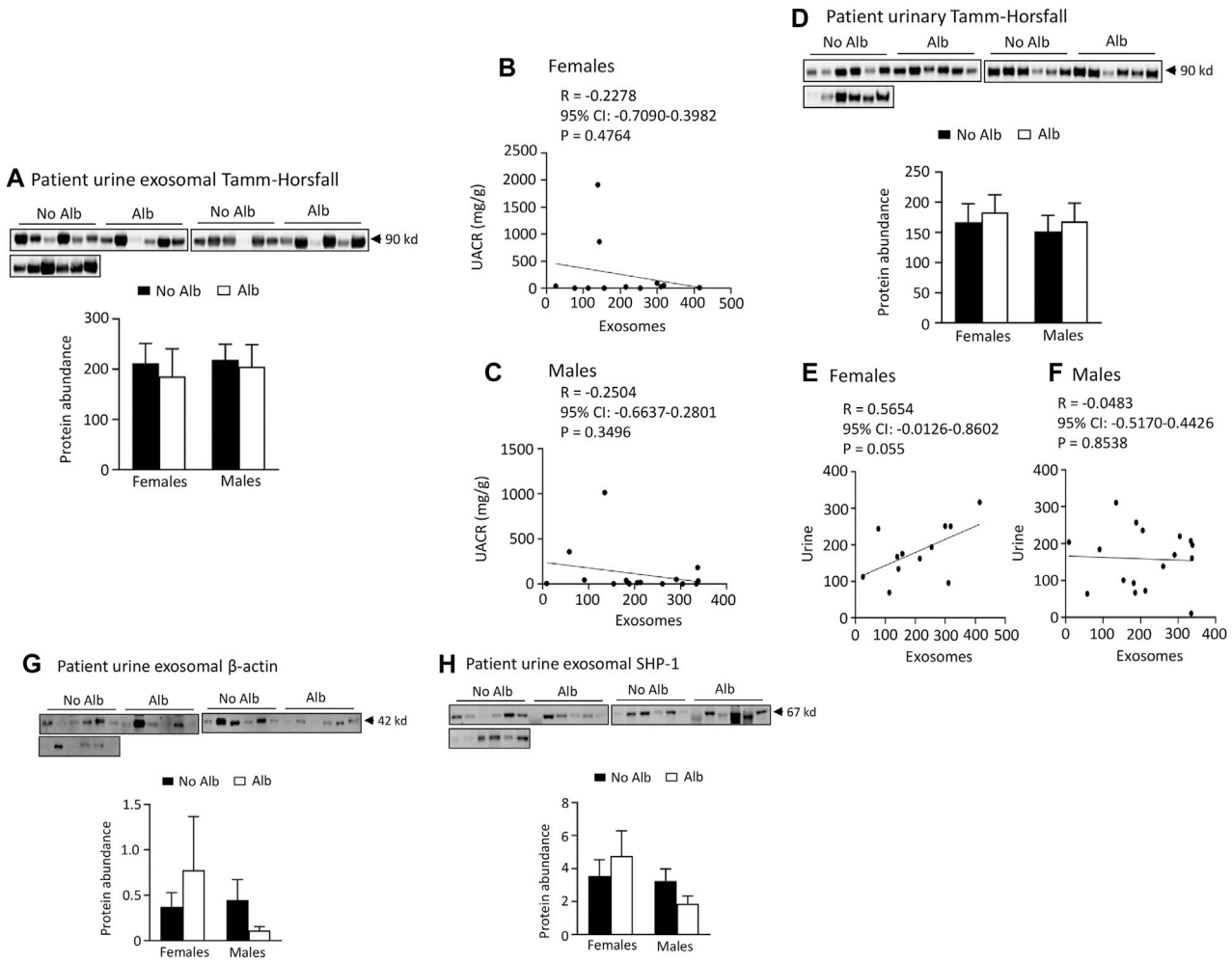

FIGURE 8
There is no association of excretion of Tamm-Horsfall protein (THP), β-actin, or SHP-1 protein in urinary exosomes with albuminuria in either male or female subjects. There is no association between excretion of THP and urine albumin creatinine ratio (UACR) in either male or female subjects. Only female subjects display a weak correlation in excretion of THP between urinary exosomes and urine. **(A)** Western blot analyses of THP in urinary exosomes (Males: n = 10 for No Alb, n = 7 for Alb, Females: n = 8 for No Alb, n = 5 for Alb). **(B,C)** No correlation was observed between the excretion of THP in urinary exosomes and UACR in either sex (Pearson test, Males: n = 9 for No Alb, n = 7 for Alb, Females: n = 7 for No Alb, n = 5 for Alb). **(D)** There is no association of urinary excretion of THP with albuminuria in either male or female subjects as examined by Western blot analysis (Males: n = 10 for No Alb, n = 7 for Alb, Females: n = 8 for No Alb, n = 5 for Alb). **(E,F)** A weak correlation in the excretion of THP between urinary exosomes and urine was found only in female subjects (Pearson test, Males: n = 10 for No Alb, n = 7 for Alb, Females: n = 7 for No Alb, n = 5 for Alb). **(G,H)** No correlation was found in the excretion of β-actin or SHP-1 protein in urinary exosomes with albuminuria in either sex (Males: n = 10 for No Alb, n = 7 for Alb, Females: n = 8 for No Alb, n = 5 for Alb).

biomarker discovery in kidney diseases. The unbiased nature of proteomic analysis allows for a comprehensive evaluation of sample contents, which is crucial in identifying potential biomarkers. In this regard, proteomic analyses of urinary exosomes have been explored for identification of potential biomarkers for early diagnosis and monitoring of various renal diseases, including acute kidney and podocyte injuries (Zhou et al., 2006b; Zhou et al. 2008; Zhou et al. 2013; Awdishu et al., 2021), glomerular kidney disease (Gutwein et al., 2010), kidney transplant rejection (Kim et al., 2022), and diabetic nephropathy (Liu et al., 2022).

With a similar approach, we observed an increase in the excretion of 164 proteins and a decrease in 176 proteins in the exosomes of mice with albuminuria compared to without. These findings were partly validated through Western blot analysis. Extending this investigation to SCD subjects, we noted a significant increase or an upward trend in the excretion of heparanase, cathepsin C, α2-macroglobulin, and SERCA3 proteins in urinary exosomes of both male and female SCD patients with albuminuria. However, female subjects demonstrated stronger correlations between these protein excretions and UACR than male subjects. Furthermore, the correlations between the excretion of heparanase, cathepsin C, and α2-macroglobulin in urinary exosomes and urine were more pronounced in female subjects compared to male subjects. In contrast, no association was found between albuminuria and the excretion of Tamm-Horsfall protein, β-actin, or SHP-1 protein in urinary exosomes of either sex. These findings suggest that the increased excretion of heparanase, cathepsin C, α2-macroglobulin,

and SERCA3 proteins from urinary exosomes or urine specifically correlates with albuminuria. The stronger correlations observed in female participants suggest a sex-specific response in the pathophysiology of SCN, possibly due to sex-specific mechanisms influencing the activity or excretion of these proteins in SCD.

The specificity of increased excretion of heparanase, cathepsin C, α2-macroglobulin, and SERCA3 proteins in urinary exosomes for SCN, as opposed to general proteinuria, warrants further investigation. In SCD, coagulation is activated, with hypercoagulability being a contributing factor to SCN (Nasimuzzaman and Malik, 2019). Heparanase plays a key role in coagulation by upregulating tissue factor (Abassi and Goligorsky, 2020), while α2-macroglobulin acts as a fibrinolysis inhibitor by targeting plasmin and thrombin (Lagrange et al., 2022). Early research indicated no significant difference in serum α2-macroglobulin levels between SCD patients and healthy controls (Hedo et al., 1993), but later findings showed elevated α2-macroglobulin in steady-state SCD patients compared to healthy subjects (Makis et al., 2000).

However, the involvement of heparanase and α2-macroglobulin in other renal diseases leading to proteinuria has been documented. Heparanase has been implicated in various experimental and human glomerular diseases associated with proteinuria, including diabetes and membranous nephropathy (Shafat et al., 2011; Gil et al., 2012; Szymczak et al., 2017). Elevated urinary protein levels and activity of heparanase are noted in patients with both Type 1 and Type 2 diabetes (Shafat, Ilan, Zoabi, Vlodavsky and Nakhoul, 2011; Rops et al., 2012), as well as in renal transplant patients with proteinuria and decreased allograft function (Shafat et al., 2012). Similarly, increased serum α2-macroglobulin levels, correlating with microalbuminuria, have been observed in diabetic patients (James et al., 1980; Ahmad et al., 2001; Yoshino et al., 2019). The roles of cathepsin C and SERCA3 in SCD, and particularly in SCN, remain largely unexplored. Nonetheless, by combining patients' history with other diagnostic tools, SCN can be differentiated from other types of disease-induced nephropathy using these potential biomarkers.

It is noteworthy that GFR, measured using a transcutaneous method, was found to be elevated in SCD mice. This observation mirrors the renal function in patients with SCD during the early stages of the disease. The potential underlying causes for this include compensatory high renal blood flow and hyperfiltration, endothelial dysfunction, altered nitric oxide metabolism, and changes in hormonal and cytokine levels (Nath and Hebbel, 2015; Kasztan et al., 2019; Afangbedji and Jerebtsova, 2022).

In summary, through proteomic analyses of urinary exosomes from humanized SCD mice, and subsequent Western blot confirmation using urine and urinary exosomes of SCD subjects, we have observed that both male and female SCD subjects exhibited an increased or trending increase in the excretion of heparanase, cathepsin C, α2-macroglobulin, and SERCA3 proteins. Notably, this increase was specifically correlated with albuminuria. Moreover, we have found that female subjects demonstrated stronger correlations between the excretion of these proteins and the UACR compared to their male counterparts. One limitation of the present study is the small size of the human subject population. Despite this, the study lays a solid foundation for further exploration into the potential use of these proteins as biomarkers for the early diagnosis of SCN and for monitoring therapeutic efficacy, particularly in female patients. The next phase of our investigation will involve using a different cohort to validate these discoveries. Subsequently, a prospective, observational study will be conducted to determine whether these protein levels increase prior to the onset of albuminuria in SCD patients' urine and urinary exosomes.

Data availability statement

The data presented in the study are deposited in the jPOST repository at the address https://repository.jpostdb.org/ with accession number PXD043401 and project number JPST002221.

Ethics statement

The studies involving humans were approved by the Institutional Review Board of National Heart Lung and Blood Institute (Clinical Trials identifier: NCT03958643). The studies were conducted in accordance with the local legislation and institutional requirements. The participants provided their written informed consent to participate in this study. The animal study was approved by the Institutional Animal Care and Use Committee of the Uniformed Services University of the Health Sciences (Protocol # MED-16-978). The study was conducted in accordance with the local legislation and institutional requirements.

Author contributions

BP: Data curation, Formal Analysis, Methodology, Writing–original draft. EL: Data curation, Methodology, Supervision, Writing–original draft, Writing–review and editing. HA: Conceptualization, Funding acquisition, Writing–review and editing. XL: Data curation, Writing–review and editing. SN: Supervision, Writing–review and editing. JO: Conceptualization, Funding acquisition, Writing–review and editing. IS: Writing–review and editing. MK: Conceptualization, Funding acquisition, Writing–review and editing. CF: Writing–review and editing, Supervision. XZ: Conceptualization, Data curation, Formal Analysis, Funding acquisition, Investigation, Methodology, Project administration, Supervision, Validation, Writing–original draft, Writing–review and editing.

Funding

The author(s) declare financial support was received for the research, authorship, and/or publication of this article. This work was funded by the grant (MED-83-3923 to XZ) from the Collaborative Health Initiative Research Program between the National Heart Lung and Blood Institute and the Henry M. Jackson Foundation for the Advancement of Military Medicine. HA was funded by the Intramural Research Programs of National Heart Lung and Blood Institute and National Institute of Allergy and Infectious Diseases (HL006196, AI001150).

Acknowledgments

The authors thank Dr. Hong Wang for analysis of podocalyxin protein abundance in urinary exosomes and urine.

Conflict of interest

The authors declare that the research was conducted in the absence of any commercial or financial relationships that could be construed as a potential conflict of interest.

The author(s) declared that they were an editorial board member of Frontiers, at the time of submission. This had no impact on the peer review process and the final decision.

Publisher's note

All claims expressed in this article are solely those of the authors and do not necessarily represent those of their affiliated organizations, or those of the publisher, the editors and the reviewers. Any product that may be evaluated in this article, or claim that may be made by its manufacturer, is not guaranteed or endorsed by the publisher.

Author disclaimer

The content and views expressed in this article are the sole responsibility of the authors and do not necessarily reflect the views or policies of the Uniformed Services University of the Health Sciences or US Department of Defense. Mention of trade names, commercial products, or organizations does not imply endorsement by the Uniformed Services University of the Health Sciences or US Department of Defense.

Supplementary material

The Supplementary Material for this article can be found online at: https://www.frontiersin.org/articles/10.3389/fphys.2024.1300667/full#supplementary-material

References

Abassi, Z., and Goligorsky, M. S. (2020). Heparanase in acute kidney injury. *Adv. Exp. Med. Biol.* 1221, 685–702. doi:10.1007/978-3-030-34521-1_28

Afangbedji, N., and Jerebtsova, M. (2022). Glomerular filtration rate abnormalities in sickle cell disease. *Front. Med. (Lausanne).* 9, 1029224. doi:10.3389/fmed.2022.1029224

Afangbedji, N., Kumari, N., Diaz, S. F., Wen, F., Taylor, J. G., Nekhai, S., et al. (2022). Soluble urokinase-type plasminogen activator receptor in sickle cell disease-associated chronic kidney disease. *Blood Adv. Sep.* 14, 1854–1857. doi:10.1182/bloodadvances.2022008374

Ahmad, J., Singh, M., and Saleemuddin, M. (2001). A study of plasma alpha-2-macroglobulin levels in type 2 diabetic subjects with microalbuminuria. *J. Assoc. Physicians India* 49, 1062–1065.

Ataga, K. I., Saraf, S. L., and Derebail, V. K. (2022). The nephropathy of sickle cell trait and sickle cell disease. *Nat. Rev. Nephrol. Jun* 18, 361–377. doi:10.1038/s41581-022-00540-9

Ataga, K. I., Zhou, Q., Saraf, S. L., Hankins, J. S., Ciccone, E. J., Loehr, L. R., et al. (2023). Sex differences in progression of kidney disease in sickle cell disease. *Haematologica* 108, 1436–1441. doi:10.3324/haematol.2022.281677

Awdishu, L., Le, A., Amato, J., Jani, V., Bal, S., Mills, R. H., et al. (2021). Urinary exosomes identify inflammatory pathways in vancomycin associated acute kidney injury. *Int. J. Mol. Sci. Mar.* 10, 22. doi:10.3390/ijms22062784

Becker, A. M. (2011). Sickle cell nephropathy: challenging the conventional wisdom. *PediatrNephrol* 26, (12), 2099–2109. doi:10.1007/s00467-010-1736-2

Caseiro, A., Barros, A., Ferreira, R., Padrão, A., Aroso, M., Quintaneiro, C., et al. (2014). Pursuing type 1 diabetes mellitus and related complications through urinary proteomics. *Transl. Res. Mar.* 163, 188–199. doi:10.1016/j.trsl.2013.09.005

Ciragil, P., Kurutas, E. B., and Miraloglu, M. (2014). New markers: urine xanthine oxidase and myeloperoxidase in the early detection of urinary tract infection. *Dis. Markers* 2014, 269362. doi:10.1155/2014/269362

Finazzi, A. E., Micali, S., Maccarrone, M., D'Amico, A., Vespasiani, G., Pasqualetti, P., et al. (2001). Urinary N-acetyl-beta-D-glucosaminidase concentration in patients with spinal cord injury: relationship with urodynamic parameters. *Urology* 58, 870–874. doi:10.1016/s0090-4295(01)01376-0

Gil, N., Goldberg, R., Neuman, T., Garsen, M., Zcharia, E., Rubinstein, A. M., et al. (2012). Heparanase is essential for the development of diabetic nephropathy in mice. *Diabetes. Jan.* 61, 208–216. doi:10.2337/db11-1024

Gutwein, P., Schramme, A., Abdel-Bakky, M. S., Doberstein, K., Hauser, I. A., Ludwig, A., et al. (2010). ADAM10 is expressed in human podocytes and found in urinary vesicles of patients with glomerular kidney diseases. *JBiomedSci* 17, 3. doi:10.1186/1423-0127-17-3

Hamideh, D., Raj, V., Harrington, T., Li, H., Margolles, E., Amole, F., et al. (2014). Albuminuria correlates with hemolysis and NAG and KIM-1 in patients with sickle cell anemia. *PediatrNephrol* 29, 1997–2003. doi:10.1007/s00467-014-2821-8

Hedo, C. C., Aken'ova, Y. A., Okpala, I. E., Durojaiye, A. O., and Salimonu, L. S. (1993). Acute phase reactants and severity of homozygous sickle cell disease. *J. Intern Med.* 233, 467–470. doi:10.1111/j.1365-2796.1993.tb01000.x

Heemskerk, S., Pickkers, P., Bouw, M. P., Draisma, A., van der Hoeven, J. G., Peters, W. H., et al. (2006). Upregulation of renal inducible nitric oxide synthase during human endotoxemia and sepsis is associated with proximal tubule injury. *Clin. J. Am. Soc. Nephrol.* 1, 853–862. doi:10.2215/CJN.00490206

Holzscheiter, L., Beck, C., Rutz, S., Manuilova, E., Domke, I., Guder, W. G., et al. (2014). NGAL, L-FABP, and KIM-1 in comparison to established markers of renal dysfunction. *ClinChemLab Med.* 52, 537–546. doi:10.1515/cclm-2013-0693

Hoorn, E. J., Pisitkun, T., Zietse, R., Gross, P., Frokiaer, J., Wang, N. S., et al. (2005). Prospects for urinary proteomics: exosomes as a source of urinary biomarkers. *Nephrol. Carlt.* 10, 283–290. doi:10.1111/j.1440-1797.2005.00387.x

Huang, da W., Sherman, B. T., and Lempicki, R. A. (2009). Systematic and integrative analysis of large gene lists using DAVID bioinformatics resources. *Nat. Protoc.* 4, 44–57. doi:10.1038/nprot.2008.211

James, K., Merriman, J., Gray, R. S., Duncan, L. J., and Herd, R. (1980). Serum alpha 2-macroglobulin levels in diabetes. *J. Clin. Pathol. Feb* 33, 163–166. doi:10.1136/jcp.33.2.163

Jerebtsova, M., Saraf, S. L., Lin, X., Lee, G., Adjei, E. A., Kumari, N., et al. (2018). Identification of ceruloplasmin as a biomarker of chronic kidney disease in urine of sickle cell disease patients by proteomic analysis. *Am. J. Hematol. Feb* 93, E45–E47. doi:10.1002/ajh.24965

Jerebtsova, M., Taye, A., Smith, N., Afangbedji, N., Stokes, D., Niu, X., et al. (2020). Association between plasma and urinary orosomucoid and chronic kidney disease in adults with sickle cell disease. *Br. J. Haematol. Jul* 190, e45–e48. doi:10.1111/bjh.16702

Kasztan, M., Aban, I., Hande, S. P., Pollock, D. M., and Lebensburger, J. D. (2020). Sex differences in the trajectory of glomerular filtration rate in pediatric and murine sickle cell anemia. *Blood Adv. Jan.* 28 (4), 263–265. doi:10.1182/bloodadvances.2019001237

Kasztan, M., Fox, B. M., Lebensburger, J. D., Hyndman, K. A., Speed, J. S., Pollock, J. S., et al. (2019). Hyperfiltration predicts long-term renal outcomes in humanized sickle cell mice. *Blood Adv.* 3 (3), 1460–1475. doi:10.1182/bloodadvances.2018028878

Kim, M. J., Lim, S. J., Ko, Y., Kwon, H. E., Jung, J. H., Kwon, H., et al. (2022). Urinary exosomal cystatin C and lipopolysaccharide binding protein as biomarkers for antibody-mediated rejection after kidney transplantation. *Biomedicines*, 10, (10), 2346. doi:10.3390/biomedicines10102346

Lagrange, J., Lecompte, T., Knopp, T., Lacolley, P., and Regnault, V. (2022). Alpha-2-macroglobulin in hemostasis and thrombosis: an underestimated old double-edged sword. *J. Thromb. Haemost. Apr* 20, 806–815. doi:10.1111/jth.15647

Lee, K., Gane, P., Roudot-Thoraval, F., Godeau, B., Bachir, D., Bernaudin, F., et al. (2001). The nonexpression of CD36 on reticulocytes and mature red blood cells does not modify the clinical course of patients with sickle cell anemia. *Blood* 98 (98), 966–971. doi:10.1182/blood.v98.4.966

Liu, T., Wang, Y., Zhao, M., Jiang, J., Li, T., and Zhang, M. (2022). Differential expression of aerobic oxidative metabolism-related proteins in diabetic urinary exosomes. *Front. Endocrinol. (Lausanne)* 13, 992827. doi:10.3389/fendo.2022.992827

Makis, A. C., Hatzimichael, E. C., Mavridis, A., and Bourantas, K. L. (2000). Alpha-2-macroglobulin and interleukin-6 levels in steady-state sickle cell disease patients. *Acta Haematol.* 104, 164–168. doi:10.1159/000046509

Micanovic, R., LaFavers, K., Garimella, P. S., Wu, X. R., and El-Achkar, T. M. (2020). Uromodulin (Tamm-Horsfall protein): guardian of urinary and systemic homeostasis. *Nephrol. Dial. Transpl. Jan. 1* 35, 33–43. doi:10.1093/ndt/gfy394

Mohtat, D., Thomas, R., Du, Z., Boakye, Y., Moulton, T., Driscoll, C., et al. (2011). Urinary transforming growth factor beta-1 as a marker of renal dysfunction in sickle cell disease. *PediatrNephrol* 26, 275–280. doi:10.1007/s00467-010-1677-9

Molitch, M. E., DeFronzo, R. A., Franz, M. J., Keane, W. F., Mogensen, C. E., Parving, H. H., et al. (2004). Nephropathy in diabetes. *Diabetes Care* 27 (1), S79–S83. doi:10.2337/diacare.27.2007.s79

Nasimuzzaman, M., and Malik, P. (2019). Role of the coagulation system in the pathogenesis of sickle cell disease. *Blood Adv.* 3 (3), 3170–3180. doi:10.1182/bloodadvances.2019000193

Nath, K. A., and Hebbel, R. P. (2015). Sickle cell disease: renal manifestations and mechanisms. *NatRevNephrol* 11, 161–171. doi:10.1038/nrneph.2015.8

Nekhai, S., Lin, X., Soni, S., Taye, A., Smith, N., Afangbedji, N., et al. (2021). Urinary kringle domain-containing protein hgfl: a validated biomarker of early sickle cell anemia-associated kidney disease. *Am. J. Nephrol.* 52, 582–587. doi:10.1159/000517056

Packialakshmi, B., Stewart, I. J., Burmeister, D. M., Feng, Y., McDaniel, D. P., Chung, K. K., et al. (2022). Tourniquet-induced lower limb ischemia/reperfusion reduces mitochondrial function by decreasing mitochondrial biogenesis in acute kidney injury in mice. *Physiol. Rep. Feb* 10, e15181. doi:10.14814/phy2.15181

Rops, A. L., van den Hoven, M. J., Veldman, B. A., Salemink, S., Vervoort, G., Elving, L. D., et al. (2012). Urinary heparanase activity in patients with Type 1 and Type 2 diabetes. *Nephrol. Dial. Transpl. Jul* 27, 2853–2861. doi:10.1093/ndt/gfr732

Scarfe, L., Schock-Kusch, D., Ressel, L., Friedemann, J., Shulhevich, Y., Murray, P., et al. (2018). Transdermal measurement of glomerular filtration rate in mice. *J. Vis. Exp.*, 58520. doi:10.3791/58520

Selma, J., Song, H., Rivera, C., Douglas, S., Akella, A., Bollavaram, K., et al. (2022). Sickle cell disease promotes sex-dependent pathological bone loss through enhanced cathepsin proteolytic activity in mice. *Blood Adv. Mar.* 8 (6), 1381–1393. doi:10.1182/bloodadvances.2021004615

Shafat, I., Agbaria, A., Boaz, M., Schwartz, D., Baruch, R., Nakash, R., et al. (2012). Elevated urine heparanase levels are associated with proteinuria and decreased renal allograft function. *PLoS One* 7, e44076. doi:10.1371/journal.pone.0044076

Shafat, I., Ilan, N., Zoabi, S., Vlodavsky, I., and Nakhoul, F. (2011). Heparanase levels are elevated in the urine and plasma of type 2 diabetes patients and associate with blood glucose levels. *PLoS One* 6 (6), e17312. doi:10.1371/journal.pone.0017312

Sharma, M., Halligan, B. D., Wakim, B. T., Savin, V. J., Cohen, E. P., and Moulder, J. E. (2008). The urine proteome as a biomarker of radiation injury: submitted to proteomics- clinical applications special issue: "renal and urinary proteomics (thongboonkerd). *Proteomics Clin. Appl.* 2 (2), 1065–1086. doi:10.1002/prca.200780153

Sundaram, N., Bennett, M., Wilhelm, J., Kim, M. O., Atweh, G., Devarajan, P., et al. (2011). Biomarkers for early detection of sickle nephropathy. *AmJHematol* 86, 559–566. doi:10.1002/ajh.22045

Szymczak, M., Kuźniar, J., Kopeć, W., Żabińska, M., Marchewka, Z., Kościelska-Kasprzak, K., et al. (2017). Increased granulocyte heparanase activity in neutrophils from patients with lupus nephritis and idiopathic membranous nephropathy. *Arch. Immunol. Ther. Exp. Warsz. Feb* 65, 83–91. doi:10.1007/s00005-016-0396-8

Tan, Y., Mui, D., Toan, S., Zhu, P., Li, R., and Zhou, H. (2020). SERCA overexpression improves mitochondrial quality control and attenuates cardiac microvascular ischemia-reperfusion injury. *Mol. Ther. Nucleic Acids* 22 (22), 696–707. doi:10.1016/j.omtn.2020.09.013

Tsai, J. F., Jeng, J. E., Chuang, L. Y., Chang, W. Y., and Tsai, J. H. (1997). Urinary transforming growth factor beta1 levels in hepatitis C virus-related chronic liver disease: correlation between high levels and severity of disease. *Hepatology* 25, 1141–1146. doi:10.1002/hep.510250516

van Balkom, B. W., Pisitkun, T., Verhaar, M. C., and Knepper, M. A. (2011). Exosomes and the kidney: prospects for diagnosis and therapy of renal diseases. *Kidney Int.* 80, 1138–1145. doi:10.1038/ki.2011.292

Voskaridou, E., Terpos, E., Michail, S., Hantzi, E., Anagnostopoulos, A., Margeli, A., et al. (2006). Early markers of renal dysfunction in patients with sickle cell/beta-thalassemia. *Kidney Int.* 69, 2037–2042. doi:10.1038/sj.ki.5000248

Wang, H., Ferraris, J. D., Klein, J. D., Sands, J. M., Burg, M. B., and Zhou, X. (2015). PKC-α contributes to high NaCl-induced activation of NFAT5 (TonEBP/OREBP) through MAPK ERK1/2. *Am. J. Physiol. Ren. Physiol.* 308, F140–F148. doi:10.1152/ajprenal.00471.2014

Wang, H., Morris, R. G., Knepper, M. A., and Zhou, X. (2019). Sickle cell disease up-regulates vasopressin, aquaporin 2, urea transporter A1, Na-K-Cl cotransporter 2, and epithelial Na channels in the mouse kidney medulla despite compromising urinary concentration ability. *Physiol. Rep. Apr* 7, e14066. doi:10.14814/phy2.14066

Wasung, M. E., Chawla, L. S., and Madero, M. (2015). Biomarkers of renal function, which and when? *ClinChimActa* 438, 350–357. doi:10.1016/j.cca.2014.08.039

Yoshino, S., Fujimoto, K., Takada, T., Kawamura, S., Ogawa, J., Kamata, Y., et al. (2019). Molecular form and concentration of serum α(2)-macroglobulin in diabetes. *Sci. Rep.* 9, 12927. doi:10.1038/s41598-019-49144-7

Zhou, H., Cheruvanky, A., Hu, X., Matsumoto, T., Hiramatsu, N., Cho, M. E., et al. (2008). Urinary exosomal transcription factors, a new class of biomarkers for renal disease. *Kidney Int.* 74, 613–621. doi:10.1038/ki.2008.206

Zhou, H., Kajiyama, H., Tsuji, T., Hu, X., Leelahavanichkul, A., Vento, S., et al. (2013). Urinary exosomal Wilms' tumor-1 as a potential biomarker for podocyte injury. *AmJPhysiol Ren. Physiol.* 305, F553–F559. doi:10.1152/ajprenal.00056.2013

Zhou, H., Pisitkun, T., Aponte, A., Yuen, P. S., Hoffert, J. D., Yasuda, H., et al. (2006a). Exosomal Fetuin-A identified by proteomics: a novel urinary biomarker for detecting acute kidney injury. *Kidney Int.* 70, 1847–1857. doi:10.1038/sj.ki.5001874

Zhou, H., Yuen, P. S., Pisitkun, T., Gonzales, P. A., Yasuda, H., Dear, J. W., et al. (2006b). Collection, storage, preservation, and normalization of human urinary exosomes for biomarker discovery. *Kidney Int.* 69, 1471–1476. doi:10.1038/sj.ki.5000273

Zhou, X., Wang, H., Koles, N. L., Zhang, A., and Aronson, N. E. (2014). Leishmania infantum-chagasi activates SHP-1 and reduces NFAT5/TonEBP activity in the mouse kidney inner medulla. *AmJPhysiol Ren. Physiol.* 307, F516–F524. doi:10.1152/ajprenal.00006.2014

frontiers | Frontiers in Physiology

TYPE Original Research
PUBLISHED 14 August 2024
DOI 10.3389/fphys.2024.1399396

OPEN ACCESS

EDITED BY
Carolyn Mary Ecelbarger,
Georgetown University, United States

REVIEWED BY
Alvaro Conrado Ucero,
Complutense University of Madrid, Spain
Xiaoming Zhou,
Uniformed Services University of the Health Sciences, United States

*CORRESPONDENCE
Mykola Mamenko,
mmamenko@augusta.edu
Irina Baranovskaya,
ibaranovskaya@augusta.edu

RECEIVED 11 March 2024
ACCEPTED 29 July 2024
PUBLISHED 14 August 2024

CITATION
Baranovskaya I, Volk K, Alexander S, Abais-Battad J and Mamenko M (2024) Lithium-induced apoptotic cell death is not accompanied by a noticeable inflammatory response in the kidney.
Front. Physiol. 15:1399396.
doi: 10.3389/fphys.2024.1399396

Lithium-induced apoptotic cell death is not accompanied by a noticeable inflammatory response in the kidney

Irina Baranovskaya*, Kevin Volk, Sati Alexander, Justine Abais-Battad and Mykola Mamenko*

Department of Physiology, Medical College of Georgia, Augusta University, Augusta, GA, United States

Lithium (Li^+) therapy is a valuable tool in psychiatric practice that remains underutilized due to safety concerns. Excessive plasma Li^+ levels are nephrotoxic and can trigger a local immune response. Our understanding of the immunomodulatory effects of Li^+ in the kidney is fragmentary. Here, we studied how immune mechanisms contribute to the development of Li^+-induced adverse effects in the kidneys of C57BL/6NJ mice placed on a 0.3% lithium carbonate diet for 28 days. We combined histochemical techniques, immunoblotting, flow cytometry, qPCR and proteome profiler arrays to characterize renal tissue damage, infiltrating immune cells and cytokine markers, activation of pyroptotic and apoptotic cascades in the kidneys of mice receiving Li^+-containing and regular diets. We found that biomarkers of tubular damage, kidney injury marker, KIM-1, and neutrophil gelatinase-associated lipocalin, NGAL, were elevated in the renal tissue of Li^+-treated mice when compared to controls. This correlated with increased interstitial fibrosis in Li^+-treated mice. Administration of Li^+ did not activate the pro-inflammatory NLRP3 inflammasome cascade but promoted apoptosis in the renal tissue. The TUNEL-positive signal and levels of pro-apoptotic proteins, Bax, cleaved caspase-3, and caspase-8, were elevated in the kidneys of Li^+-treated mice. We observed a significantly higher abundance of CD93, CCL21, and fractalkine, accumulation of $F4.80^+$ macrophages with reduced M1/M2 polarization ratio and decreased $CD4^+$ levels in the renal tissue of Li^+-treated mice when compared to controls. Therefore, after 28 days of treatment, Li^+-induced insult to the kidney manifests in facilitated apoptotic cell death without an evident pro-inflammatory response.

KEYWORDS

anti-inflammatory, apoptosis, lithium, nephrogenic diabetes insipidus, renal damage, macrophage polarization

Introduction

Lithium (Li^+) stands out as one of the most effective tools in the psychiatric pharmacological arsenal, particularly in the treatment of bipolar disorder. Randomized clinical trials and real-world evidence studies establish Li^+ as a mood stabilizer for bipolar patients with unique disease-modifying benefits including well-documented effective control of acute mania, prevention of manic as well as depressive episodes, improvement of the long-term disease trajectory, reduction of suicide rates and all-

cause mortality (Malhi and Bauer, 2023; Kessing, 2024). Li^+ can also improve cognition, reduce the incidence of dementia and has a promising therapeutic potential to combat Alzheimer's, Parkinson's and Huntington's disease, as well as addiction disorders (Grandjean and Aubry, 2009; Singh et al., 2023).

Wider use of Li^+ has been limited due to its perceived toxicity manifesting only at excessively high plasma levels (Rybakowski, 2018). Li^+ has a narrow therapeutic window of 0.6–1.2 mM in plasma (Malhi and Bauer, 2023; Kessing, 2024), and chronic exposure to high doses of Li^+ has been linked to a range of kidney pathologies. By far, the most common renal complication of Li^+ therapy is impairment of vasopressin-dependent water reabsorption in the collecting duct principal cells leading to nephrogenic diabetes insipidus (NDI) that is observed in up to 40% of treated patients (Grunfeld and Rossier, 2009). Several studies report that Li^+ can induce distal renal tubular acidosis, manifesting in increased urine pH and ammonia excretion, possibly due to altered proton and ammonia secretion by the collecting duct intercalated cells (Perez et al., 1975; Weiner et al., 2014). The prevalence of severe renal complications in Li^+-treated population is relatively low (Vestergaard et al., 1979; Bendz et al., 2010). Infrequent observations of proximal tubular atrophy, progressive interstitial fibrosis, nephrotic syndrome, formation of microcysts, chronic kidney disease and renal failure have been reported in a small percentage of long-term Li^+ users (Markowitz et al., 2000; Kripalani et al., 2009; Azab et al., 2015; Alsady et al., 2016; Rybakowski, 2018; Mehta et al., 2022). On the other hand, a mounting body of evidence demonstrates protective effects of Li^+ in the kidney (Gong et al., 2016). Long-term therapy with low doses of Li^+ as a monotherapy or in combination with other drugs demonstrated renoprotective effects in animal models of acute kidney injury and can be beneficial in chronic kidney disease (Bao et al., 2015; Alsady et al., 2016; Mehta et al., 2022; Shimizu et al., 2023). A better understanding of the mechanisms underlying Li^+-induced adverse effects will allow mitigating the risks and ensure broader utilization and better outcomes of Li^+-based therapies.

Li^+-induced insult to the kidney can induce a local immune response. The accrued data draws a complex and often contradictory picture of the immunomodulatory action of lithium in the kidney. Intoxication observed at high plasma Li^+ concentrations activates proinflammatory factors in the kidney and induces pyroptosis (Jing et al., 2022). At the same time, long-term administration of Li^+-containing diet, resulting in therapeutically acceptable circulating Li^+ levels, reportedly induces interstitial fibrosis in rat kidneys but is associated with minimal inflammatory activity (Walker et al., 2013). Other studies reveal anti-inflammatory properties of Li^+ that can affect renal function. Lithium has been shown to inhibit the synthesis of prostaglandins, reduce renal injury and attenuate inflammation in several models of acute kidney injury and renal disease (Nahman et al., 2012; Azab et al., 2015; Gong et al., 2016). This creates a strong momentum for further evaluation of Li^+-induced immune mechanisms in the kidney.

Based on the previous studies reporting insidious progression of Li^+-induced renal injury, we hypothesized that Li^+-induced insult to the kidney is not accompanied by a pronounced inflammation in the renal tissue. In this study, we placed C57BL/6NJ mice on a regular rodent chow containing 0.3% lithium carbonate for 4 weeks to achieve therapeutically acceptable serum Li^+ levels and establish the contribution of immune mechanisms to nephrotoxic effects of lithium in the kidney. We demonstrate that administration of Li^+ for 28 days induces NDI and moderate renal injury, likely due to apoptosis of tubular epithelial cells. The immune response localized to the kidneys of Li^+-treated mice does not exhibit a distinctive proinflammatory phenotype and has characteristic anti-inflammatory features.

Materials and methods

Experimental animals

7-week-old male C57BL/6NJ mice (Jackson Laboratories, United States) weighing between 20–22 g were randomly assigned to receive Teklad 2,918 chow (control group) and Teklad 2,918 chow supplemented with 0.3% lithium carbonate (Li^+-treated group) over the course of 28 days. All animal procedures were approved by the Institutional Animal Care and Use Committee of the Medical College of Georgia at Augusta University (AUP 2017-0844) and were conducted under the National Institutes of Health Guide for the Care and Use of Laboratory Animals. All mice had unrestricted access to water and food, were maintained under conditions of a 12:12 h light-dark cycle, constant temperature, and humidity. Animal wellbeing was monitored daily throughout the study. Body weight was recorded twice a week. At the end of each experimental week, the animals were transferred to metabolic cages (Tecniplast, Italy) for a 24-h period with *ad libitum* access to water and food. Urine volume, osmolarity, and the amount of consumed water were measured to assess NDI manifestations. At the end of the study, all animals were euthanized by exsanguination under 5% isoflurane anesthesia. Blood samples were collected through cardiac puncture into BD Vacutainer serum separation tubes to measure serum ion concentrations using the CareLyte Plus electrolyte analyzer (Diamond Diagnostics) or into BD Vacutainer blood collection tubes with sodium heparin for blood urea nitrogen (BUN) assessment with the STAT Profile Prime Plus Gas Analyzer (Nova Biomedical). Renal tissue was dissected and used for immune cell extraction, fixed for histological analysis, or rapidly frozen in liquid nitrogen and stored at −80°C for further molecular biology analysis.

Histopathological staining

Fresh renal tissue was fixed in 10% neutral-buffered formalin for 24 h, embedded into paraffin, cut into 5 µm sections, mounted on slides, and stained with picrosirius red according to a routinely used histological protocol. Slides were scanned using Aperio Versa (40x) and digital images were downloaded into QuPath platform (version 0.5.0) (Bankhead et al., 2017). Interstitial fibrosis, interstitial thickness, and tubular dilation were analyzed in the cortex in a blinded manner (N = 5 per each animal group), Briefly, by loading a threshold classifier we identified the tissue as an area

with the signal above the background (to exclude tubular lumen, arteries, and any technical voids in the tissue). This approach was used for all further analysis, including fibrosis and interstitial thickness. Tubular dilation was determined in the cortex by measuring the area with the signal equal to the background, manually excluding arteries, glomeruli, and any tissue-free space other than tubular lumen from consideration. Then, an object classifier was created and trained by the provided RTrees algorithm to detect the interstitial regions of the tissue area, which was further applied to calculate the interstitial area in the cortex (named interstitial thickness). Finally, by creating an additional threshold classifier in the red channel we calculated the percentage of interstitial fibrosis normalized on the whole cortex area (% of cortex) or the cortical interstitial area (% of interstitium).

Evaluation of DNA fragmentation in formalin fixed paraffin embedded kidney sections

To evaluate cell apoptosis in the renal tissue, DNA fragmentation was visualized in the kidney sections using a terminal deoxynucleotidyl transferase dUTP nick end labeling (TUNEL) assay with a 3, 3 -diaminobenzidine (DAB)–horseradish peroxidase (HRP) detection staining, TUNEL-HRP-DAB kit (Abcam), according to the manufacturer's guidelines. Briefly, 5 μm sections cut from the paraffin-embedded kidney blocks fixed in 10% formalin were deparaffinized, rehydrated and permeabilized with proteinase K for 20 min. Endogenous peroxidase activity was inhibited by a 3% H_2O_2 solution in methanol. This was followed by an application of TUNEL reaction mixture in a humidified chamber for 90 min, and a subsequent 10 min incubation in a blocking buffer. The sections were incubated with the streptavidin-HRP conjugate for 30 min, followed by an application of DAB for 10 min and methyl green counterstain for another 3 min. Quantification of the number of TUNEL-positive cells was manually performed in a blinded manner across the entire cortex area using an inverted Nikon Eclipse Ti2 microscope equipped with a 40x Nikon Plan Fluor Objective. The cortex area for each sample was calculated using the QuPath platform (version 0.5.0). The number of TUNEL-positive cells per square millimeter (mm^2) in the cortex was used for statistical analysis. Representative images were taken with a Nikon DS-Fi3 digital camera.

Western blotting

Renal tissue was homogenized in an ice-cold 5% sorbitol, 5 mM histidine/imidazole buffer (pH = 7.5) supplemented with a protease and phosphatase inhibitor cocktail (Thermo Scientific). Homogenate samples were further centrifugated at 2000 g for 10 min at +4°C and protein concentration was measured using standard Bradford assay protocol. Each sample was mixed with Laemmli sample buffer containing 5% β-mercaptoethanol and incubated for 5 min at +95°C. Then, samples were separated by SDS PAGE using 4%–15% precast polyacrylamide gel (Bio-Rad). Trans-Blot Turbo RTA Midi 0.2 μm nitrocellulose transfer kit (Bio-Rad) and Trans-Blot turbo transfer system (Bio-Rad) were used for protein transfer according to the manufacturer's protocol. The membrane was stained with Ponceau red for protein load verification. Membranes were washed in Tris-buffered saline with 0.1% Tween-20 (TBST), blocked in 5% non-fat milk or in 5% BSA (for IL-1β and ASC detection) in TBST for 1 h at room temperature and further incubated with one of the primary antibodies for NGAL, KIM-1, Bax, Bcl-xL, Caspase-8, Cleaved Caspase-8, Cleaved Caspase-3, IL-1β, caspase-1, cleaved caspase-1, NLRP3, ASC, and Bid overnight at +4°C (Supplementary Table S1). The incubation with secondary horseradish peroxidase-conjugated antibody was performed for 1 h at room temperature. Stripping was performed when needed in a buffer containing 0.2 M Glycine, 3.5 mM SDS, and 1% Tween 20 (pH = 2.2) for 10 min. Information about the antibodies used and their working dilutions is provided in the Supplementary Material. Chemiluminescent SuperSignal Pico Plus kit and West Femto Maximum Sensitivity Substrate kits (Thermo Scientific), Azure C600 Imaging System (Azure Biosystems) and ChemiDoc (Bio-rad) were used for protein detection. Densitometric analysis was performed in ImageJ 1.50 software (NIH). The levels of specific protein bands were normalized to the total protein signal according to Ponceau red staining.

Quantitative PCR analysis

Renal tissue was homogenized in TRIzol reagent (Invitrogen) using Fisherbrand 150 Handheld homogenizer (Fisher Scientific). RNA extraction and RNA samples digestion with DNAse (Promega) was followed by complementary DNA synthesis using Reverse Transcriptase Kit (Promega) and according to the manufacturer's instructions. Quantitative PCR analysis was performed using Universal SYBR Green Supermix (Bio-Rad) and QuantStudio 3 RT-PCR System (Applied Biosystems). Primers were synthesized by Integrated DNA Technologies and provided in the Supplementary Table S1. The relative expression of Fn-1, Col1-a1, NLRP3, caspase-1, IL-1β and ASC genes in renal tissue homogenates was calculated by $2^{-\Delta\Delta CT}$ method, and Rn18s/45s ribosomal RNA was used for normalization.

Protein array analysis

Proteome Profiler Mouse XL Cytokine Array (R&D systems) was used for cytokine profile screening according to the manufacturer's instructions. Renal tissue homogenate samples isolated from Li^+-treated or control mice (N = 6 per group) were pooled together for each group and incubated on the nitrocellulose membranes containing capture antibodies printed in duplicates. Loading volume for each sample was adjusted using the Bradford assay. Dot blot densitometric analysis was performed in the ImageJ 1.50 software (NIH). To calculate the relative protein abundance, densities of all dots were normalized on the average density of the dots on the membrane with control group samples. Mean values of relative protein abundances were calculated for a pair of membranes containing samples from control and Li^+-treated groups. Cytokine profiling was performed 4 times for each group.

TABLE 1 Endpoint physiological parameters for experimental mice.

Parameter	Control		Li^+-treated		Significance
	Mean	SEM	Mean	SEM	*p*-Value
Final body weight, g	27.67	0.96	21.47	0.48	< **0.0001** ζ
Total kidney weight, mg	338.3	11.12	261.2	7.99	< **0.0001**
Total kidney to body weight, %	1.22	0.02	1.22	0.03	0.82
Serum Li^+, mmol/L	ND	-	1.34	0.23	
Serum Na^+, mmol/L	148.7	0.31	153.0	1.50	**0.020** ζ
Serum K^+, mmol/L	4.37	0.42	4.95	0.43	0.35
Serum Cl^-, mmol/L	113.7	0.32	117.9	0.90	**0.001** ζ
BUN, mg/dL	23.80	2.40	22.40	1.81	0.65
Water intake, ml/24 h	1.86	0.12	19.88	2.40	< **0.0001** ζ
Urinary volume, ml/24 h	0.89	0.02	15.96	3.26	< **0.01** ζ
Urinary osmolality, mOsm/L	1,608.00	140.00	153.00	37.64	< **0.01** ζ

A Student's t-test (with Welch's correction for samples with unequal variances–ζ) was used for statistical comparisons. Data are presented as mean ± SEM. $N = 10$ for each group. ND, not determined. *P* values lower than 0.05 are indicated in bold.

Immune cell isolation and analysis

Immune cell isolation from the renal tissue was performed using a well-established protocol as previously described (Walton et al., 2023). In brief, freshly isolated renal tissue was minced using a razor blade and incubated in the RPMI-1640 medium (Gibco) containing 0.1% collagenase type IV (Worthington) and 10 µg/mL DNAse I (Sigma-Aldrich). The incubation was carried out for 30 min at +37°C. To obtain single-cell suspension, kidney homogenates were sequentially filtered through a series of filters with pore sizes of 100, 70, and 40 µm. Subsequently, mononuclear cells were separated using Percoll density gradient centrifugation (Sigma-Aldrich). Isolated cells were counted using a hemocytometer. For further analysis, 1 million cells from each sample were incubated with antibodies against CD16/CD32 to block non-specific antibody binding. To identify specific immune cell populations, we used previously published panel of fluorochrome-conjugated antibodies (Saleh et al., 2016): CD45-BV510, F4/80-AlexFluor488, CD3-APC, CD4-APC/H7, and CD8a-PE/Cy7. Live and dead cells were distinguished using DAPI staining (1 µg/mL, BioLegend). Flow-cytometric analysis of the stained cells was performed using a 5-Laser AURORA Spectral Cytometer (Cytek). The gating strategy employed for the identification and analysis of immune cell populations is illustrated in Supplementary Figure S1.

Macrophage extraction

Positive selection of the renal single-cell suspensions was performed by column separation using MicroBeads against F4.80 (Miltenyi Biotec) according to the manufacturer's instructions. The purification quality was checked by flow cytometry and was more than 90%. RNA was extracted from samples using RNeasy Mini Kit (Qiagen). RNA samples were further used for RT-qPCR experiments, where the relative expression of IL-12β and Arg-1 mRNA was performed by $2^{-\Delta\Delta CT}$ method (Supplementary Table S1).

Statistical analysis

Statistical analysis and data visualization were performed in GraphPad Prism 9.41. Longitudinal data on urine osmolarity and volume, water consumption and body weight changes were analyzed by a two-way mixed-design ANOVA with a Greenhouse-Geisser correction. A Student's t-test (with Welch's correction for samples with unequal variances) was used to compare the endpoint data between control and Li^+-treated groups. Values of $P < 0.05$ were considered statistically significant. Data are presented as mean ± SEM.

Results

Therapeutic serum Li^+ levels cause a moderate insult to the renal tissue

After 28 days on a 0.3% Li_2CO_3 diet, serum Li^+ levels in mice were elevated to 0.7–1.5 mmol/L (Table 1). This is below the serum Li^+ toxicity range (>1.5 mmol/L) reported for psychiatric patients (Grandjean and Aubry, 2009). Water intake, serum sodium and chloride concentrations, urine volume were significantly higher, and urine osmolarity was markedly lower in Li^+-treated mice than in controls (Table 1; Figures 1A–C), strongly indicative of nephrogenic diabetes insipidus (NDI). Otherwise, Li^+ intake did not appear to affect renal function, as indicated by similar endpoint BUN concentrations in Li^+-treated and control mice (Figure 1D).

Renal histology revealed morphological changes in the renal cortex including a higher percentage of fibrotic tissue, increased interstitial thickness, tubular dilation, and clear signs of hydronephrosis in renal papillae of Li^+-treated mice compared to the control group (Figures 2A–C). Quantitative RT-PCR showed that the expression of genes encoding

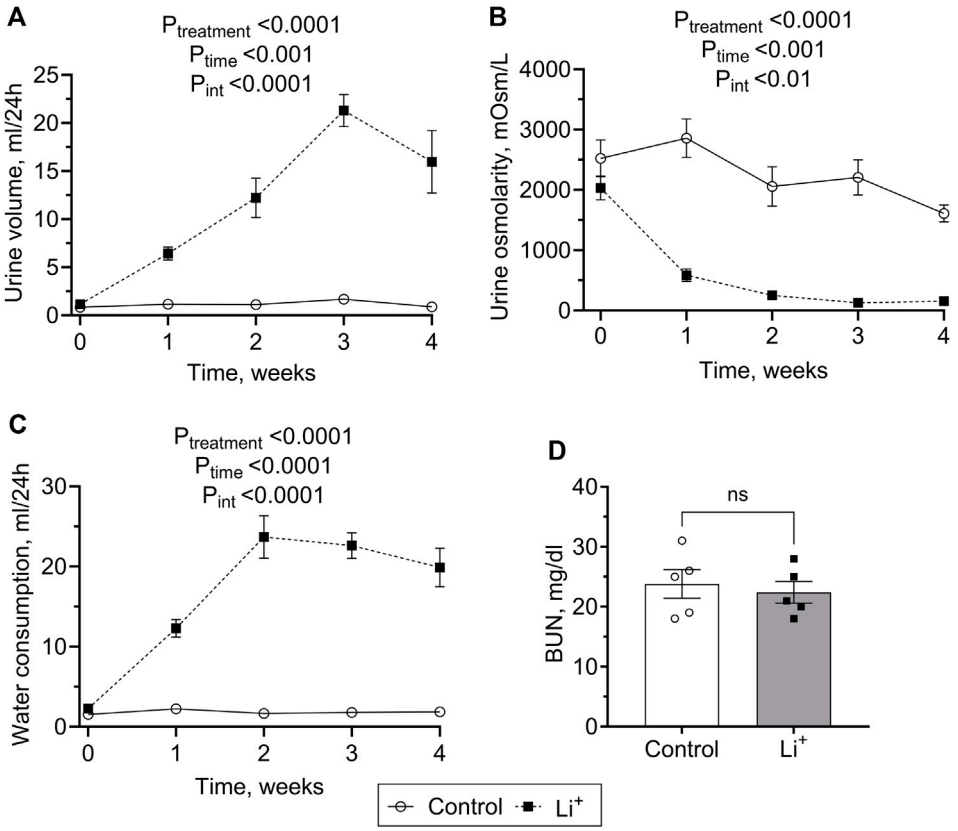

FIGURE 1
Lithium carbonate intake induces NDI symptoms in mice. Summary plots showing 24-h urine volume **(A)**, urine osmolarity **(B)** water consumption **(C)** measured over the course of 4 weeks and the endpoint BUN **(D)** observed in Li^+-treated and control mice. Data are shown as mean ± SEM. Differences between group means were analyzed by a two-way mixed-design ANOVA with a Greenhouse-Geisser correction **(A–C)** and a Student's t-test **(D)**. N ≥ 5 animals per group.

extracellular matrix proteins associated with increased interstitial thickness and fibrosis, collagen type I alpha 1 (Col1a1) and fibronectin 1 (Fn1), was significantly higher in renal tissue homogenates isolated from Li^+-treated mice than in controls (Figure 2D). Protein abundance of the proximal and distal tubule cell damage markers, kidney injury molecule, KIM-1 (Figure 2E) and neutrophil gelatinase-associated lipocalin, NGAL (Figure 2F), were moderately but significantly elevated in the renal tissue of Li^+-treated mice when compared to controls.

Li^+ changes the cytokine profile and alters the levels of lymphoid and myeloid cells in the renal tissue

To investigate if Li^+-induced damage is accompanied by an inflammatory response in the renal tissue, we performed cytokine and chemokine screening in the renal tissue samples from Li^+-treated and control mice using a multiplex cytokine array. The abundance of anti-inflammatory markers, pentraxin 2, adiponectin and CD93, was higher in the renal tissue of Li^+-treated mice than in controls. The levels of pro-inflammatory markers, CD26, CLCX16, PCSK9, and osteopontin, were not significantly different in the renal tissue samples isolated from Li^+-treated and control mice. Interestingly, the abundance of CCL21/6Ckine and fractalkine/CX3CL1 was elevated in the kidneys of Li^+-treated mice when compared to controls (Figures 3A, B).

Next, we performed immunophenotyping of the renal tissue samples isolated from control and Li^+-treated mice using flow cytometry. There were no detectable differences in the total number of immune cells ($CD45^+$ per mg renal tissue) and in the percentage of T cells ($CD3^+$, %) between the groups (Figures 4A, B). Interestingly, the percentage of helper T lymphocytes ($CD4^+CD8^-$, %) was significantly lower and the proportion of cytotoxic T lymphocytes ($CD4^-CD8^+$, %) – significantly higher in the kidneys of Li^+-treated mice than in control (Figure 4D). The proportion of macrophages ($F4.80^+$, %) was almost two-fold higher in the renal tissue of Li^+-treated mice when compared to the control group (Figure 4C). Based on earlier reports (Orecchioni et al., 2019), we used the ratio of IL-12β/arginase-1 gene expression to assess macrophage polarization along the M1/M2 (pro-/anti-inflammatory) axis. The IL-12β/arginase-1 mRNA ratio was significantly lower in the renal tissue macrophages of Li^+-treated mice (Figure 4E). This shift in macrophage polarization is consistent with a reduced inflammatory response in the kidneys of Li^+-treated mice when compared to controls.

10.3389/fphys.2024.1399396

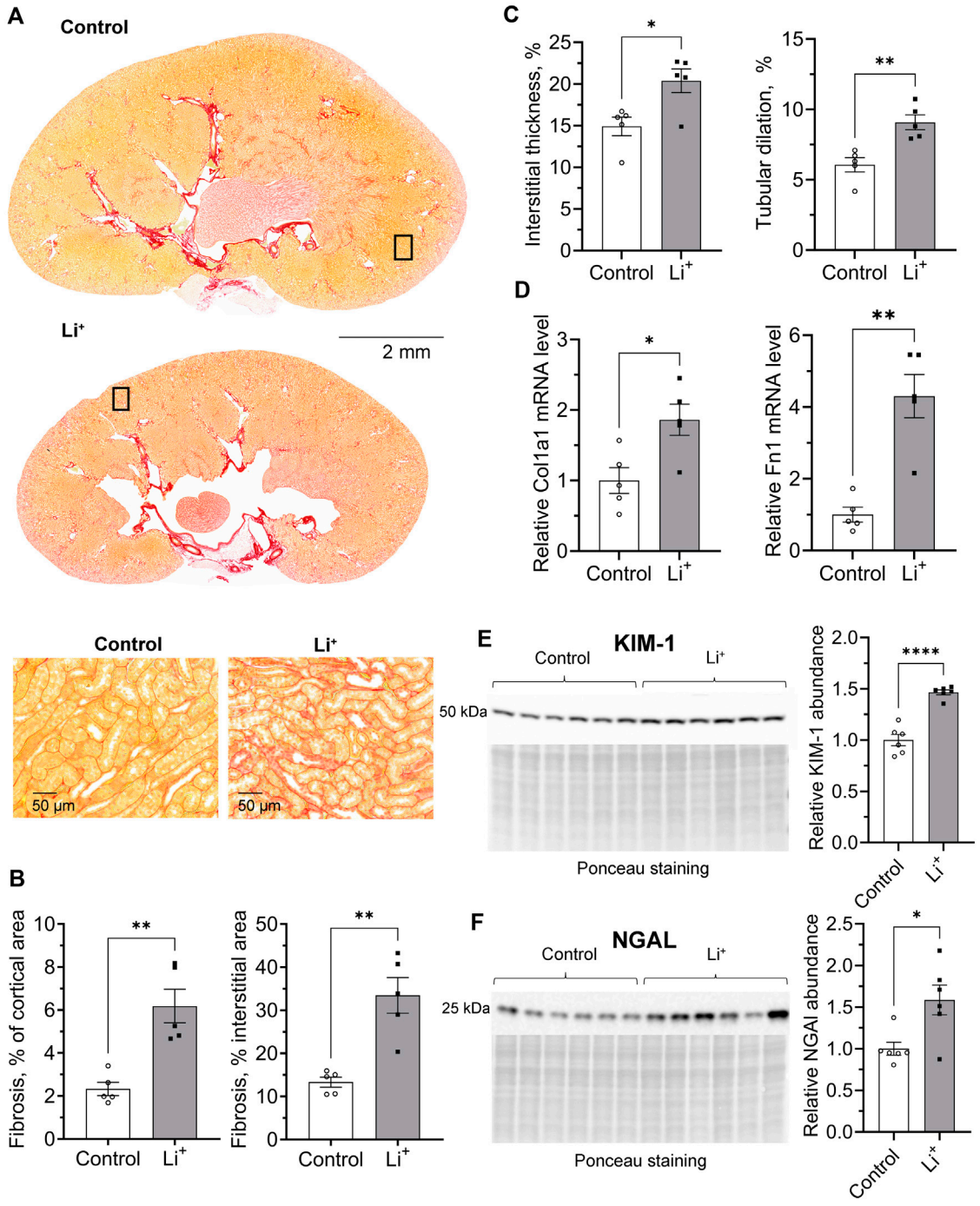

FIGURE 2
Chronic exposure to lithium causes a moderate insult to the renal tissue. **(A)** Representative microphotographs showing renal tissue fibrosis evaluated by the picrosirius red staining in control and Li$^+$-treated mice. **(B)** Summary plots on the interstitial fibrosis that was calculated as the percentage of the fibrotic area in the cortex and cortical interstitium. **(C)** Graphs summarizing the quantitative analysis of the interstitial thickness and tubular dilation in the cortex. **(D)** Summary plots showing the relative expression levels of Collagen type I alpha 1 and Fibronectin 1 in renal homogenates by RT-qPCR. Graphs summarizing protein abundances of kidney injury markers, KIM-1 **(E)** and NGAL **(F)** detected by immunoblotting in renal tissue homogenates. Data are shown as mean ± SEM. Differences between groups were analyzed using a Student's t-test with Welch's correction for samples with unequal variances. * – $p < 0.05$, ** – $p < 0.01$, **** – $p < 0.0001$, $N \geq 5$ animals per group.

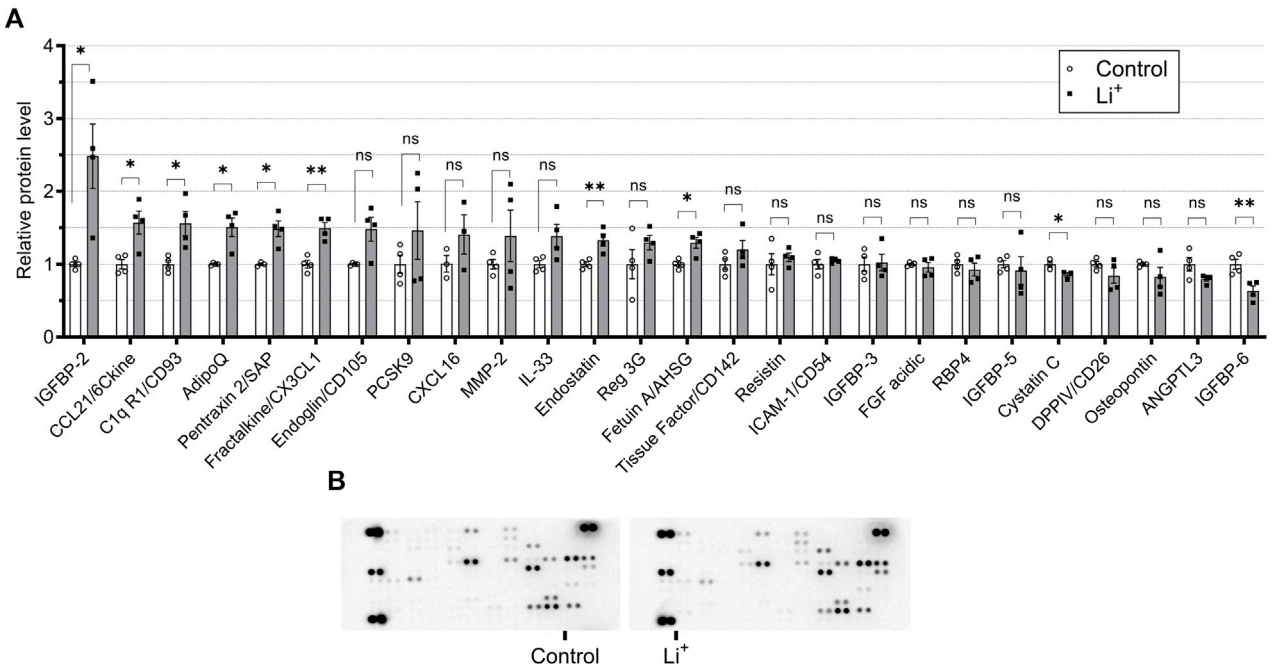

FIGURE 3
Administration of lithium does not trigger a pro-inflammatory response in the kidney. **(A)** A plot summarizing cytokine array data on the cytokines and chemokines in the renal tissue isolated from control and Li^+-treated mice. **(B)** Representative images of dot-blot cytokine array membranes visualizing the reporting signal density from kidney homogenates of control and Li^+-treated mice. Data are shown as mean ± SEM. Differences between groups were analyzed using a Student's t-test with Welch's correction for samples with unequal variances. * – $p < 0.05$, ** – $p < 0.01$. N = 6 mice per group. To perform the cytokine screening, renal tissue homogenates from all control or Li^+-treated mice were pooled together and applied onto respective membranes. The procedure was repeated 4 times.

Li^+ activates apoptosis, but does not stimulate the pro-inflammatory NLRP3 inflammasome cascade in the kidney

Serum Li^+ levels (>2.5 mmol/L) exceeding the toxicity threshold reportedly result in the activation of NLRP3 inflammasome triggering inflammatory cell death through pyroptosis in the mouse kidney (Jing et al., 2022). The priming stage of NLRP3 inflammasome activation results in NFκB-mediated transcriptional upregulation of the inflammasome components and substrates. Thus, next we assessed the expression of genes associated with NLRP3 inflammasome – interleukin-1β pathway, known to induce pyroptosis and the release of inflammatory cytokines. The mRNA levels of NLRP3, caspase-1, and IL-1β were similar in the renal tissue of Li^+-treated and control mice (Figure 5A). Renal abundance of uncleaved caspase-1 protein was comparable in both mouse groups, while the protein levels of NLRP3, cleaved caspase-1 and IL-1β were significantly lower in the kidneys of Li^+-treated mice when compared to controls (Figures 5B–F). Interestingly, the expression of apoptosis-associated speck-like protein containing a caspase activation and recruitment domain (ASC) gene and its protein abundance was markedly higher in the renal tissue isolated from Li^+-treated mice when compared to controls (Figures 5A, B, D). Importantly, while ASC is required for inflammasome activation, it also has a pronounced apoptotic function and can induce apoptosis in a p53-dependent manner (Protti and De Monte, 2020).

We used TUNEL assay to examine DNA fragmentation as an indicator of apoptotic cell death in the renal tissue. The number of TUNEL-positive cells was significantly higher in the renal cortex of Li^+-treated mice than in controls (Figure 6A). Since apoptotic, necrotic and even proliferating cells with increased rates of DNA repair may exhibit TUNEL-positive staining, we further compared the abundance of apoptotic markers in the renal tissue of Li^+-treated and control mice with immunoblotting. Signaling cascades that induce apoptotic cell death converge on the cleavage and activation of caspase-3 that plays a major role in the executive phase of apoptosis. We found that cleaved caspase-3 was significantly more abundant in the kidney homogenates isolated from Li^+-treated mice than in controls, corroborating our TUNEL staining data on the activation of apoptosis in the renal tissue of Li^+-treated mice (Figure 6B). Thus, Li^+ induces apoptotic cell death in the kidney, but does not activate NLRP3 inflammasome mediated pyroptosis.

Li^+ triggers apoptosis in the kidney through both extrinsic and mitochondrial pathways

Apoptosis can be induced through intrinsic and extrinsic pathways. The intrinsic pathway activation relies on a mitochondrion-centered interaction between pro-apoptotic and anti-apoptotic proteins from Bcl-2 family, such as Bax and Bcl-xL, that either promotes apoptotic cell death or

10.3389/fphys.2024.1399396

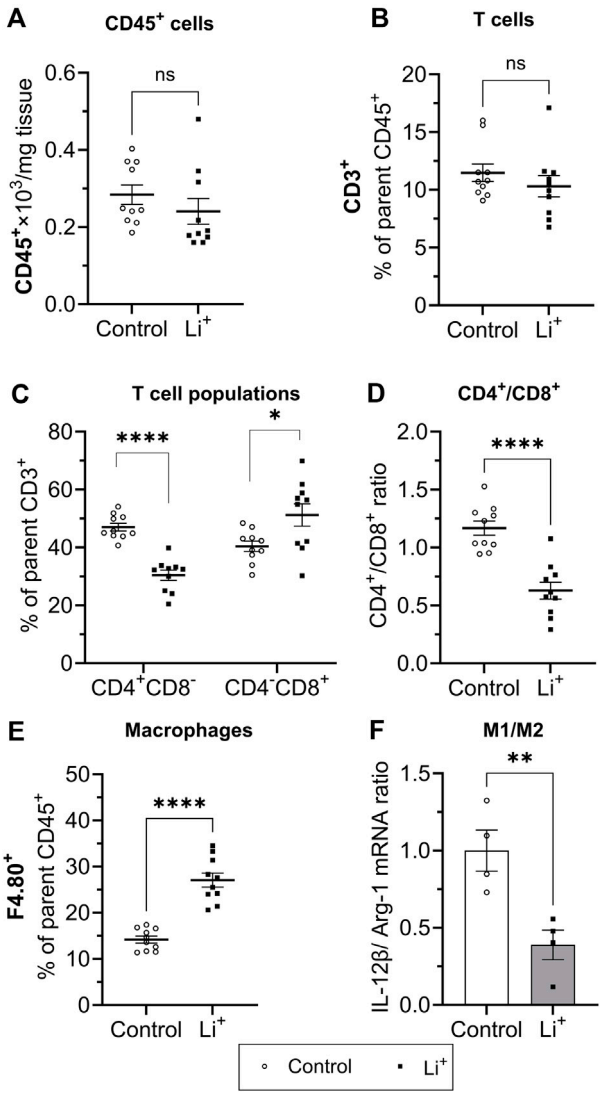

FIGURE 4
Lithium changes the immune cell landscape in the kidney. Summary plots demonstrating flow-cytometric analysis of immune cells isolated from the renal tissue: total lymphocytes [CD45$^+$, **(A)**]; T lymphocyte [CD3$^+$, **(B)**; helper (CD4$^+$CD8$^-$] and cytotoxic (CD4$^-$CD8$^+$) T lymphocytes **(C)**; the ratio of CD4$^+$/CD8$^+$ T lymphocytes **(D)**; macrophages [F4.80$^+$, **(E)**]. **(F)** A summary graph showing the ratio of IL-12b/arginase-1 mRNA expression in a purified F4.80$^+$ macrophage fraction. Data are shown as mean ± SEM. Differences between groups were analyzed using a Student's t-test with Welch's correction for samples with unequal variances. *$p < 0.05$, **$p < 0.01$, ****p < 0.0001, N ≥ 4 mice per group.

generates a pro-survival signal. We found that the abundance of the pro-apoptotic Bax protein is significantly higher in the renal tissue from Li$^+$-treated mice than in controls, while the level of the pro-survival Bcl-xL protein is similar in both groups (Figure 7A). The extrinsic receptor-mediated apoptotic pathway induces cleavage and activation of caspase-8. The abundance of cleaved caspase-8 was two times higher in the renal tissue from Li$^+$-treated mice than in controls, while the levels of uncleaved pro-caspase-8 were significantly lower in the kidneys of Li$^+$-treated mice (Figure 7B). In addition to its central role in the extrinsic apoptotic pathway, caspase-8 can activate the BH3 interacting-domain death agonist, Bid (Kantari and Walczak, 2011). The activation of Bid, a Bcl-2 protein family member, amplifies the caspase-8 mediated pro-apoptotic signal and links the extrinsic receptor-mediated and intrinsic mitochondria-driven apoptotic pathways. We observed similar levels of Bid protein in the renal tissue samples isolated from Li$^+$-treated and control mice (Figure 7C). Therefore, chronic lithium intake independently activates receptor-mediated and mitochondrial apoptotic pathways in the renal cells.

Discussion

In this study, C57BL/6NJ male mice were placed on a 0.3% lithium carbonate diet for 28 days to achieve serum lithium concentrations below the reported toxicity range for psychiatric patients and explore chronic effects of Li$^+$ on the kidney. This intervention led to the development of NDI, renal tissue fibrosis, and elevated levels of kidney injury markers, KIM-1 and NGAL. Li$^+$ administration did not result in activation of the NLRP3 inflammasome pathway in the renal tissue but promoted apoptosis in tubular cells. Protein abundance of CD93, CCL21, and fractalkine, important for efficient macrophage infiltration, was significantly higher in the kidneys of Li$^+$-treated mice when compared to controls. And, indeed, we observed markedly elevated levels of F4.80$^+$ macrophages in the renal tissue of Li$^+$-treated mice with a polarization shift towards M2 phenotype. The abundance of anti-inflammatory markers, including pentraxin 2 and adiponectin, was increased in the kidneys of mice receiving Li$^+$ when compared to controls, while pro-inflammatory cytokines remained mostly unaffected. Consistent with the anti-inflammatory profile of Li$^+$-induced immune response in the kidney, the levels of pro-inflammatory proteins, associated with NLRP3-inflammasome activation, caspase-1, NLRP3, and IL-1β, were lower in the renal tissue of Li$^+$-treated mice. While a 4-week treatment with Li$^+$ did not elevate the levels of immune cells (CD45$^+$) in the renal tissue, significant alterations were found in the T cell population balance. The numbers of CD4$^+$ cells were significantly lower and the levels of CD8$^+$ cells were markedly elevated in the kidneys of Li$^+$-treated mice when compared to controls.

We show that after 28 days on 0.3% Li_2CO_3 diet mice attained serum Li$^+$ concentrations in the range of 0.7–1.5 mmol/L, and their kidneys exhibited clear signs of damage and fibrosis (Figure 2). Long-term exposure to lithium has been associated with tubular atrophy and interstitial fibrosis in human and rodent models (Walker et al., 2013; Alsady et al., 2016). The accrued evidence suggests the involvement of glycogen synthase kinase-3 beta (GSK-3β), a negative regulator of Wnt/β-catenin activity (Huang et al., 2023). Prolonged activation of the Wnt-pathway can exacerbate fibrotic kidney diseases and accelerate the progression of chronic kidney disease (CKD) (Xiao et al., 2016). Lithium, as a GSK-3β inhibitor, can over-activate the Wnt/β-catenin pathway, thereby promoting the development of renal fibrosis (Alsady et al., 2016). Higher levels of KIM-1 and NGAL markers in the kidneys of Li$^+$-treated mice corresponded to the renal damage occurring in the proximal

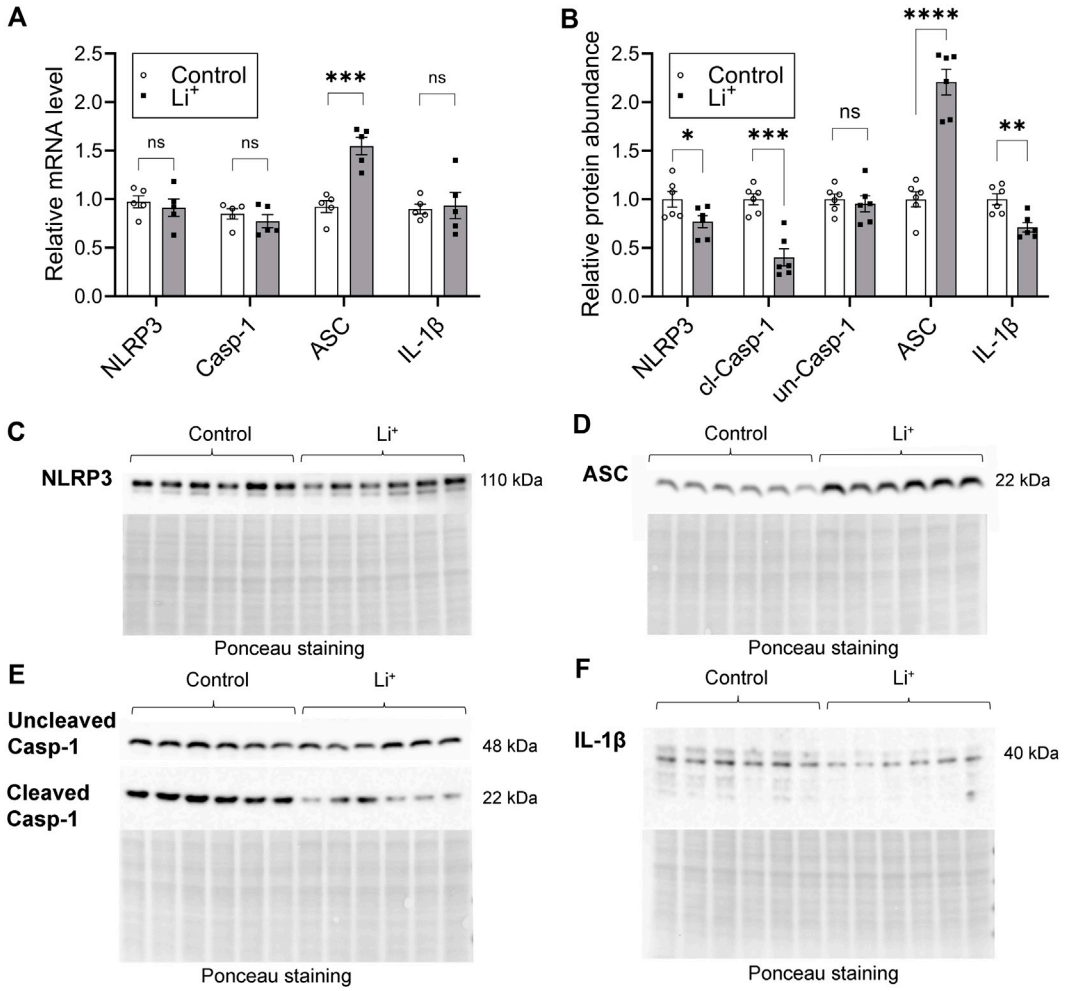

FIGURE 5
Lithium does not activate the NLRP3 inflammasome cascade in the kidney. **(A)** A summary plot demonstrating relative expression of inflammasome-associated genes: NLRP3, caspase 1, ASC, IL-1β in the renal tissue of control and Li^+-treated mice. **(B)** A summary plot showing the abundance of NLRP3, uncleaved and cleaved caspase 1, ASC, IL-1β proteins in the kidney homogenates isolated from control and Li^+-treated mice. **(C–F)** Representative image of membranes stained for NLRP3, uncleaved and cleaved caspase 1, ASC, IL-1β proteins. Total protein Ponceau staining is shown below the respective bands of interest. Data are shown as mean ± SEM. Differences between groups were analyzed using a Student's t-test with Welch's correction for samples with unequal variances. *$p < 0.05$, **$p < 0.01$, ***$p < 0.001$, ****$p < 0.0001$. $N \geq 5$ mice per group.

and distal tubular segments, respectively. Excessive accumulation of Li^+ in these nephron segments has been linked to proximal tubular atrophy, dysregulation of AQP2 trafficking and expression, and loss of principal collecting duct cells (Alsady et al., 2016). Thus, the dietary intervention and experimental timeline used in our study are reflective of chronic exposure to Li^+ in psychiatric patients and animal models.

Comparison of the cytokine and immune cell profiles in the renal tissue samples from Li^+-treated and control mice strongly suggests the absence of an evident proinflammatory response after 28 days on Li^+ diet. Administration of Li^+ did not significantly change the abundance of pro-inflammatory markers, such as CD26, CXCL16, PCSK9, and osteopontin in the kidney. At the same time the levels of anti-inflammatory markers, including pentraxin 2 and adiponectin, were significantly elevated in the renal tissue of Li^+-treated mice compared to control animals (Figure 3A). The levels of $CD45^+$ remain comparable in both groups, while the number of $CD4^+$ T cells, associated with inflammation in multiple renal disorders, including salt-sensitive hypertension (Walton et al., 2023), was significantly lower in the renal tissue of Li^+-treated mice when compared to controls (Figure 4). We also show that the abundance of a pro-inflammatory protein CD26, expressed on the activated $CD4^+$ T cells under Th1 polarization (Ohnuma et al., 2008), was comparable in the renal homogenates isolated from Li^+-treated and control mice (Figure 3A). Moreover, the ratio of IL-12β/arginase-1 gene expression, reflecting the proinflammatory macrophage polarization along the M1/M2 axis, was significantly lower in the renal tissue macrophages of Li^+-treated mice when compared to controls (Figure 4F). Finally, the protein abundance of cleaved caspase-1, critical for initiation of an inflammatory response, was remarkably lower in the renal tissue of Li^+-treated mice compared to controls (Figure 5E). Earlier studies demonstrate that treatment with Li^+ reduces the levels of pro-inflammatory cytokines in the blood of bipolar patients (Boufidou et al., 2004)

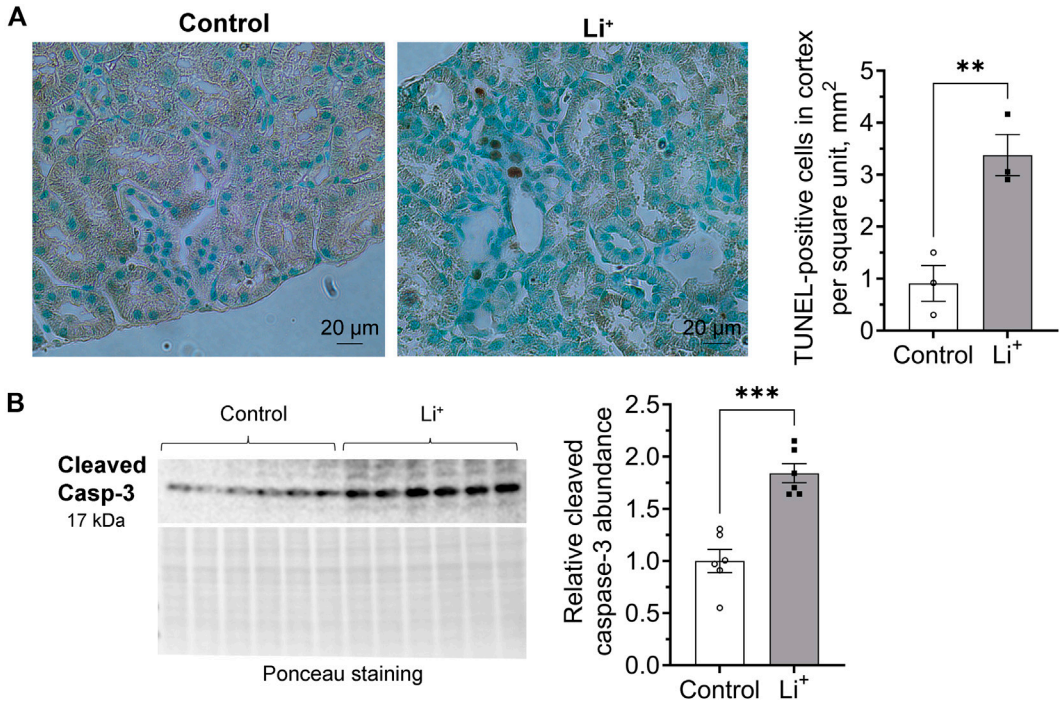

FIGURE 6
Lithium induces apoptosis in the renal tissue. **(A)** Representative images of kidney sections isolated from control and Li^+-treated mice stained with an HRP/DAB TUNEL assay kit (left). A graph summarizing the analysis of TUNEL-staining data (right). **(B)** A representative image of the membrane stained for cleaved caspase-3 and total protein (Ponceau) and a summary graph showing the abundance of cleaved caspase-3 in the renal tissue homogenates isolated from control and Li^+-treated mice. Data are shown as mean ± SEM. Differences between groups were analyzed using a Student's t-test with Welch's correction for samples with unequal variances. **p < 0.01, ***p < 0.001. N ≥ 3 mice per group.

and decreases neuroinflammation in rats (Basselin et al., 2010). An animal study shows that long-term administration of Li^+-containing diet over the course of 6 months induces apoptosis in the epithelium of dilated and atrophic cortical tubules in rat kidneys but is accompanied with minimal inflammatory activity (Walker et al., 2013). Thus, our observations are consistent with previously reported anti-inflammatory properties of lithium.

Intoxication caused by excessively high levels of Li^+ (>2.5 mmol/L) in serum and renal tissue has been associated with an inflammatory reaction in mouse kidney, including the activation of NLRP3 inflammasome and pyroptosis (Jing et al., 2022). At serum Li^+ levels below 1.5 mmol/L in our experimental cohort, we did not observe elevated transcription of NLRP3 inflammasome-related genes or increased abundance of respective protein products in the renal tissue of Li^+-treated mice (Figure 5). This is in line with our findings pointing to the anti-inflammatory nature of Li^+-induced immune response in the kidney. One notable exception was significantly higher expression of ASC in the kidneys of Li^+-treated mice compared to controls (Figures 5A, B, D). While ASC is critical for inflammasome-mediated cell death through pyroptosis, it also plays an essential role in the intrinsic mitochondrial pathway of apoptosis through the p53-Bax network (Protti and De Monte, 2020). We confirmed the activation of apoptosis in the renal tissue of Li^+-treated mice. The number of tubular epithelial cells with DNA fragmentations characteristic of apoptosis was significantly elevated in the renal cortex of Li^+-treated mice (Figure 6A). Cleavage of the effector caspase-3 (Figure 6B), associated with activation of apoptosis, and Bax/Bcl-xL ratio (Figure 7A), indicative of mitochondrial apoptotic pathway activation, were markedly higher in the kidneys of Li^+-treated mice when compared controls. The observed elevated levels of cytotoxic ($CD8^+$) T lymphocytes in the renal tissue of Li^+-treated mice indicate that Li^+ may also rely on the extrinsic pathway to induce apoptosis (Diamond and Gill, 2000). Indeed, we saw higher levels of cleaved caspase-8, an initiator caspase in receptor-mediated apoptotic cell death, in the kidneys of mice receiving Li^+ (Figure 7B). Caspase-8 activated through the extrinsic pathway can cleave Bid protein that gets translocated into mitochondria, where it promotes Bax activation, linking the extrinsic receptor-mediated and intrinsic mitochondria-dependent pathways (Kantari and Walczak, 2011). This linkage amplifies the apoptotic receptor-mediated apoptotic signal by engaging the mitochondrial pathway. However, Bid levels were comparable in the renal tissue of Li^+-treated and control mice (Figure 7C), indicative of independent activation of mitochondrial and extrinsic pathways by Li^+ administration. Thus, we conclude that chronic exposure to lithium likely contributes to the induction of apoptosis in the kidney through both mitochondrial and extrinsic pathways, without appreciable involvement of inflammasome or pyroptosis.

We found significantly elevated levels of CD93, fractalkine/CX3CL1, CCL21, and IGFBP-2 in the renal tissue samples

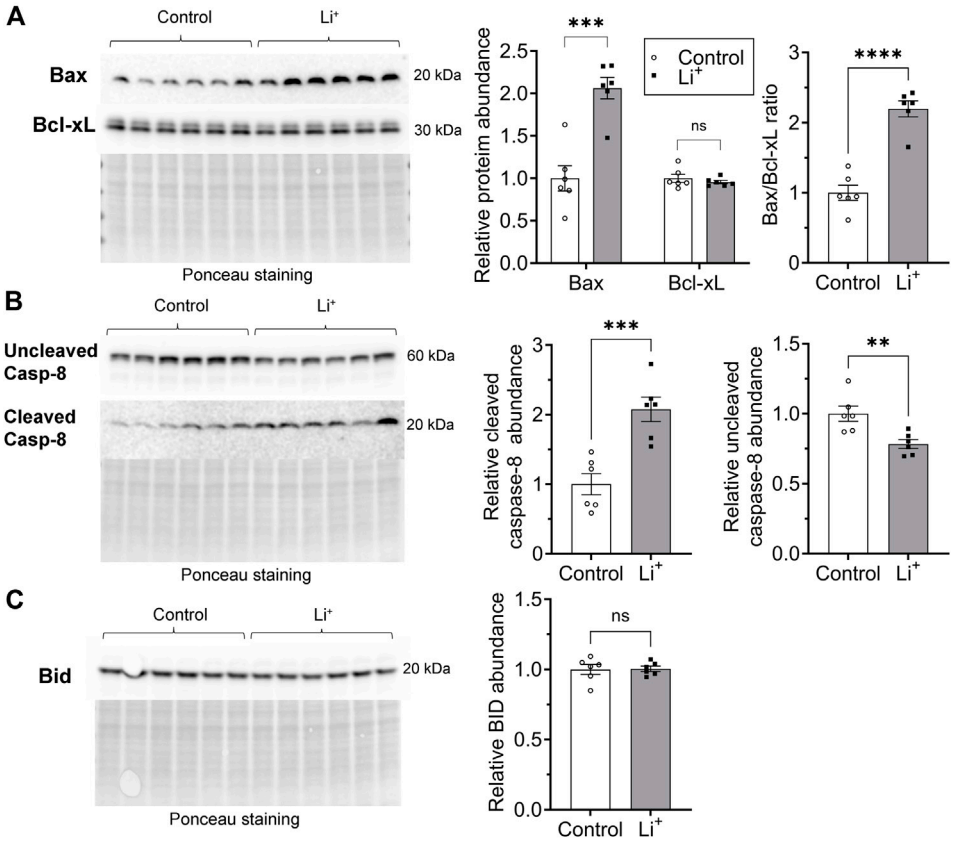

FIGURE 7
Lithium induces apoptosis in renal cells via extrinsic and intrinsic pathways. **(A)** Representative images of the membranes and summary graphs showing the abundance of Bax and Bcl-xL in the renal tissue homogenates isolated from control and Li^+-treated mice. **(B)** Representative images of the membranes and summary graphs showing the abundance of full and cleaved caspase-8 in the renal tissue of control and Li^+-treated mice. **(C)** A representative image of the membrane and a summary plot demonstrating the abundance of Bid protein in the kidneys of control and Li^+-treated mice. Images of the membranes stained with Ponceau to control protein loading are presented for each experiment. Data are shown as mean ± SEM. Differences between groups were analyzed using a Student's t-test with Welch's correction for samples with unequal variances. **p < 0.01, ***p < 0.001, ****p < 0.0001, N ≥ 5 mice per group.

isolated from Li^+-treated mice (Figure 3A). CD93 glycoprotein is a phagocytic receptor required for efficient clearance of apoptotic cells by macrophages *in vivo* (Norsworthy et al., 2004). CX3CR1, a receptor for fractalkine, reportedly contributes to CKD progression (Cormican and Griffin, 2021). However, it can also promote macrophage trafficking to apoptotic sites, the release of anti-inflammatory mediators, such as interleukin-1 receptor antagonist and prostaglandin E2 (Zhuang et al., 2017). CX3CR1 deficiency was previously associated with a shift toward M1 dominant macrophages in the liver (Ni et al., 2022). The role of IGFBP-2 in renal pathophysiology and modulation of immune response remains to be fully understood. Proinflammatory and proapoptotic effects were reported in diabetic kidney disease (Wang et al., 2024), while in cancer IGFBP2 can induce M2 macrophage polarization (Zhang et al., 2024). Finally, CCL21 and its receptor CCR7 also facilitate the accumulation of macrophages and $CD45^+$ type I collagen+ fibroblasts into the renal tissue (Tang et al., 2019). It was shown that anti-CCL21 therapy successfully suppresses the infiltration of bone-marrow-derived fibroblasts ($CD45^+/ColI^+$) and reduces renal fibrosis (Sakai et al., 2006). In our study, renal tissue $F4.80^+$ macrophages were almost 2 times more abundant in Li^+-treated mice than in controls and exhibited polarization toward M2 type. M2 polarization of macrophages is known to be profibrotic in the kidney (Feng et al., 2018) and could potentially contribute to the development of renal fibrosis, a known pathology of chronic lithium treatment. This provides a strong rationale for further research investigating molecular determinants of Li^+-induced immune response in the renal tissue.

Overall, we demonstrate that administration of lithium for 28 days, resulting in circulating Li^+ levels below the clinically reported toxic threshold, causes an insidious insult to the kidney. Li^+ promotes apoptosis in tubular cells but does not induce pronounced inflammation in the renal tissue. On the contrary, Li^+-induced immune response in the kidney exhibits distinct anti-inflammatory features. Future experiments assessing the molecular determinants of apoptotic cell death and characterizing the subsets of lymphoid and myeloid cells in the renal tissue and at the systemic level will be critical to better understand the beneficial effects and pathophysiological sequelae of chronic lithium administration on the kidney.

Data availability statement

The raw data supporting the conclusions of this article will be made available by the authors, without undue reservation.

Ethics statement

The animal study was approved by the Institutional Animal Care and Use Committee of the Medical College of Georgia at Augusta University. The study was conducted in accordance with the local legislation and institutional requirements.

Author contributions

IB: Conceptualization, Writing–original draft, Writing–review and editing, Data curation, Formal Analysis, Investigation, Methodology, Validation, Visualization. KV: Formal Analysis, Investigation, Methodology, Writing–review and editing. SA: Investigation, Methodology, Writing–review and editing. JA-B: Investigation, Methodology, Writing–review and editing. MM: Conceptualization, Data curation, Funding acquisition, Investigation, Project administration, Resources, Supervision, Writing–original draft, Writing–review and editing.

Funding

The author(s) declare that financial support was received for the research, authorship, and/or publication of this article. This work was supported by the National Institute of Diabetes and Digestive and Kidney Disease (NIDDK) R01DK125464 grant to MM.

Acknowledgments

We would like to thank Nichole Mumuney for her technical assistance in animal handling; Drs. David Mattson, Brandi Wynne, and Daria Ilatovskaya for their overall support of this research; the Histology and Electron Microscopy Core Laboratory at Augusta University and Georgia Research Pathology Service for their technical assistance with tissue processing and histological staining; the Georgia Cancer Center Flow Cytometry Shared Resource Laboratory for the assistance in flow cytometry; Georgia Cancer Center Biorepository for their assistance with slide scanning.

Conflict of interest

The authors declare that the research was conducted in the absence of any commercial or financial relationships that could be construed as a potential conflict of interest.

Publisher's note

All claims expressed in this article are solely those of the authors and do not necessarily represent those of their affiliated organizations, or those of the publisher, the editors and the reviewers. Any product that may be evaluated in this article, or claim that may be made by its manufacturer, is not guaranteed or endorsed by the publisher.

Supplementary material

The Supplementary Material for this article can be found online at: https://www.frontiersin.org/articles/10.3389/fphys.2024.1399396/full#supplementary-material

References

Alsady, M., Baumgarten, R., Deen, P. M., and de Groot, T. (2016). Lithium in the kidney: friend and foe? *J. Am. Soc. Nephrol.* 27 (6), 1587–1595. doi:10.1681/ASN.2015080907

Azab, A. N., Shnaider, A., Osher, Y., Wang, D., Bersudsky, Y., and Belmaker, R. H. (2015). Lithium nephrotoxicity. *Int. J. Bipolar Disord.* 3 (1), 28. doi:10.1186/s40345-015-0028-y

Bankhead, P., Loughrey, M. B., Fernandez, J. A., Dombrowski, Y., McArt, D. G., Dunne, P. D., et al. (2017). QuPath: open source software for digital pathology image analysis. *Sci. Rep.* 7 (1), 16878. doi:10.1038/s41598-017-17204-5

Bao, H., Ge, Y., Peng, A., and Gong, R. (2015). Fine-tuning of NFκB by glycogen synthase kinase 3β directs the fate of glomerular podocytes upon injury. *Kidney Int.* 87 (6), 1176–1190. doi:10.1038/ki.2014.428

Basselin, M., Kim, H. W., Chen, M., Ma, K., Rapoport, S. I., Murphy, R. C., et al. (2010). Lithium modifies brain arachidonic and docosahexaenoic metabolism in rat lipopolysaccharide model of neuroinflammation. *J. Lipid Res.* 51 (5), 1049–1056. doi:10.1194/jlr.M002469

Bendz, H., Schon, S., Attman, P. O., and Aurell, M. (2010). Renal failure occurs in chronic lithium treatment but is uncommon. *Kidney Int.* 77 (3), 219–224. doi:10.1038/ki.2009.433

Boufidou, F., Nikolaou, C., Alevizos, B., Liappas, I. A., and Christodoulou, G. N. (2004). Cytokine production in bipolar affective disorder patients under lithium treatment. *J. Affect Disord.* 82 (2), 309–313. doi:10.1016/j.jad.2004.01.007

Cormican, S., and Griffin, M. D. (2021). Fractalkine (CX3CL1) and its receptor CX3CR1: a promising therapeutic target in chronic kidney disease? *Front. Immunol.* 12, 664202. doi:10.3389/fimmu.2021.664202

Diamond, A. S., and Gill, R. G. (2000). An essential contribution by IFN-gamma to CD8+ T cell-mediated rejection of pancreatic islet allografts. *J. Immunol.* 165 (1), 247–255. doi:10.4049/jimmunol.165.1.247

Feng, Y., Ren, J., Gui, Y., Wei, W., Shu, B., Lu, Q., et al. (2018). Wnt/β-Catenin-Promoted macrophage alternative activation contributes to kidney fibrosis. *J. Am. Soc. Nephrol.* 29 (1), 182–193. doi:10.1681/ASN.2017040391

Gong, R., Wang, P., and Dworkin, L. (2016). What we need to know about the effect of lithium on the kidney. *Am. J. Physiol. Ren. Physiol.* 311 (6), F1168–F1171. doi:10.1152/ajprenal.00145.2016

Grandjean, E. M., and Aubry, J. M. (2009). Lithium: updated human knowledge using an evidence-based approach: Part I: clinical efficacy in bipolar disorder. *CNS Drugs* 23 (3), 225–240. doi:10.2165/00023210-200923030-00004

Grunfeld, J. P., and Rossier, B. C. (2009). Lithium nephrotoxicity revisited. *Nat. Rev. Nephrol.* 5 (5), 270–276. doi:10.1038/nrneph.2009.43

Huang, R., Fu, P., and Ma, L. (2023). Kidney fibrosis: from mechanisms to therapeutic medicines. *Signal Transduct. Target Ther.* 8 (1), 129. doi:10.1038/s41392-023-01379-7

Jing, H., Wang, F., and Gao, X. J. (2022). Lithium intoxication induced pyroptosis via ROS/NF-κB/NLRP3 inflammasome regulatory networks in kidney of mice. *Environ. Toxicol.* 37 (4), 825–835. doi:10.1002/tox.23446

Kantari, C., and Walczak, H. (2011). Caspase-8 and bid: caught in the act between death receptors and mitochondria. *Biochim. Biophys. Acta* 1813 (4), 558–563. doi:10.1016/j.bbamcr.2011.01.026

Kessing, L. V. (2024). Why is lithium [not] the drug of choice for bipolar disorder? a controversy between science and clinical practice. *Int. J. Bipolar Disord.* 12 (1), 3. doi:10.1186/s40345-023-00322-7

Kripalani, M., Shawcross, J., Reilly, J., and Main, J. (2009). Lithium and chronic kidney disease. *BMJ* 339, b2452. doi:10.1136/bmj.b2452

Malhi, G. S., and Bauer, M. (2023). Lithium first: not merely first line. *Bipolar Disord.* 25 (1), 7–8. doi:10.1111/bdi.13299

Markowitz, G. S., Radhakrishnan, J., Kambham, N., Valeri, A. M., Hines, W. H., and D'Agati, V. D. (2000). Lithium nephrotoxicity: a progressive combined glomerular and tubulointerstitial nephropathy. *J. Am. Soc. Nephrol.* 11 (8), 1439–1448. doi:10.1681/ASN.V1181439

Mehta, P. M., Gimenez, G., Walker, R. J., and Slatter, T. L. (2022). Reduction of lithium induced interstitial fibrosis on co-administration with amiloride. *Sci. Rep.* 12 (1), 14598. doi:10.1038/s41598-022-18825-1

Nahman, S., Belmaker, R. H., and Azab, A. N. (2012). Effects of lithium on lipopolysaccharide-induced inflammation in rat primary glia cells. *Innate Immun.* 18 (3), 447–458. doi:10.1177/1753425911421512

Ni, Y., Zhuge, F., Ni, L., Nagata, N., Yamashita, T., Mukaida, N., et al. (2022). CX3CL1/CX3CR1 interaction protects against lipotoxicity-induced nonalcoholic steatohepatitis by regulating macrophage migration and M1/M2 status. *Metabolism* 136, 155272. doi:10.1016/j.metabol.2022.155272

Norsworthy, P. J., Fossati-Jimack, L., Cortes-Hernandez, J., Taylor, P. R., Bygrave, A. E., Thompson, R. D., et al. (2004). Murine CD93 (C1qRp) contributes to the removal of apoptotic cells *in vivo* but is not required for C1q-mediated enhancement of phagocytosis. *J. Immunol.* 172 (6), 3406–3414. doi:10.4049/jimmunol.172.6.3406

Ohnuma, K., Takahashi, N., Yamochi, T., Hosono, O., Dang, N. H., and Morimoto, C. (2008). Role of CD26/dipeptidyl peptidase IV in human T cell activation and function. *Front. Biosci.* 13, 2299–2310. doi:10.2741/2844

Orecchioni, M., Ghosheh, Y., Pramod, A. B., and Ley, K. (2019). Macrophage polarization: different gene signatures in M1(LPS+) vs. Classically and M2(LPS-) vs. Alternatively activated macrophages. *Front. Immunol.* 10, 1084. doi:10.3389/fimmu.2019.01084

Perez, G. O., Oster, J. R., and Vaamonde, C. A. (1975). Incomplete syndrome of renal tubular acidosis induced by lithium carbonate. *J. Lab. Clin. Med.* 86 (3), 386–394.

Protti, M. P., and De Monte, L. (2020). Dual role of inflammasome adaptor ASC in cancer. *Front. Cell. Dev. Biol.* 8, 40. doi:10.3389/fcell.2020.00040

Rybakowski, J. K. (2018). Challenging the negative perception of lithium and optimizing its long-term administration. *Front. Mol. Neurosci.* 11, 349. doi:10.3389/fnmol.2018.00349

Sakai, N., Wada, T., Yokoyama, H., Lipp, M., Ueha, S., Matsushima, K., et al. (2006). Secondary lymphoid tissue chemokine (SLC/CCL21)/CCR7 signaling regulates fibrocytes in renal fibrosis. *Proc. Natl. Acad. Sci. U. S. A.* 103 (38), 14098–14103. doi:10.1073/pnas.0511200103

Saleh, M. A., Norlander, A. E., and Madhur, M. S. (2016). Inhibition of interleukin 17-A but not interleukin-17F signaling lowers blood pressure and reduces end-organ inflammation in angiotensin II-induced hypertension. *JACC Basic Transl. Sci.* 1 (7), 606–616. doi:10.1016/j.jacbts.2016.07.009

Shimizu, M. H. M., Volpini, R. A., de Braganca, A. C., Nascimento, M. M., Bernardo, D. R. D., Seguro, A. C., et al. (2023). Administration of a single dose of lithium ameliorates rhabdomyolysis-associated acute kidney injury in rats. *PLoS One* 18 (2), e0281679. doi:10.1371/journal.pone.0281679

Singh, A., Arora, S., Chavan, M., Shahbaz, S., and Jabeen, H. (2023). An overview of the neurotrophic and neuroprotective properties of the psychoactive drug lithium as an autophagy modulator in neurodegenerative conditions. *Cureus* 15 (8), e44051. doi:10.7759/cureus.44051

Tang, P. M., Nikolic-Paterson, D. J., and Lan, H. Y. (2019). Macrophages: versatile players in renal inflammation and fibrosis. *Nat. Rev. Nephrol.* 15 (3), 144–158. doi:10.1038/s41581-019-0110-2

Vestergaard, P., Amdisen, A., Hansen, H. E., and Schou, M. (1979). Lithium treatment and kidney function. A survey of 237 patients in long-term treatment. *Acta Psychiatr. Scand.* 60 (5), 504–520. doi:10.1111/j.1600-0447.1979.tb00559.x

Walker, R. J., Leader, J. P., Bedford, J. J., Gobe, G., Davis, G., Vos, F. E., et al. (2013). Chronic interstitial fibrosis in the rat kidney induced by long-term (6-mo) exposure to lithium. *Am. J. Physiol. Ren. Physiol.* 304 (3), F300–F307. doi:10.1152/ajprenal.00182.2012

Walton, S. D., Dasinger, J. H., Burns, E. C., Cherian-Shaw, M., Abais-Battad, J. M., and Mattson, D. L. (2023). Functional NADPH oxidase 2 in T cells amplifies salt-sensitive hypertension and associated renal damage. *Am. J. Physiol. Ren. Physiol.* 325 (2), F214–F223. doi:10.1152/ajprenal.00014.2023

Wang, X., Zhang, Y., Chi, K., Ji, Y., Zhang, K., Li, P., et al. (2024). IGFBP2 induces podocyte apoptosis promoted by mitochondrial damage via integrin α5/FAK in diabetic kidney disease. *Apoptosis* 29, 1109–1125. doi:10.1007/s10495-024-01974-1

Weiner, I. D., Leader, J. P., Bedford, J. J., Verlander, J. W., Ellis, G., Kalita, P., et al. (2014). Effects of chronic lithium administration on renal acid excretion in humans and rats. *Physiol. Rep.* 2 (12), e12242. doi:10.14814/phy2.12242

Xiao, L., Zhou, D., Tan, R. J., Fu, H., Zhou, L., Hou, F. F., et al. (2016). Sustained activation of wnt/β-catenin signaling drives AKI to CKD progression. *J. Am. Soc. Nephrol.* 27 (6), 1727–1740. doi:10.1681/ASN.2015040449

Zhang, X., Sun, X., Guo, C., Li, J., and Liang, G. (2024). Cancer-associated fibroblast-associated gene IGFBP2 promotes glioma progression through induction of M2 macrophage polarization. *Am. J. Physiol. Cell. Physiol.* 326 (1), C252–C268. doi:10.1152/ajpcell.00234.2023

Zhuang, Q., Cheng, K., and Ming, Y. (2017). CX3CL1/CX3CR1 Axis, as the therapeutic potential in renal diseases: friend or foe? *Curr. Gene Ther.* 17 (6), 442–452. doi:10.2174/1566523218666180214092536

Frontiers in Physiology

Understanding how an organism's components work together to maintain a healthy state

The second most-cited physiology journal, promoting a multidisciplinary approach to the physiology of living systems - from the subcellular and molecular domains to the intact organism and its interaction with the environment.

Discover the latest Research Topics

See more →

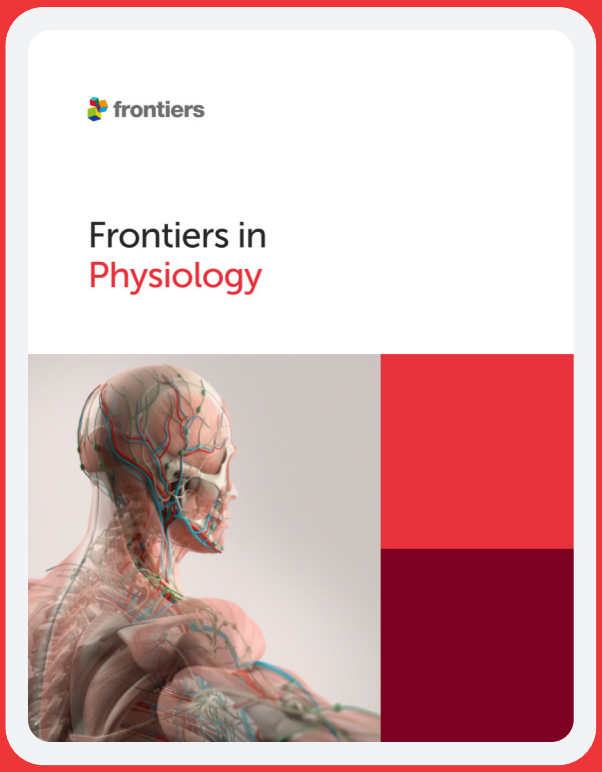

Frontiers

Avenue du Tribunal-Fédéral 34
1005 Lausanne, Switzerland
frontiersin.org

Contact us

+41 (0)21 510 17 00
frontiersin.org/about/contact